EUROCORR 2022

28 August – 1 September 2022 · Berlin · Germany

EUROCORR 2022

European Corrosion Congress

Corrosion in a Changing World – Energy, Mobility, Digitalization

© visitBerlin, Foto: Dirk_Mathesius

ABSTRACTS / EXTENDED PAPERS FOR POSTERS

www.eurocorr2022.org

DECHEMA
Gesellschaft für Chemische Technik und Biotechnologie e.V.

GfKORR
Gesellschaft für Korrosionsschutz e.V.

EFC
EUROPEAN FEDERATION OF CORROSION
EFC Event-Number 472

EUROCORR
The European Corrosion Congress

GOLD SPONSORS

Since 1949, Trenton has pioneered the development of microcrystalline wax-based anticorrosion products. Most well known is the Wax-Tape® brand wrap system, used with primers & outerwraps. Wraps meet a variety of needs, above and below ground and in high temperature applications. For additional protection, Trenton offers a range of outerwraps. Benefits of Trenton's products include: minimal surface prep, ease of application, conformable to irregular surfaces, removable for inspection, compatible with other coatings, environmentally friendly. **www.trentoncorp.com**

VDM Metals, is part of the Acerinox Group. VDM Metals develops and manufactures nickel, copper, cobalt and zirconium alloys as well as high-alloyed special stainless steels for the most demanding applications in different industries. Each one of the company's alloys is characterized by a unique combination of properties, depending on their chemical composition and the manufacturing process.

High-performance materials made by VDM Metals pass very stringent quality control. They are used in mission-critical applications and many of today's key technologies for large-scale implementation and safe handling of corrosive and high-temperature processes and procedures. VDM Metals is well prepared for the future. **www.vdm-metals.com**

SILVER SPONSORS

Gamry Instruments designs, manufactures, and sells electrochemical instrumentation and accessories, designed to fit your needs and budget. This includes basic DC corrosion measurements, electrochemical impedance, noise, and frequency modulation. We have a variety of single and multichannel potentiostats, QCMs, multiplexer, RCE setups, and cells/accessories.

In the DACH region, **C3** has been the contact for Gamry products for 25 years. We guarantee fast technical support, take care of sales and provide competent application consulting. **www.gamry.com**

At COMSOL, we develop mathematical modeling software that drives new breakthroughs in physics and engineering — and we love what we do. Our flagship product, COMSOL Multiphysics®, is used in all fields of engineering, manufacturing, and scientific research for modeling multiphysics systems. Our customers use the software to understand, predict, innovate, and optimize product designs and processes.

The **Corrosion Module** add-on to the COMSOL Multiphysics® platform includes features, interfaces, and example models that enable a straightforward approach to the simulation of all electrochemical corrosion processes. **www.comsol.de**

Framatome supports the safe & efficient operation of key equipment in demanding environments. Our expertise is based on decades working on materials, coating, welding and corrosion. We operate comprehensively equipped laboratories for destructive testing and NDE, for customized corrosion testing in various environments, and welding and manufacturing optimization. We perform root cause analyses, fracture mechanics and fitness-for-service assessments – servicing nuclear and non-nuclear industries. **www.framatome.com**

OLI Systems is a pioneer and established global leader in water chemistry and its applications in industrial processes. Delivering comprehensive process modeling and intelligent simulation insights for chemical processes that enhance operational efficiency and engineering productivity.

OLI Systems provides domain expertise with an extensive chemistry property database, differentiated thermodynamic and kinetic models and proven software platforms. Only OLI Systems can accurately simulate and automate multiple water chemistry-based processes in oil & gas, power generation, metals & mining, chemicals, water treatment and related industrial markets that maximize environmental sustainability and reduce OPEX. **olisystems.com / OLI on LinkedIn**

BRONZE SPONSOR

Seppeler – we make it work. This motto is more than just a promise. It is the Seppeler Group's claim to be a strong, flexible and long-term partner to every customer. As a producer and service provider for hot dip galvanizing, coating, container technology or gratings production. For any challenge. In any industry. For this reason we at the Seppeler Group capitalise on specialist expertise and personal commitment.

We love things that are long-lasting. In over 100 years, Seppeler has developed into a flexible group of companies with regionally anchored locations. The business units in Germany, Poland and Switzerland form a strong network with almost 1,600 members of staff. Thanks to individual solutions, advanced techniques and a strong focus on service, we offer our customers the best solution. And we offer our employees secure, valuable employment. **www.seppeler.de**


3X ENGINEERING
AMPP
automa
BioLogic
C3 PROZESS- UND ANALYSENTECHNIK
Distributor in D, A, CH of:
GAMRY INSTRUMENTS
CLAMPON
ULTRASONIC INTELLIGENT SENSORS
COMSOL
CORMET
Testing Systems
CORTEC
CORPORATION
DUVINE
www.duvine.co.uk
EFC
EUROPEAN FEDERATION OF CORROSION
ELANTAS
FEAC
ENGINEERING | REALIZE YOUR DIGITAL TWIN
framatome
GUARANT
INTERNATIONAL
EUROCORR
AUGUST 27 - 31, 2023
BELGIUM BRUSSELS
THE ANNUAL CONGRESS OF THE EUROPEAN FEDERATION OF CORROSION
IPS
Elektroniklabor GmbH & Co. KG
IVIUM TECHNOLOGIES
LUNALABS
Metrohm
Autolab B.V.
MONTIPOWER
Surface Preparation Technologies
Part of Monti Group
OLI
systems, inc.
PalmSens
Parr
Pietro Fiorentini
Q-LAB
RECORRTech
ROCHOLL
GmbH
SFTec
TRENTON Europe
VDM Metals
A company of ACERINOX
THE WORLD CORROSION ORGANIZATION

POSTER TOPICS

- A Corrosion and Scale Inhibition (WP 1)
- B Corrosion by Hot Gases and Combustion Products (WP3)
- C Nuclear Corrosion (WP4)
- D Environment Sensitive Fracture (WP 5)
- E Corrosion Mechanisms, Methods and Modelling (WP 6 & 8)
- F Marine Corrosion (WP 9)
- G Microbial Corrosion (WP 10)
- H Corrosion of Steel in Concrete (WP11)
- J Corrosion in Oil and Gas Production (WP 13)
- K Coatings (WP 14)
- M Automotive Corrosion (WP 17)
- N Tribo-Corrosion (WP 18)
- O Corrosion of Polymer Materials (WP 19)
- P Corrosion and Corrosion Protection of Drinking Water Systems (WP 20)
- Q Corrosion of Archaeological and Historical Artefacts (WP 21)
- R Corrosion Control in Aerospace (WP 22)
- S Corrosion Reliability of Electronics (WP 23)
- T CO_2-Corrosion in Industrial Applications (WP 24)
- U Atmospheric Corrosion (WP 25)
- V TF: Corrosion in Green & Low Carbon Energy Technologies

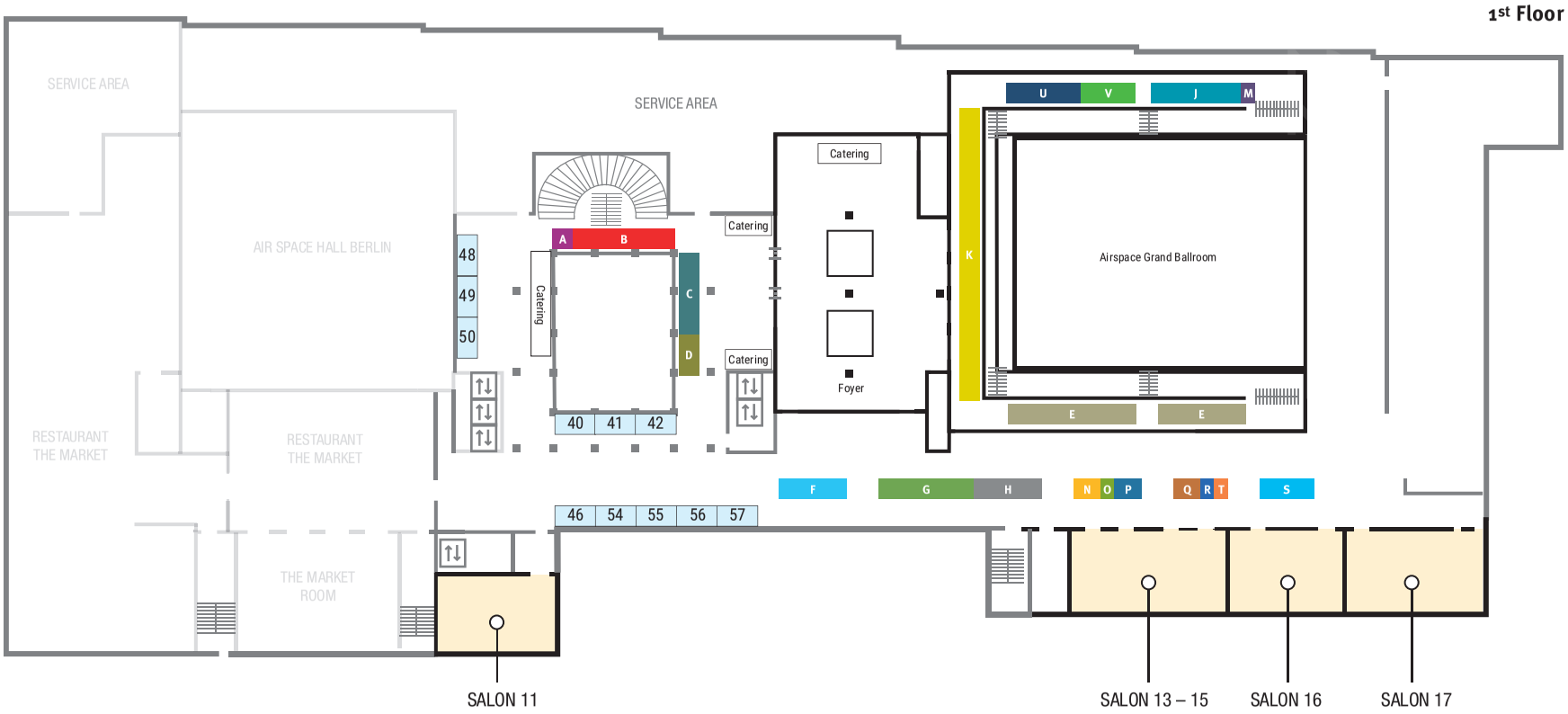

Corrosion and Scale Inhibition (WP 1)

P 1.01 **Green corrosion inhibitors – Development of eco-friendly products of low cost from industrial waste.**
J. Rocha[1]; M. V. Casanova Monteiro[1]; E. D›Elia[1]; J. da Cunha Ponciano Gomes[1]; [1] Federal University of Rio de Janeiro, Rio de Janeiro/BR

P 1.02 **Advanced sensor based on EIS for continuous corrosion monitoring in an Icelandic geothermal power plant**
L. Freire[1]; I. Ezpeleta[1]; J. Sánchez[1]; A. Aimen[1]; [1] AIMEN, Porriño/E

Corrosion by Hot Gases and Combustion Products (WP3)

P 2.01 **Cyclic oxidation resistance of IN625 produced by Laser Beam Melting, influence of the building direction**
S. Mercier[1]; T. Gheno[1]; A. Morel[1]; D. Boivin[1]; E. Rimpot[1]; C. Rio[1]; [1] ONERA, Université Paris Saclay, Chatillon/F

P 2.02 **A systematic study of the effect of the nickel and cobalt respective proportions in M–30Cr alloys (M = Ni and/or Co) on their behavior in oxidation at high temperature**
A. Padox[1]; M. Jollain[1]; L. Aranda[2]; P. Berthod[2]; [1] University of Lorraine, Vandoeuvre-lès-Nancy/F; [2] University of Lorraine, Nancy/F

P 2.03 **Exploration of the high temperature oxidation of the M–30Cr alloys (M = Co and/or Ni) containing tantalum in absence of carbon**
F. Schumacher[1]; Y. Ait-Meddour[2]; L. Aranda[3]; P. Berthod[4]; [1] University of Lorraine, Vandoeuvre-lès-Nancy/F; [2] University of Lorraine, Vandoeuvre-lès-Nancy/F; [3] University of Lorraine, Nancy/F; [4] Université de Lorraine, Nancy/F

P 2.04 **Characteristics and resistance against spallation of the oxides formed at high temperature on {Co, Ni}–based chromium–rich cast alloys containing titanium**
S. Ozouaki Wora[1]; P. Berthod[2]; [1] University of Lorraine, Vandoeuvre-lès-Nancy/F; [2] Université de Lorraine, Nancy/F

P 2.05 **Oxidized states of chromium–rich {Ni,Co}–based alloys rich in tantalum to form TaC carbides after exposure at 1250°C in air**
J. Gomis[1]; P. Berthod[2]; [1] University of Lorraine, Vandoeuvre-lès-Nancy/F; [2] Université de Lorraine, Nancy/F

Nuclear Corrosion (WP4)

P 3.01 **Microstructural investigation of oxide films on Alloy 182 weld metal formed under BWR zinc water chemistry**
A. Mackiewicz[1]; S. Ritter[1]; K. Chen[1]; H. Seifert[1]; S. Virtanen[2]; [1] Paul Scherrer Institut (PSI), Villigen/CH; [2] Friedrich-Alexander University Erlangen-Nürnberg, Erlangen/D

P 3.02 **Slow strain rate testing of Fe-10Cr-4Al ferritic steel in liquid lead and lead-bismuth eutectic**
C. Petersson[1]; [1] royal institute of technology KTH, Stockholm/S

P 3.03 **Effect of oxidants produced by radiolysis on aqueous corrosion of iron**
T. Ota[1]; S. Ajito[2]; T. Hojo[2]; M. Koyama[2]; E. Akiyama[2]; [1] Tohoku University, Aoba Ward, Sendai City, Miyagi /J; [2] Tohoku University, Sendai City/J

P 3.04 **Corrosion assessment for the evaluation of the long-term integrity of containers in crystalline rock**
C. Stephan-Scherb[1]; J. Eckel[2]; T. Fass[2]; T. Weyand[2]; C. Dietl[1]; A. von Oertzen[1]; L. Maerten[1]; [1] Bundesamt für die Sicherheit der nuklearen Entsorgung, Berlin/D; [2] Bundesamt für die Sicherheit der nuklearen Entsorgung, Köln/D

Environment Sensitive Fracture (WP 5)

P 4.01 **Failure Analysis of a High Pressure Temperature Turbine Blade of an Aircraft Jet Engine**
M. García-Martínez[1]; J. del Hoyo Gordillo[1]; M. Valles González[1]; A. Pastor Muro[1]; B. González Caballero[1]; [1] INTA, Torrejón de Ardoz (Madrid)/E

P 4.02 **Design and experimental validation of hydrogen trapping features in Ni model alloys**
A. Prasad[1]; A. Dreano[2]; L. Couturier[1]; F. Christien[2]; F. Tancret[1]; [1] Nantes Université, Institut des Matériaux de Nantes – Jean Rouxel (IMN), CNRS UMR, Nantes/F; [2] Mines Saint-Etienne, Univ Lyon, CNRS, UMR, Saint-Etienne/F

Corrosion Mechanisms, Methods and Modelling (WP 6 & 8)

P 5.01 **Integrated corrosion resistance index for biomaterials**
C. Dias dos Reis Barros[1]; E. Janzen Kassab[1]; J. Ponciano Gomes[1]; [1] UFRJ, Rio de Janeiro/BR

P 5.02 **Use of modified NiTi alloys for biomedical applications**
E. Kassab[1]; C. Dias dos Reis Barros[1]; J. C. P. Gomes[1]; [1] Federal University of Rio de Janeiro, Rio de Janeiro/BR

P 5.03 **A stochastic model for high-temperature corrosion in nickel-based superalloys.**
F. Antonelli[1]; S. Mori[1]; J. Sumner[1]; R. Wells[2]; N. Chapman[2]; N. Simms[1]; [1] University of Cranfield, Cranfield, Bedfordshire./UK; [2] Siemens Energy, Lincoln/UK

P 5.04 **Effect of Anodic Behavior of Al Alloy on Galvanic Corrosion Resistance of AA6016/Steel Couple in Chloride Environment**
M. Kadowaki[1]; H. Katayama[1]; M. Yamamoto[2]; [1] National Institute for Materials Science (NIMS), Tsukuba/J; [2] Tohoku University, Sendai/J

P 5.05 **Comparison of Corrosion Behavior of Two Different Aluminium Alloys for Lid Foil from Industrial Point of View**
A. Kabil[1]; E. Harputlu[1]; H. Mollaoglu Altuner[1]; [1] Assan Aluminyum San. ve Tic. A.S, Kocaeli/TR

P 5.06 **Kinetics of the oxygen reduction reaction on passive films formed Fe-Cr alloy**
Y. Wang[1]; D. Blackwood[1]; M. Ng[2]; [1] National University of Singapore, Singapore/SGP; [2] Institute of High Performance Computing, Agency for Science, Technology and Research, Singapore, Singapore/SGP

P 5.07 **Corrosion performance of 4xxx aluminium alloy with high scrap content for construction applications**
P. Alexopoulou[1]; A. Flampouri[1]; M. Koklioti[1]; E. Aivazoglou[1]; T. Tzevelekou[1]; G. Kalkantzis[2]; G. Ziogas[2]; A. Mavroudis[2]; [1] ELKEME - Hellenic Research Centre for Metals S.A., Oinofyta/GR; [2] Elval, Aluminium Rolling Division of ElvalHalcor S.A., Oinofyta/GR

P 5.08 **Study of metallic-aqueous interfaces from a multiscale approach and its application to corrosion inhibition**
E. de Freitas Martins[1]; I. Cole[2]; P. Ordejón[3]; [1] RMIT University, Barcelona/E; [2] RMIT University, Melbourne/AUS; [3] Catalan Institute of Nanoscience and Nanotechnology, Barcelona/E

P 5.09 **Construction of a data driven corrosion risk model as a novel method for corrosion management**
W. Witteveen[1]; J. Horvath[1]; K. De Baere[1]; S. Gelareh[2]; G. Potters[1]; J. Tacq[3]; [1] Antwerp Maritime Academy, Antwerp/B; [2] Université d'Artois, Béthune/F; [3] Sirris, Zwijnaarde/B

P 5.10 **Corrosion inhibitor structures for automotive steel - A computational chemistry perspective**
S. Jeschke[1]; I. Cole[1]; P. Eiden[2]; R. Mishra[2]; P. Deglmann[2]; J. Gorges[2]; C. Rein[2]; P. Keil[3]; [1] RMIT University, Melbourne/AUS; [2] BASF SE, Ludwigshafen am Rhein/D; [3] BASF Coatings GmbH, Muenster/D

P 5.11 **A multiscale approach to bias dependent electrochemical processes at metallic-aqueous interfaces**
J. Castillo Robles[1]; E. de Freitas Martins[1]; P. Ordejón[2]; I. Cole[3]; [1] RMIT University, Barcelona/E; [2] ICN2, Barcelona/E; [3] RMIT University, Melbourne/AUS

P 5.12 **Interpretation of ENA data from accelerated exposure of modified ZRP based on modelling of coating electrical properties as related to corrosion of the substrate**
B. Eremias[1]; L. Mindos[1]; L. Turek[1]; [1] SVUOM Ltd., Prague/CZ

P 5.13 **Advances in understanding the anomalous alkalinization of the electrolyte during the anodic polarization of Mg**
R. Montoya[1]; A. Ortiz[2]; J. Genescá[2]; [1] UNAM, N.L. Mexico/MEX; [2] UNAM, APODACA/MEX

P 5.14 **Effect of delayed inhibitor supply on the local degradation and protection kinetics of IMs in AA2024-T3**
M. Mopon[1]; S. Garcia[1]; [1] TU Delft, Delft/NL

P 5.15 **Improving phase-field models to simulate the aqueous corrosion phenomena**
J. Amador[1]; J. Vega[1]; F. Varas Merida[2]; M. Lekka[1]; E. García-Lecina[1]; [1] CIDETEC, San Sebastian/E; [2] Universidad Politecnica de Madrid, Madrid/E

P 5.16 **Numerical contribution in DCVG method for a reliable and quantified detection of coating defects on buried pipelines**
D. Garcia[1]; E. Sassine[1]; S. Deharo[1]; R. François[1]; C. Barthe[2]; [1] CORROHM, Ramonville-Saint-Agne/F; [2] Trapil, Poissy/F

P 5.17 **Possibilities and Recent Advances in Respirometric Monitoring of Corrosion Rates**
M. Strebl[1]; M. Bruns[1]; S. Virtanen[1]; [1] Friedrich-Alexander-Universität Erlangen-Nürnberg (FAU), Erlangen/D

P 5.18 **Effects of Microalloying on the local corrosion processes in High-Manganese Twinning-Induced Plasticity Steel**
T. Olugbade[1]; C. Das[1]; A. Wetzel[1]; J. Witt[1]; O. Ozcan[1]; [1] Bundesanstalt für Materialforschung und -prüfung (BAM), Berlin/D

P 5.19 **Effect of passivation after additive manufacturing of titanium alloy on corrosion resistance and protein binding**
S. Nikpour[1]; [1] Western University of Ontario, London/CDN

P 5.20 **Corrosion behavior of Al-based structurally complex alloys**
K. Młynarek-Żak[1]; R. Babilas[1]; [1] Silesian University of Technology, Gliwice/PL

P 5.21 **Metal Release of CoCrMo Alloy in Protein-Rich Solutions–Effect of Sliding and Manufacturing Process**
Z. Wei[1]; V. Romanovski[2]; L. Filho[3]; C. Persson[3]; S. Sanaei[4]; M. Atapour[4]; Y. Hedberg[1]; [1] University of Western Ontario, London/CDN; [2] University of Virginia, Charlottesville/USA; [3] Uppsala University, Uppsala/S; [4] Isfahan University of Technology, Isfahan/IR

P 5.22 **Corrosion resistance of rapid solidified $Al_{85}(Ni,Fe,Cu)_{10}Y_5$ alloys in 3.5% NaCl solution**
R. Babilas[1]; K. Młynarek-Żak[1]; A. Radoń[1]; [1] Silesian University of Technology, Gliwice/PL

P 5.23 **Low Voltage SEM/EDS-analyses of 304 and 347 Stainless Steels Oxidized at 600-800 °C**
J. Juhanoja[1]; T. Nguyen[1]; [1] Top Analytica Ltd, Turku/FIN

P 5.24 **Influence of phosphorus segregation and grain boundary misorientation on intergranular corrosion of α-Fe**
K. Tojima[1]; S. Ajito[1]; Y. Zhang[1]; T. Hojo[1]; G. Miyamoto[1]; M. Koyama[1]; T. Furuhara[1]; E. Akiyama[1]; [1] Tohoku University, Katahira, Aoba-ku, Sendai/J

P 5.25 **Modeling of Electrochemical Oxide Film Growth**
I. Bösing[1]; J. Thöming[1]; F. La Mantia[1]; [1] University of Bremen/D

Marine Corrosion (WP 9)

P 6.01 **The effect of dissolved CO_2 on SCC of pipeline steel in simulated marine environments**
S. Abubakar[1]; S. Mori[1]; J. Sumner[1]; [1] Cranfield University, Bedford/UK

P 6.02 **Corrosion testing in a laboratory container - Corrosion testing with artificial seawater and sediment**
K. Zekhnini[1]; S. Grabowski[1]; Q. Le[1]; A. Burkert[1]; M. Babutzka[1]; [1] Bundesanstalt für Materialforschung und -prüfung (BAM), Berlin/D

P 6.03 **Rapid assessment of corrosion susceptibility of mild steel in simulated splash zone condition**
V. Kalikivayi[1]; K. Mondal[2]; S. Singh[2]; [1] Indian Institute of Technology Kanpur, Kapur, Uttar Pradesh, India/IND; [2] Indian Institute of Technology Kanpur, Kanpur/IND

P 6.04 **Internal corrosion studies of equipment and pipings involved in offshore Power-to-X (PtX) platforms**
S. Sankaran[1]; W. Fürbeth[1]; [1] DECHEMA - Forschungsinstitut, Frankfurt am Main/D

P 6.05 **Investigation of corrosion of carbon steel under insulation**
J. Edet[1]; T. Green[2]; S. Roy[2]; [1] University of Strathclyde, Montrose Street, Glasgow/UK; [2] University of Strathclyde, Glasgow/UK

Microbial Corrosion (WP 10)

P 7.01 **Microbiologically influenced corrosion of steel sheet pilings in a Dutch harbor- fast corrosion and unexpected mass loss**
N. Noël-Hermes[1]; M. Salta[1]; [1] Endures B.V., Den Helder/NL

P 7.02 **Hierarchical surface texturing in stainless steel as an alternative to prevent biocorrosion in marine environments**
J. Castillo Lagos[1]; E. Ramos-Moore[2]; G. Pizarro P.[2]; [1] Pontificia Universidad Católica de Chile, La Florida/RCH; [2] Pontificia Universidad Católica de Chile, Santiago/RCH

P 7.03 **Pitting corrosion of 316L stainless steel caused by SRB´s in DGR environment**
R. Bureš[1]; J. Stoulil[1]; V. Hlaváčková[2]; D. Dobrev[3]; [1] University of Chemistry and Technology Prague/CZ; [2] Technical University of Liberec/CZ; [3] ÚJV, Řež/CZ

P 7.04 **The effects of Calcigel bentonite naturally occurring microorganisms on corrosion of cast iron**
V. Sushko[1]; N. Matschiavelli[1]; T. Wei[1]; T. Stumpf[1]; A. Cherkouk[1]; [1] Helmholtz-Zentrum Dresden - Rossendorf (HZDR) , Dresden/D

P 7.05 **Intersectoral Bridging in the Fragmented Field of Microbiologically Influenced Corrosion**
J. Knisz[1]; J. Stoulil[2]; [1] University of Public Service, Baja/H; [2] University of Chemistry and Technology, Prague/CZ

P 7.06 **Anaerobic microbial corrosion of carbon steel under conditions relevant for deep geological repository of nuclear waste**
R. Shrestha[1]; T. Černoušek[2]; J. Stoulil[3]; H. Kovářová[4]; K. Sihelská[5]; R. Špánek[6]; A. Ševců[7]; J. Steinová[8]; [1] Technical University of Liberec, Liberec/CZ; [2] Research Center Řež, Husinec-Řež/CZ; [3] University of Chemistry and Technology, Prague/CZ; [4] Research Center Řež , Husinec-Řež/CZ; [5] Research Center Řež , Husinec-Řež/CZ; [6] Technical University of Liberec, Liberec/CZ; [7] Technical University of Liberec , Liberec/CZ; [8] Technical University of Liberec and Charles University in Prague, Liberec, Prague/CZ

Corrosion of Steel in Concrete (WP11)

P 8.01 **Corrosion of embedded steel in alkaline activated mortars manufactured from slag**
A. Bautista[1]; S. Shagñay[1]; I. Ramon[1]; F. Velasco[1]; M. Torres-Carrasco[1]; [1] Universidad Carlos III de Madrid, Leganes/E

P 8.02 **Licorice extract as corrosion inhibitor in mortar**
R. Naderi[1]; A. Bautista[2]; S. Shagñay[2]; M. Torres-Carrasco[2]; F. Velasco[2]; [1] University of Tehran, Tehran/IR; [2] Universidad Carlos III de Madrid, Leganes/E

P 8.03 **Impact of electromigration treatment on chloride binding properties of cement**
M. Reiser[1]; M. Kouril[2]; F. Bayer[1]; S. Msallamova[1]; [1] University of Chemistry and Technology, Prague, Prague/CZ; [2] University of Chemistry and Technology, Praha/CZ

P 8.04 **Investigation of the effect of fuel ageing and corrosion in oxymethylene ether (OME)**
M. Irawan-Pieperhoff[1]; [1] OWI Science for Fuels gGmbH, Herzogenrath/D

P 8.05 **Application of a reinforcement anode on an historical building**
X. Hallopeau[1]; E. Marie-Victoire[2]; C. Annede-Villeau[3]; [1] SECCO Corrosion Consulting, Vélizy-Villacoublay/F; [2] Sorbonne Universités, Champs-sur-Marne/F; [3] Freyssinet International & Cie, Rueil-Malmaison/F

Corrosion in Oil and Gas Production (WP 13)

P 9.01 **Appraising the effect of cooling rates during solutioning on the long term corrosion and pitting resistance of SLM Inconel 718 alloy**
M. Siddiqui[1]; M. Abdelgadir[1]; A. Adesina[1]; ; [1] King Fahd University of Petroleum and Minerals, Dhahran/SAR

P 9.02 **Effects of surface roughness on anaerobic marine biofilm formation and microbiologically-influenced corrosion of UNS G10180 carbon steel**
L. Jones[1]; M. Salta[2]; T. Skovhus[3]; K. Thomas[4]; T. Illson[4]; J. Wharton[1]; J. Webb[1]; [1] University of Southampton, Southampton/UK; [2] University of Portsmouth, Portsmouth/UK; [3] VIA University College, Horsens/DK; [4] DNV – Energy Systems, Loughborough/UK

P 9.03 **Effect of building orientation on corrosion kinetics and mechanism of 3D printed AlSi10Mg alloy in saline medium**
A. Meroufel[1]; C. Linders[1]; A. Gordon[1]; [1] RISE, Kista/S

P 9.04 **Anticorrosive and Persistency Properties of Arabian Crude Oils**
L. AlSharif[1]; C. Canto Maya[1]; [1] Saudi Aramco Oil Company, Dhahran/SAR

P 9.05 **Optimization of Extraction Conditions for Production of Halophyte-based Biocides for Microbiologically Influenced Corrosion (MIC) Mitigation**
J. Stein[1]; T. Chaturvedi[1]; T. Skovhus[2]; M. Thomsen[1]; [1] Aalborg University, Esbjerg/DK; [2] VIA University College, Horsens/DK

P 9.06 **Acoustic Emission Sensing for Early Damage Detection and Localization In Pressurized Vessels**
M. Alerwi[1]; C. Canto Maya[2]; [1] Saudi Aramco, Dhahran Saudi Arabia/SAR; [2] Saudi Aramco, Dharan/SAR

P 9.07 **Mechanistic understanding of the effect of initial microstructure of low-alloy carbon steel on its CO2-corrosion resistance in simulated formation water chemistry**
K. Gupta[1]; S. Haratian[1]; A. Larsson[2]; G. Abbondanza[2]; E. Lundgren[2]; R. Ambat[1]; [1] Technical University of Denmark, Kgs. Lyngby/DK; [2] Lund University, Lund/S

P 9.08 **The influence of hydrogen sulfide concentration on the corrosion and hydrogenation of steel 07Cr18Ni6**
M. Khoma[1]; S. Halaichak[1]; M. Chuchman[1]; C. Vasyliv[1]; B. Datsko[1]; N. Ratska[1]; H. Pokhmurska[4]; [1] Karpenko Physico-Mechanical Institute of the NAS of Ukraine, Lviv/UA; [4] TU Chemnitz /D

P 9.09 **Influence of $CeCl_3$ on the inhibitory activity of imidazoline-based corrosion inhibitor**
G. Bilić[1]; T. Borko[2]; [1] University of Zagreb, Faculty of Mining, Geology and Petroleum Engineering, Zagreb/HR; [2] INA, d.d., Zagreb/HR

P 9.10 **Influence of Micro-Alloying Elements Upon the CO_2 Preferential Weld Corrosion Rate of Carbon Steel**
J. L. Cardoso[1]; Z. Panossian[2]; B. B. Andrade[1]; M. Henrique[1]; R. S. Marques[1]; P. Zumpano Jr[3]; I. P. Baptista[4]; [1] FIPT Foundation for support of the Institute for Technological Research, São Paulo/BR; [2] IPT Institute for Technological Research, São Paulo/BR; [3] Petrobras, São José dos Campos/BR; [4] Petrobras, Rio de Janeiro/BR

P 9.11 **Q-BI – Purple Yams Waste (Ipomoea Batatas) as Organic Corrosion Inhibitors for Carbon Steel in Oil and Gas Industry: Substitute of Chemical Compound**
G. Putra[1]; [1] Pertamina , Jaarta /RI

Coatings (WP 14)

P 10.01 **DIGICOAT: EIS and FTIR data analysis for protective coatings**
A. Gutierrez[1]; A. Ruesca[1]; [1] Survey and Foresee Technologies SLL, Las Palmas de Gran Canaria/E

P 10.02 **Control of the degradation rate and corrosion resistance of ZK60 magnesium alloy by coating via HiPIMS and SolGel**
A. Claver Alba[1]; I. Zalakain[1]; I. Fernández[2]; J. Santiago[2]; I. Quintana[3]; L. Mendizabal[3]; J. García[1]; [1] Institute for Advanced Materials and Mathematics (INAMAT2), Universidad Pública de Navarra (UPNA), Pamplona/E; [2] Nano4Energy SL, Madrid/E; [3] Fundación Tekniker, Eibar/E

P 10.03 **Evolution in microstructure, wear, corrosion, and tribocorrosion behavior of Mo- containing high-entropy alloy coatings fabricated by laser**
Y. Fu[1]; C. Du[1]; X. Li[1]; [1] University of Science and Technology Beijing, Beijing/CN

P 10.04 **Flash Plasma Electrolytic Oxidation of an Additively Manufactured Al-Si alloy**
M. Mohedano[1]; E. Lopez[1]; R. Del Olmo[2]; E. Matykina[1]; R. Arrabal[1]; [1] University Complutense of Madrid, Madrid/E; [2] Military University of Technology, Warsaw/PL

P 10.06 **Development of an innovative quasi-ceramic layer for the hot forming of galvanized medium manganese steels with variable strengths**
A. Anthes[1]; W. Fürbeth[1]; [1] DECHEMA - Forschungsinstitut, Frankfurt am Main/D

P 10.07 **Increasing the corrosion resistance of AZ91 magnesium alloy by plasma electrolytic oxidation**
M. Štrbák[1]; B. Hadzima[2]; J. Sovík[3]; [1] University of Žilina, Žilina/SK; [2] University of Žilina Research Centre, Žilina/SK; [3] University of Žilina, Martin/SK

P 10.08 **Enhancing corrosion resistance on magnesium alloy EV31 by PEO process**
V. Knap[1]; B. Hadzima[2]; M. Štrbák[2]; V. Obertová[2]; [1] University of Zilina, Príbovce/SK; [2] University of Žilina, Zilina/SK

P 10.09 **Zr-Mo-Mn Conversion Coating as a Sealing Option to AA2024-T3 Anodized Layers**
J. Salles Pinheiro[1]; J. Zoppas Ferreira[1]; [1] UFRGS, Porto Alegre/BR

P 10.10 **Plasma Electrolytic Oxidation (PEO) for Production of High-Performance Coatings on Ti-Al Intermetallic Compounds**
K. Munassar[1]; B. Mingo[1]; A. Yerokhin[2]; [1] University of Manchester, Manchester/UK; [2] University of Manchester, Manchester/UK

P 10.11 **ZnO-based nanostructured electrodes for biosensors: Corrosion behavior in Ringer's physiological solution**
K. Aleksić[1]; A. Stankovic[1]; I. Stojkovic Simatovic[2]; S. Markovic[1]; [1] Serbian Academy of Sciences and Arts, Belgrade/SRB; [2] University of Belgrade, Belgrade/SRB

P 10.12 **Fabrication of Novel Hybrid Sol-Gel/Urethane Coatings for the Protection of Mild Steel Substrate against Corrosion in the Saline Medium**
R. Suleiman[1]; B. Alkhuraim[1]; [1] King Fahd University of Petroleum & Minerals (KFUPM), Dhahran/SAR

P 10.13 **Sealing of Anodized Aluminum Alloy by Acrylic Acid Polymerization**
A. Dąbrowski[1]; Z. Buczko[1]; [1] Łukasiewicz Research Network, Warsaw/PL

P 10.14 **Physical and tribological properties of infrared dried coatings**
I. Cindrić[1]; I. Stojanovic[1]; L. Turkalj[1]; I. Juraga[1]; D. Rakela Ristevski[2]; [1] Faculty of Mechanical Engineering and Naval Architecture, Zagreb/HR; [2] Končar Steel Structures Inc., Zagreb/HR

P 10.15 **Influence of Hydrogel Coatings on Corrosion and Fatigue of Iron in Simulated Body Fluid**
J. Huang[1]; M. Voigt[1]; S. Wackenrohr[2]; C. Ebbert[1]; A. Keller[1]; H. Maier[2]; G. Grundmeier[1]; [1] Paderborn University, Paderborn/D; [2] Leibniz Universität Hannover, Garbsen/D

P 10.16 **Efficient coating process using robots and water-based coating material**
Š. Jurišić[1]; I. Stojanovic[1]; V. Šimunović[1]; M. Kurtela[1]; V. Alar[1]; M. Bilmez[2]; [1] Faculty of Mechanical Engineering and Naval Architecture, Zagreb/HR; [2] Ember Kamin, Velika/HR

P 10.17 **Self-assembled monolayers of phosphonic acids for improved bronze protection by polyurethane coating**
N. Carek[1]; D. Mikic[1]; A. Kapitanovic[1]; H. Otmacic Curkovic[1]; [1] Faculty of Chemical Engineering and Technology, University of Zagreb/HR

P 10.18 **Poly-aminoindoles as alternative coatings against corrosion: Electrochemical study in simulated seawater**
E. Castañeda[1]; J. Armijo[1]; I. Vargas[1], [1] Pontificia Universidad Católica de Chile, Santiago/RCH

P 10.19 **The impact of bioactive coatings on bone implants corrosion**
D. Bjelić[1]; M. Finšgar[1], [1] Faculty of chemistry and chemical engineering, Maribor/SLO

P 10.20 **Modified epoxy coatings on cast iron**
M. Kurtela[1]; V. Šimunović[1]; V. Alar[1]; M. Samardžija[2]; [1] Faculty of Mechanical Engineering and Naval Architecture, University of Zagreb, Zagreb/HR; [2] Faculty of Mining-Geology-Petroleum Engineering, University of Zagreb, Zagreb/HR

P 10.21 **Assessment of the Antibiofilm Performance of Chitosan-Based Surfaces in Marine Environments**
M. Lima[1]; L. Gomes[1]; M. Romeu[1]; J. Valcarcel[2]; J. Vázquez[2]; M. Cerqueira[3]; L. Pastrana[3]; A. Bourbon[3]; E. Jong[4]; J. Sjollema[4]; F. Mergulhão[1]; [1] Faculty of Engineering of University of Porto, Porto/P; [2] Instituto de Investigaciones Marinas, Vigo/E; [3] International Iberian Nanotechnology Laboratory, Braga/P; [4] University Medical Center Groningen, Groningen/NL

P 10.22 **An effective poly (ethylene) oxide sol-gel coating reinforced with SiO_2 nanoparticles to enhance the corrosion resistance of PEO-coated $AZ_{31}B$ Mg alloys**
E. Merino Abad[1]; A. Durán[1]; Y. Castro[1]; [1] Consejo Superior de Investigaciones Científicas (CSIC), Madrid/E

P 10.23 **Ultrasonically enhanced cerium based conversion chemistry for the corrosion protection of aluminum alloys**
L. Ruhm[1]; P. Vieth[1]; G. Grundmeier[1], [1] Paderborn University, Paderborn/D

P 10.24 **Cost effective sealing of porous PEO coating on AZ_{31} magnesium alloy by removable water and oil based preservatives**
F. Pastorek[1]; M. Štrbák[1]; B. Hadzima[1]; J. Pastorková[1]; [1] University of Žilina, Žilina/SK

P 10.25 **Effect of Laser Surface Melting on the Corrosion Resistance of Adhesive/Al 7075 Alloy Interfaces**
P. Vieth[1]; C. Weinberger[1]; M. Tiemann[1]; G. Grundmeier[1]; [1] Universität Paderborn, Paderborn/D

P 10.26 **Fabrication and characterisation of additive manufactured $Ti_{-6}Al_4V$ parts by laser powder bed fusion (L-PBF) technique**
N. Godja[1] [1] CEST Konpetenzzentrum für elektrochemische Oberflächentechnologie GmbH, Wiener Neustadt/A

P 10.27 **Hybrid PEO/sol-gel coatings loaded with Ce for corrosion protection of AA2024**
E. Lopez[1]; R. Del Olmo[2]; M. Mohedano[1]; E. Matykina[1]; R. Arrabal[1]; [1] Universidad Complutense de Madrid, Madrid/E; [2] Military University of Technology, Warsaw/PL

P 10.28 **Aluminium alloy corrosion inhibition by two-stage modified zeolite**
S. Korniy[1]; I. Zin[1]; L. Kwiatkowski[2]; M. Danyliak[1]; O. Khlopyk[1]; [1] Karpenko Physico-Mechanical Institute of NAS of Ukraine, Lviv/UA; [2] Łukasiewicz Research Network - Institute of Precision Mechanics, Warsaw/PL

P 10.29 **Effect of boron dispersion phase content on the microstructure and corrosion resistance of the Ni-B/B composite coatings**
K. Skroban[1]; A. Gajewska-Midziałek[1]; G. Cieślak[1]; M. Gostomska[1]; T. Ciciszwili[1]; E. Pęśko[1]; A. Kapuścińska[1]; M. Trzaska[1]; Z. Buczko[2]; [1] Łukasiewicz Research Network - Institute of Precision Mechanics, Warsaw/PL; [2] Łukasiewicz Research Network, Warsaw/PL

P 10.30 **New waterborne zinc primers**
U. Paszek[1]; [1] Polish Corrosion Society, Gdańsk/PL

Automotive Corrosion (WP 17)

P 12.01 **Corrosion-induced hydrogen absorption and embrittlement of Ultra-high-strength steel with Zn-based coatings in neutral aqueous conditions**
H. Bang[1]; J. Park[1]; Y. Park[1]; S. Jung[2]; S. Kim[1]; [1] Sunchon National University, Suncheon/ROK; [2] Hyundai Steel, DangJin/ROK

Tribo-Corrosion (WP 18)

P 13.01 **Improvement of the tribocorrosion properties of tungsten carbide (WC-Co) samples coated via PVD**
J. García[1]; A. Claver Alba[1]; M. Marqués[1]; E. Almandoz[2]; J. Fernandez de Ara[2]; J. Fernández Palacio[2]; [1] Institute for Advanced Materials and Mathematics (INAMAT2), Universidad Pública de Navarra (UPNA), Pamplona/E; [2] Centre of Advanced Surface Engineering (AIN), Cordovilla/E

P 13.02 **Galvanic corrosion between Ti and CoCrMo alloy in human synovial fluids**
Y. Bao[1]; A. Muñoz[1]; S. Mischler[1]; [1] EPFL, Lausanne/CH

Corrosion of Polymer Materials (WP 19)

P 14.01 **Sol-Rec2 Case Study: Assessment of Corrosion Behaviour of Aluminium and Degradation of Polymers During Delamination of Multi-Material Packaging Systems**
B. Syrek-Gerstenkorn[1]; [1] University of Leicester, Leicester/UK

Corrosion and Corrosion Protection of Drinking Water Systems (WP 20)

P 15.01 **Long-term corrosion monitoring: A prediction tool using the "SOCORRO" system**
B. Karabulut[1]; B. Verhoeven[1]; G. Potters[2]; S. Gelareh[3]; R. Dewil[1]; B. Rossi[4]; [1] KU Leuven, Sint-Katelijne-Waver/B; [2] Antwerp Maritime Academy, Antwerp/B; [3] University of Artois, Béthune/F; [4] University of Oxford, Oxford/UK

P 15.02 **New process for interior pipe rehabilitation with environmentally friendly coating materials**
H. Jost[1]; R. Feser[1]; E. Tarfeld[1]; H. Blache[1]; D. Kovoussoglou[1]; T. Tillmann[1]; D. Mollenhauer[2]; S. Grahammer[2]; N. Gräßle[2]; [1] Fachhochschule Südwestfalen, Iserlohn/D; [2] Fa. Warnecke&Böhm, Schliersee/D

Corrosion of Archaeological and Historical Artefacts (WP 21)

P 16.01 **Restoration of iron supporting structure of historic suspension bridge**
H. Geiplova[1]; P. Fialova[2]; L. Mindos[2], M. Vlachova[1]; [1] SVUOM Ltd., Praha/CZ; [2] SVUOM Ltd., Prague/CZ

P 16.02 **Indoor environment and its aggressivity toward cultural heritage objects made of Lead and its alloys**
D. Majtás[1]; P. Fialová[2]; [1] Institute of Theoretical and Applied Mechanics of the Czech Academy of Sciences, Prague/CZ; [2] SVÚOM ltd., Prague/CZ

Corrosion Control in Aerospace (WP 22)

P 17.01 **Modification of tartaric-sulphuric acid anodizing bath by a short chain monocarboxylic acid based additive**
E. Šrámková[1]; V. Záliš[1]; [1] Czech aerospace research centre, Prague/CZ

Corrosion Reliability of Electronics (WP 23)

P 18.01 **Practical methods for Moisture Level Indication inside Printed Circuit Boards**
J. Christensen[1]; [1] FORCE Technology, Brøndby/DK

P 18.02 **Effect of solder mask surface properties and water film build-up on PCBA failure**
A. Lakkaraju[1]; H. Conseil-Gudla[1]; R. Ambat[1]; D. Schucht[2]; J. Tekath[2]; [1] Technical University of Denmark, Kongens Lyngby/DK; [2] Lackwerke Peters GmbH & Co, Kempen/D

P 18.03 **Electrochemical testing for characterization of sinterability of DCB substrates with Cu, Ag and NiAu metallization**
S. Klengel[1]; J. Dumke[2]; D. Wilke[2]; M. Hahn[2]; [1] Fraunhofer IMWS, Halle/D; [2] Elektrochemie Halle GmbH, Halle/D

P 18.04 **Developing strategies for protecting Li-ion powered hearing aids from the user environments.**
M. Asikainen[1]; A. Yadav[2]; R. Ambat[1]; [1] Technical University of Denmark, Lyngby/DK; [2] WS Audiology A/S, Lynge/DK

CO_2-Corrosion in Industrial Applications (WP 24)

P 19.01 **Water absorption in dense phase CO_2**
B. Morland[1]; A. Dugstad[1]; G. Svenningsen[1]; [1] Institute for Energy Technology, Kjeller/N

Atmospheric Corrosion (WP 25)

P 20.01 **Deposition of Chloride Ions in the Vicinity of Road I/11 in the Czech Republic**
M. Vacek[1]; V. Krivy[1]; K. Kreislova[2]; M. Kubzova[1]; [1] Faculty of Civil Engineering, VSB – Technical University of Ostrava, Ostrava - Poruba/CZ; [2] SVUOM Ltd, Prague/CZ

P 20.02 **Resistometric sensors for atmospheric corrosion monitoring of surface treated or naturally corroded metals**
M. Reiser[1]; F. Bayer[1]; A. Marešová[1]; Š. Havíř[1]; M. Kouřil[1]; [1] University of Chemistry and Technology Prague, Prague/CZ

P 20.03 **Waterborne coating for bronze corrosion protection**
A. Kapitanovic[1]; H. Otmacic Curkovic[1]; [1] Faculty of Chemical Engineering and Technology, Zagreb/HR

P 20.04 **Applicability of the paste electrolyte cell for the evaluation of atmospheric corrosion of cultural heritage metals**
I. Šoljić[1]; S. Martinez[2]; [1] University of Zagreb, Faculty of Chemical Engineering and Technology, Zagreb/HR; [2] Faculty of Chemical Engineering and Technology, University of Zagreb, Zagreb/HR

P 20.05 **Determination of the corrosion product layer resistance on zinc samples by using gel electrolytes**
S. Valet[1]; M. Babutzka[1]; [1] Bundesanstalt für Materialforschung und -prüfung (BAM), Berlin/D

TF: Corrosion in Green & Low Carbon Energy Technologies

P 21.01 **Study of the anodized Al sealing process, using new sealing solutions that are more respectful of the environment**
H. Salhi[1]; A. Chilali[2]; [1] Research and Development Center of Air Force, Alger/DZ; [2] National Preparatory School for Engineering Studies, Alger/DZ

P 21.02 **Corrosion of Pt in fuel cell electrodes of different structure**
A. Krasnova[1]; A. Nechitailov[1]; N. Glebova[1]; A. Kastsova[1]; N. Zelenina[1]; A. Seyeux[2]; P. Marcus[2]; N. Cam[3]; P. Volovitch[2]; [1] Ioffe Institute, Saint-Petersburg/RUS; [2] Institut de Recherche de Chimie Paris, Paris/F; [3] Placamat, Pessac/F

P 21.03 **Evaluation of the susceptibility to hydrogen-induced corrosion of various metallic materials for offshore power-to-X plants**
S. Schewe[1]; W. Fürbeth[1]; [1] DECHEMA-Forschungsinstitut, Frankfurt am Main/D

P 21.04 **Carbon steel corrosion and fusion bonded coating deterioration in the liquid phase of anaerobic digestion**
X. Wen[1]; [1] University of Southampton, Southampton/UK

(Programme as of 20 August, subject to change)

Green corrosion inhibitors – Development of eco-friendly products of low cost from industrial waste.

Authors: Janaina Cardozo da Rocha[a], Eliane D'Elia[b], Mariana V. Casanova Monteiro[a] and José Antônio da Cunha Ponciano Gomes[a]

Due to the environmental requirements currently imposed, for corrosion inhibitors to be considered environmentally suitable, there is a growing interest in natural antioxidants from plant extracts, as they have low toxicity in relation to synthetic antioxidants. Green inhibitors are obtained from plant extracts or biodegradable material and lead to a reduction in the intensity of dissolution of metals, decreasing their corrosion rate. Research carried out in recent years reports that the activity of corrosion inhibitors in many of these plant extracts may be due to the presence of constituents such as alkaloids, flavonoids, tannins, cellulose and polycyclic compounds, which can lead to formation of a film on the metal surface, thus preventing corrosion. The approach on green inhibitors in the literature is almost always aimed at applications in acidic media, while the performance in neutral media has been little studied, so there is a need for a better understanding of the mechanisms involved in the process of inhibition of these compounds in neutral media. Another technological gap within this line of research is the existence of few works that emphasize the importance of reusing industrial waste as a source of potential corrosion inhibitors. Thus, since the amount of waste generated is very large, adding value to by-products can be interesting from an economic, scientific and technological point of view. This paper will present the history of the development of green inhibitors from plant extracts for application in neutral and acid media carried out in Labcorr / COPPE / UFRJ. The orange peel, mango peel, passion fruit peel, cashew peel, papaya seed and grape pomace extracts were studied. These extracts were obtained by three different extraction methodologies: infusion extraction, polarity gradient extraction and hydroalcohol extraction. The performance of extracts was good in both media studied. The efficiency of these inhibitors was more significant in 1 mol L^{-1} hydrochloric acid media, with efficiencies above 93% in weight-loss measurement, while the best inhibition efficiency in neutral media was of 74%.

a Laboratório de Corrosão, Programa de Engenharia Metalúrgica e de Materiais, COPPE/UFRJ
b Departamento de Química Inorgânica, Instituto de Química, UFRJ.

Advanced sensor based on EIS for continuous corrosion monitoring in an Icelandic geothermal power plant

Ezpeleta Ignacio, Sánchez Julio, Castro Rubén, Freire Lorena

[1]AIMEN Technology Centre, O Porriño, Spain, ignacio.ezpeleta@aimen.es

Abstract

Corrosion and scaling are the major issues in the exploitation of geothermal sources. Geothermal fluids are very complex mixtures consisting of dissolved gases and high salinity solutions, which creates very aggressive environments. Besides, the high temperature of the geothermal fluids increases corrosion rates promoting failures related to stress and fatigue corrosion. On the other hand, reinjection of cooled brine exiting the heat-exchanger favors scaling onset, since the chemicals dissolved in geothermal waters may tend to precipitate promoting inorganic depositions on the casing.
Corrosion and scaling phenomena are difficult to detect visually or monitor continuously. Standard techniques based on pH, temperature and pressure measurements, chemistry composition and fluid physical properties are habitually applied as indirect methods for corrosion rate control. Other traditional techniques such as mass loss probes or electrical resistance measurements have been introduced more recently for corrosion data registration. These methods, however, lack of enough robustness for accurate and reliable measuring and evaluating corrosion behavior of materials employed in geothermal systems.
In this scenario, a novel system is proposed for online corrosion monitoring of materials. A dedicated electrochemical-based test system will be designed and developed by AIMEN for on-line and continuous monitoring of the corrosion/scaling rate of different materials exposed to the real plant conditions at different locations. This system will use non-standard methods based on Electrochemical Impedance Spectroscopy (EIS) to follow corrosion rates in real time in a demonstration plant sited in Iceland within the GECO project.

Keywords

EIS, geothermal brine, scaling, corrosion monitoring.

Introduction

Geothermal power is cost effective, reliable, sustainable, and environmentally friendly and UE recognize geothermal energy's essential role in the European energy transition towards net-zero greenhouse gas emissions in 2050. Recent estimations indicate that the global production capacity for geothermal electricity is at about 14GW (installed capacity in 2018) and is expected to rise to just over 17GW by 2023.

The economic feasibility of geothermal installations relies on continuous operation of the geothermal loop. However, exploitation of these power plants is usually accompanied by corrosion damages and formation of scale deposits in the pipelines and power equipment, leading to the efficiency reduction.

The overall economic losses connected with the formation of deposits and corrosion of metal at the plants comprise the costs for measures taken to remove the consequences and prevent the occurrence of the above-mentioned problems and the costs connected with underproduction of electricity due to failures and disconnection of equipment, forced outages, and degraded efficiency of the power station.

In this scenario, corrosion resistant components made of titanium alloys and high-alloyed stainless steels are commonly employed for dealing with these problems. However, if inexpensive carbon steel or low alloying stainless steel components could be used, this would improve the power plant's economic factors by generating a considerable reduction in capital investment. Moreover, if the system could be monitored to know the material condition at real time, a decrease in the costs of operations and maintenance through optimized maintenance schedules would result.

The goal of GECO project is to advance the ability to provide cleaner and cost-effective non-carbon emitting energy across EU and the world. Thus, the aims of the project include a detailed and consistent monitoring program, geothermal analysis and comprehensive modelling that will allow to characterize the consequences of fluid flow in diverse field demo sites.

As the laboratory testing cannot completely mimic all the complex processes that occur in real operation conditions, a detailed demonstration and monitoring development for evaluating the materials resistance at each demo site will be elaborated. Each site specific plan will include tracer monitoring of the chemistry of fluids in the injection and GECO will develop strategies to monitor possible corrosion of infrastructure like casing pipes.

In this work, an innovative monitoring system is introduced to be installed in the geothermal piping for on-site and on-line corrosion monitoring using Electrochemical Impedance Spectroscopy (EIS) to determine the corrosion rate and the scaling degree of pipes under realistic circumstances in Iceland (Hellisheidi plant). This involves designing of a cell configuration based on 3 electrodes for evaluating the corrosion resistance of selected materials and the identification of corrosion mechanisms, corrosion rate and scaling formation occurring in the internal wall of the pipes.

Structural and electrical design of this corrosion probe will be realized together with the selection of materials and components to construct the monitoring system according to the specific geothermal characteristics at the site. The test will also allow the comparison between the behavior of different materials under the exposure conditions and to establish a ranking of materials from the most resistant to the least.

Experimental

The corrosion monitoring systems provided by AIMEN are based on the principles of a conventional 3-electrode-configuration cell for electrochemical measurements. EIS will be performed on selected metallic materials and the probe will respond in real time to changes in the corrosion rate of the materials exposed in the geothermal installation. A detailed description of the system design and operation will be presented in the following sections.

Design requirements

For the design of the electrochemical probe, the following requirements should be accomplished:

- The system requires three electrodes: a reference electrode (RE), a counter-electrode (CE) and a working electrode (WE). This configuration is selected as optimum to perform reliable EIS measurements.
- Multi-material: Different alloys will be tested; therefore, it is necessary a probe incorporating several materials to be studied under the same conditions. Moreover, an insulating material must be selected to electrically isolate the electrodes.
- Dismountable: Materials need to be easily dismantled once the testing campaign has been completed.
- Easy installation: The whole system (the probe and the data acquisition system) should be simple to install to avoid disruptions in the plant operation.
- Autonomous: Sensor operation should be unassisted since there are no personnel available at the plants to configure or collect data during its continuous operation. The measurements must be periodically scheduled and transmitted through wireless technology to an online server to be interpreted and analyzed by AIMEN.
  Working conditions: the design must withstand the harsh working conditions of the installation area and the geothermal fluid chemistry (T=96ºC, P=14 bar).

Based on those specified requirements, a conceptual design of the complete system is firstly created, including both the sensor geometry and the electrodes distribution, and the electronics for data acquisition, processing, and transmission.
A cylindrical body, divided in different segments simulating the pipe sections, with an internal diameter equal to the piping diameter is proposed. Using these dimensions, the fluid will pass through the installed probe without any load loss due to section changes. The segments, in form of rings (WE), will be manufactured with the previous selected combinations substrate materials, on which the electrochemical measurements will be performed to determine the corrosion rate under real conditions.
Taking as reference the configuration of a conventional three-electrode electrochemical cell, on both sides of each WE, two CE with the same geometry and a RE will be placed. This disposition was selected to obtain a better distribution of the electric field over the WE.
These rings should be separated by an insulating material that has to withstand the operating conditions promoting a tight seal of the assembly. After manufacturing, the definitive monitoring probe should be tested at laboratory scale to check its behavior under high-pressure and high-temperature conditions to guarantee its integrity prior installation. Likewise, preliminary electrochemical tests were realized to validate the proper operation of the electrodes distribution. An outline of the described preliminary design of the probe manufactured for Iceland is shown in Figure 1.

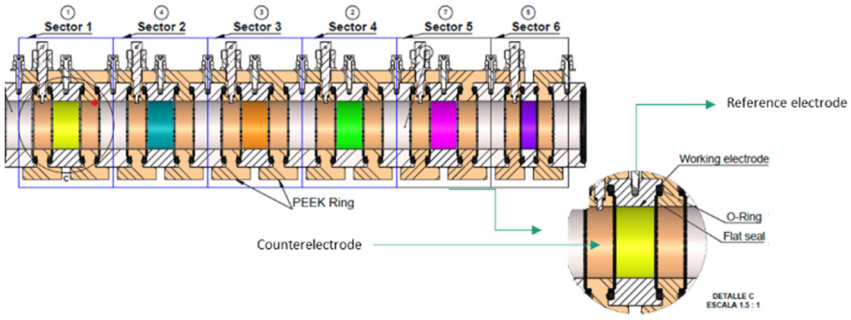

Figure 1: Scheme of the 3-electrode electrochemical probe

Thus, the whole probe would be composed by several electrochemical cells (one for each selected material) placed sequentially and connected independently for being electrochemically assessed. The selected materials for Icelandic plant are compiled in Table 2. All this set will be linked to the rest of the piping system by coupling flanges connected to a pipe test section. This testing section should facilitate the installation of the monitoring system in the geothermal plant without affecting the operation. The electrical connections of the electrodes will be taken to the outside part of the probe where a control unit equipped with a potentiostat will be installed. Moreover, to measure the cells individually, a multiplexer should be introduced.

Table 1: Materials selected for the monitoring system to be installed in Iceland

WE	Mat	Ni	Cr	Mo	Mn	Fe
1	**Incon 625**	>58	20-23	8-19	<0.5	<5
2	**AISI 316**	10-12	16-18	2	<2	bal.
3	**2507**	6-8	24-26	3-5	<1.2	bal.
4	**SMO254**	18	20	6.1	0.8-1.4	bal.
5	**P265GH**	<0.3	<0.3	<0.08		bal.
6	**K55**					bal.

The measurement procedure will be controlled by a specific software (developed in AIMEN) executed remotely on a PC. These measurements will be transmitted through a 3G modem and supervised periodically from AIMEN staff.

Corrosion measurements. Electrochemical Impedance Spectroscopy (EIS)

The main innovation of the corrosion monitoring system is related with the continuous updating of the corrosion state of the exposed materials in real time by using EIS measurements.
EIS is a sophisticated electrochemical technique extensively used in laboratory testing of protective coatings or materials corrosion performance [1]. EIS measurements are also being made in the field on materials in service in different industrial environments. In the field, EIS is a method to monitor the material condition, rate of deterioration, remaining life, etc.[2], information that is valuable in planning maintenance programs.
EIS is a non-destructive technique and so can provide time-dependent quantitative information about the electrode processes and complex interfaces. The standards, as ISO 16773:2016, deal with instrumental setup, data validation, performing EIS measurement and

experimental results, but does not give guidelines for data interpretation, which is more complex.
EIS method consists in measuring the response of an electrode to a sinusoidal potential modulation at different frequencies. At low frequency range, the system will remain excited for a long time, exciting and relaxing all the partial steps involved in the process, including the slower ones. On the contrary, as the frequency increases, only response from the faster process (having short relaxation time) will be observed. Having this in mind and considering that ion migration process through the electrolyte is a fast process, they will be visible in the high frequency range, providing an estimation of the conductivity of the medium (> 10kHz). On the other hand, the corrosion processes of the material, involving oxidation-reduction reactions, are slower processes that will be distinguishable in the lower frequency range (1kHz-1mHz). Thus, it is essential to define the frequency range to be explored so that all the processes involved can be studied. The main advantage of EIS lies in its high sensitivity, detecting changes in the material long before any visible damage occurs.
One popular format for evaluating EIS data, consists of plotting the imaginary impedance (Zim) versus the real impedance component (ZRe) at each excitation frequency. This is called the Nyquist plot.
Further spectra analysis allows formulation of a hypothesis on the electrical behaviour of the system and establishment of an equivalent circuit model. EIS data is commonly analysed by fitting it to an equivalent electrical circuit model consisting of passive elements such as resistors, capacitors and inductors. The different impedance parameters involved in the selected EIS model were obtained by a regression procedure based on a simplex strategy. Literature proposes different models of equivalent circuits to interpret the impedance data [3,4,5] however, to be useful, the elements in the model should have a physical meaning in the electrochemistry of the system. Thus, this technique is relatively easy to apply, but the data extracted from it are not, in most cases, directly interpretable, and require a deep prior knowledge of the real system. As a simpler way to assess the corrosion resistance of the materials, the impedance modulus (|Z|) at low frequencies, as the polarization resistance (Rp), is employed as a quantitative parameter to determine materials corrosion performance.
There is a good linear relationship between average corrosion current and the polarization resistance, therefore, higher Rp implies higher corrosion resistance and, in consequence, better barrier properties.
EIS measurements will be obtained by using a potentiostat PGSTAT20 AUTOLAB from Ecochemie®. Impedance will be measured in the frequency range between 100kHz and 0.1Hz (5 points per decade) with a selected AC potential perturbation which will be dependent of the testing materials resistivity. EIS measurements are daily executed and registered every 8 hours to follow the behaviour of the materials exposed under real conditions in the well during a period of one year.
Additionally, visual examination of the WE section and microscopical studies will allow at determining the type of frequency.

Results

The corrosion monitoring system was installed in Hellisheidi plant (Iceland) in October - November 2021.

The measurement period has started in November 2021, and it is expected to extend it for 12 months. The first results obtained indicate clear differences between the corrosion mechanisms found on stainless steel and carbon steel materials as shown in Nyquist plots of Figure 2.

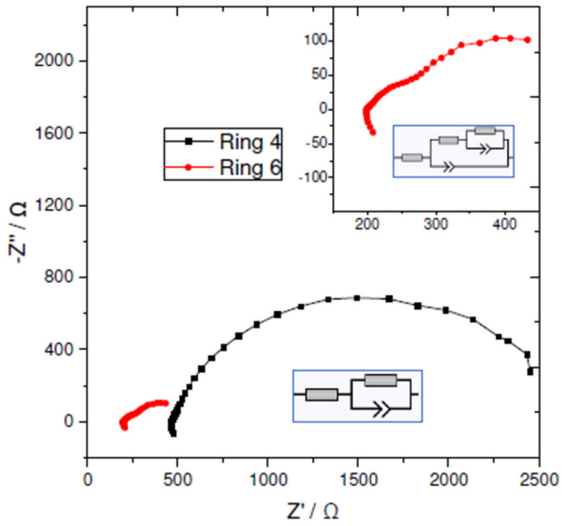

Figure 2: Nyquist plot obtained for SMO254 ss (WE4) versus carbon steel (WE6).

Stainless steels spectra describe a unique high impedance arc, that can be fitted to a standard Randles equivalent circuit (Figure 2, WE4). This circuit is composed by a first pure resistance, associated to the electrolyte resistance (Re), followed by a resistance parallel to a capacitance (R1C1). These two elements correspond to the Polarization Resistance (R1=Rp) and to the double layer capacity (C1).

For the case of carbon steel (WE6), two different arcs are observed, so a different circuit need to be used to fit the measurements. An additional couple of Resistance capacitance parallel to the previous RC elements (R-R(RC)C) is required. This new element corresponds to the passive oxide film formed between the electrolyte and the carbon steel substrate. In this case, Rp does not only correspond to the diameter of the first arc, but it is the sum of both differentiated arcs.

Thus, an evolution can be detected during the measurement period. Figure 3 shows weekly Rp average values represented for each WE at different weeks.

As shown in the graph, Rp is higher for stainless steels (WE1, WE2, WE3 and WE4), as expected, while WE5 and WE6 present higher variability and lower Rp values. K55 (WP6) present the lowest values during this period, thus it is the least corrosion resistant.

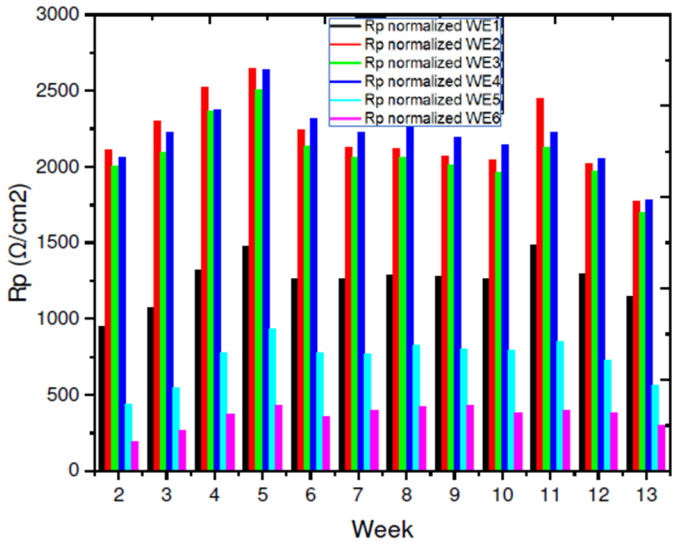

Figure 3: Results of Rp (average values) obtained during 13 weeks for each WE.

These results are not necessarily constant during testing time, because the nature of the layers over the metal can change, grows or scaling phenomena could appear. For instance, apparition of single peaks in the resistance values can be explained by the irregularities in the flowrate: when the flowrate decreases, the impedance increases abruptly, probably due to the formation of deposits on the metal substrates.
The obtained results so far allow to establish a scale of materials from the highest corrosion resistant to the lowest under the conditions of Iceland plant: WP4 (SMO 254)>WP2(AISI 316) > WE3 (Superduplex 2507) >WE1 (INCONEL 625) >WE5 (P265GH) >WE6 (K55)
Deep analysis will be performed to optimize the best combination of material/fluid for each installation and maximize the durability and the efficiency of the plant.

Conclusions

GECO project proposes a detailed and consistent monitoring program to provide cleaner and cost-effective non-carbon emitting geothermal plants.
A dedicated corrosion monitoring equipment for online and continuous monitoring of materials degradation for geothermal plants will be designed, developed and installed by AIMEN Technologic Centre in the demo sites located in Iceland (Hellisheidi) to run under high temperature and pressure conditions for one year.
EIS measurements will be registered and evaluated in real time to compare the corrosion performance of the selected materials and anticipate potential damages in the infrastructures. Following the impedance measurements allows detecting how the outages or plant malfunctions can affect the corrosion processes on the piping materials anticipating leakages due to pipe damages and, in consequence, avoiding long non-operational periods and high repair costs.

References

1. H. P. Hack and J. R. Scully, Defect Area Determination of Organic Coated Steels in Seawater Using Breakpoint Frequency Method, J. Electrochemical Soc., Vol. 138, No. 1, pp. 33-40 (1991)
2. Shreepathi, A. Guin, S. M. Naik, M. Rao Vattipalli, Service Life Prediction of Organic Coatings: Electrochemical Impedance Spectroscopy vs Actual Service Life, J. Coatings Technology and Research 8(2):191 (2011)
3. Calderón-Gutiérrez, F. E. Bedoya-Lora, Barrier property determination and lifetime prediction by electrochemical impedance spectroscopy of a high-performance organic coating, Dyna, year 81, no. 183, pp. 97-106 (2014)
4. M. Orazem et B. Tribollet, Electrochemical Impedance Spectroscopy (2008)
5. L. Freire, M.J. Carmezim, M.G.S. Ferreira, M.F. Montemor, The passive behaviour of AISI 316 in alkaline media and the effect of pH: A combined electrochemical and analytical study, Electrochim. Acta Vol 55, 21, pp 6174-6181 (2010)

Acknowledgements

The research leading to these results was developed under the framework of GECO project. This project has received funding from the European Union's Horizon 2020 research and innovation program under grant agreement No 818169.

Cyclic oxidation resistance of IN625 produced by Laser Beam Melting, influence of the building direction

Sébastien Mercier[1]; Thomas Gheno[1]; Ariel Morel[1]; Denis Boivin[1]; Etienne Rimpot[1]; Catherine Rio[1];

[1]DMAS, ONERA, Université Paris Saclay, F92322, Chatillon, France

Additive manufacturing of metals is increasingly used in the industry. However, if major improvements have been made in recent years to obtain dense and sound materials with good chemical and mechanical properties, there are still challenges regarding the long term evolution of these properties in aggressive environments, and the application of this manufacturing technology to more critical applications such as thermomechanical fatigue in high temperature oxidative environment.

In this paper, the isothermal and cyclic oxidation properties of as-built Laser-Beam-Manufacturing (LBM) IN625 was investigated as a function of the orientation of the coupons with respect to the main construction direction in the LBM tank. Isothermal and 1h cycle cyclic oxidation tests were carried out at 1000°C on vertical, horizontal and 45° coupons. Coupons of IN625 fabricated by conventional means (casting and cold-rolling) were included in the tests as reference. While no influence of the construction orientation was found in isothermal oxidation, a significant effect was found in cyclic oxidation. Indeed the horizontal coupons had a longer cyclic oxidation lifetime than the 45° coupons, which themselves had a longer life time than the vertical coupons. An oxidation-spallation model was fitted to the cyclic mass change data. This is used to identify the impact of the LBM process and building orientation on oxidation kinetics and spallation behavior, compared to conventional IN625. The influence of the manufacturing process on the oxidation properties is then analyzed based on microstructural observations and composition profiles in the metal below the oxide scale.

Corrosion by Hot Gases and Combustion Products (WP3)

A systematic study of the effect of the nickel and cobalt respective proportions in M–30Cr alloys (M = Ni and/or Co) on their behavior in oxidation at high temperature

Aurore Padox, Matthias Jollain, Lionel Aranda, Patrice Berthod

University of Lorraine, Nancy/France

Nickel and cobalt are frequently present together in cast superalloys. For instance nickel is almost systematically present in the chemical composition of cobalt alloys to help the austenitic structure to remain stable despite temperature variations in service. It is often observed that the oxidation behavior at high temperature is better in great presence of nickel than in great presence of cobalt. The aim of this study is to explore the effect of the Co/Ni ratio in the case of simple cast alloys composed of nickel, cobalt and chromium only. Thermogravimetric tests were carried out in air at 1200°C, followed by post–mortem characterization of the oxidized samples (XRD, SEM, EDS). Globally, the obtained results confirm the well-known tendencies concerning the additions of cobalt to nickel alloys (mass gain rates in) and the additions of nickel on cobalt alloys (promoting chromia as main or single oxide). However, some expected influences were not really observed, this suggesting that the roles of Ni and Co may be more complex as it can be thought. This may be related to the particular high level of the test temperature.

Keywords : binary and ternary alloys, nickel, cobalt, chromium, high temperature oxidation, mass gain kinetic, oxidation products

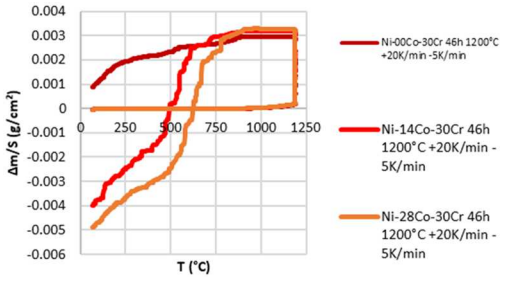

	Co-30Cr	Co-14Ni-30Cr	Co-28Ni-30Cr
Cr_2O_3	✓	✓	✓
$CoCr_2O_4$	✓	✗	✗
CoO	✓	✗	✗

{Δm/S versus T}–plots of Ni–30Cr alloys with various Co additions (left) and table summarizing the presence of not of different kinds of oxides formed on Co–30Cr alloys with various Ni additions (right)

Exploration of the high temperature oxidation of the M–30Cr alloys (M = Co and/or Ni) containing tantalum in absence of carbon

Florian Schumacher, Yona Ait Meddour, Lionel Aranda, Patrice Berthod

University of Lorraine, Nancy/France

Tantalum is often present in chromia–forming polycrystalline superalloys based on cobalt or on nickel. It may plays a double role in the strengthening, as solid solution hardener and as a strong carbide–forming element (TaC carbides, generally). In carbon containing superalloys Ta is present in the matrix as well as in the primary carbides (and secondary in case of precipitation heat treatment). Tantalum is also easy to oxidize and it takes part to the phenomena during the high temperature oxidation of the concerned alloys. The related phenomena may depend on the forms with which Ta is present in the alloy. In this work, by avoiding the presence of carbon in the considered alloys ((Co, Ni)–30Cr–4Ta with various Ni/Co ratios), the presence of Ta in solid solution only is favored. Thermogravimetric tests at 1200°C were performed, followed by post–mortem characterization. It was observed that tantalum effectively played a significant (detrimental in some cases) role on the oxidation sequences, notably on the adherence of the oxide scales formed externally.

Keywords : ternary and quaternary carbon–free alloys, nickel, cobalt, chromium, tantalum, high temperature oxidation, mass gain kinetic, oxidation products

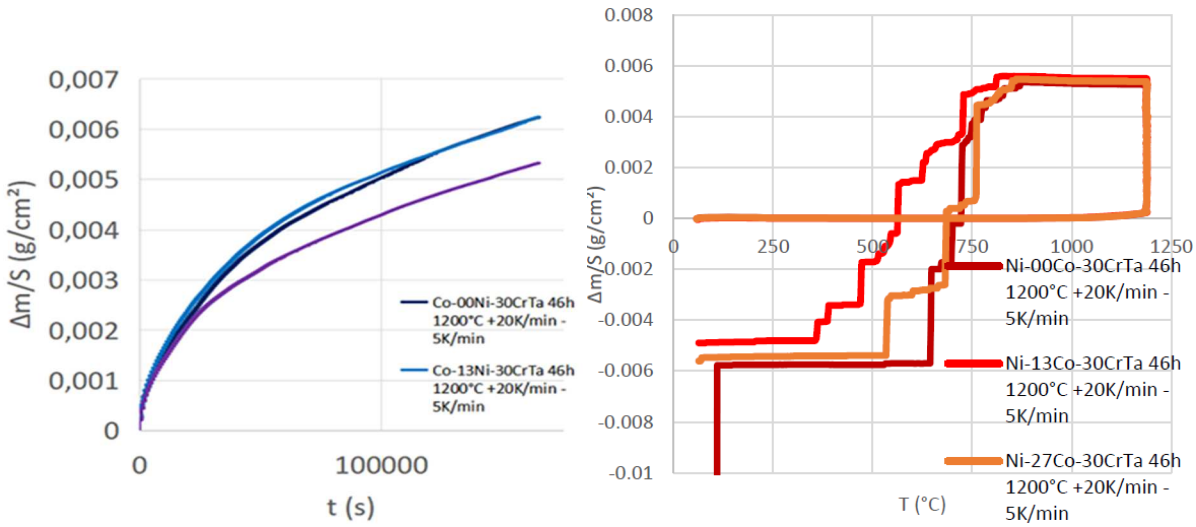

{Δm/S versus t}–plots of Co–30Cr alloys with various Ni additions (left) and {Δm/S versus T}–plots of Ni–30Cr alloys with various Co additions (right)

Characteristics and resistance against spallation of the oxides formed at high temperature on {Co, Ni}–based chromium–rich cast alloys containing titanium

Synthia Annick Ozouaki Wora, Patrice Berthod

University of Lorraine, Nancy/France

Titanium is a MC carbide–forming element which can be used to obtain carbides, in addition to other carbides or as single carbide present, able to take part to the interdendritic mechanical reinforcement for resisting stresses at high temperature. However, this element can strongly react with oxygen or nitrogen. Consequently its presence may influence the general behavior of chromia–forming alloys in oxidation at high temperature, by promoting the formation of other oxides than chromia. In this work, a series of samples all containing 25 wt.%Cr, 0.4wt.% C and 1.6wt.%Ti, with a base element shared between nickel and cobalt in various proportions, were exposed at 1250°C during 70 hours to achieve rather severe oxidized states. The variation of mass during a -5°C min^{-1} cooling was monitored using a thermo–balance and the oxidized states and deteriorated sub-surfaces after return to room temperature were characterized. The loss of oxide scales during the cooling was significant but variable between the alloys. The remaining parts of scales allowed specifying the oxides. Chromia was present in all cases but oxides involving titanium were well present. It was notably observed that an outermost TiO_2 thin scale developed along the external face of chromia and separated it from the oxidizing gas.

Keywords : {Ni, Co}–based alloys, titanium, carbides, chromia, TiO_2, oxide spallation

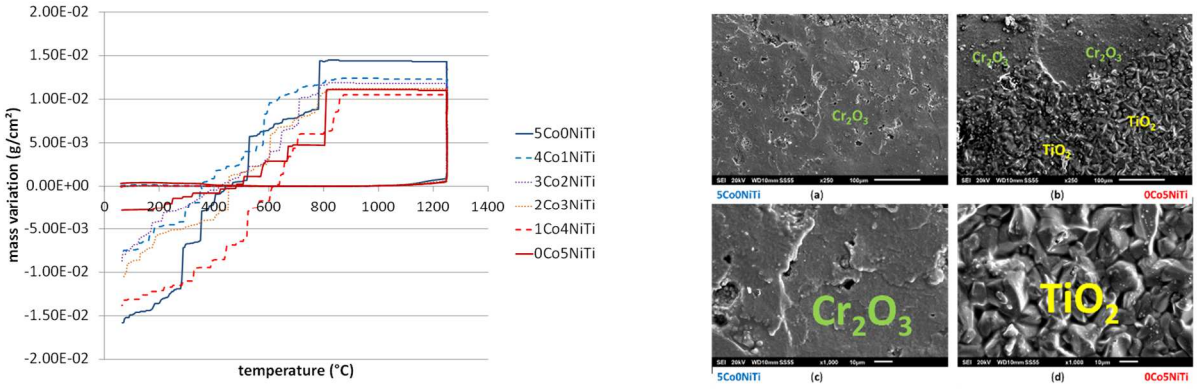

{Δm/S versus T}–plots of the six {Ni, Co}–25Cr–0.4C–1.6Ti alloys (left) and SEM/SE micrographs of the surface states for two of them (right)

Oxidized states of chromium–rich {Ni,Co}–based alloys rich in tantalum to form TaC carbides after exposure at 1250°C in air

Jean-Paul Gomis, Patrice Berthod

University of Lorraine, Nancy/France

Tantalum carbides are among the most stable MC primary carbides of cast superalloys when they are exposed at elevated temperature. When chromium is present in the chemical composition for achieving high resistance against hot oxidation and hot corrosion, the TaC carbides are particularly present in cobalt–based superalloys, but less in the nickel–based ones for equivalent contents in tantalum and carbon. In all cases a part of the tantalum atoms stays in solid solution in the matrix and Ta atoms are able to diffuse toward the oxidation front. The purpose of this work is to examine, after exposure at a temperature high enough to facilitate the dissociation of TaC carbides and a fast diffusion of the Ta atoms, how tantalum behaved and where it went, in the case of {Ni, Co}–based alloys containing 25 wt.%Cr – 0.4wt.%C – 6wt.%Ta. It appears that, for the nickel–richest alloys, all the tantalum atoms which were oxidized, had reached the interface with the external oxide scales. In the case of the cobalt–richest alloys a significant part of tantalum was internally oxidized as $CrTaO_4$ islands along the sub–surface close to the metal/scale interface. One can note also that the presence of tantalum did not preserve the cobalt–richest alloys starting a generalized oxidation with the formation of spinels $CoCr_2O_4$ and even of CoO.

Keywords : {Ni, Co}–based alloys, tantalum, carbides, chromia, $CrTaO_4$ distribution

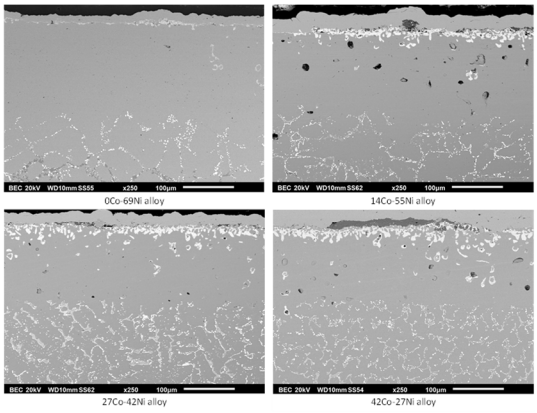

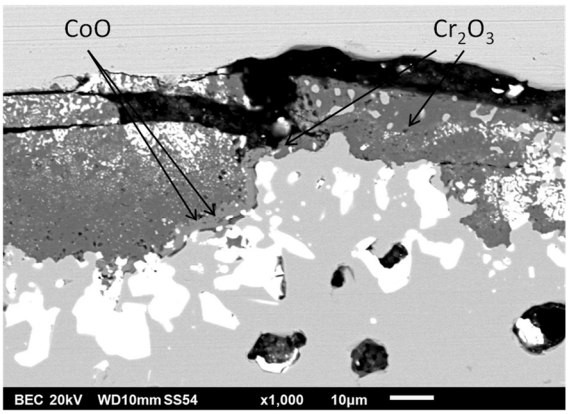

General view of the oxidized surface and sub-surface states for four of the alloys (left) and detailed view in the case of the nickel-free Co–based one (right) in which the white areas are $CrTaO_4$; SEM in BSE mode on cross–sections

Microstructural investigation of oxide films on Alloy 182 weld metal formed under BWR zinc water chemistry

Adrianna Mackiewicz, Paul Scherrer Institute (PSI), Villigen/Switzerland, adrianna.mackiewicz@psi.ch
Stefan Ritter, Paul Scherrer Institute (PSI), Villigen/Switzerland
Kai Chen, Paul Scherrer Institute (PSI), Villigen/Switzerland
Hans-Peter Seifert, Paul Scherrer Institute (PSI), Villigen/Switzerland
Sannakaisa Virtanen, Friedrich-Alexander University Erlangen-Nürnberg, Erlangen/Germany

For many years now, boiling water reactors (BWRs) have been using zinc (Zn) injection into the coolant to reduce the radioactive corrosion build-up caused by neutron-activated Co^{60} isotopes. Some studies have indicated that Zn might also positively influence stress corrosion cracking (SCC) mitigation of nickel-based alloys and stainless steels. However, the potential effects of Zn injection regarding their SCC behavior require further quantification and resolving of the oxidation kinematics.
Therefore, the impact of Zn injection on the SCC behavior of a nickel-based weld metal (Alloy 182) in BWR environment is investigated in the framework of a research project at PSI. Tensile tests are performed in simulated BWR environment studying the SCC initiation behavior. Chen et al. present these results at the same conference in the paper “Effect of zinc injection on mitigating stress corrosion cracking of structural materials in LWR primary water”. Additionally, specimens are exposed to Zn-free and Zn-containing BWR water in autoclaves with recirculating loops and their oxide films are studied. Different microstructural characterization techniques (e.g., electron microscopy, electron dispersive X-ray spectroscopy, Raman spectroscopy, etc.) are used to identify zinc incorporation into the oxide film. The first results are presented and discussed at the current poster. They show that Zn is present in the oxide film and that the oxide film properties vary after the Zn treatment.

Slow strain rate testing of Fe-10Cr-4Al ferritic steel in liquid lead and lead-bismuth eutectic

Christopher Petersson, Royal institute of technology KTH, Stockholm/Sweden

Peter Szakalos, Royal institute of technology KTH, Stockholm/Sweden

Daniel Stein, Royal institute of technology KTH, Stockholm/Sweden

Abstract

The susceptibility of an Fe-10Cr-4Al steel to liquid metal embrittlement (LME) in low oxygen liquid lead and lead-bismuth eutectic (LBE) environments has been investigated, using a newly developed slow strain rate testing (SSRT) technique that can be employed at elevated temperatures. The results from this study showed that the Fe-10Cr-4Al steel suffered from embrittlement when exposed to LBE over a wide temperature range. The embrittlement, here measured as reduction in total strain at rupture, was observed already at the melting temperature of LBE and reached a maximum at approximately 375°C. At temperatures above 425 °C the materials ductility regained its original levels. The exposures in liquid lead showed no indications of embrittlement but instead a ductile behavior over the entire temperature range studied (340-480 °C).

Effect of oxidants produced by radiolysis on aqueous corrosion of iron

T. Ota, S. Ajito, T. Hojo, M. Koyama, E. Akiyama, Tohoku University, Sendai/Japan

In March 2011, Fukushima Daiichi Nuclear Power Plant (1F) in Japan lost their functions due to the earthquake and tsunami. Currently, the 1F is scheduled to be decommissioned. Since the nuclear fuel in the primary containment vessel melted and leaked by the accident, debris emitting gamma-rays produces H_2O_2 and NO_x etc. through the radiolysis of coolant water and purged nitrogen. These produced oxidants may accelerate the corrosion of structure consisting of carbon steel[1]. Therefore, it is important to understand the corrosion behavior of the carbon steel in this specific environment to ensure the integrity of the containment vessels during the long-term decommissioning.

Thus, in this study, O_3 and NO_x, which are generated by the radiolysis, were introduced into the aqueous solution to simulate the irradiation environment. The corrosion behavior of the iron in the aqueous solution simulating the radiation environment was investigated by using immersion test and electrochemical analysis.

The specimen used in this study was an iron sheet (purity: 99.5 wt.%). The solution was 0.1 M acetic acid/sodium acetate aqueous buffer solution with pH 5.5. The air containing O_3 and NO_x was introduced into the aqueous solution with bubbling. After the introduction, polarization resistance and cathodic polarization measurements of the iron sheet were carried out in the solution.

The corrosion rate of the iron sheet obtained by the polarization resistance measurement increased with increasing the amount of the introduced oxidants. The result of the polarization measurement showed that the cathodic reaction was enhanced by the introduction of the oxidants. From these results, it was found that the corrosion of the iron sheet was accelerated by the introduced oxidants due to the enhancement of the cathodic reaction of the oxidants.

Reference

1) K. Daub, X. Zhang, J.J. Noël, J.C. Wren, Electrochimica Acta, 55 (2010) 2767

Corrosion assessment for the evaluation of the long-term integrity of containers in crystalline rock

C. Stephan-Scherb, J. Eckel, T. Fass, T. Weyand, C. Dietl, A. von Oertzen, L. Maerten, Bundesamt für die Sicherheit der nuklearen Entsorgung, Berlin/Germany

Crystalline rock is a potential host rock for a repository site for high level radioactive waste in Germany. In safety concepts for crystalline host rocks, in contrast to the host rocks rock salt and claystone, the canister in combination with geotechnical barriers may function as the essential barrier – and is therefore with regard to radionuclide retaining properties of greater importance than the host rock. The long-term integrity of the waste canister depends on various parameters such as canister material, microstructure, anti-corrosive coating, geotechnical barrier properties, local pore water composition, radiolysis on the inside of the container and tectonic strain.

The presentation addresses the challenge of determining the durability of a waste container in crystalline host rock by comparing and evaluating different international concepts for canister design and discussing their applicability to the requirements in Germany. The focus lies on the geochemical environment and material characteristics – while considering the tectonic environment within the repository.

The contribution will highlight the activities of BASE with regard to evaluating the corrosion properties of different potential canister materials such as copper, cast iron and stainless steel. The aim is to deepen the understanding of individual processes, their combined effects, as well as their classification into favorable or unfavorable processes and conditions for the derivation or justification of regulatory requirements.

Failure study of an aircraft engine high pressure turbine (HPT) first stage blade

García-Martínez, María[1], del Hoyo Gordillo, Juan Carlos[1], Valles González, Mª Pilar[1], Pastor Muro Ana[1]; González Caballero, Beatriz[1]

[1] *National Institute for Aerospace Technology (INTA). Torrejón de Ardoz (Madrid), Spain, garciamam@inta.es.*

Abstract

In jet engines, almost 50% of failures are located in turbine blades and disc damages. Turbine blades often fail due to creep, corrosion and fatigue. Corrosion pitting can be one of the factors contributing to fatigue mechanisms, as it occurs in this study. This paper presents the study to determine the root cause of the failure of a high-pressure temperature (HPT) blade in a turbofan engine. The incident, which involved the fracture of one of the 1st Stage HPT gas turbine blades, took place before the aircraft entered the runway, with no consequences for the rest of the aircraft.

Visual observation of the blades indicated that initially one blade was fractured. Subsequently, detachment of the airfoil from this blade and its impact with the rest of the blades of the first turbine disc trigged a catastrophic damage to them and affected later stages blades. Chemical, microstructural and mechanical characterization determined that blade material corresponded to René 142 type nickel superalloy, presenting the typical microstructure of the second generation nickel superalloy, formed by fine rectangular ɣ' (Ni_3Al) precipitates in a ɣ Ni matrix.

The observed fractographic characters by optical and scanning electron microscopy showed that the fracture of the first damaged blade was due to a fatigue mechanism. The fatigue phenomenon was initiated by corrosion pitting on the root surface of the mentioned blade, on the intrados, and progressed due to the cyclic stresses and temperature gradients, typical factors in the usual operation of a gas turbine.

Keywords

HPT Turbine; blade; corrosion-fatigue; thermo-mechanical fatigue; fractography

Introduction

Fatigue is a degradation process of a material subjected to cyclic loads of values below those that would be capable of causing it to fail under static loading. During this process, a crack is generated which, given the right conditions, will grow until the part ruptures when a sufficient number of cycles are applied. The number of cycles required will depend on several factors such as applied load, presence of notches, etc. Fatigue failure requires, therefore, the combined action of repeated variable loads and time.
The fatigue failure mechanism, or thermomechanical fatigue (TMF), as is the case in this study, is one of the main failure mechanisms of turbine blades, as demonstrated in the extensive literature on the failure analysis of turbine blade [1-4]. TMF is therefore the dominant life-limiting factor that must be taken into account in the design of turbine blades [1]. A critical value should be defined for the crack depth, for which the designed parts should not fail during the expected operating hours. Inspections of the parts should be carried out to verify that this critical value is not reached, at which point the parts will need to be replaced or, if possible, repaired. If the crack reaches a certain depth, it propagates to form ductile striations. Subsequently, partial ruptures due to static overloading usually occur, with the appearance of dimples and pseudo-cleavages, finally leading to rupture of the remaining section by static overloading. When considering the factors that can influence the fatigue phenomenon, it should be emphasized that the fatigue mechanism can operate either by initiating and propagating a crack, or only by propagating a crack generated by another pre-existing mechanism or defect.

Background

This paper presents the procedure followed to determine the cause of the catastrophic failure of a turboprop engine. The events occurred after ignition and taxiing of the aircraft with all parameters within limits indicating normal operation of the turboprop engine propulsion group. At the runway, an explosion was heard followed by an uncontrolled increase of the ITT indicator or inter-turbine temperature, which rose to 1341°C, while before the incident it was 863ºC. Boroscopic inspections of the engine found that most of the blades of the two-stage gas turbine were affected as a consequence of the impact suffered by the fragment detached from the blade that had broken off at the dovetail, which was designated as blade 0 (Figure 1).

a) 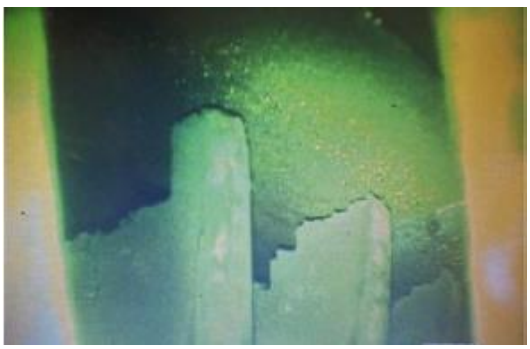 b) 

Figure 1. a) Image obtained in the boroscopic inspection of the first stage of the high pressure turbine (HPT). b) Disassembled HPT disc: Blade area close to the one fractured by the dovetail (blade 0).

Materials and methods

The material chemical analysis of the first stage high-pressure turbine (HPT) blades was carried out by using a Panalytical X-ray fluorescence (XRF) equipment model Setium and by the combustion technique with Leco CS600 equipment.
A microstructural study was carried out, by embedding the longitudinal section of one of the blades of the first stage in conductive resin and, after a suitable polishing and a chemical etching with a reagent composed of lactic acid 50ml, nitric acid 30ml and hydrofluoric acid 2ml, its microstructure was observed in a Leica MEF4M optical microscope (OM). The presence and thickness of the coating was determined using the same OM. The coating was analyzed by a ThermoScientific APREO C field emission scanning electron microscope (FESEM), obtaining its semi-quantitative chemical composition by an Oxford AZTEC Energy Dispersive X-Ray Spectroscopy (EDX).
A microhardness test was performed on the base material of a metallographic specimen containing both the root and the airfoil of one of the blades, using a Future FM7 microhardness equipment with a test force of 0.5 Kgf.
A Leica DVM6 digital microscope (DM) and the FESEM, which incorporates EDX, were used for the fractographic study of blade 0, fractured by the dovetail. In addition, an exhaustive study of blade surface defects was carried out, using metallographic specimens of longitudinal sections, which were observed without etching by OM and FESEM.

Results and discussion

Visual observation and macro-fractographic study

Naked eye and DM observations of the blades were performed. The fracture of blade 0 occurred on a plane perpendicular to the longitudinal axis of the blade, at the location of the letters engraved on the intrados face root (Figure 3a). The fracture surface is perpendicular to the normal component of the tensile stresses (the sum of the lift and rotational tensile loads). The rest of the adjacent blades ruptured at the airfoil. These blades showed plastic macrodeformation in the fracture area (Figure 2). Finally, the cooling passages were inspected and did not appear to be obstructed.

Figure 2. Blade 0 and several blades affected by the impact with the fragment of blade 0

The fracture of blade 0 started at the intrados face root, where corrosion pitting was found on the blade surface and was subsequently studied in more detail (Figure 3).

a) 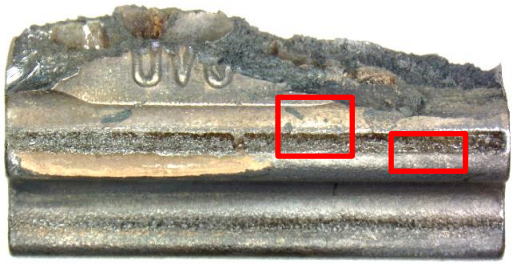 b) 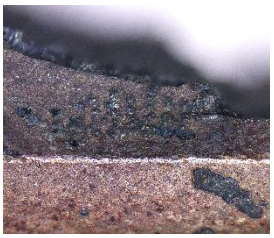 c) 

Figure 3. a) MD view of the fractured blade 0 intrados profile. Detail at higher magnification (red squares) in b) and c) where corrosion pitting was observed.

The macromorphological characters observed on the fracture surface of blade 0, such as the presence crack progression marks (CPMs) (Figure 4b), probably due to the existence of successive stresses, indicated the direction of fracture propagation and the point of origin of the fracture located on the outer surface of the blade. This origin coincides with the corrosion signs observed on the intrados face root (Figure 3). Two textures were observed on the fracture surface, both with low light reflectivity: the first one slightly smooth matte, in the area of the origin and up to the end of the CPMs, and the second one fibrous on the remaining part of the fracture surface (Figure 4a). Finally, small reflective spots were detected that were molten metal particles caused by overheating and hot sparks generated by friction

a) 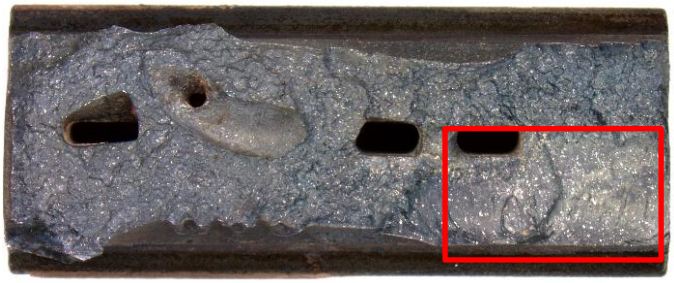 b) 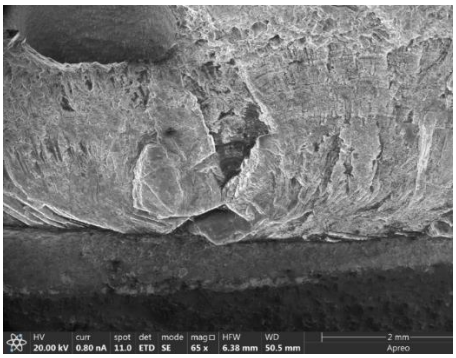

Figure 4. Macrofractographic characters on the fracture surface of blade 0: a) By DM, the fracture surface: slightly smooth matte texture with some reflective spots (framed in red) and the remaining fracture rough matte texture. b) By FESEM, detailed picture of the fracture surface with possible origin and CPMs.

Study of defects on the blade surface

Signs of corrosion on the intrados face root were found on most of the blades, including blade 0. Some of these pitting had a depth of 55 µm, penetrating the corrosion almost to the base material (Figure 5b).

In addition, cracks were detected at the intrados face root on a large part of the blades. It should be noted that these cracks were in the same area and position as the fracture in blade 0, just below the engraved letters (Figure 5e). These cracks crossed the coating perpendicularly reaching the base material and with a total crack depth of approximately 60-185 µm (Figure 5f). In most of these cracks, corrosion was observed within the cracks (Figure 5g).

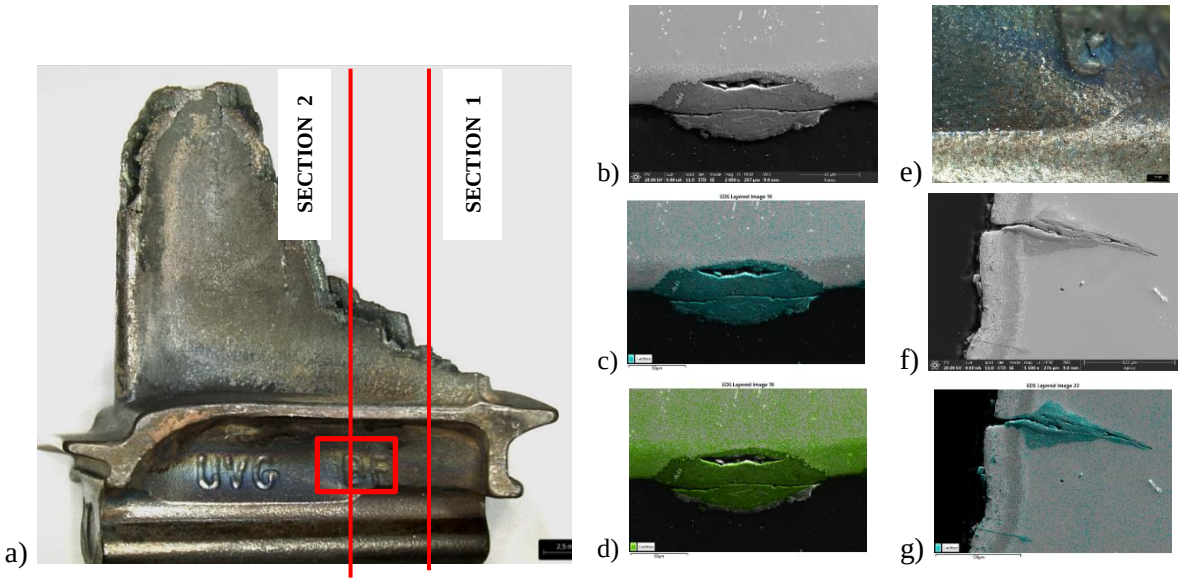

Figure 5. a) By MD, view of the intrados of one of the affected blades, with sections 1 and 2 cuts for metallographic specimens. b) FESEM image of a 55 µm deep corrosion pitting of a section 1 metallographic specimen. c) and d) Distribution map by EDX of elements O (blue) and Al (green) in the pitting corrosion. e) Detail picture at higher magnification (red box) where cracks were observed. f) By FESEM, picture of cracks in the section 2 metallographic specimen. g) Distribution map by EDX of element O in the cracks.

Material characterization

The chemical composition of the blade material, obtained by XRF and by the combustion technique, expressed as a percentage by weight, is shown in **Table 1**

Balance	**C**	**Al**	**Co**	**Cr**	**Hf**	**Mo**	**Ta**	**Re**	**W**
Ni	0.11	6.1	11.4	6.4	1.6	1.3	5.7	≅2.1	4.5

Table 1. Chemical composition (wt%).

According to the composition obtained from the chemical analysis, and taking into account the allowed tolerances, the base material of the blades would correspond to a René 142 nickel-based superalloy, in accordance with metallographic databases such as Total Materia [5]. The René 142 superalloy belongs to the type of columnar growth grain nickel-based superalloys, known as second generation, whose high temperature resistance is similar to that of Single Crystal (SC) alloys, which have been used as critical materials for turbine blades in aviation, aerospace and gas turbines [6-8]. Since the early 1950s, research has been carried out to develop an optimized material for gas turbine blades with all the required properties. The history of gas turbine blades shows the evolution of base material from wrought materials to Single Crystal (SC) superalloys, and of coatings from thermal barriers, through diffusion aluminides as in the present case, to the combination of EB-PVD (Electron-Beam Physical Vapor Deposition) coatings and Thermal Barrier Coatings (TBCs) [9].

Regarding the microstructure at the blade root, large columnar growth grains (Figure 6a) and a dendritic structure typical of this type of superalloys were observed. Such microstructure consisted of thin rectangular precipitates of ɣ' (Ni_3Al) in a Ni ɣ matrix, which has a face-

centered cubic (FCC) structure, and also exhibited eutectic ɣ/ɣ' islands [10,11] (Figure 6b). The microstructure study revealed also, that the blades had suffered overheating due to the dissolution of the rectangular ɣ' precipitates into the ɣ' matrix in the airfoil zone (Figure 6c). This is consistent with the overheating observed immediately after the incident.

a) b) c)

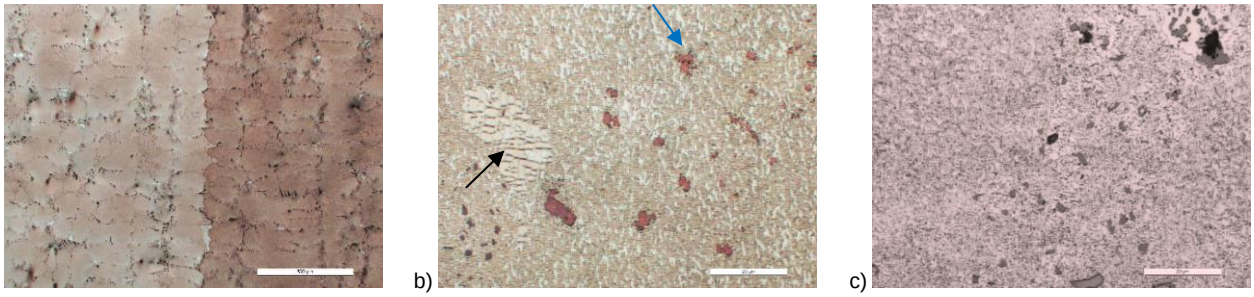

Figure 6. MO images of the microstructure at the root of one of the blades. a) Boundary between two columnar grains and dendritic structure. b) Typical structure: thin rectangular ɣ' precipitates in a ɣ' matrix, Hf and Ta carbide precipitates (blue arrow) and eutectoid ɣ/ɣ' islands (black arrow). c) Dissolution of thin rectangular ɣ' precipitates into ɣ' matrix.

Precipitates of hafnium and tantalum carbides, typical of the microstructure of this type of nickel-based superalloys, were identified in the FESEM by EDX (Figure 7).

a) b)

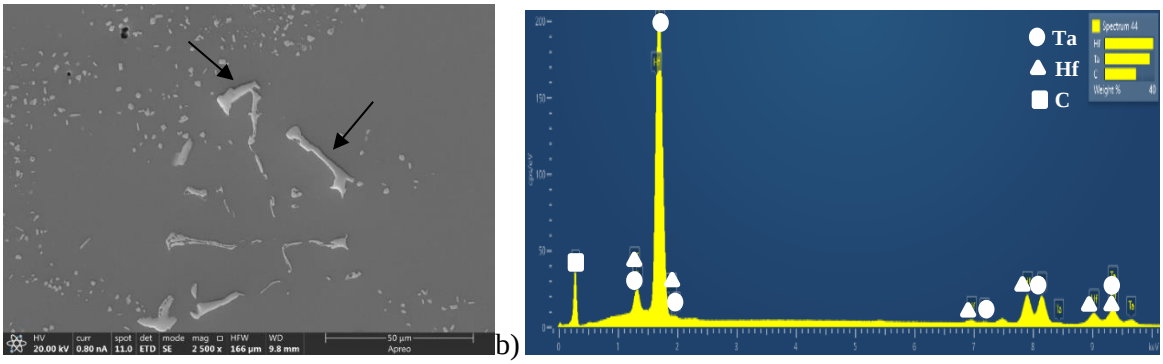

Figure 7. FESEM a) Image of the base material at the root with Hf and Ta carbide precipitates (black arrow). b) EDX spectrum of one of the precipitates that contains Ta, Hf and C as the major elements.

The hardness values on the Vickers scale, obtained in the base material core, are shown in Tabla 2. It was observed that they were lower in the airfoil than in the root, which is consistent with the fact that the superalloy had suffered overheating and with the observed microstructure, since the root, being embedded in the turbine disk and not directly affected by the combustion gases, is more protected against such overheating.

Area	Average HV 0,5 Kgf
Root	430,7±17,9
Airfoil	391,7±16,6

Tabla 2. Microhardness values on the Vickers scale.

Coating characterization

The study of the metallographic specimen by OM (Figure 8) showed an Al-Pt diffusion coating used to protect the nickel-based superalloy from the high temperatures resulting from the

combustion gases [12]. It had a homogeneous profile and thickness, both in intrados and extrados, of about 70-80 μm. The coating thickness decreased from the lower part of the blade platform and eventually disappeared towards the middle of the blade root. In addition, cracks were observed crossing the coating but not penetrating the base material. These cracks are characteristic of this type of coatings; they are formed by the difference in thermal expansion coefficients of the coating elements and the base material.

On the intrados, it was observed that, as the coating thickness decreased at the root, it was oxidized and the oxide layer increased as the coating thickness decreased (Figure 9).

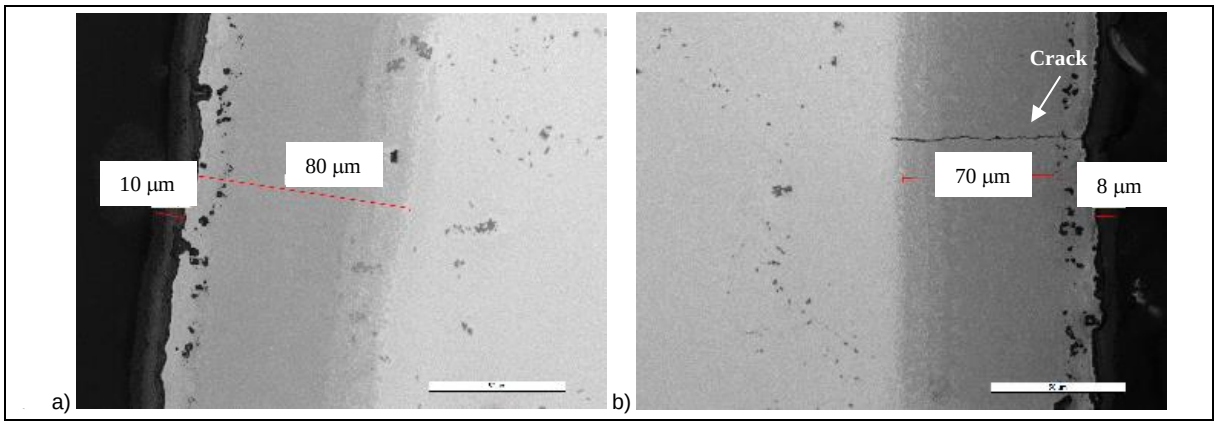

Figure 8. OM images of the diffusion coating: with a uniform thickness of 70-80, μm and a top oxide layer of approximately 8-10 μm in both a) intrados and b) extrados.

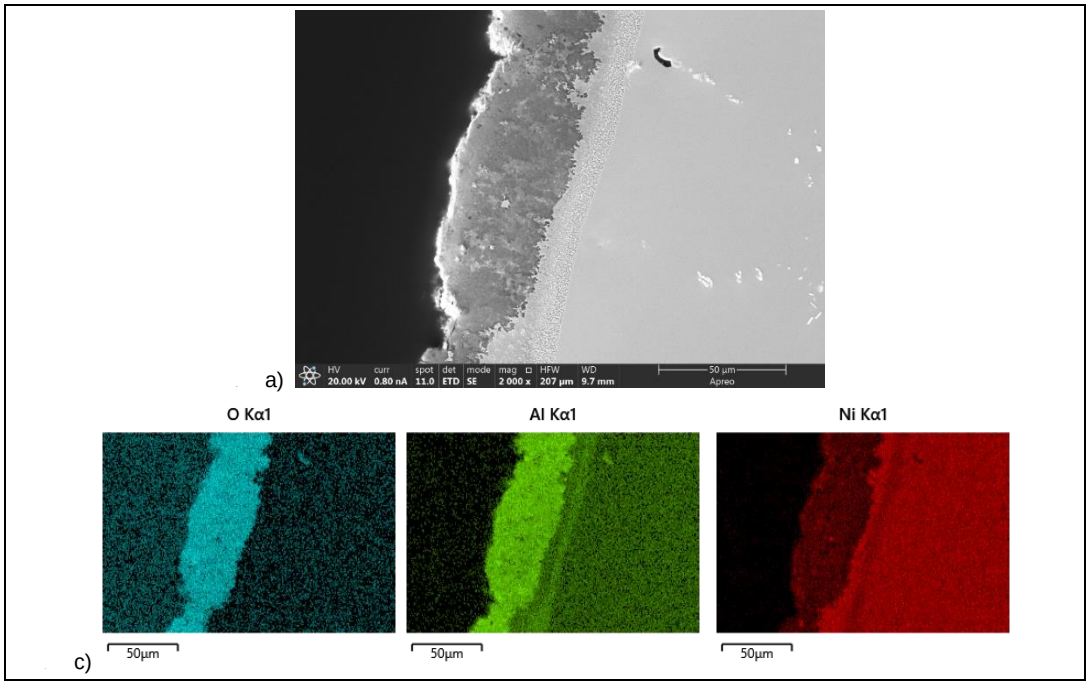

Figure 9. By FESEM, photo of the oxidized diffusion coating on the root in intrados, in the area where the coating ends. b) EDX map of element distribution: O (blue), Al (light green) and Ni (red)

A more detailed study of the coating, performed on the FESEM, showed that it consisted of three layers, typical of a protective diffusion coating against oxidation and corrosion at high temperatures [13-15]. The layers were analyzed by EDX with the following result (Figure 10): a top layer of protective aluminum oxide, intermediate layer of the diffusion coating rich in Al, Pt and Ni where Al and Pt came from the coating while Ni came from the diffusion of the base

material, and inner layer of the diffusion coating, rich in precipitates, in this case of W and Cr according to EDX analysis.

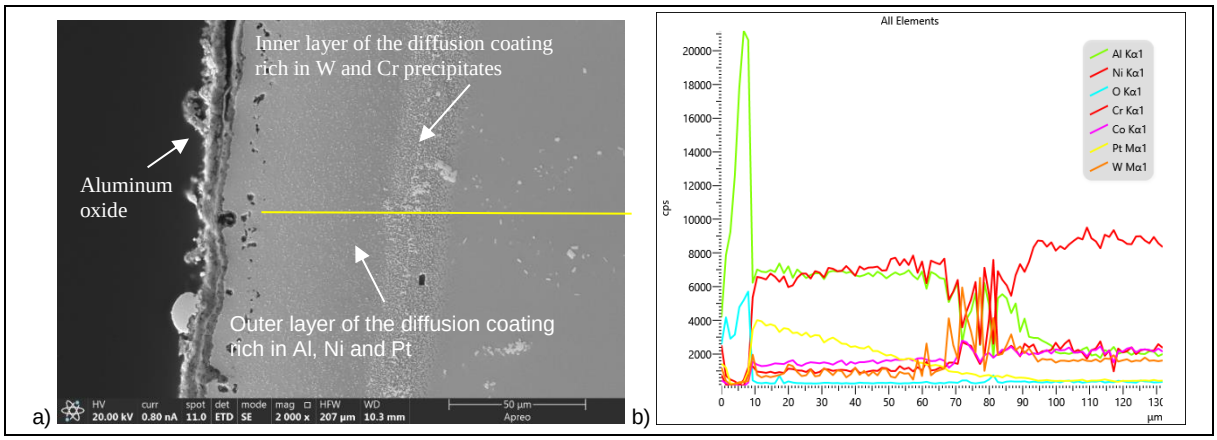

Figure 10. By FESEM: a) General picture of the diffusion coating. b) Line spectrum by EDX showing the evolution of the elements concentration according to the yellow line that crosses the coating until it reaches the base material of the nickel base superalloy

Micro-fractographic study

The microfractographic characters observed on the fracture surface of blade 0 by FESEM, as the ductile fatigue striations (Figure 11a and Figure 11b), indicated that the fracture mechanism was fatigue [16]. In the area where the fracture ended, dimples were observed (Figure 11c), indicating that the fracture was terminated by static overload in the remaining section of the blade. In addition, zones with molten material were observed (Figure 11c), which corresponded to the reflective spots seen with the DM. This molten material was possibly formed due to post-incident heating and hot sparks generated by friction

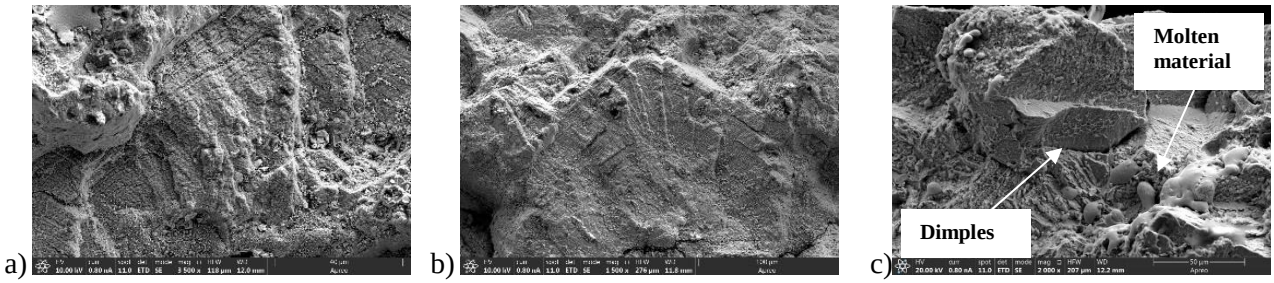

Figure 11. Microfractographic characters on the fracture surface of blade 0. In the FESEM: a) and b) Fatigue striations in different areas. c) Dimples and molten material.

Based on the obtained results, it can be concluded that the fracture process of blade 0 started with the formation of corrosion pits on the surface. Then, the crack incubation took place from these corrosion pits on the surface of intrados face blade, coinciding with the zone of maximum tensile stresses, and propagated by the application of successive static loads of short duration such as turbine vibrations, in accordance with a fatigue phenomenon. Subsequently, the crack originated grew towards the interior of the root, in a perpendicular direction to the blade axis by fatigue mechanism. Finally, the remaining section ruptured by static overloading. The presence of cyclic stresses and temperature gradients is an accelerating factor for crack growth once formed. Lastly, from the detachment of the blade 0 airfoil, and as a consequence of its impact with the rest of the blades of the first turbine disk, those blades suffered catastrophic damage and, probably, affected later turbine stages.

Turbine blades are subjected to the combined action of variable mechanical loads induced by centrifugal force and lift and thermal loads caused by the high temperature gas in service. Due to this combination of mechanical and thermal loads, some authors call this type of fatigue thermomechanical fatigue (TMF) [1,17,18].

Conclusions

This study has determined the cause of an accident that occurred in a turboprop aircraft engine when it was at the runway head. The material of the first stage fractured blades of the high pressure turbine (HPT) was studied and was discarded as the possible cause. From the visual observation and the fractographic study, it was concluded that the cause of the accident was the breakage of one of the blades, called blade 0, due to a thermo-mechanical fatigue process. This process started in the corrosion pitting on the intrados face at the root of blade 0 and progressed by a fatigue mechanism, due to the existence of cyclic stresses and temperature gradients, typical factors in the normal operation of a gas turbine. Finally, from the detachment of the blade 0 airfoil, and as a consequence of its impact with the rest of the blades of the first turbine disc, those blades suffered catastrophic damage and, probably, affected later stages of the turbine.

In light of the observed results and the factors that may have influenced this incident, a series of recommendations were made. It was suggested to carry out conscientious and frequent aircraft washings, including engines, to ensure the elimination of the remains of any substances that may have been ingested during the flights and, especially, when the flights have taken place in coastal areas and with ash ingestion.

Acknowledgment

Authors would like to thank all staff of Metallic Materials Area and especially the Microanalytical and Microstructural Characterization Laboratory.
This research has not received any specific grant from public, commercial or not-profit funding agencies.

References

1. R. Wang, B. Zhang, D. Hu, K. Jiang, H. Liu, J. Mao, F. Jing, X. Hao, Thermomechanical fatigue experiment and failure analysis on a nickel-based superalloy turbine blade, Eng Fail Anal. **102** (2019) 35-45.
2. Swati Biswas, M.D. Ganeshachar, Jivan Kumar, V.N. Satish Kumar, Failure Analysis of a Compressor Blade of Gas Turbine Engine, Procedia Eng. **86** (2014) 933-939.
3. Marko Katinić, Dražan Kozak, Ivan Gelo, Darko Damjanović, Corrosion fatigue failure of steam turbine moving blades: A case study, Eng Fail Anal, **106** (2019) 104136.
4. Hyeok-Jun Kwon, Dooyoul Lee, Young-Kook Lee, Failure analysis of blades and vanes of a compressor for a gas turbine engine, Eng Fail Anal, **124** (2021) 105386.
5. Total Materia [Internet] [cited 2021 April 8]. Available from: https://www.totalmateria.com.
6. A. D. Cetel, D. N. Duhl. Second generation columnar grain nickel-base Superalloys. The Minerals, Metals & Materials Society, 420 Commonwealth Dr, Warrendale, PA 15086, USA. (1992) pp.287-296.
7. Tin, S. and Pollock, T.M. Nickel-Based Superalloys for Blade Application: Production, Performance and Application. In Encyclopedia of Aerospace Engineering (eds R. Blockley and W. Shyy), (2010**).**

8. G. L. Erickson. Superalloy Development for Aero and Industrial Gases. ASM International. (1994). ISBN 0-87170-487-0.
9. B. Swain, P. Mallick, S. Patel, R. Roshan, S.S. Mohapatra, S. Bhuyan, M. Priyadarshini, B. Behera, S. Samal, A. Behera, Failure analysis and materials development of gas turbine blades, Mater Today Proc, **33(8)** (2020) 5143-5146.
10. J. Belan, A. Vaško, E. Tillová, Microstructural analysis of DV – 2 Ni – base superalloy turbine blade after high temperature damage, Procedia Eng. **177** (2017) 482-487.
11. Xiaotong Guo, Weiwei Zheng, Chengbo Xiao, Longfei Li, Stoichko Antonov, Yunrong Zheng, Qiang Feng, Evaluation of microstructural degradation in a failed gas turbine blade due to overheating, Eng Fail Anal, **103** (2019) 308-318.
12. A.B Smith, A Kempster, J Smith, Vapour aluminide coating of internal cooling channels, in turbine blades and vanes, Surf Coat Technol, **120-121** (1999) 112-117.
13. Xie, Feng, Dingjun Li, and Weixu Zhang, Long-Term Failure Mechanisms of Thermal Barrier Coatings in Heavy-Duty Gas Turbines, Coatings, **10(11)** (2020) 1022.
14. Clarke, D.R., Oechsner, M. & Padture, N.P. Thermal-barrier coatings for more efficient gas-turbine engines. MRS Bulletin, **37** (2012) 891-898.
15. Wojciech J. Nowak, Tadeusz Kubaszek, Marek Góral, Bartek Wierzba, Durability of underaluminized thermal barrier coatings during exposure at high temperature, Surf Coat Technol, **382** (2020) 125236.
16. Pintado, J. Fallo en Servicio de los Materiales Metálicos. Instituto Nacional de Técnica Aeroespacial. (1992). ISBN: 84-60-6-09-1.
17. Andre Pineau, Stephen D. Antolovich, High temperature fatigue of nickel-base superalloys – A review with special emphasis on deformation modes and oxidation, Eng Fail Anal, **16(8)** (2009) 2668-2697.
18. H. Zhou, H. Harada, Y. Ro, I. Okada, Investigations on the thermo-mechanical fatigue of two Ni-based single-crystal superalloys, Mater Sci Eng A, **394(1-2)** (2005) 161-167.

Design and experimental validation of hydrogen trapping features in Ni model alloys.

Aman Prasad[1,2], *Alixe Dreano*[2], *Laurent Couturier*[1], *Frédéric Christien*[2], *Franck Tancret*[1]

1. *Nantes Université, Institut des Matériaux de Nantes – Jean Rouxel (IMN), CNRS UMR 6502, 2 rue de la Houssinière, BP 32229, 44322 Nantes Cedex 3, France*
2. *Mines Saint-Etienne, Univ Lyon, CNRS, UMR 5307 LGF, Centre SMS, F - 42023 Saint-Etienne France*

Presence of hydrogen in nickel alloys can lead to embrittlement of the alloys, causing catastrophic failure. One way to circumvent this is by designing alloys with features that traps hydrogen. Most of the phases formed in Nickel alloys leads to an increase in hydrogen embrittlement. However, MC carbides and γ' precipitates with high γ/ γ' lattice misfit have been evidenced to trap hydrogen in austenitic steels. To experimentally study this in nickel alloys, nickel alloys containing only TiC carbides or γ' precipitates with tailored γ/ γ' lattice misfit were designed using a combination of computational thermodynamics, genetic algorithm multi-objective optimization, and physical models. These alloys were designed such that the phases can be dissolved at high temperatures and precipitated by heat treatment to quantify the role of these features in hydrogen trapping. After designing, the alloys were synthesized in the laboratory. The alloy with TiC carbides was studied with and without the presence of precipitates using electrochemical permeation and thermal desorption spectroscopy. Further, a local equilibrium approach was used to fit the experimental permeation and TDS curves and extract the trapping parameters (i.e. trapping energies and trap densities). Finally, the efficiency of the designed model alloys to control hydrogen trapping will be discuss in the light of experimental and numerical results.

Integrated corrosion resistance index for biomaterials

Camila D. R. Barros, Federal University of Rio de Janeiro (UFRJ), Rio de Janeiro/Brazil; Elisa J. Kassab, Federal University of Rio de Janeiro (UFRJ), Rio de Janeiro/Brazil; José Antônio C. Ponciano Gomes, Federal University of Rio de Janeiro (UFRJ), Rio de Janeiro/Brazil

Abstract

Corrosion resistance is a crucial requirement for a suitable host response during the service life of biomaterials [1-10]. Although for some specific applications the dissolution kinetics can play an important role, as in the case of temporary devices, high corrosion resistance is a basic requirement for biomaterial used by permanent devices [1]. The selection of alloys for biomedical applications requires excellent mechanical and chemical properties, together with non-cytotoxicity characteristics, making the material suitable for the biological environment. For orthopedics, vascular, and dental applications several alloys types can be selected, including stainless steel, silver-palladium, gold and gold-palladium, nickel-chromium, cobalt-chromium-molybdenum, nickel-titanium, titanium alloys, and commercially pure titanium [1,2]. The corrosion resistance can be influenced by the chemical composition, amounts of trace elements or impurities, processing route, microstructure, and surface conditions (morphology and composition). Besides the basic characteristics of the metallic material, the environment properties, which means composition, pH, temperature, and oxygen dissolved, will define the corrosion resistance achieved [1]. In the case of stainless steel based on their compositions, the correlation amount of Cr, Mo, and N elements allowed to establish an index for corrosion behavior expressed by the pitting resistance equivalent number (PREN), which is applicable for chloride-containing environments [1-4]. However, PREN index does not consider the composition of the environment in contact with the alloy. The corrosion resistance of biomaterials can be assessed by parameters obtained through electrochemical methods as OCP (open circuit potential) and anodic polarization results [1]. The present work describes one corrosion resistance index proposal, based on parameters obtained from electrochemical tests carried out in body fluid simulated solutions. For the formulation of the corrosion resistance index, the database of investigations carried out by our research group from 2003 to the present was used [5-10]. Results include stainless

steel, silver-palladium alloys, gold alloys, nickel-chromium alloys, cobalt-chromium-molybdenum alloys, nickel-titanium alloys, commercially pure titanium, and titanium alloys. In addition, studies in the literature that reports the same selected parameters for similar alloys are also considered.

References

1. N. Eliaz. Materials (2019) 12, 407.
2. Y. Yoo, S. Jang, K. Oh, J. Kim, Y. Kim. J. Biomed Mater Res Part B: Appl Biomater(2008) 86B:310-220
3. D. Mareci, G. Neomti, N. Aelenei, C. Bocanu. European Cells and Materials (2005) 10
4. M. Tattimani, M.C.Y., B. Reddy, S.B. Badi. Journal of Advanced Scentific Reserarch (2021) 12, 2.
5. E. Kassab, C.D.R. Barros, P.G. Silva, L. F. Silva, J.A.C. Ponciano Gomes. Journal of Materials Engineering and Performance (2020)
6. C.D.R. Barros, J.A.C. Ponciano Gomes. Materials Research (2021) 24(2) e20200369
7. C.D.R. Barros, J.C. Rocha, B.F.Braz, R.E. Santelli, J.A.C.P.Gomes. Int. J. Electrochem. Sci. (2020) 15. 394 – 411.
8. C.D.R. Barros; J.A.C. Ponciano Gomes. Journal of the Mechanical Behavior of Biomedical Materials (2020) 112, 104015
9. C.D.R. Barros, J.C. Rocha, J.A.C. Ponciano Gomes. Journal of Bio- and Tribo-Corrosion (2020) 6:117
10. C.D.R. Barros, J.C. Rocha, J.A.C. Ponciano Gomes. Journal of Bio- and Tribo-Corrosion (2021) 7:73

Use of modified NiTi alloys for biomedical applications

Elisa Kassab, Camila D.R. Barros, José Antônio C. P. Gomes, Federal University of Rio de Janeiro (UFRJ), Rio de Janeiro/Brazil;

Nickel titanium (NiTi) based alloys are very suitable to manufacture a wide range of biomedical devices, such as orthodontics and endodontics components, self-expanding stents, and implant devices. Alloying a third or a fourth element to the NiTi alloy is na alternative commonly considered to improve the mechanical properties, adjust critical transformation temperatures or promote adequate radiopacity. This work aims to make a review of the performance of modified NiTi alloys, considering the advantages of adding new elements and the consequences of it, especially regarding the corrosion resistance in physiological environments.

The addition of copper (Cu) to NiTi alloys can be very beneficial in terms of mechanical properties by narrowing the stress hysteresis in the stress-strain curve and stabilizing the superelasticity characteristics under cyclic deformation [1]. The poor radiopacity of NiTi can be improved by alloying with a high-density ternary element, such as tantalum (Ta), platinum (Pt), or palladium (Pd) [2]. Regarding the effects on the transformation temperatures of NiTi-based alloys, the addition of Cu, iron (Fe), vanadium (V), cobalt (Co), and chromium (Cr) reduces them, while the addition of hafnium (Hf), Ta, Pd, Pt, and gold (Au) increases the transformation temperatures of NiTi alloys [3].

Despite the many advantages presented by modified NiTi alloys, the addition of ternaries and quarternaries elements to the alloy can change the nature of the oxide film and affect the corrosion resistance of such alloys. Metallic elements deriving of the third element addition were found whitin the TiO_2 film of NiTiCu and NiTiPd alloys [4]. An increase in localized corrosion susceptibility was observed when Cu, Fe, Pd, Co, and Cr were added as ternary elements [4,5].

[1] Gil, F. J., Planell, J. A. (1999). J Biomed Mater Res, 48(5), 682-688.

[2] Baker, H. L. (2019). Doctoral dissertation, University of Birmingham.

[3] Zarinejad, M., Liu, Y. (2008). Adv Function Mat, 18(18), 2789-2794.

[4] Kassab, E., et. al. (2014). Mater Corr, 65(1),

[5] dos Reis Barros, C.D., Gomes, J.A.D.C.P. (2020). J Mech Behav Biomed Mater, 112, 104015.

A stochastic model for high-temperature corrosion in nickel-based superalloys

Federico Antonelli, Cranfield University, Cranfield, United Kingdom
Stefano Mori, Cranfield University, Cranfield, United Kingdom
Joy Sumner, Cranfield University, Cranfield, United Kingdom
Roger Wells, Siemens Energy, Lincoln, United Kingdom
Neil Chapman, Siemens Energy, Lincoln, United Kingdom
Nigel Simms, Cranfield University, Cranfield, United Kingdom

Abstract

Gas turbines have been extensively used in aviation and power generation since the first part of the 20th century. Despite their successes, internal components such as vanes and blades can be subjected to a form of degradation known as high-temperature corrosion or hot corrosion, which is detrimental to their respective service lives. This degradation mechanism occurs when components come into contact with alkali compounds derived from the fuels or external environments. Broadly speaking, compounds such as sodium sulphates melt because of high temperatures and attack metals by damaging thermal barrier coatings and depleting oxide scales. Predictive models of hot corrosion are needed, however the creation of a deterministic model has not proved to be practicable. This is because corrosion damage depends on many variables such as changes in gas and metal temperatures, gas partial pressures, gas composition, materials' characteristics, etc. Cranfield University has developed an extensive database from accelerated hot corrosion laboratory tests in which nickel-based superalloys have been exposed to a variety of conditions (~500-1050 °C; 50-10,000 ppm SO_X; 50-10,000 ppm HCl; 0-100 µg/cm^2/h of various salt mixtures; up to 1000h exposure, etc.). Metal loss data have then been obtained using dimensional metrology to get cumulative distributions of metal loss (with and without internal damage). These datasets have formed the basis for predictive metal loss modelling development. This paper reports the development of a new stochastic model of hot corrosion degradation. Data were treated as random variables and the time evolution has been predicted by using the information contained in the experimental data. The model, which produces realistic predictions, has been validated against experimental data and is consistent with the underlying physics of the system.

Effect of Anodic Behavior of Al Alloy on Galvanic Corrosion Resistance of AA6016/Steel Couple in Chloride Environment

Mariko Kadowaki [1], Hideki Katayama [1], Masahiro Yamamoto [2]

1: National Institute for Materials Science (NIMS), Tsukuba, Japan

2: Tohoku University, Center for Fundamental Research on Nuclear Decommissioning, Sendai, Japan

Background

Because of the demand for reducing car-weight and CO_2 emission, the use of multi-material structures of aluminum alloys and steels has been increased. However, the galvanic corrosion becomes serious problem at the joint parts. In this study, the galvanic corrosion behavior of aluminum alloy AA6016/ carbon steel SM490A couple was investigated in NaCl solutions.

Experimental conditions

AA6016 Al-Mg-Si alloy (0.99 mass% Si, 0.15 mass% Fe, 0.49 mass% Mg) and SM490A carbon steel (0.15 mass% C, 0.02 mass% Si, 0.85 mass% Mn) sheets were used. Galvanic corrosion tests were conducted in NaCl solutions. The concentration of NaCl was varied from 0.05 to 5 wt.%. In addition to the experiments, potential and current distributions during galvanic corrosion were simulated by finite element method (FEM) using COMSOL Multiphysics® software.

Results

According to the galvanic current values measured during immersion in NaCl solutions, it was found that AA6016 and SM490A were basically anodic and cathodic sites, respectively. The galvanic corrosion behavior of AA6016/ SM490A couple depended on NaCl concentration. At high NaCl concentration, some localized corrosion initiated on AA6016 while the surface of SM490A was almost not corroded. On the other hand, at low NaCl concentration, both AA6016 and SM490A surfaces were severely corroded. The results of FEM simulation indicated that the change in the galvanic corrosion behavior was attributed to the change in the anodic polarization characteristics of AA6016.

Kinetics of the oxygen reduction reaction on passive films formed Fe-Cr alloy

Ying Wang[1], Daniel John Blackwood[1], Man-Fai Ng[2], [1]National University of Singapore, Singapore, [2]Institute of High Performance Computing, Agency for Science, Technology and Research, Singapore*

The role of stainless steel in the industry is still of considerable significance and are presently irreplaceable. However, stainless steels are vulnerable to localized pitting and crevice corrosion. In the case of pits, these can re-passivate if the oxide film can repair itself prior to acidification of the occluded pit solution exceeding a critical threshold value. The rate of acidification is partly controlled by the supply of cathodic current available to drive metal dissolution within the active pit, with this cathodic current predominately coming from the reduction of dissolved oxygen at the passive film/ electrolyte interface.

The efficiency of oxygen reduction reaction (ORR) on the passive film is partially determined by the composition and conductivity of the oxides on the metal's surface. In this study, the evolution of the passive films on a series of Fe-Cr alloys ($Fe_{85}Cr_{15}$, $Fe_{80}Cr_{20}$, $Fe_{75}Cr_{25}$, $Fe_{50}Cr_{50}$ and $Fe_{25}Cr_{75}$) manufactured by the arc-melting. Results from rotating disc studies conducted in 0.1 M NaOH suggested that mixed Fe/Cr oxides were more favorable for ORR than either pure Fe or pure Cr oxides. This finding is supported by DFT calculations that $FeCr_2O_4$ is a better catalyst for ORR than Fe_2O_3 and Cr_2O_3.

This work may provide a different perspective to elucidate the formation and breakdown of the passive oxides and the subsequent development of localized corrosion. Indeed, it may one day be possible to tune the passive films on high-entropy alloys or during additive manufacturing process to minimize the kinetics of the ORR and thereby increase the likelihood of pit re-passivation.

Corrosion performance of 4xxx aluminium alloy with high scrap content for construction applications

P. Alexopoulou[1], A. Flampouri[1], M. Koklioti[1], E. Aivazoglou[1], Th. Tzevelekou[1], G. Kalkantzis[2], G. Ziogas[2], A. Mavroudis[2]

[1]ELKEME - Hellenic Research Centre for Metals S.A. [2]Elval, Aluminium Rolling Division of ElvalHalcor S.A., 61st km Athens-Lamia Nat. Road, GR 32011, Oinofyta, Viotia, Greece

Recycling is a key enabler for the aluminium industry to fulfill sustainability commitments, as it minimizes energy consumption, greenhouse gas emissions and waste generation. Expanding the range of alloy applications, which can absorb high percentage of scrap for their production, supports the transition towards a low carbon and resource efficient economy, yielding multiple environmental and economic benefits for the manufacturers and end users. Examining products performance prior to market launch is of vital importance to ensure their quality and longevity.

In this work, the corrosion performance of 4xxx alloy aluminium sheets produced using 100% scrap and coated with various paint systems, for general construction products was studied. Selected samples were subjected to Filiform Corrosion test and Acetic Acid Salt Spray test and evaluated according to EN 1396. The effect of critical alloying elements content on the obtained corrosion behaviour was also assessed. Microstructure examination using optical and scanning electron microscope of the corroded samples was performed. Respective phases were further calculated by Thermo-Calc software.

According to the results, the coated 4xxx aluminium sheets exhibited good corrosion resistance, yielding similar behaviour compared to corresponding coil coated systems of 3xxx alloy, typically used for this application. Microstructural examination revealed that α-Al(Mn,Fe)Si and (Si) precipitates were dominant particles. The corrosion mechanism is associated with the nature, size and distribution of the intermetallic particles in the aluminium matrix and the respective electrochemical potential difference. Chemical composition can be adjusted to support improved performance. Present research demonstrates that there is potentially space to expand the use of 4xxx alloy with increased scrap content up to 100% in construction applications, contributing to sustainable development without compromising products quality and durability.

Study of metallic-aqueous interfaces from a multiscale approach and its application to corrosion inhibition

Ernane de Freitas Martins[a,b]; Ivan Cole[b]; and Pablo Ordejón[a]

[a] Catalan Institute of Nanoscience and Nanotechnology, Barcelona/Spain

[b]RMIT University, Melbourne/Australia

Metallic surfaces in contact with air or aqueous solutions are prone to corrosion, a natural process that can lead to many dangerous problems. That can be mitigated by several corrosion inhibition (CI) technics where the use of inhibitor compounds to cover the metallic surface stands out. Understanding the processes occurring at the metallic-inhibitors-aqueous solution interfaces is crucial in CI since it affects the reactivity of inhibitors and their movement at the surfaces, besides helping in understanding the double layer formation and polarization of the surfaces. Those processes are usually related to atomistic phenomena, and molecular modelling emerges as an excellent tool. Here we propose using a quantum mechanics/molecular mechanics (QM/MM) approach to address the metallic-aqueous interface, providing a good balance between accuracy and computational cost. We aim to use a multiscale QM/MM approach to investigate the Au-H_2O interface, comparing the results with those widely reported in the literature for this system using methods with less accuracy. We will also provide a benchmark analysis using ab initio molecular dynamics (MD) to validate the QM/MM method proposed, making possible the use of this method to investigate the interaction between other metals relevant to corrosion inhibition, the environment, and the inhibitors compounds. We tested two sets of Lennard-Jones parameters reported in the literature to describe the metal-water interaction using QM/MM MD and compared their performance against ab initio MD for different supercells. Our results show that the layering of water above the metal is very sensitive to the parameters used, which may substantially affect the metal-water interaction. The mTIP3P water model improved the results, satisfactorily reproducing our benchmark ab initio calculations. Our findings show that the proposed approach can be used to describe the structural properties of the Au-H_2O interface at a reduced computational cost and satisfactory accuracy, paving the way for applications in CI to explore the underlying mechanisms involved in the interfacial processes.

Construction of a data driven corrosion risk model as a novel method for corrosion management

Wikke Witteveen, Antwerp Maritime Academy, Antwerp, Belgium
Joeri Horvath, Antwerp Maritime Academy, Antwerp, Belgium
Kris De Baere, Antwerp Maritime Academy, Antwerp, Belgium
Shahin Gelareh, Dept. Réseaux et Télécom, IUT de Béthune, Université d'Artois, Béthune, France
Geert Potters, Antwerp Maritime Academy, Antwerp, Belgium
Jeroen Tacq, SIRRIS, Zwijnaarde, Belgium

Corrosion is an often unrecognized, complex phenomenon, caused by non-linear interactions of various physicochemical causes (temperature, pH, salinity, oxygen concentration...), aggravated by even less understood bacterial activities. Nevertheless are the damages due to this “phenomenon” daunting, ranging from an average 3.8% of the gross domestic product globally, to even 19.9% in maritime surroundings. To obtain an operational predictive model, a series of long-term lab tests were performed, measuring instantaneous corrosion rates (using LPR sensors) and correlating the outcomes with the physicochemical conditions in the environment. A number of expected correlations among environmental parameters and between environmental parameters and corrosion rate have been confirmed. Other correlations such as between dissolved oxygen and corrosion rate could not be reproduced. These laboratory test data have provided indispensable insight in the way in which sensors, especially LPR corrosion sensors, respond to long-term exposure to a changing environment. In addition, the importance of and correlations between the environmental parameters is better understood. Furthermore, several data preprocessing strategies were compared, leading to the adoption of a Savitsky-Golay filter. Afterwards, the corrosion data as well as the physicochemical conditions provided a basis to develop a machine learning approach to create a predictive model of corrosion in a maritime and industrial environment. This model is currently being validated in a number of field demonstrations within the Interreg 2 Seas project SOCORRO. Together with the insights gained in these demonstrations, the predictive model will provide further insights in the pros and cons of long term use of sensors and how to interpret them in function of corrosion management strategies.

Corrosion inhibitor structures for automotive steel - A computational chemistry perspective

Steffen Jeschke[1], Ivan S. Cole[1], Philipp Eiden[2], Ratan K. Mishra[2], Peter Deglmann[2], Jan N. Gorges[2], Christian Rein[2], Patrick Keil[3]

[1] Manufacturing Materials and Mechatronics Engineering, School of Engineering, RMIT University, Melbourne VIC 3001, Australia
[2] BASF SE, Carl-Bosch-Strasse 38, 67056 Ludwigshafen am Rhein, Germany
[3] BASF Coatings GmbH, Glasuritstrasse 1, 48165 Muenster, Germany

With increasing awareness of sustainability issues, the development of organic and environmentally friendly corrosion inhibitors is in high demand. Most of the published screening studies predominantly utilise quantum chemical methods based on density functional theory (DFT) together with statistical or machine learning approaches to reveal quantitative structure-property relationships (QSPRs). However, datasets used in such investigations so far have often been limited to a small confined chemical space of potential lead structures and have neglected the structural diversity of the metal surface leading to very generalised, potentially even oversimplified predictive models. Experimentally, the complexity of environmental aspects like temperature, salinity, pH and other factors are also often simplified, making it complicated to derive a mechanistic understanding of inhibition or guidelines for corrosion inhibitor selection.

In the automotive industry, steel has been an important material for body construction over several decades. Challenged by the regulatory demands for safer, cleaner, and more fuel-efficient vehicles, numerous steels of different composition and mechanical properties are used, predisposing resulting multi-substrate assemblies to localised corrosion. Zn-based coatings are applied via galvanisation processes for corrosion protection. However, additional organic corrosion inhibitors are required to provide active protection over a longer lifetime.

Here, we present computational modelling insights of a comprehensive experimental study including so far about 150 organic heterocyclic small molecules covering a broad chemical space. The experimental electrochemical measurements are conducted under different conditions of pH and salinity, with fully immersed samples as well as droplet set-ups. In order to develop QSPR-models, computational methods are employed using DFT-based methods such as the conductor-like screening model for real solvents (COSMO-RS) to collect molecular descriptors for the organic inhibitor candidates. Additionally, the interactions between the steel surface and the inhibitor is modelled to allow a more detailed understanding of mechanisms.

A multiscale approach to bias dependent electrochemical processes at metallic-aqueous interfaces.

Jose Maria Castillo-Robles[a,b], Ernane de Freitas Martins[a,b], Pablo Ordejón[a], Ivan Cole[b]

[a]ICN2, Barcelona/Spain; [b]RMIT University, Melbourne/Australia;

Corrosion is a major problem in the industry, and to mitigate it, toxic inorganic compounds are often used as corrosion inhibitors. However, over the last few years, they are being replaced by more environmentally friendly compounds. The fundamental mechanism determining their inhibition performance are still far from understood. Computational simulations can provide us important insights into those mechanisms allowing for a detailed analysis of the metallic-inhibitor-aqueous interface. Nonetheless, the actual simulations reported in the literature present some main gaps in their works, such as 1) the use of too simple surface models, 2) neglect of solvent, 3) absence of bias effects, and 4) absence of cathodic/anodic reactions. To address precisely those gaps, an innovative approach commonly used in electronic transport calculations is proposed. A setup where the aqueous solution and inhibitors are sandwiched by two electrodes kept under a bias voltage will be used to address the structural and dynamical properties of the involved interfaces. As preliminary results, we investigated the adsorption of 2-mercaptobenzimidazole (MBI) on Cu(111) surfaces. The relative stability of MBI and the Cu(111) surfaces were evaluated using density functional theory (DFT). To consider the vdW interactions, Grimme's semiempirical dispersion model (DFT-D2) is used throughout the calculations. All calculations were carried out in the SIESTA code. Several adsorption sites of MBI on the Cu surface were tested, leading to hollow Cu sites as the most stable ones, in terms of the binding energy (E_B). To sample different coverages at the surface, it was considered several slabs shapes, with different superficial areas and exposed Cu atoms. After that, the calculations will be extended to include the effect of the electrode potential on both adsorbed inhibitors and metallic surfaces. That can be achieved by combining DFT and the non-equilibrium Green's functions (NEGF) formalism, using TranSIESTA module. A quantum mechanics/molecular mechanics (QM/MM) method will be applied to fully account for the solvent effects, including a realistic number of solvent molecules in the simulations, using the QM/MM module in SIESTA.

Interpretation of ENA data from accelerated exposure of modified ZRP based on modelling of coating electrical properties as related to corrosion of the substrate

Boleslav Eremias[1], Lubomir Mindos[1], Libor Turek[1]

[1]SVUOM Ltd., Prague/Czech Republic, eremias@svuom.cz

Abstract
The possible differences in the protective performance of modified ZRP with the same OPVC (40 vol. %) but with different type of fillers were confirmed by new interpretation of ENA data in combination with single frequency (1 kHz) impedance test results. By this approach changes of resistivities and dielectric constants (identified on tested coating systems in the end of accelerated exposure) can be related to delamination tendency of given type of coating in 0.05 M NaCl after 168 hrs of exposure. It was found the electrical properties of tested coting systems were changed with immersion time rather differently for combination of Zn dust with MIO or aluminium type of fillers. Water/electrolyte uptake determination based on modelling of coating electrical properties by the above-mentioned approach provided evidence of different polymer changes during exposure for combinations of Zn/MIO or Zn/Al particles distributed within this type of coatings.

Keywords Modified ZRP; ENA; SIFT; water uptake; interfacial delamination.

Introduction

Opposite with epoxy zinc rich coatings (ZRP) the modified type of ZRP with partial substitution of Zn by different type of fillers have not yet been widely studied, especially concerning of water uptake effect on deterioration in conditions of the use for tests low electrolyte (NaCl) concentration. In fact, for evaluation of barrier properties of mentioned type of coatings it should be remembered the more dilute the salt solution the greater can be the water uptake by the paint and the earlier the onset of paint breakdown [1]. As recent findings show delamination kinetics of four modified ZRP with the same OPVC (65 vol. %) investigated by means of ENA during immersion tests in 0.05 M NaCl seems to be really comparable with water diffusion trough the coating characteristics [2]. In this work an estimation of delaminated corroding area A_d at the steel/coating interface was made based on increase of double layer capacitance c_{dl} data obtained by analysis of noise impedance spectra at different times of exposure. As tested coatings had been previously examined on water uptake in 0.05 M NaCl by means of capacitance measurements water diffusion trough the coating characteristics were calculated and compared with A_d. This approach can be improved by new interpretation of ENA data in combination with single frequency (1 kHz) impedance test (SIFT) results [3]. In this case differences in water uptake estimated by SIFT can be used to provide information concerning the coating capacitance C_c and the coating resistance (pore resistance) R_{po}. If during exposure for tested modified ZRP no swelling (volume and area increase) is observed, capacitance should be considered to be proportional to product $\varepsilon.\varepsilon_0$ (ε is the coating dielectric constant, ε_0 is the permittivity constant for vacuum). On the other hand, for R_{po} values obtained by SIFT Haruyama et al. [4] suggestions (that the decrease of R_{po} and the increase of c_{dl} with exposure time are due to increase of delamination area A_d) can be used for monitoring of coating resistivity ρ if value of A_d («A) is known (A = total specimen area).

Considering possible similarity of EIS spectra with noise impedance spectra at low and intermediate frequencies procedure for determination of ρ and ε by combination of ENA data with SIFT data can so also be used for possible calculation of the break point frequency f_b and minimum frequency f_{min} with the use of Mansfeld and Tsai [5] analysis. It was shown recently if those effective values for f_b and f_{min} are used then the ratio $(f_b - f_{min})/(f_b/f_{min})$ for Zn and MIO pigmented epoxy coating tested in 0.05 M NaCl can be proportional to absorption of water in this coating [3]. As mentioned above ratio is combination of the relations between two types of parameters (f_b and f_{min} dependent on A_d and ρ while f_b/f_{min} is dependent only on A_d) it becomes at longer stage of exposure dependent on additional absorption of water in defects formed at the filler/binder interface. By comparing of this ratio values in the end of exposure can so be information on this effect obtained even for ZRP coatings with reduced Zn content, but modified by MIO or Al additions improving barrier properties.

In order to prove connection of this effect with expected lower coating resistance against electrolyte permeation into the coating/metal interface for the MIO particles compared to Al one [6] two modified ZRP with Zn/MIO or Zn/Al combinations were chosen for demonstration of possible application of this approach. Apart of electrochemical measurements more advanced microscopic method was used for metallographic analysis of tested coating systems. EDX mapping and structure (SEM-SE image) of cross-sections were chosen for this purpose.

Experimental

Two types of modified Zn pigmented epoxy coatings with partial replacement of Zn by other type of fillers were prepared with the same value of OPVC = 40 vol. % but with different polymer matrix components.

Table 1 – Characteristics of ZRP modified by different type of fillers

sample	OPVC (vol. %)	vol. % ratio Zn/filler	filler	binder	hardener
AKAl 117	40	82:18	Alumstapa 2NL	Epicote 1010	Epicure 3115
AKM 28	40	5:5	Miox SF	CHS Epoxy 222	Telalit 160

While for preparation of AKAl 117 were used Al particles (supplied in paste by Eckart GmbH, Germany) mixed with Zn dust and epoxy resin components, for preparation of AKM 28 was used as filler Miox SF (supplied by Kartner Montan Industrie, Austria) mixed with Zn dust and epoxy resin components. For dissolution of mixture with given type of components dissolver Netzsch and cooling water condition were used. Zn dust for preparation of both coatings was 4P16 (supplied by UMICORE Zinc Alloys and Chemicals Co., Belgium). Both tested coatings were applied by a spreader bar to steel C4Q panels previously polished and degreased. The average thickness of dry film was 55 μm.

Immersion tests using ENA for tested coatings on steel substrate specimens were performed with use of the same experimental set-up as described earlier [7]. The potential and current noise (ENP and ENC) values (for given data set measured for given immersion time) were collected for measurement periods of 600 s with sampling rate of 20 Hz (12 000 points for period) using GAMRY ESA 410 software in the end of 168 hrs exposure test in 0.05 M NaCl.

These data were used to obtain MEM noise impedance spectrum characteristics (MEM curves) providing information about c_{dl} values as well as A_d values in the end of immersion time. For this purpose, A_d values were estimated from c_{dl} values measured at given time t (μF) by means of empirical equation $A_d = c_{dl}(t)/20$ if 20 is the typical value of the bare steel double layer capacitance adopted to estimate the underlying metallic active interface (μF/cm^2) [8]. In addition to it immediately after EN measurements in the end of exposure single frequency (1 kHz) impedance test with the use of HIOKI LCR HITESTER was performed to estimate values of R_{po} and C_c for the same time of exposure.

Results and discussion

It is believed for tested types of coatings MIO particles can improve coating resistance against disbonding by increasing the coating resistance against electrolyte permeation but are not so effective as Al particles causing during exposure $Al(OH)_3$ precipitation on the steel surface and inside coating pores [6]. As it can be seen by comparing Noise Impedance spectra (MEM curves) obtained for tested coating systems in the end of exposure (Fig. 1) this effect seems to be confirmed. The same conclusion concerning this effect can be made by comparing values of c_{dl}, A_d, R_{po} and C_c together with calculated values of ρ and ε for tested coating systems in the end of exposure (Table 2).

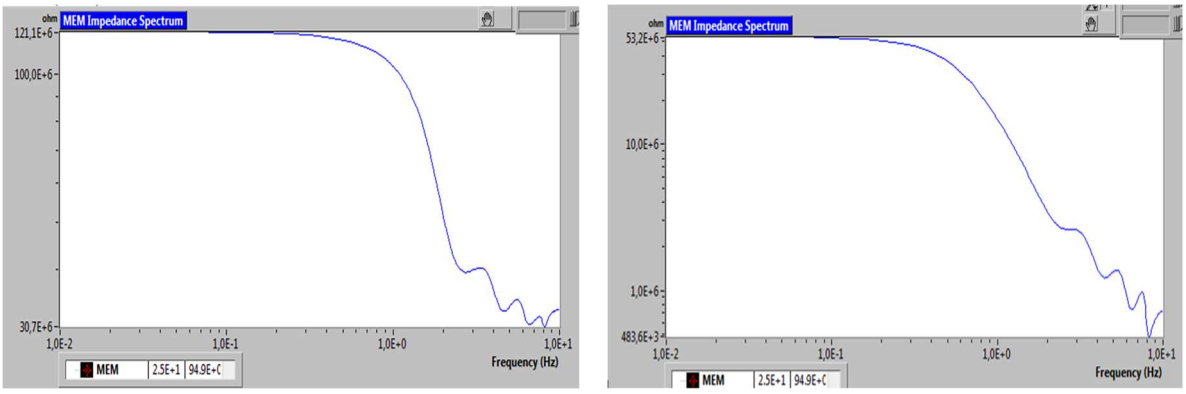

Figure 1: Noise Impedance spectra for AKAl 117 (left) and AKM 28 (right) at 168 hrs of exposure in 0.05 M NaCl

Table 2 – Values of c_{dl}, A_d, R_{po} and C_c together with calculated values of ρ and ε as estimated for tested coating systems in the end of exposure

sample	c_{dl} (F)	A_d (cm^2)	R_{po} (Ω)	C_c (F)	ρ (Ω.cm)	ε
AKAl 117	9,38 E-10	4,69 E-05	37,24 E06	47,94 E-12	3,17 E05	7,80
AKM 28	8,03 E-09	4,01 E-04	1,25 E06	156,27 E-12	1,28 E05	25,42

Considering the additional absorption of water at defects formed at the filler/binder interface this occurs during exposure mainly in AKM 28 sample. For AKAl 117 and AKM 28 the ratio $(f_b - f_{min})/(f_b/f_{min})$ values with use of Mansfeld and Tsai analysis can be calculated to confirm also suggestion of larger deterioration connection with delamination tendency for tested coating systems (Table 3).

Table 3 – Values of the ratio $(f_b - f_{min})/(f_b/f_{min})$ as estimated with use of parameters involved in Table 2 for tested coating systems in the end of exposure

sample	ratio $(f_b - f_{min})/(f_b/f_{min})$ (Hz)
AKAl 117	15.60
AKM 28	69.71

From Table 3 can be seen this suggestion is quite well confirmed by presented data. In fact, found differences in the ratio $(f_b - f_{min})/(f_b/f_{min})$ can also be compared with previously found differences in values of the volume of water in capillaries ($x_{v,cap}$) and the volume of water in polymer solution ($x_{v,\,sol}$) estimated for tested coating systems from capacitance measurements (Table 4).

Table 4 – Values of $x_{v,cap}$ and $x_{v,\,sol}$ calculated from previously obtained capacitance vs. time plots during 168 hrs exposure of tested coating systems in 0.05 M NaCl with the use of Touhsaent and Leidheiser analysis [9]

sample	$x_{v,cap}$ (vol. %)	$x_{v,\,sol}$ (vol. %)
AKAl 117	2.54	5.85
AKM 28	6.24	26.19

From Table 4 can be seen that differences in $x_{v,\,sol}$ values found for both tested coatings are comparable with differences in the ratio $(f_b - f_{min})/(f_b/f_{min})$ values. In the case of AKM 28 the start of additional absorption of water during exposure means also the start of some Cl^- ions penetration into coating and possible redistribution of Zn and MIO particles in polymer matrix. Both effects can be confirmed by comparison of differences in the structure for exposed tested coating systems (Figure 2).

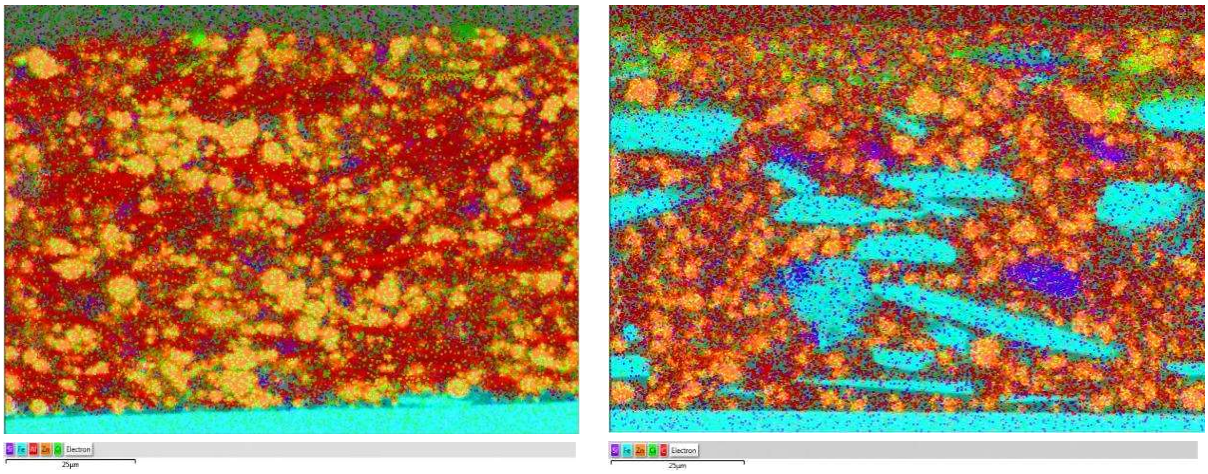

Figure 2: EDX mapping and structure (SEM-SE image) of cross-sections for AKAl 117 (left) and AKM 28 (right) after exposure

Conclusions

By new interpretation of ENA data in combination with SIFT results was checked information concerning of water uptake effect on deterioration of two modified ZRP with Zn/MIO or Zn/Al combinations at OPVC = 40. It was found this method based on modelling of coating electrical properties related to corrosion of substrate can help in study of water uptake and interface delamination effects on coating deterioration.

Acknowledgements

This paper was prepared with financial support of DKRVO project from MPO ČR.

References

1. D.M. Brasher, T.J. Nurse, J. Appl. Chem., **9** (1959) 96.
2. B. Eremias, L. Mindos, L. Turek, L. Hochmannova, EUROCORR 2019.
3. B. Eremias, L. Mindos, L. Turek, METAL 2022.
4. S. Haruyama, S. Asari, T. Tsuru, Electrochem. Soc. Interface, **87** (1987) 197.
5. F. Mansfeld, C.H. Tsai, Corrosion, **47** (1991) 958.
6. B. Nikravesh, B. Ramezandeh, A.A. Sarabi, S.M. Kasiriha, Cor. Sci., **53** (2011) 1592
7. B. Eremias, L. Mindos, L. Turek, EUROCORR 2013.
8. C.I. Elsner, E. Cavalcanti, O. Ferraz, A.R. Di Sarli, Progress in Org. Coating, **48** (2003) 50.
9. R.E. Touhsaent, H. Leidheiser, Jr., Corrosion, **28** (1972) 435.

Advances in understanding the anomalous alkalinization of the electrolyte during the anodic polarization of Mg

R. Montoya, A. Ortiz, J. Genescá.

PUNTA-UNAM, Apodaca N.L., Mexico

Experimental methods based on the collection of H_2 gas have been used to quantify the anomalous cathodic reaction during Mg alloys dissolution. However, the hydrogen evolution could be proportional to the OH^- production.

The objective of this work is to investigate if during the anodic polarization of Mg alloys determining the propagation rate of alkaline profiles is really equivalent to the collection of H_2 .

Since the important convective effects generated during the corrosion of Mg alloys could be even turbulent, it becomes extremely difficult to measure (or modeling) the pH evolution into the electrolyte while the dissolution takes place. To avoid the convective effects into the electrolyte, a gel instead of a liquid electrolyte was used. The gel electrolyte was doped with phenolphthalein in order to visually track the propagation of alkaline fronts generated during the galvanic corrosion of magnesium alloys. The propagation rate was obtained by tracking the evolution of the system through proper lens and image softwares to clearly distinguish the color borders.

The experimental setup presented here has the unique capability to simultaneously register the electrochemical behavior of magnesium alloys at several anodic over-potentials.

Findings proved an important conjecture made (but not proved) for some researchers in the past: an acidification process is present during the Mg dissolution. It was also demonstrated that such acidification is quickly neutralized by the water reduction reaction and a mechanism is provided.

Effect of delayed inhibitor supply on the local degradation and protection kinetics of IMs in AA2024-T3

Marlon Mopon Jr., and Santiago J. Garcia

Novel Aerospace Materials, Faculty of Aerospace Engineering, Delft University of Technology, Delft, Netherlands

Recent studies have reported on the de-alloying process of intermetallics present in AA2024-T3 beyond their reported relative anodic or cathodic potentials. Highly spaced and temporally resolved in situ optics provided information on the degradation kinetics and degradation steps of a range of intermetallics. Similarly, other studies have reported on the local interaction of Cerium and Lithium salts with IMs. In most corrosion inhibitor studies the metals are exposed directly to solutions with a certain inhibitor concentration, a case unlikely to happen in real applications when the inhibitors are embedded in the coating. In real life systems, the inhibitor at the desired concentration may take some time to be released. Little is therefore known about the inhibition and degradation kinetics of intermetallic when the corrosion inhibitor is supplied at different stages within the IM degradation process (i.e. activation, dealloying, trenching).

In this work, we study how the inhibitor (cerium nitrate) time-dependent availability with respect to the local corrosion process affects the local IM corrosion kinetics in AA2024. For this purpose we used a hyphenated optical-electrochemical technique that provides real-time optical and electrochemical (in this case electrochemical noise) information of local IM activity supported with ex-situ characterization such as SEM-EDX and Raman spectroscopy.

Improving phase-field models to simulate the aqueous corrosion phenomena

J. Amador[1], J.M. Vega[1], F. Varas[2], M. Lekka[1], E. García-Lecina[1]

[1]CIDETEC, Basque Research and Technology Alliance (BRTA), Po. Miramón196, 20014 Donostia-San Sebastián, Spain

[2]School of Aerospace Engineering, Universidad Politécnica de Madrid (UPM), Plaza Cardenal Cisneros 3, 28040 Madrid, Spain

Nowadays, numerical models at the mesoscale typically consider mass and charge conservation in the solid (i.e., metal) and electrolyte, separately, using electrode kinetics as a boundary condition. The main drawback is the presence of a sharp interface which requires a continuous re-meshing of the domain to simulate the interface motion. This significantly increases the computational cost, especially to simulate more complex and long-lasting situations.

Currently, one promising alternative are the phase-field models which are able to minimise the energy of the system by introducing an order parameter (it implicitly indicates the movement of the interface). These models were developed in metallurgy and have been successfully extrapolated to different fields such as corrosion science, establishing a thermodynamically coherent approach.

One of the first attempts by Mai et al.[1] simulated the pitting corrosion, where the corrosion phenomenon was controlled by metal cation diffusion. Recently, Ansari et al.[2] have added reactions occurring in the electrolyte, and considering Butler-Volmer kinetics. However, there are still certain limitations: (i) it is not fully realistic (especially regarding the introduction of the potentials), (ii) reactions such as the oxygen reduction one are not considered yet in the model, (iii) the model is not fully validated.

Therefore, this work proposes a further improvement to phase-field models for corrosion application (e.g., steel, stainless steel), addressing the limitations above and including the validation of the model with experimental results.

References

1. W. Mai, S. Soghrati, and R. G. Buchheit, *Corros. Sci.*, **110**, 157–166 (2016) https://www.sciencedirect.com/science/article/pii/S0010938X16301408.

2. T. Q. Ansari et al., *npj Comput. Mater.*, **4**, 38 (2018) https://doi.org/10.1038/s41524-018-0089-4.

Numerical contribution in Direct Current Voltage Gradient (DCVG) method for a reliable and quantified detection of coating defects on buried pipelines

David Garcia, CORROHM, Toulouse/France

Elie Sassine, CORROHM, Toulouse/France

Simon Deharo, CORROHM, Toulouse/France

Christophe Barthe, Trapil, Poissy/France

Raoul François, CORROHM, Toulouse/France

The DCVG (Direct Current Voltage Gradient) is a commonly used technique by oil and gas transporters during coating integrity inspection of buried pipelines. The main challenge exposed in this paper is to improve the estimation of the surface area of coating defects.

Traditional method consists in measuring the potential gradient using two electrodes along the buried pipeline, which is strongly modified at the coating defects level. In order to estimate their surface, a transversal gradient measurement is then performed and compared to the one generated by a metallic coupon of known dimensions placed on the soil surface and electrically connected to the buried pipeline.

This method is particularly effective in detecting the location of the various coating defects but the estimation of their surface remains unpredictable at this time.In this context, a large part of the error is due to the uncertainty in the offset distance that the operator shall adopt to measure the transversal gradient generated by the metallic coupon. This offset distance actually depends on a multitude of geometrical (metallic coupon surface, depth of the buried pipeline...) and physicochemical factors – as soil resistivity. It is for this reason that the estimation of the coating defects surface is particularly sensitive.

This article shows the relevance of 3D numerical simulation in taking into account these different parameters and perform a reliable estimation of the defects surface based on potential gradient measurements. Several experimental configurations are studied to demonstrate the robustness of this innovative approach.

Possibilities and Recent Advances in Respirometric Monitoring of Corrosion Rates

Michael G. Strebl, Mark P. Bruns, Sannakaisa Virtanen, Institute for Surface Science and Corrosion, Friedrich-Alexander Universität Erlangen-Nürnberg, Erlangen/Germany

Accurate measurement of the corrosion rate of metals and alloys is fundamental to study mechanisms of corrosion processes or the development of new corrosion protection measures. Recently, novel respirometric methods to monitor real-time corrosion rates in situ during atmospheric corrosion [1,2] and immersion [3] were established by the authors. The straightforward approach is based on monitoring the rate of the O_2 reduction reaction, the H_2 evolution reaction or both cathodic reactions simultaneously. The proposed methods range from advanced gravimetric experimental setups to closed manometric setups to sophisticated flow cell experimental setups. Any metallic material with any type of coating or surface modification can be studied with the introduced universal techniques.

The respirometric methods provide information that was not accessible previously. Corrosion rates can be monitored in real-time without interfering with the corrosion process. The methods prove to be sensitive enough to detect even low corrosion rates. Validation with independent mass loss measurements showed an excellent correlation. Furthermore, the corrosion rate and the relative contribution of the cathodic reactions can be followed in situ to study the effect of different exposure conditions during atmospheric corrosion and immersion. Especially for atmospheric corrosion, where electrochemical methods are difficult to apply, the respirometric approach opens up a new window to investigate corrosion processes. This includes to study in the lab the effect of wet-dry cycling, temperature, gas atmosphere and salt contamination in the context of atmospheric corrosion, accelerated testing and field exposure. On the other hand, biodegradable implant materials can be tested under realistic immersion conditions to determine the effect of electrolyte composition, temperature and flow on the corrosion rate and corrosion mechanism. Moreover, the respirometric approach was coupled with electrochemical measurements to add control over the current or potential of the electrode under investigation [4]. Precise decomposition of the net electrical current into partial currents is possible with this combined approach.

This presentation gives an overview of the different respirometric experimental setups. Example measurements are presented to highlight the opportunities afforded by the respirometric method. The latest results regarding respirometric monitoring during potentiodynamic polarization curves or during simultaneous EIS measurements will be shared.

[1] M. Strebl, S. Virtanen, Real-Time Monitoring of Atmospheric Magnesium Alloy Corrosion, Journal of The Electrochemical Society 166 (2019) C3001-C3009. https://doi.org/10.1149/2.0011911jes.

[2] M. Strebl, M. Bruns, S. Virtanen, Editors' Choice—Respirometric in Situ Methods for Real-Time Monitoring of Corrosion Rates: Part I. Atmospheric Corrosion, J. Electrochem. Soc. 167 (2020) 21510. https://doi.org/10.1149/1945-7111/ab6c61.

[3] M.G. Strebl, M.P. Bruns, G. Schulze, S. Virtanen, Respirometric In Situ Methods for Real-Time Monitoring of Corrosion Rates: Part II. Immersion, J. Electrochem. Soc. 168 (2021) 11502. https://doi.org/10.1149/1945-7111/abdb4a.

[4] M.G. Strebl, M.P. Bruns, S. Virtanen, Coupling Respirometric HER and ORR Monitoring with Electrochemical Measurements, Electrochimica Acta 412 (2022) 140152. https://doi.org/10.1016/j.electacta.2022.140152.

Effects of Microalloying on the local corrosion processes in High-Manganese Twinning-Induced Plasticity Steel

Temitope Olumide Olugbade, Chayanika Das, Annica Wetzel, Julia Witt, Ozlem Ozcan

Bundesanstalt für Materialforschung und -prüfung (BAM), Berlin, Germany.

Abstract

Delayed fracture and low resistance to corrosion especially under aggressive corrosive environment often limits the wide application of twinning-induced plasticity (TWIP) steel. To address this issue, the present work investigates the effect of microalloying on the corrosion properties of Fe-Mn-C-Al-Cr TWIP steel. Base and microalloyed TWIP steels were synthesized via arc melting process under argon atmosphere. Thermal homogenization treatments were performed by varying the temperature and duration to generate different microstructures. The macroscopic corrosion properties were investigated in 3.5 wt. % NaCl electrolyte at room temperature via potentiodynamic polarization and electrochemical impedance spectroscopy (EIS). Scanning electron microscopy (SEM), energy dispersive X-ray spectroscopy (EDX) and Scanning Kelvin Probe Microscopy (SKPFM) were used to investigate the correlation between the processing parameters and the resulting alloy microstructure and the electrical properties of the surface oxides. In situ atomic force spectroscopy (AFM) was used to investigate local corrosion properties especially with a focus on the effect of the homogenization treatments.

Our results indicate that microalloying is a successful strategy to improve the corrosion resistance of Fe-Mn-C-Al-Cr TWIP steels. Among different alloying elements, titanium has shown improvement of corrosion properties for both local and general corrosion. As the superiority of TWIP steels lies in their advantageous mechanical properties, this presentation will summarize the synergies and conflicts between different microalloying elements in terms of mechanical and corrosion properties.

Effect of passivation after additive manufacturing of titanium alloy on corrosion resistance and protein binding

S. Nikpour, Dept. Chemistry, The University of Western Ontario, Canada

M. Biesinger, Surface Science Western, The University of Western Ontario, Canada

Y. Hosein, ADEISS, The University of Western Ontario, Canada

D. Holdsworth, Dept. Medical Biophysics, The University of Western Ontario, Canada

Y. Hedberg, Dept. Chemistry and Surface Science Western, The University of Western Ontario, Canada

Titanium alloys such as Ti-6Al-4V (6 wt.% Al and 4 wt% V) are commonly used for dental implants and total joint replacements, including hip and knee, as they can offer high corrosion resistance and biocompatibility. The oxide layer is formed on the surface as soon as these alloys are exposed to air or water. Then, it hinders further metal oxidation (corrosion) and acts as a barrier against aggressive ions to access the bare metal surface. The chemical environment in the human body is complex and dynamic. Major corrosive factors are inflammatory conditions (oxidative, acidic), wear/micromotions, chlorides and complexing agents such as proteins. Interactions between proteins and metals in the formed surface oxide or as released metal ions can alter the corrosion behavior of metallic implants during their service life in multiple ways. The way implants are fabricated is also crucial. Increasingly, additive manufacturing (AM) is utilized for biomedical implants, as AM implants can be custom-shaped. Some of the AM companies, moreover, apply a standardized passivation process through immersion in nitric acid, according to ASTM F86-13, to increase the corrosion resistance of AMed implants. This study aims at understanding whether surface passivation after manufacturing AM Ti-6Al-4V has any effect on corrosion and metal release under benign and harsh physiological conditions, where the harsh environment simulates a crevice environment in a joint implant. We employed electrochemical methods to determine corrosion resistance, solution analysis by means of inductively coupled plasma mass spectrometry to determine the amount of released metals, and X-ray photoelectron spectroscopy to determine any changes in surface composition. It could be concluded that the passivation had a positive (corrosion-decreasing) effect on smooth (mirror-polished) but not rough (sand-blasted) surfaces of Ti-6Al-4V intended for implant materials.

Corrosion behavior of Al-based structurally complex alloys

Katarzyna Młynarek-Żak, Rafał Babilas,

Silesian University of Technology, Department of Engineering Materials and Biomaterials, Gliwice, Poland

Aluminum alloys with additions of transition metals (TM) such as Cr, Cu, Ni, Fe are increasingly studied group of materials. The presence of structurally complex alloy phases (SCAPs), including quasicrystals, was identified for some Al-(Cr, Cu, Ni)-Fe alloys [1,2]. The presence of such phases in the structure provides such as high electrical conductivity at elevated temperature, low thermal conductivity, high hardness, low friction, and good corrosion resistance, which can be used for modern and advanced applications, for example as blades in helicopter engines [3].

The aim of the study was to evaluate the corrosion behavior of the following alloys: $Al_{65}Cr_{20}Fe_{15}$, $Al_{71}Cr_{24}Fe_5$, $Al_{65}Cu_{20}Fe_{15}$, $Al_{71}Ni_{24}Fe_5$ produced at two different cooling rates (slow and rapid solidification). Structural studies were carried out using X-ray diffraction, neutron diffraction, transmission electron microscopy and scanning electron microscopy. In order to describe the corrosion mechanisms, potentiodynamic measurements and electrochemical impedance spectroscopy (EIS) tests were carried out. Corrosion products were identified using the X-ray photoelectron spectroscopy (XPS).

In the conducted studies, the structure of the alloys was characterized: $Al_{65}Cr_{20}Fe_{15}$ (binary phase alloy with SCAP), $Al_{71}Cr_{24}Fe_5$ (multiphase alloy with SCAP), $Al_{65}Cu_{20}Fe_{15}$ (multiphase alloy with an icosahedral phase), $Al_{71}Ni_{24}Fe_5$ (multiphase alloy with a decagonal phase). Corrosion tests showed that the rapidly solidified $Al_{71}Ni_{24}Fe_5$ alloy has the best corrosion resistance due to the low value of the corrosion current density (j_{corr}= 0.2 μA/cm^2) and high polarization resistance (R_p= 74 kΩcm^2). The worst resistance was found for slowly cooled $Al_{65}Cr_{20}Fe_{15}$ alloy.

The work was supported by the National Science Centre of Poland under research project no. 2018/29/B/ST8/02264.

References

[1] K. Młynarek-Żak et al., Electrochim. Acta. 409, 139836 (2022) 1-16.

[2] R. Babilas et al., J. Alloys Compd. 868 (2021) 1-11.

[3] J-M. Dubois, Chem. Soc. Rev. 41 (2012) 6760-6777.

Metal Release of CoCrMo Alloy in Protein-Rich Solutions–Effect of Sliding and Manufacturing Process

Zheng Wei[1], Valentin Romanovski[2,3], Luimar Filho[4], Cecilia Persson[4], Saber Sanaei[5], Masoud Atapour[5], Yolanda Hedberg[1]

[1]Dept. Chemistry, University of Western Ontario, London, Ontario, Canada

[2]Dept. Materials Science and Engineering, University of Virginia, Charlottesville, VA, USA

[3]Science and Research Centre of Functional Nano-Ceramics, National University of Science and Technology "MISIS", Moscow, Russia

[4]Uppsala University, Division of Applied Materials Science, Department of Materials Science, Uppsala, Sweden

[5]Department of Materials Engineering, Isfahan University of Technology, Isfahan, Iran

CoCrMo alloys, which have excellent corrosion and wear resistance, are widely used for dental and orthopedic implants in the human body. However, there are interfacial reactions occuring between the metal surface and the biological environment. Adverse health effects can sometimes be caused by tiny amounts of released metals from the surface of the CoCrMo alloy. Hence, it is very important to investigate the mechanism of corrosion behavior of CoCrMo in protein-rich solutions under sliding conditions and for different manufacturing processes. CoCrMo alloys usually are used in bearing and wearing parts of implants, where they are exposed to load, friction, and a protein-rich environment. Hence, the effect of sliding, protein aggregation and metal precipitation on metal release from CoCrMo were investigated. The metal release under sliding conditions was increased in the presence of bovine serum albumin. However, protein aggregation and metal precipitation can result in underestimation of the extent of metal release from CoCrMo in mixed protein solutions, especially under sliding conditions. In addition, the effect of the print direction during laser powder bed fusion of CoCrMo alloys on corrosion resistance and metal release was investigated, with minor effects observed. All these studies deepen our insight in the extent and mechanism of metal release from CoCrMo alloys in protein-rich solutions, which helps to minimize adverse health effects.

Corrosion resistance of rapid solidified $Al_{85}(Ni,Fe,Cu)_{10}Y_5$ alloys in 3.5% NaCl solution

Rafał Babilas, Katarzyna Młynarek-Żak, Adrian Radoń

Silesian University of Technology, Department of Engineering Materials and Biomaterials, Gliwice, Poland

Al-based alloys with an amorphous structure are characterized by favourable corrosion resistance compared to crystalline ones. Relatively better anticorrosion properties resulted from the chemical homogeneity and the absence of defects in the structure. Data from the literature indicate alloys with amorphous structure in chemical compositions, e.g.: Al-Ni-Y, Al-Ni-Fe, Al-La-Ni-Fe, and Al-Ni-Y-Co.

The aim of the work was to evaluate the corrosion behavior of $Al_{85}Ni_{10}Y_5$, $Al_{85}Ni_5Fe_5Y_5$, $Al_{85}Ni_{3.33}Fe_{3.33}Cu_{3.33}Y_5$ alloys prepared by induction melting pure metals in a ceramic crucible in an atmosphere of argon. Rapid solidified ribbons were prepared by remelting the master alloys in quartz crucibles and casting onto a rotating Cu wheel. Phase identification was performed using X-ray diffraction. To determine how the composition and casting method influenced the structure and the local environment of Fe, Mössbauer spectroscopy was applied. Electrochemical measurements were performed in 3.5% NaCl at 25 ^oC solution using an Autolab 302N potentiostat equipped with a three-electrode cell controlled by NOVA software.

The best corrosion resistance indicated the amorphous $Al_{85}Ni_5Fe_5Y_5$ alloy (E_{corr} = -0.375 V, j_{corr} = 2.1 μA/cm^2, R_p = 3.7 kΩcm^2). The addition of Fe also had a positive effect on the corrosion behavior compared to the composition of the $Al_{85}Ni_{10}Y_5$ ribbon. In the case of the addition of copper to $Al_{85}(Ni,Fe,Cu)_{10}Y_5$ alloy the corrosion resistance was the worst, which is related to the large difference between the electrochemical potential of copper and aluminum. The data in the literature indicate that amorphous alloys are characterized by good corrosion resistance. However, the chemical composition is one of the factors responsible for the behavior of the material in an electrochemical environment.

Acknowledgments

The work was supported by the National Science Centre of Poland under research project no. 2018/29/B/ST8/02264.

Low Voltage SEM/EDS-analyses of 304 and 347 Stainless Steels Oxidized at 600-800 °C

Jyrki Juhanoja and Thao Nguyen , Top Analytica Ltd, Turku/Finland

Austenitic stainless steels such as 304 and 347 have excellent mechanical properties and corrosion resistance at high temperatures. The good corrosion resistance of stainless steels is based on the formation of a very dense and thus protective chromium oxide (Cr_2O_3) on the steel surface. The composition,and the crystal structure of the protective layer as well the physical properties like porosity on the metal-oxide interphase are the key parameters determining the corrosion resistance.

Scanning electron microscopy (SEM) with energy dispersive spectroscopy (EDS) is one of the most used techniques for the analyses of oxide layers, but the lateral resolution in EDS-analyses is typically limited to a micrometer scale, which is not enough to resolve the fine structure of the oxide layer. In this work we have done EDS-analyses at 3 kV accelerating voltage and used L-lines of the main components (Cr, Fe, Ni and Mn) and managed to improve the resolution down to 10-50 nm.

The analyses are made from samples oxidized at 600- 800 °C in a laboratory furnace with ambient air. The cross-sections of the samples are made with Ar-beam cross-section polisher. The results show the elemental distribution of the elements, identified compounds and the voids on the interphases.

Influence of phosphorus segregation and grain boundary misorientation on intergranular corrosion of α-Fe

Kazuya Tojima, Saya Ajito, Yongie Zhang, Tomohiko Hojo, Goro Miyamoto, Motomichi Koyama, Tadashi Furuhara, Eiji Akiyama, Institute for Materials Research, Tohoku University, Sendai/Japan

1. Introduction

Phosphorus (P) in iron and steel is known to segregate at grain boundary (GB) and cause intergranular corrosion (IGC). It has been reported that IGC was accelerated as the amount of P segregation at GB increased in Fe-P binary alloys [1]. Both elemental segregation and IGC strongly depend on GB character. Thus, it is important to investigate the relationship between the GB character and the IGC behavior caused by P segregation. However, this relationship of Fe-P alloys has not been investigated, and the detailed mechanism of IGC with P segregation has not been clarified. In this study, immersion tests and GB misorientation analysis of two types of Fe-P alloys with different amounts of P segregation at GB were conducted, and the effects of P segregation and GB misorientation on IGC of iron were discussed.

2. Experimental procedure

Fe-0.01P (mass%) alloy was used in this study. The specimens were annealed at 600°C for 24 hours and 700°C for 1 hour (hereinafter called HT600 and HT700). The P concentrations at GB of HT600 and HT700 were assumed to be about 4 at.% and 2 at.%, respectively. GB misorientation distribution was analyzed by electron backscatter diffraction measurement. Subsequently, the specimens were subjected to immersion tests in a 0.1 M sodium sulfate aqueous solution. After the immersion test, the corrosion products were mechanically removed for subsequent surface observations.

3. Results and discussion

In the case of HT600, corrosion products were deposited on the surface after immersion test for 8 hours. The corrosion grooves were observed at the GBs after the removal of the corrosion products. On the other hand, HT700 hardly corroded after the immersion test for 18 hours. These results indicated that the iron specimen with a large amount of P segregation at GB was susceptible to IGC. In the presentation, the relationship between IGC and GB misorientation will be discussed.

[1] J. Küpper, H. Erhart and H.J. Grabke, *Corros. Sci.*, 3 (1981), 227.

Modeling of Electrochemical Oxide Film Growth

Ingmar Bösing, Jorg Thöming, Fabio La Mantia; Universität Bremen, Deutschland

Our civilization would not be possible without the phenomena passivity, which describes the growth of stable oxide films on metal surfaces. These oxide films, also known as passive films, can slow down corrosion about three orders of magnitude, and thus passive films enable the use of different metals for construction works, in the medical sector, in the mobility sector and beyond.

Even though, metal oxides play a crucial role in our daily lives, the mechanism behind oxide film growth are not fully understand and there remain several open questions regarding this topic. Several approaches to model oxide film growth under external potential have been proposed to deepen the understanding of the underlying mechanism and to deliver new insights in to the investigated processes. Nowadays the most popular model is the Point Defect Model, which was developed in the 1980s in Macdonald's working group. The Model describes oxide growth by interfacial reactions and the transport of defects through the film itself. Even though, the model is widely used it is based on different assumptions, as a constant electric field, the neglection of electrons and holes and a linear dependency on pH and potential of the potential drop at the film/solution interface.

To overcome these assumptions, to test the assumptions and to present a more comprehensive model we developed a continuum model based on the PDM which takes into account the impact of electrons and holes, calculates the electric field based on physical reasonable equations and involves a transpassive breakdown mechanism of the oxide film. Furthermore, the Refined-PDM (R-PDM) allows to simulate time depending oxide film growth of the whole polarization behavior of metals, from active dissolution, over the active/passive transition, the passive film growth and transpassive breakdown.

Comparison of Corrosion Behavior of Two Different Aluminium Alloys for Lid Foil from Industrial Point of View

Ahmet Kabil, Ece Harputlu, Hatice Mollaoglu Altuner,

Assan Aluminyum San. ve Tic. A.S., Turkey/Istanbul

Aluminium alloys are widely used in packaging applications due to their excellent impermeability and barrier properties, corrosion resistance, and compatibility with printing processes, high strength and high formability. Due to these superior properties, aluminium foils are widely used in lid applications for dairy products such as yogurt. Since both side of the foil is lacquered or coextrusion coated, aluminium foil does not come into direct contact with corrosive media unless there is any defect on the coating such as holes. On the other hand, in case of any defect in the coating, the corrosion behavior of the aluminium foil directly affects the delamination of the package.

The objective of this study was to assess the differences between the corrosion behaviors of two different aluminium alloys –EN AW-8006 and EN AW-8079 as lid foil by means of OCP and cyclic potential tests. Additional to electrochemical tests two bare foils were immersed into 50 ml HCl %37 +10 g CuSO4 #1000 ml solution for different times ranging from 10 s to 5 min and their surfaces were examined by SEM. The purpose of using this method, which is normally used to rapid check for the continuity of the coating on laminated structures, was to observe the corrosion propagation on the aluminium foil surface in case it is exposed to corrosive media due to any defect on the coating.

SEM examinations of the foil surfaces revealed that pitting starts earlier in EN AW-8006 alloy. It was also observed that while the pits progress through the thickness of the foil and creates individual small holes on EN AW-8079 alloy after extended time, the depth of the pits remained lower but the total surface area of pits were larger during the same contact time on EN AW-8006 alloy. Cyclic polarization curves of the two alloys revealed that despite the 8006 alloy is more active; it tends to passivate the existing pits earlier than 8079 alloy. This result is consistent with the SEM observations. Even if the rapid passivation of the 8006 alloy prevents the pit propagation through the thickness of the foil, since it leads to larger corroded area on the surface increases the risk of delamination of the lid during the shelf life of the product. For this reason EN AW-8079 alloy is more favorable for lid applications in terms of corrosion behavior.

Dissolved CO_2 effect on SCC of pipeline steels in simulated marine environments

Abubakar S. A., Mori S., Sumner J.

Cranfield University, Bedfordshire, MK43 0AL, UK.

Offshore pipelines are subjected to various forms of stresses which are induced by internal fluid flow, ocean currents, mechanical vibrations of other nearby installed equipment, earth movement etc. These stresses in combination with corrosive environment and in presence of trace gases particularly O_2, CO_2 and H_2S can cause an increase in corrosion of these pipelines and subsequently failure can occur when higher pressures are applied. Proper understanding of the effects of these trace gases can help in setting up corrosion mitigation strategies, and hence reduce risks associated with corrosion related failures.

In this research work the corrosion behaviour and susceptibility of API 5L X70 and X100 pipeline carbon steels to stress corrosion has been investigated in 4 tests in 3.5% NaCl solution with either N_2 or CO_2 bubbled through at 5 ^oC or 25 ^oC. Tests involving N_2 bubbling acted to reduce dissolved O_2. C-ring specimens were stressed to 80% and 95% yield strength. Linear polarization resistance technique monitored the corrosion potentials and rates. Corrosion extent and morphology were studied by optical microscopy (to measure the cumulative probability of metal loss exceedance), followed by SEM observation.

Results obtained from the control experiment (N_2 gas) show correlations between corrosion rates and both temperature and stress conditions. An increase in corrosion rate of more than 100% was observed with increasing temperature from 5 ^oC to 25 ^oC. At 5 ^oC the cumulative probability of metal loss exceedance of X70 increases with applied stress, while at 25 ^oC, the higher the stress the lower the cumulative probability of metal loss exceedance. Similar trends in change in metal were observed for X100 at both 5 ^oC and 25 ^oC. At 25 ^oC, deeper pitting corrosion was observed on the surfaces, with different morphology from that formed at 5 ^oC. A considerable degree of anodic dissolution was observed on the samples at 5 ^oC; it was greater at 25 ^oC. Results with CO_2 show more rapid rates of corrosion. No SCC cracks were observed on the specimens exposed with dissolved N_2 only. Data is still been collected for the dissolved CO_2 conditions.

Corrosion testing in a laboratory container - Corrosion testing with artificial seawater and sediment

Khalid Zekhnini[1], Sven Grabowski[2], Quynh Hoa Le[1], Andreas Burkert[1], Martin Babutzka[1]

[1] Bundesanstalt für Materialforschung und -prüfung (BAM)

Division 7.6 Corrosion and Corrosion Protection

Unter den Eichen 87, 12205 Berlin, Germany

[2] Bundesanstalt für Materialforschung und -prüfung (BAM)

Division 6.7 Surface Modification and Measurement Technology

Unter den Eichen 44-46, 12203 Berlin, Germany

Electricity generation by offshore wind turbine generators (WTG) is an important pillar of the energy transition. Corrosion processes on WTGs pose a particular challenge with regard to safe operation over longer periods of time due to the highly corrosive conditions in the offshore area. BAM is therefore conducting research to ensure a safe operation of the turbines over their intended service life to protect people and the environment.

In a joint research project, different corrosion-relevant areas of a WTG foundation structure were specifically simulated in test basins within a laboratory container. The aim of the work was, on the one hand, the gravimetric and electrochemical determination of corrosion rates in different areas of a WTG that are relevant for cathodic corrosion protection (CCP): Underwater and sediment zone as well as the transition area between these two zones. Also, targeted tests were carried out under CCP. In addition, investigations regarding calcareous deposition during CCP were carried out on idealized specimens under laboratory conditions to better assess its influence on the protection process. The investigations were carried out in a laboratory container with different basins, which were filled with sand as sediment and artificial seawater according to ISO 15711 and connected via a closed water circuit.

The presentation at Eurocorr will provide an overview of the investigations and the most important results. It will be evaluated, if a simulation of offshore corrosion conditions is possible to a certain extent in an idealized system with artificial seawater and sediment.

Rapid assessment of corrosion susceptibility of mild steel in simulated splash zone condition

K Vishwanath, S. S. Singh and K. Mondal
Department of Materials Science and Engineering,
Indian Institute of Technology, Kanpur-208016, UP, India

Abstract:

Mild steels or their derivative steels in the carbon range of 0.1-0.25 wt.% C are used in almost all the common engineering applications, such as construction, bridges, household, agriculture, etc. On the other hand, constructions in offshore or river always experience a hostile environment leading to severe corrosion of the steel structures as well as reinforced bars embedded in the concrete. Therefore, a quick assessment of corrosion in a laboratory scale is extremely important in order to facilitate the selection of suitable materials for varied corrosion environments in off-shore areas. Hence, the present work concentrates on the quick evaluation of corrosion of a mild steel, in annealed condition, under the influence of waves in 3.5 wt. % NaCl solution. A novel simulated marine environment device is developed to evaluate the corrosion behavior in various marine zones (atmosphere zone, splash zone, and immersion zone). The Raman and FTIR Spectroscopic analysis of the corrosion products, formed at various zones, revealed the formation of α-FeOOH, γ-FeOOH, β-FeOOH, and Fe_3O_4. The morphologies of the corrosion product formed in various zones, as characterized by scanning electron microscope (SEM), show that the corroded region of the splash zone contains cracks and porous rust layer in comparison to that of the other regions, indicating instability of the corrosion products. Moreover, the thickness of the corrosion product layer was found to be more in the splash zone in comparison to that of the other zones due to cyclic wetting and drying. Additionally, electrochemical measurements (linear polarization (LP), electrochemical impedance spectroscopy (EIS), and Tafel polarization) were conducted on the corroded surface of various zones without the removal of the rust layer, suggesting a strong relationship of rust layer composition and phase fraction with corrosion rates.

Keywords: Steel; Rust; Splash zone; Electrochemical impedance spectroscopy (EIS).

Internal corrosion studies of equipment and pipings involved in offshore Power-to-X (PtX) platforms

Shivasarathy Sankaran, DECHEMA-Forschungsinstitut, Frankfurt a.M., Germany
Wolfram Fürbeth, DECHEMA-Forschungsinstitut, Frankfurt a.M., Germany

It is important to promote renewable energy-based sources to accelerate the global endeavor in decarbonizing various industry sectors. Over the last decade, offshore wind power energy systems are becoming important in most parts of the world. The electricity produced through offshore wind turbines is green and has zero carbon footprint. Using the PtX process, a process of converting electrical energy into chemical energy through electrolysis, seawater can be split into hydrogen and oxygen. The produced hydrogen can further be converted into synthetic sustainable fuels such as methane, methanol, or ammonia. This alluring process comes with a threat in the form of corrosion occurring in the PtX offshore platform.

The internal corrosion of equipment and pipings are to be evaluated fundamentally using electrochemical and spectroscopic methods. The risk of microbiologically influenced corrosion (MIC) of components (cooling systems, wastewater pipes) depending on the bacterial species and environmental conditions will be thoroughly analyzed. Furthermore, the effect of chlorides on the degradation of electrode materials used for seawater electrolysis will be evaluated. In addition, the surface morphologies of the materials will be carefully characterized using XRD, electron microscopic methods and other advanced characterization techniques.

Investigation of corrosion of carbon steel under insulation

John Edet, Todd Green and Sudipta Roy

Department of Chemical and Process Engineering, University of Strathclyde, G1 1XJ, United Kingdom

Abstract

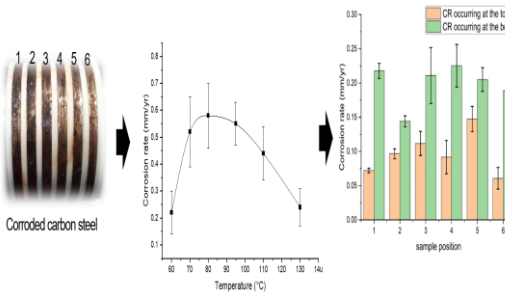

Corrosion under insulation (CUI) is the degradation of metals due to the presence of water and contaminants such as chlorides[1]. CUI is influenced by factors such as temperature, quantity, and distribution of electrolyte in insulation as well as presence of inhibitors. Studies reporting the influence of these factors for insulated structures are quite scarce. Therefore, this study is aimed at evaluating the effect of these parameters on CUI using gravimetric measurement.

Results indicated an increase in corrosion rate up to 80 ^{o}C, which decreased when the temperature increased to 130 ^{o}C. This could be attributed to rapid drying of the mineral wool insulation at higher temperatures. Higher corrosion rates were observed at the bottom part of the rings compared to the top due to accumulation of more test solution (1 wt. % NaCl) within this region. Furthermore, vapour phase corrosion inhibitor (VpCI 619) consisting primarily of sodium molybdate was observed to mitigate CUI by 89.2 % at 80 ^{o}C but decreased to 83 % as temperature was increased to 130 ^{o} C. This could be due to partial desorption of the inhibitor from the surface of the metal at higher temperatures[2].

In conclusion, this study indicates that CUI increases with temperature up to 80 ^{o}C but decreased on further increase in temperature due to rapid drying of the insulation. Also, the inhibitor showed good inhibition efficiency at temperatures where aggressive CUI have been speculated. This may provide technical guidance for design and material selection to prevent failure of insulated structures.

References

1. Caines, S., Khan, F., Shirokoff, J. and Qiu, W. (2015). *Journal of Loss Prevention in the Process Industries,* 33:39-51.
2. Shams, A. M., Din, E. and Wang, L (1996). Mechanism of corrosion inhibition by sodium molybdate. *Desalination*, 107:29-43.

Microbiologically influenced corrosion of steel sheet pilings in a Dutch harbor- fast corrosion and unexpected mass loss

Nanni NOËL-Hermes[1] and Maria SALTA[1]

[1] Endures B.V., 1781 AT Den Helder, The Netherlands
**nanni.noel@endures.nl*

Microbiologically influenced corrosion (MIC) is the deterioration of metals as a result of metabolic activity of microorganisms. Different genera of microorganisms convert nutrients which are available in soil and water. Such nutrients are often converted to acids and other corrosive by-products which change the environmental conditions and may accelerate corrosion processes. MIC can be recognized very well by its typical tubercles or corrosion products, being relatively soft layered structures consisting of orange iron hydroxide products and black products containing iron sulfide. These layers are only weakly attached to the steel surface and underneath the steel is shiny, with pits, craters and holes.

During regular inspection of steel sheet pilings in a Dutch harbor fast corrosion and unexpected mass loss was detected. Next to complete perforations, reddish brown spots on the surface of the steel sheet pilings were found. A complete failure analysis including microbial investigations was carried out to clarify if the observed failure was a result of MIC or if another corrosion mechanism was involved. Cconspicuous spots of the steel sheet piling structure were chosen for further analysis. Potential measurements were carried out and sheet samples were taken for microbial analysis and microbial related failure analysis. Next to the detection and identification of present corrosion relevant microorganisms (MPN, qPCR) a microscopic approach was used to determine if these organisms are directly active on the surface of the metal structure. Scanning Electron Microscopy (SEM) analysis was done with main focus on sulfur related compounds under corrosion products on metal coupons.

Results showed that stray-current could be excluded as corrosion mechanism. Based on the findings it is likely that MIC was the responsible failure mechanism of the fast corrosion and unexpected mass loss.

Hierarchical surface texturing in stainless steel as an alternative to prevent biocorrosion in marine environments

Javiera Castillo[1,2], Esteban Ramos-Moore[1], and Gonzalo E. Pizarro P[1,2];* (1) *Pontificia Universidad Católica de Chile, Santiago, Chile.* (2) *Marine Energy Research & Innovation Center. Chile. * jccastillo2@uc.cl*

In terms of economic cost, biocorrosion and biofouling are relevant problems to be solved within the marine industry[1]. Seawater contains nutrients and provides environmental conditions that promote bacterial colonization, usually resulting in the formation of biofilms on metal surfaces. Understanding the initial surface settlement of pioneer colonizers and the following biofilm formation is necessary to control the effect of biocorrosion and design methods for its prevention.

Several studies have shown that bacterial settlement can be controlled to a certain degree using patterned surfaces featuring repeating topographical elements of sizes ranging from nanometers to micrometers. For example, wetting functionalization has been achieved thanks to the fabrication of hierarchical structures with controlled shapes and sizes at the micro-scale and nanoscale[1]. Nevertheless, and to the best of our knowledge, there is a lack of systematic studies in the bio-interfaces research literature. In this work, we aim to understand how hierarchical the surface texturing of stainless-steel surfaces influences the bacterial colonization phenomena in marine environments. The leading hypothesis of this interdisciplinary research is that bacterial colonization on stainless steel exposed to seawater is significantly affected by both topography and surface chemistry, and that both can be tailored by hierarchical surface texturing. Our preliminary results in copper show a strong correlation between surface area and pattern scale with the bacterial settlement[2].

1. Ouyang Y, Zhao J, Qiu R, Hu S, Zhang Y, Wang P. Bioinspired superhydrophobic and oil-infused surface: Which is the better choice to prevent marine biofouling? *Colloids Surfaces A Physicochem Eng Asp*. 2018;559(September):297-304. doi:10.1016/j.colsurfa.2018.09.060
2. Caro-Lara L, Ramos-Moore E, Vargas IT, et al. Initial adhesion suppression of biofilm-forming and copper-tolerant bacterium Variovorax sp. on laser microtextured copper surfaces. *Colloids Surfaces B Biointerfaces*. 2021;202(November 2020). doi:10.1016/j.colsurfb.2021.111656

Pitting corrosion of 316L stainless steel caused by SRB´s in DGR environment

Richard Bureš[1], Jan Stoulil[1], Veronika Hlaváčková[2], David Dobrev[3]

[1]University of Chemistry and Technology, Prague/Czech Republic;

[2]Technical University, Liberec/Czech Republic

[3]ÚJV a.s., Řež/Czech Republic

The contribution is focused on estimation of threshold conditions for pitting initiation of the 316L stainless steel in the environment of deep geological repository for spent nuclear fuel. There exists a risk of pitting, due to possible synergistic effect of sulphate reducing bacteria (SRB) and radiolysis, producing thiosulphates responsible for passive layer local dissolution. Measurements were performed in synthetic bentonite pore solution and in slurry with Czech bentonite BCV. A tested parameters were temperature up to 50°C and random concentrations of thiosulphates up to 12 mmol/l. A short term electrochemical potentiodynamic experiments were performed as well as long term exposure tests. Part of the experiments were carried out in irradiation facility with ^{60}Co source under dose rate 1 Gy/h. The results show significant risk of pitting especially at 50°C. The pits show shallow morphology without significant enrichment of sulphur inside. Thiosulphates are probably important as depassivator for pit initiation, but pH drop of occluded solution is more important for pit propagation.

The effects of Calcigel bentonite naturally occurring microorganisms on corrosion of cast iron

V. Sushko, N. Matschiavelli, T. Wei, T. Stumpf, A. Cherkouk,

Helmholtz-Zentrum Dresden-Rossendorf, Institute of Resource Ecology, Dresden/Germany

In light of Germany's exploration of clay formations as potential hosts for deep geological repositories (DGR), and the most likely use of bentonite as a buffer material, copper or carbon steel/cast iron would be the most appropriate container material [1]. The surface of the metal containers is a subject to anaerobic corrosion and microbially influenced corrosion in a DGR. The interactions at the metal/bentonite interface can determine the performance of such a multi barrier system [2].

This study investigates the microbial processes that can occur at the interface between metal container and bentonite, and evaluates the effects of the microbial communities naturally occurring in bentonite may have on the corrosion of the nuclear waste container.

Microcosm experiments as described in [3] were performed with Calcigel bentonite. The microcosms, containing GGG40 cast iron coupons, artificial Opalinus Clay porewater and bentonite, were incubated in N_2-atmosphere at 37 °C. Some of the microcosms were supplemented with sodium lactate to stimulate microbial activity. After the incubation period the content of the microcosms was investigated by various geochemical analysis, DNA isolation and amplification for microbial community analysis, SEM-EDX and RAMAN spectroscopy to characterize the surface structure of the cast iron coupons. Geochemical investigation of the samples showed a slight lactate consumption. Surface analysis of the coupons with SEM confirmed a corrosion ofr the coupons incubated with Calcigel bentonite, as well as crystalline structures covering the coupons to some extent. The cast iron coupons incubated with bentonite including naturally occurring microorganisms showed a faster corrosion than control samples with sterilized bentonite. To get a better overview about the ongoing microbial processes, microbial diversity analysis and incubations for a longer time-frame are currently still under investigation.

References

1. Nieder-Westerman, G.H., et al. 2013, Radioactive Waste Management and Contaminated Site Clean-Up, 462-488.
2. Kaufhold, S., et al. 2020, ACS Earth Space Chem. 4, 5, 711–721.
3. Matschiavelli, N. et al., 2019, Environ. Sci. Technol., 53, 17, 10514–10524

Intersectoral Bridging in the Fragmented Field of Microbiologically Influenced Corrosion

Judit Knisz, University of Public Service, Baja, Hungary

Jan Stoulil, University of Chemistry and Technology, Prague, Czech Republic

Microbiologically influenced corrosion (MIC) causes billions of dollars of damage to the industry each year. Although many scientists and industrial operators understand the severity of MIC and the importance of research and investment in its detection, monitoring and mitigation, there are still many who are either unaware of this phenomenon or underestimate its gravity. Over the past decade, our understanding about the microorganisms and mechanisms involved in and factors influencing this deterioration process has grown enormously, still many questions are unanswered. Development is slowed by a large gap between academia and industry; often important scientific findings in industrial sectors remain concealed due to fear of public reaction, while in academia research is carried out that is far from the actual need of the industry.

A recent initiative has aimed to overcome these challenges and close or at least narrow the gap between industry and academia. The Euro-MIC COST Action (*CA2013* – *European MIC Network - New paths for science, sustainability and standards*) aims to develop an interdisciplinary and intersectoral network that will encourage synergistic communication and collaboration between material scientists, corrosion engineers, microbiologists, chemists and integrity managers. By creating a united European MIC community, MIC research, standardization can greatly advance and may bring about new innovations.

To achieve a collaborative MIC community, first we have to critically review the status quo in MIC and provide a secure platform for data and knowledge sharing. The presentation will provide insights into the challenges of and potential solutions for intersectoral bridging.

Anaerobic microbial corrosion of carbon steel under conditions relevant for deep geological repository of nuclear waste

Rojina Shrestha [a], Tomáš Černoušek [b], Jan Stoulil [c], Hana Kovářová [b], Kristína Sihelská [b], Roman Špánek [a], Alena Ševců [a], Jana Steinová[a,d],

[a] Institute for Nanomaterials, Advanced Technologies and Innovations, Technical University of Liberec, Bendlova 1407/7, Liberec 1 461 17, Czech Republic

[b] Research Center Řež, Department of Nuclear Fuel Cycle, Husinec-Řež 130 25068, Czech Republic

[c] University of Chemistry and Technology, Department of Metals and Corrosion Engineering, Technická 5, Prague 166 28, Czech Republic

[d] Department of Botany, Faculty of Science, Charles University in Prague, Benátská 2, Prague 128 01, Czech Republic

Abstract

The globally accepted strategy to dispose spent nuclear fuel and high-level radioactive waste is deep geological repository. The absolute barrier of this disposal system is intact metal canister, which will prevent the direct release of radionuclides into the repository environment. Safe performance of metal canister may be, however, affected by microbially influenced corrosion (MIC), as many studies have shown active presence of anaerobic microorganism in pore water and bentonite buffer. This study aims to provide a better understanding of corrosion processes relevant to deep underground repositories. Microbial corrosion of carbon steel in synthetic bentonite pore water inoculated with natural underground water containing microorganisms over a period of 780-days under sterile and anaerobic conditions was performed. Corrosion behaviour was determined using the mass loss method, SEM-EDS analysis and Raman spectroscopy, while qualitative and quantitative changes in the microbial community were analysed using molecular biological tools. Corrosion rates were significantly higher in the biotic environment with significant localization of corrosion attacks of up to 1 mm arising within 12-months. High abundance of *Methyloversatilis* correlating with periods of highest localised corrosion penetrations, suggests that this bacterium plays an important role in MIC. Our results indicate that nitrate-reducing bacteria could represent a potential threat to waste canisters under nuclear repository condition.

Corrosion of embedded steel in alkaline activated mortars manufactured from slag

A. Bautista, S. Shagñay, I. Ramón, F. Velasco, M. Torres-Carrasco
Universidad Carlos III de Madrid, Leganés, Madrid / Spain

Many concrete structures require embedded steel for complaining with their flexural and tensile requirements. The corrosion of reinforcing steel bars in concrete can easily compromise the durability of concrete structures, especially when they are exposed to chloride-rich environments or carbonatation by atmospheric CO_2 takes place.

Cement is worldly the second highest consumed material, just after the steel, and cement (PC) manufacturing is considered one of the most contaminating industries at the present moment. Hence, it is mandatory to develop and implement alternatives to the PC, with lower or no clinker content (less polluting) and that can offer a suitable in-service behavior when steel bars are embedded.

The present research evaluates the manufacturing of mortars from blast furnace slag (a waste) as precursor. Though there have already been many investigations about materials with alkaline activation, most of them have been focused on their microstructure and/or their porosity and mechanical properties. Alkali-activated slags (AAS) are materials obtained from the alkaline activation of slag, and clearly nice results have been obtained with them regarding properties different from corrosion. AAS have shown to be prone to suffering severe curing shrinkage. Our studies have checked that this shrinkage is usually associated to surface cracking. This microcracking cannot be especially relevant for mechanical properties, but acts as preferential diffusion path for chloride diffusion, as results obtained in our laboratory proves. So, special formulations of AAS, with balanced shrinkage, must be designed if steel bars are being embedded in them.

In this study, corrosion results of corrugated carbon steel reinforcements embedded in different mortars and submitted to cycles of immersion in NaCl solution and drying are shown. The performance of the steel-mortar samples is monitored with electrochemical impedance spectroscopy (EIS). The morphology of the attack and the associated mass losses are studied. Chlorides and pH profiles through the different mortar covers are measured, so factors determining the corrosion improvement achieved can be properly discussed.

Licorice extract as corrosion inhibitor in mortar

R. Naderi[1,2], A. Bautista[1], S. Shagñay[1], M. Torres-Carrasco[1], F. Velasco[1]

[1] Universidad Carlos III de Madrid, Leganés, Madrid / Spain

[2] School of Metallurgy and Materials Engineering, Faculty of Engineering, University of Tehran, Tehran / Iran

Corrosion of reinforcement in concrete structures has huge economic implications as well as social issues including endangering the safety of people who are working in industries. One of the methods to reduce steel corrosion is the use of corrosion inhibitors. The adverse effects of majority of the synthesized corrosion inhibitors (*e.g.*, traditional nitrites) on the environment have led to widespread efforts to replace them. The green inhibitors extracted from plants are an attractive alternative to traditional inorganic ones (*e.g.*, nitrites). Our previous research has shown the possibility of using licorice for reducing the corrosion rate of the steel bars in simulated concrete pore solutions with chlorides [1]. In this research, the feasibility of reducing the corrosion rate of steel rebar in mortar is tested.

Corrugated carbon steel bars conformed by thermomechanical treatment [2] were embedded in a mortar made of Portland cement type IV. The corrosion performance of the reinforcements was characterized without inhibitor and adding 2% licorice to the mortar. Cement/sand dose for mortars was 1/3. Moreover, water/cement ratio was 0.5. 1.25% (by wt.) of $CaCl_2$ related to cement was added. The electrochemical behavior was monitored by electrochemical impedance spectroscopy (EIS) and positive results are obtained. Moreover, the effect of inhibitors in the porosity and mechanical strength of mortars was also studied.

After curing for 28 days, results show that very slight reduction on porosity take place when adding the natural inhibitor, not affecting mechanical properties. Impedances measured in licorice containing mortars are always higher than those measured on specimens without inhibitor, during the whole testing period (86 days).

[1] R. Naderi et al. J. Molec. Liq. 346 (2022) 117856.

[2] A. Bautista et al. Constr. Build. Mater. 229 (2019) 116899.

Impact of electromigration treatment on chloride binding properties of cement

Reiser Matej, Kouril Milan, Frantisek Bayer, Sarka Msallamova

University of Chemistry and Technology Prague, Technicka 5, Prague, Czech Republic

Direct electrical current is used in several ways for its healing effect in reinforced concrete structures. In long-term application, it is used for cathodic protection, both in preventive and remedial mode. In the latter case, higher current densities are introduced from an external power source. In both of these cases, the DC current induces the migration of chloride ions from the cathodic reinforcement to the surface anode. DC current applied for a short time is used for electrochemical extraction of chlorides. The principle based on chloride migration is the same, except that higher current densities are applied. The passage of current through an ionic conductor, such as wet concrete, induces the transport not only of chloride but also of other ions such as hydroxides or calcium and sodium ions. This can cause local concentration changes, dissolution and changes in the microstructure of the cement binder and affect its sorption properties towards chlorides. Thus, concrete after chloride extraction may be less resistant to future chloride penetration. Series of concrete samples based on Portland cement (OPC) and samples containing supplementary materials (fly ash, microsilica) were prepared. Binding isotherms on intact and differently treated samples were acquired in order to reveal the effect of DC current on various microstructural components and their involvement in chloride binding. Concentrations of free and bound chlorides was monitored for a set of chloride concentrations. The results showed significant impact of DC treatment on cement binding properties. Such a finding was confirmed for all three kinds of concrete samples.

Investigation of the effect of fuel ageing and corrosion in oxymethylene ether (OME)

M. Irawan-Pieperhoff, S. Feldhoff, OWI Science for Fuels gGmbH an der RWTH Aachen

V. Arya, R. Reitz, MPA-IfW TU Darmstadt, Germany

The development of sustainable synthetic fuels requires optimum properties not only for use in internal combustion engines, but also materials compatibility with the installed components. In addition to the required properties, it is necessary to investigate changes in the physicochemical properties of fuels, for example due to longer storage times in fuel tanks. The associated fuel ageing can influence the (long-term) functional reliability of installed vehicle components. In addition, changes in the physico-chemical properties of fuels have negative effects on the combustion process in the engine.

As part of the BMBF-funded research project NAMOSYN, OWI and MPA are investigating the effects of fuel ageing on metallic components of industrial interest. From very large number of chemical compounds that could be used as fuels, a selection was made based on available Combustion data, namely oxymethylene ether (OME) as the most promising diesel fuel alternative. Specifically, corrosion properties of metallic materials used in the fuel system are studied. In accordance with VDA 230-207, the materials are stored in the fresh fuels at 60°C for up to 3 months, half immersed in liquid phase and half in gas phase. in tightly sealed glass containers Fuel properties such as density, water content, viscosity, oxidation stability, vapor pressure, ignition temperature, and sediment formation during storage are determined and analyses are used to evaluate their conformity to standards and to assess possible ageing or decomposition reactions. Initial results have shown that the various fuels interact very differently with the materials. For certain combinations of fuel and material, colour changes can be observed, indicating strong interfacial interactions. For Example, particularly significant colour changes are observed in the fuel blend of OME with diesel B0 when in contact with tin-coated field components. A decolouration or selective oxidation of tin surface is seen and ‘browning’ of fuel sample indicating presence of oxides. However, the results of the fuel analysis (requirement parameters according to DIN EN 590) were essentially unremarkable. In this context, the compatibility of metallic materials in the fuel system with OME and OME Blend will be determined as well.

Application of a reinforcement anode on an historical building

Xavier Hallopeau, SECCO Corrosion Consulting, Vélizy-Villacoublay, France

This presentation reports the development of a new impressed current anode for the cathodic protection of steel reinforced rebar in concrete.
The application of a DC current on a carbon fiber reinforced polymer, used both as a structural reinforcement and as an anode surface, allows to polarize the steel in concrete. The key to success in the development of this surface reinforcement-anode is the possibility of obtaining uniform distribution of current. Application on beams and columns of matrix and meshes is reported.

Appraising the effect of cooling rates during solutioning on the long term corrosion and pitting resistance of SLM Inconel 718 alloy

Murtaza Siddiqui[1], Abdelgadir M. Abdelgadir[1] , Akeem Y. Adesina[2]*

[1]Mechanical Engineering Department, King Fahd University of Petrolum & Minerals, Dhahran, 31261, Saudi Arabia

[2]Interdisciplinary Research Center for Advacned Materials (IRC-AM), King Fahd University of Petrolum & Minerals, Dhahran 31261, Saudi Arabia

Corresponding author's email: adesina@kfupm.edu.sa

Abstract

In this study, the effect of cooling rate during solutioning heat treatment on the corrosion and pitting resistance of SLM Inconel 718 alloy was investigated. The IN718 samples were subjected to solutioning at a temperature of 1100 ^{o}C for a duration of 1 h and then cooled via quenching, air, and furnace cooling to attain a fast, medium, and slow cooling rates, respectively. Subsequently, electrochemical techniques were used to evaluate the corrosion and pitting resistance behavior in 3.5 % NaCl solution. The effect of immersion duration for up to 168 h was also assessed on the samples cooled with different cooling rates. The microstructure, morphology and mechanical properties were examined by XRD, SEM, optical microscopy, and microindentation. The mechanical properties was slightly improved for the air cooled sample, however, there is no/little increment in the hardness for the water quenched and furnaced cooled samples. Similarly, the electrochemical corrosion meaurements showed that air cooling shows the best corrosion and pitting resistance followed by the water quenched, while the furnace cooling was the least improvement.

Effects of surface roughness on anaerobic marine biofilm formation and microbiologically-influenced corrosion of UNS G10180 carbon steel

Liam Jones[1], Maria Salta[3], Torben Lund Skovhus[4], Kathryn Thomas[5], Timothy Illson[5], Julian Wharton[2], Jeremy Webb[1]

[1]School of Biological Sciences, University of Southampton, Southampton, United Kingdom

[2]School of Engineering and Physical Sciences, University of Southampton, Southampton, United Kingdom

[3]School of Biological Sciences, University of Portsmouth, Portsmouth, United Kingdom

[4]Research Center for Built Environment, Energy, Water and Climate, VIA University College, Horsens, Denmark

[5]DNV, Holywell Park, Ashby Road, Loughborough, United Kingdom

The challenge in understanding and predicting microbiologically influenced corrosion (MIC) is the lack of robust and reproducible model biofilm systems that reflect real-world operating conditions. Furthermore, there are no internationally recognised standards or test methods with which to evaluate control strategies effective against MIC. Current industrial standards provide insightful guidance when it comes to the detection, testing and evaluation of MIC; however, less than 25% of risk-based inspections analyse sessile biofilm samples when investigating corrosion.

This work aims to develop and validate a model biofilm system to investigate the role of biofilm communities within MIC. The effect of surface roughness on MIC and biofilm formation between As Received ($R_{a\ Control}$ = 2.2360 ± 0.3450 µm & $R_{a\ Test}$ 2.4971 ± 0.6720 µm), and 25 µm polished ($R_{a\ Control}$ = 1.3938 ± 0.0897 µm & $R_{a\ Test}$ 1.6781 ± 0.1133 µm) carbon steel coupons (UNS G10180) will be investigated. The objective is to run two CDC biofilm reactors, one control and one test reactor inoculated with an anaerobic marine sediment sample. Both reactors will be run with an electrochemical cell setup and H_2S microsensor, whilst maintaining anaerobic conditions.

Corrosion rates will be monitored daily via linear polarization resistance and electrochemical impedance spectroscopy measurements, with potentiodynamic polarization performed at the end. Similarly, changes in H_2S concentration will be monitored daily (will reflect the activity of sulphate-reducing prokaryotes). Once the experiment is complete, biofilm viability through LIVE/DEAD imaging and monitoring of ATP activity will be assessed alongside any changes in prevalence and activity of different species within the biofilm using molecular microbial methods (qPCR and 16S rRNA amplicon sequencing). Gravimetric analysis alongside surface profilometry will be performed to assess the extent of the corrosion degradation. In combination these methods will provide a holistic understanding, providing novel insights into the effect of surface roughness on MIC.

We hypothesise that carbon steel coupons with greater surface roughness will facilitate biofilm attachment and growth, and thus exhibit higher corrosion rates.

Effect of building orientation on corrosion kinetics and mechanism of 3D printed AlSi10Mg alloy in saline medium

Abdelkader Meroufel, Clara Linders, Andrew Gordon, RISE, Kista, Sweden

Corrosion behavior of 3D printed alloys is dictated by specific microstructure features. Among the most studied alloys, Aluminum attracted a lot of research interest with aim to understand corrosion mechanism and improve the printing process for better compromise between mechanical and corrosion resistance properties. Selective Laser Melting (SLM) of aluminum alloys play a major part in applications in different fields, from aerospace to automotive and robotics, due to their high strength-to-weight ratio. AlSi10Mg was studied with focus on its mechanical properties versus microstructure features in different building directions/orientations. However, few studies aimed to understand the differences in corrosion performance versus orientation building of this alloy.

In this study the corrosion behavior of an aluminum alloy printed through SLM was studied using open circuit (OCP), Electrochemical Impedance Spectroscopy (EIS) and Potentiodynamic (PD) tests. All the tests were performed in stagnant saline medium for three different orientation buildings (horizontal, vertical and 45 angle) at ambient temperature. The results highlighted the higher corrosion rate for horizontal orientation, porous electrode behavior and similar open circuit potential. Relationship between corrosion parameters and microstructure features was established.

Anticorrosive and Persistency Properties of Arabian Crude Oils

Layan AlSharif, Christian Canto, Saudi Aramco, Dhahran/Saudi Arabia

With the continuous increase of water in the oil production corrosion becomes a challenging task to understand and tackle. Nevertheless, the economic production can still persist with the production of high-water fractions. It is known that some compounds in the crude oil could have anticorrosive properties able to hinder the internal corrosion. Understanding the effect of the multiple variables in the corrosion process inside the pipelines is critical for the selection of adequate mitigation strategies. In this study, a Eulerian approach is undertaken to determine anti-corrosive properties of crude oil by investigating adsorption properties under scenarios of long exposure periods to oil wetting conditions. Experimental studies are conducted by electrochemical techniques to investigate the oil's ability to actively displace water from the metal surface, and correspondingly, inhibit steel corrosion. The corrosion rate was measured under typical operating conditions of pressure and temperature inside the lines. The formation of a crude oil film on the steel surface were studied by immersing the test sample into crude oil and testing with Electrochemical Impedance Spectroscopy (EIS) exposed to different shear stresses inside an electrochemical glass cell. Preliminary results showed that some crude oil presents inhibiting capabilities, and these results are used to validate a semi-empirical electrochemical model that predicts uniform CO_2 corrosion rates under different oil immersion times and shear forces.

Key Words: corrosion rate, water content, corrosion inhibition, electrochemical testing, semi-empirical model.

Optimization of Extraction Conditions for Production of Halophyte-based Biocides for Microbiologically Influenced Corrosion (MIC) Mitigation

Jakob L. Stein, Aalborg University, Esbjerg, Denmark; Tanmay Chaturvedi, Aalborg University, Esbjerg, Denmark; Torben L. Skovhus, VIA University College, Horsens, Denmark; Mette H. Thomsen, Aalborg University, Esbjerg, Denmark

Halophytes are plants that grow in saline water and salt-affected soil. To survive these conditions, the plants synthesize various phytochemicals to survive, some of which are biocidal and easily extractable. Offshore structures and subsea pipelines are susceptible to Microbiologically influenced corrosion (MIC) caused by sulfate-reducing prokaryotes (SRP). MIC is especially prevalent due to favorable growth conditions for these microorganisms and is currently mitigated by adding biocides to the pipelines and physically scraping away biofilm. Estimates put MIC at 40% of the corrosion-related maintenance costs.

Our previous studies [1] have shown that these halophyte extracts can lower the activity of SRB to negligible levels, lower the relative abundance of common SRB species, and facilitate the breakdown of established biofilms. Different compounds are extracted from the plants as the extraction temperature increases. Some are biocidal, while others can promote growth, such as xylose and other sugars from the breakdown of the plant cells. Moreover, a lower extraction temperature will significantly reduce the production cost on a future commercial scale. Hence, optimization of the extraction temperature is essential. Our current ongoing study examines the biocidal efficacy of extracts from a single halophyte species produced at five different temperatures. Studies are being done in 100 ml serum bottles with Postgate medium and extracts. The bottles are inoculated with a microbial culture from water obtained from a production separator after a MIC afflicted pipeline in the North Sea.

Specifics of the process and the plant are part of an ongoing patent application and cannot be disclosed yet.

[1] Stein, J. L., Chaturvedi, T., Skovhus, T. L. & Thomsen, M. H. Clean Biocide Project: Halophilic plant extracts for prevention of microbiologically influenced corrosion (MIC). in *IWA Biofilm Reactor Conference. Books of Abstracts* 154–158 (2021).

Acoustic Emission Sensing for Early Damage Detection and Localization In Pressurized Vessels

Alerwi Maher, Saudi Aramco, Saudi Arabia; Canto Maya Christian, Saudi Aramco, Saudi Arabia

Abstract

This study presents a Structural Health Monitoring (SHM) solution developed using a low-cost, single channel Acoustic Emission (AE) system to detect damage initiation and growth in pressurized steel structures. The system consists of a commercial AE sensor and an in-house designed data acquisition and processing unit. The system is safe to use in high hazard industrial zones and can be permanently installed on assets operating in sour environments to detect and localize material damage for further non-destructive testing. Laboratory trials were conducted using a controlled test rig where Hydrogen-induced cracking (HIC) was induced in a HIC-susceptible steel coupon to mimic HICs observed in oil & gas pressurized vessels. These tests helped determine Key Performance Indicators (KPI) regarding cracking damage: amplitude, duration, energy, frequency content and spectrum shape were considered. The system was validated for field applications during a high-pressure production trap (HPPT) vessel shutdown and start-up. The vessel's pressurization produced several AE events on which a handful have been identified as damage indicators. The damage-signal's KPIs agree with those obtained from the lab trials and those reported in the literature. Additionally, the AE events identified during the pressurization of vessel were correlated with the before and after Advanced Ultrasonic testing results and the vessel operational conditions (pressure, temperature, level, etc). As a result, acoustic emission sensing is considered a promising technology for early damage detection and localization of pressurized vessels, and cornerstone for future asset health monitoring and digital twin implementations.

Key Words: Acoustic emission (AE); Asset Integrity; Early damage detection; Asset health monitoring; digital twin.

Mechanistic understanding of the effect of initial microstructure of low-alloy carbon steel on its CO_2-corrosion resistance in simulated formation water chemistry

Kapil Kumar Gupta[1], Saber Haratian[1], Alfred Larsson[2, 3], Giuseppe Abbondanza[2, 3], Edvin Lundgren[2, 3] Rajan Ambat[1]

[1]Department of Mechanical Engineering, Technical University of Denmark, Produktionstorvet, Building 425, 2800 Kgs. Lyngby, Denmark

[2] Lund University, Division of Synchrotron Radiation Research, Lund, Sweden

[3] NanoLund, Lund University, Box 118, 22100 Lund, Sweden

During CO_2 corrosion of steels, corrosion scale including carbonates phases as well as several kinds of (hydro-) oxides is most often formed on the material surface. The corrosion products can affect the protectiveness of the substrate, thereby manipulating the corrosion behavior. CO_2 corrosion of mild steel and how the precipitation of the corrosion products could affect the protectiveness of the underlying material have been extensively investigated during the last decades. It is established in literatures that the initial microstructure of material could highly affect the mechanisms responsible for CO_2 corrosion as well as the resistance of the material against further dissolution. However, limited number of research works have been conducted to mechanistically understand the influence of initial steel microstructure on its corrosion resistance when exposed to the CO_2-saturated sweet environments in realistic conditions, i.e., formation aqueous solution chemistry.

The detailed investigations in this study is therefore focused on understanding the effect of initial material microstructure on CO_2 corrosion resistance and the development of corrosion scale in the surface region of the low-grade steel. In order to obtain different initial microstructure, L80-1Cr steels were heated to austenitizing temperature and subsequently cooled at different rates. The heat-treated specimens were then electrochemically exposed to CO_2-saturated simulated formation water chemistry. Corrosion behavior of heat-treated samples was determined by understanding the electrochemical behavior of the steels using both DC and AC techniques. Surface characterizations before and after corrosion experiments were assessed using scanning electron microscopy and lab-source X-ray Diffraction. Furthermore, depth-resolved phase identification of the corrosion scales was performed using synchrotron X-ray diffraction to determine the sequence and the extension of corrosion products across the depth. The CO_2 corrosion mechanism is comprehensively discussed in light of the materials' electrochemical response, morphology and the microstructure of the corrosion scale developed on the surface of steels with different initial microstructure.

The influence of hydrogen sulfide concentration on the corrosion and hydrogenation of steel 07Cr18Ni6*C.*

Ch.Vasyliv [1] **,** ***M. Khoma*** [1]**,** ***M. Chuchman*** [1]**,** ***B. Datsko*** [1]**,** ***N. Ratska*** [1]**,** ***S.Halaichak*** [1]**,** ***H. Pokhmurska*** [2]

[1] *Karpenko Physico-Pechanical Institute of the NAS of Ukraine, Ukraine,*
e-mail: Chrystyna.vasyliv@gmail.com
[2] *Technische Universität Chemnitz , Chemnitz , Germany*
e-mail: hanna.pokhmurska@mb.tu-chemnitz.de

Abstract The corrosion and hydrogenation of steel 07Cr18Ni6 in standard NACE solution at the different concentration of hydrogen sulfide were studied.
Steel 07Cr16Ni6 in chloride-acetate solutions corrodes in the electrochemically active state regardless of the hydrogen sulfide concentrations. The presence of H_2S in the solution does not change the nature of the cathode processes, but accelerates them by 7… 9 times. Increase of hydrogen sulfide concentrations accelerates the anodic processes by 20… 35 times and changes its mechanism. Unstable passivation was detected in solution with $C_{H2S} \leq 100$ mg/dm^3, which turns into pitting at higher potentials.
The corrosion rate of steel 07X16H6 in solution at a C_{H2S}=100…1500 mg/dm^3 decreases by ~ 5 times for 720 h. Corrosion products on the surface of steel include nickel sulfides. Corrosion products consist of two layers at $C_{H2S} \geq 500$ mg/dm^3, the upper of which loses continuity due to cracking.
Steel 07Cr16Ni6 absorbs ~4.2, ~8.0 and ~17.5 ppm of hydrogen during corrosion in solution at concentrations C_{H2S} = 100, 500, and 1500 mg/dm^3 for 720 h. It is mostly diffusion-active hydrogen (C_{200} = 62… 70%), contained in traps with low activation energy.
Keywords: hydrogen sulfide, corrosion, hydrogenation, steel

Introduction The presence of hydrogen sulfide and other gases in oil and gas can create major problems, especially during the operation of deep wells. Hydrogen sulfide accelerates continuous and ulcerative corrosion of steels and simultaneous intense their hydrogenation and crack formation [1-4]. Such corrosion-mechanical destruction of steels is one of the most dangerous causes of structural damage in the oil and gas industries.
Much attention is paid to study mechanisms of hydrogen sulfide corrosion of steels, corrosion products morphology and their influence on the corrosion rate and hydrogen penetration. The corrosion and mechanical failure ability of steels depends on many factors: the hydrogen sulfide partial pressure, pH, temperature, chemical composition and structure of steels and corrosion products, mechanical stresses [5-7].
Aqueous hydrogen sulfide solution contains HS^-, S^{2-}, H_2S ions and is corrosion active to steels: it mostly accelerates both anodic iron dissociation reactions and cathodic hydrogen evolution reactions, but under certain conditions it can also inhibit corrosion [3,4] when a protective sulfides layer is formed on the surface.
A number of corrosion products are formed in the system depending on the hydrogen sulfide concentration, pH of the solution, temperature, redox potential, etc.: unstable maquinavit $Fe_{(1+x)}S$ (x = 0… 0.1); troilite FeS; pyrrhotite $Fe_{(1-x)}S$ (0 <x <0.2); the most stable pyrite FeS_2 [3,4]. The corrosion rate is determined by the morphology of sulfides [2,5]: dense species can inhibit corrosion, permeable species can increase and localize it due to the formation of galvanocouples, in which sulfides are the effective cathode.
If the partial pressure of hydrogen sulfide increases, the corrosion rate of steels changes ambiguously: it increases at low pressure and decreases after reaching a certain critical value. Corrosion acceleration is associated with additional cathodic reactions of hydrogen sulfide dissociation products. The acceleration of the corrosion rate is due to the formation of a protective layer of iron sulfides.
The effect of a solution pH on the corrosion rate of steels is also ambiguous. There is a sharp deterioration of the corrosion resistance of some martensitic steels in hydrogen sulfide solutions with the pH<3.5 due to depassivation and intensification of anode processes [8]. The effect of the pH on

corrosion processes also depends on the concentration of hydrogen sulfide. The corrosion rate of steel decreases linearly with increasing the pH at the low concentrations of H_2S. At higher concentrations of hydrogen sulfide, the products of its dissociation are involved in the cathode reactions. Concentration of sulfide species increases, when the pH rises. It contributes to the formation of various iron sulfides on the surface, which could slow down the corrosion rate [5-9].

Temperature accelerates all the processes associated with hydrogen sulfide corrosion: diffusion, electrochemical and chemical reactions with the precipitation of iron sulfides. The solubility of hydrogen sulfide also decreases and the solubility of corrosion products changes. Depending on these processes, the corrosion rate may increase or decrease. If protective sulfides are not formed on the surface, which is typical for the very low pH, the corrosion growth with increasing temperature. On the other hand, if the conditions of a protective film formation are favorable, and the temperature accelerates both corrosion and the corrosion products formation, a maximum of corrosion at a certain temperature should be expected.

Hydrogen sulfide in the environment causes also hydrogenation of steels and corrosion cracking. Hydrogen sulfide diffuses through the surface film or penetrates through the porous structure and forms metal sulfides with the release of hydrogen, which is absorbed by the metal. A thin sulfide film can play the role of a near-surface tank, constantly filled with hydrogen, which triggers and constantly maintains its absorption. Depending on the morphology and porosity, corrosion products can also inhibit the penetration of hydrogen into the metal, even with elastic or plastic deformation [10-12].

Martensitic stainless steels are often used in the oil and gas industry due to their high corrosion resistance and mechanical stability. Also they are cheaper from ferritic-austenitic steels. They are stable in environments with pH> 4, but at lower pH lose their properties due to depassivation, acceleration of anode processes, formation of corrosion products, hydrogenation and cracking [8].

Despite the large number of publications about hydrogen sulfide corrosion-mechanical fracture, the mechanisms of hydrogen sulfide corrosion of steels currently are insufficiently studied.

The purpose of this work was to deep knowledge about the regularities of corrosion and hydrogenation of martensitic steel 07X16H6 in chloride-acetate solutions at the different concentrations of hydrogen sulfide.

Experimental technique Cylindrical samples of steel 07Cr16Ni6 (% mass: 0.07 C; 5.3 Ni; 0.38 Ti; 17 Cr; ≤0.8 Si and Mn; ≤0.02 S; 0.035 P, the rest - Fe) were tested. They were pressed into the fluoroplastic sleeve; the side surface was insulated. The working part was a disk with a diameter of 1 cm. Volt-ampere curves were performed after stabilization of the corrosion potential (~0.5 h) with a scan rate of 1 mV / s at a temperature of 25°C in a a standard aqueous NACE solution (mass.%: 5% NaCl + 0.5% CH_3COOH (pH = 2.7)) with a concentration of hydrogen sulfide: 0; 25; 100; 500; 1000; 1500; 2000; 2800 mg/dm^3. The solutions were purged with gas mixture of hydrogen sulfide and argon of appropriate concentrations for 2 h.

Hydrogen sulfide was obtained by hydrolysis of aluminum sulfide, which guaranteed its purity. The concentration of H_2S up to 50 mg/dm^3 in the solution was determined by photocolorimetric method using N, N-dimethyl-p-phenylenediamine; and iodometric method was used at higher concentrations of H_2S (Standard GOST 22387.2-97).

PI-2MK-10A potentiostat, silver chloride reference electrode and auxiliary platinum electrode were used. Tafel coefficients were determined by graph analytical method. Taking into account the electrochemical equivalent of iron, the electrochemical corrosion index was converted to mass according to the formula: $K_m = K_i \cdot k_e$, where K_m is the mass index of corrosion rate, g/(m^2·h); K_i - electrochemical corrosion index, A/m^2; $k_e = M/(z \cdot F)$ - electrochemical equivalent of the metal, g/(A h); M is the atomic mass of the metal, g; z is the number of electrons involved in the redox reaction; F – Faraday constant, A·h.

A hydrogen concentration in steels was determined by the vacuum extraction method. Samples were heated in vacuum and a volume of released from the metal hydrogen was fixing at 200 ºC (C_{H200}) and 800 ºC (C_{H800}). Liquid differential pressure gauge was used, which was filled by dibutyl phthalate. Diffusion-moving hydrogen releases at 200 ºC and residual hydrogen - at 800 ºC. The volume of absorbed hydrogen by the 1 dm^2 of metal surface was presented in cm^3/dm^2.

After long-term exposure of the samples in the environment, the corrosion rate was determined gravimetrically.

Metallographic investigation of the surface layers has been done by a scanning electron microscope EVO 40XVP with a system of micro X-ray spectral analysis on the energy-dispersive spectrometer INCA ENERGY 350.

The results of the experiment and their discussion According to polarization curves, the addition of 25 mg/dm^3 of hydrogen sulfide to a solution of 5% NaCl + 0.5% CH_3COOH causes a shift of the corrosion potential of steel 07Cr16Ni6 to negative values by ~ 70 mV; corrosion rate increases by an order of magnitude (Fig.1, table.1). The controlling corrosion factor changes from anode to cathode. If the concentration of H_2S increases from 100 to 2800 mg/dm^3, the potential changes only by ~ 30 mV, and the values of the corrosion current remain in the range of 0.14...0.18 mA/cm^2. Hydrogen sulfide does not change the nature of cathodic processes: the Tafel coefficient is in the range of 108…115 mV per decade, but their corrosion rate increases by 7…9 times. In the presence of H_2S, the rate of anodic reactions increases by 20… 35 times, and the Tafel coefficient increases from 53 to 93… 107 mV per decade, which indicates a change in their mechanism.

In general, steel in acetate-chloride solution is in the electrochemically active state. However, a decrease in the polarization current is observed at a potential of ~ -245 mV, which indicates the development of passivation processes. At a potential of ~ -160 mV, the current increases again and pitting corrosion develops (Fig.2).

The same character of polarization curves is observed at hydrogen sulfide concentrations 25…100 mg/dm^3, and the values of the characteristic potentials are shifted towards more positive values. The signs of passivation disappear at concentrations of H_2S 1000…2800 mg/dm^3 and an active corrosion process takes place. In general, the corrosion of steel 07Cr16Ni6 in these solutions causes the formation of corrosion products of black color on the surface. Likely it is oxide-sulfide composition, which do not passivate the surface of steel and it is permeable to corrosive environments.

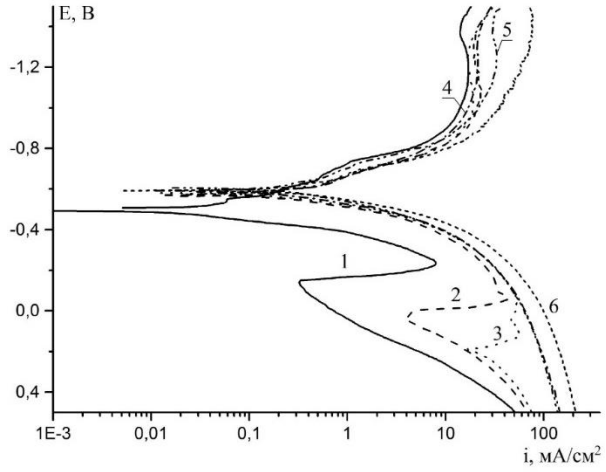

Fig.1. Polarization curves of steel 07Cr16Ni6 in solution 5% NaCl + 0,5% CH_3COOH with different H_2S concentration, mg/dm^3: 1 – 0, 2 – 25, 3 – 100, 4 – 1000, 5 – 1500, 6 – 2800.

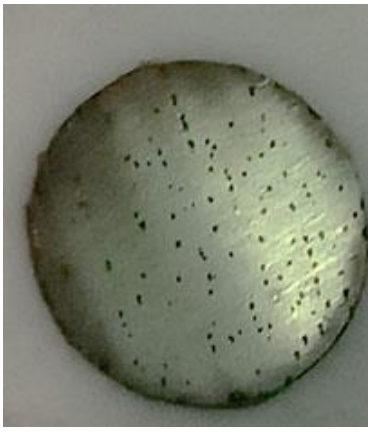

Fig. 2. Pitting damage on the surface of steel 07Cr16Ni6 in solution 5% NaCl + 0,5% CH_3COOH.

Table 1. Corrosion potentials and rates of steel 07Cr16Ni6 in solution 5% NaCl + 0,5% CH_3COOH with different H_2S concentration

H_2S concentration, mg/dm^3	E_{corr}, V	$i_к$ at E_{corr}, mA/cm^2	i_a at E_{corr}, mA/cm^2	i_{corr}, mA/cm^2	b_a,	$b_к$,
					mV	
0	-0,490	0,020	0,014	0,014	0,053	-0,107
25	-0,560	0,151	0,302	0,151	0,093	-0,107
100	-0,570	0,182	0,288	0,182	0,093	-0,113
500	-0,570	0,170	0,295	0,170	0,098	-0,114

1000	-0,570	0,182	0,302	0,182	0,098	-0,114
1500	-0,580	0,178	0,501	0,178	0,098	-0,114

The dependence of the corrosion rate *Km* of steel 07X16H6 in solution on the exposure time was studied. It was found that in the absence of hydrogen sulfide, the corrosion rate increases slightly during the first 200 h of exposure, and then decreases by an order of magnitude due to the formation of passivating films (Fig.3, curve 1).

In the presence of hydrogen sulfide in the solution, dark sulfide films are formed on the samples surface, which reduce the oxidation rate of steel. Thus, at C_{H2S} = 100 mg/dm^3 *Km* decreases from 1.68 g/(m^2·h) twice during the first 100 h, and then gradually decreases, reaching 0.37 g/(m^2·h) after 720 h of exposure (Fig.3, curve 2).

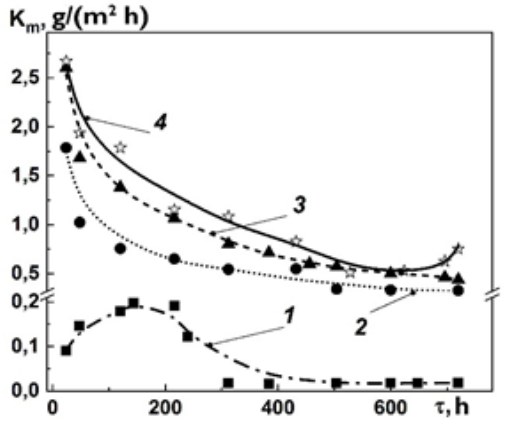

Fig.3. Change of corrosion rate during the exposure time of steel 07Cr16Ni6 in solution 5% NaCl + 0,5% CH_3COOH with different H_2S concentration of hydrogen sulfide (mg/dm^3): 1– 0; 2– ~ 100; 3 - ~ 500; 4 - ~ 1500.

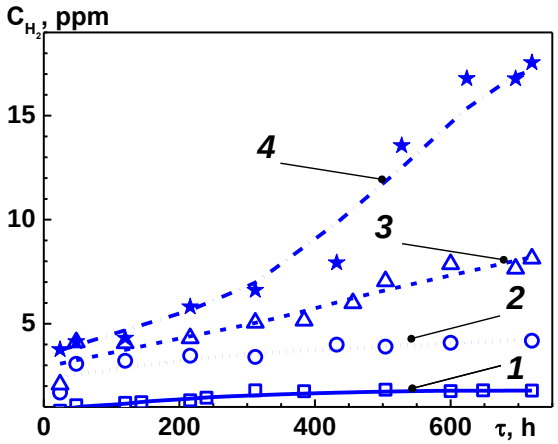

Fig. 4. Dependence of the hydrogen desorption on the exposure time of steel 07Cr16Ni6 in a solution of 5% NaCl + 0.5% CH_3COOH + H_2S. C_{H2S} (mg/dm^3): 1 – 0; *2* ~100; *3*– ~500; *4* – ~1500. Exposure time 720 h.

In the solution with C_{H2S} = 500 and 1500 mg/dm^3 (Fig. 3, curves 2,3) the corrosion rate is ~1.5 times higher than at C_{H2S} = 100 mg/dm^3. Over time it decreases exponentially and is equal to ~0.50 g/(m^2·h) after 600 h. This change in the corrosion rate could be associated with the formation sulfides of different composition and morphology on the steel surface [3,11]. The corrosion rate in a solution with C_{H2S} = 1500 mg/dm^3 increases after ~600 h of exposure due to the transformation of sulfides.

Steel 07X16H6 absorbs ~4.2, ~8.0 and ~17.5 ppm of hydrogen after 720 h corrosion in chloride-acetate solution at C_{H2S} = 100, 500, and 1500 mg / dm^3. It is mostly diffusion-active hydrogen (C_{200} = 62… 70%), contained in traps with low activation energy. At C_{H2S} = 1500 mg/dm^3, hydrogenation increases significantly (Fig.4). Defects in the corrosion layer can be a "reservoir" for hydrogen trapping.

A corrosion products deposite on the steel surface in a solution. The thickness of corrosion layer reaches 60 ... 70 μm after exposition for 720 h and practically does not depend on the H_2S concentration in the solution (fig. 5). The corrosion layer is homogeneous at C_{H2S} = 100 mg/dm^3, its structure is fine, concentration of elements throughout the thickness is stable (Fig. 5a, b). There is up to 3.5 wt.% sulfur, the concentration of nickel is three times greater than inside the sample, which may indicate the formation of nickel sulfides, which are thermodynamically more stable than iron sulfides [8]. The grain boundaries of corrosion products are consistent with the grain boundaries in the steel structure, but they are distincter (Fig. 5, b). Dendritic corrosion products, probably nickel sulfides, were found at the boundary with the metal between the martensite needles [8].

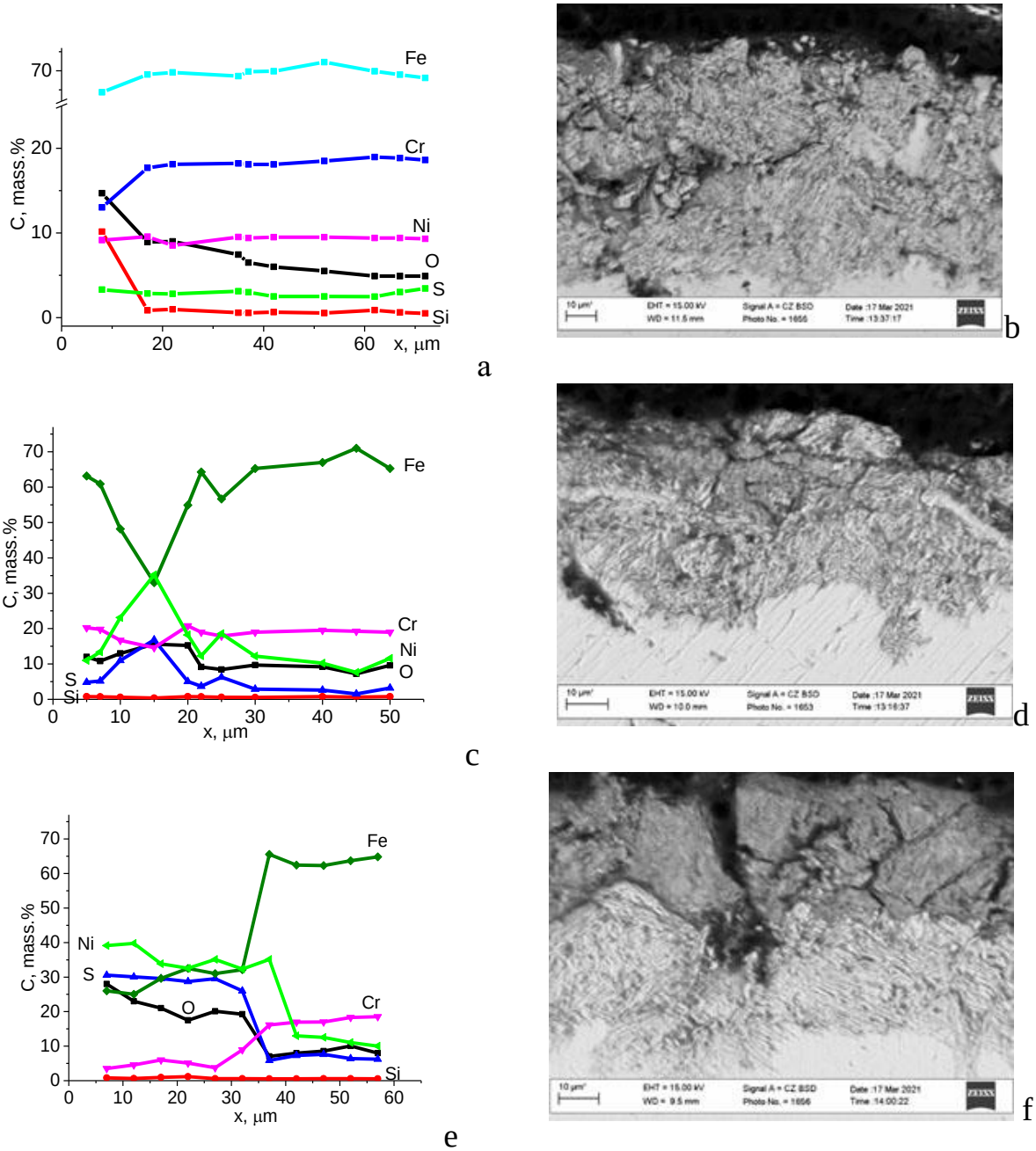

Fig.5. Concentration of elements in the corrosion layer and its microstructure after testing of steel 07Cr16Ni6 in a solution of 5% NaCl + 0.5% CH_3COOH at a concentration of hydrogen sulfide: a, b - 100 mg/dm^3; c, d - 500 mg/dm^3; e, f - 1500 mg/dm^3.

Corrosion products consist of two layers at the C_{H2S} = 500 mg/dm^3, that differ in structure and chemical composition (Fig. 5d). The outer zone with a thickness of ~ 20 μm consists of grains up to 10 μm in size, often separated by cracks. The concentration of sulfur and nickel in the outer layer is higher than in the inner layer and reaches 16 and 35 wt.%, respectively. It indicates different sulfides in the layers of corrosion products. The chemical composition and structure of the inner layer are similar to those formed in an environment with a C_{H2S} = 100 mg/dm^3 (Fig.5, c).

The thickness of the outer corrosion layer increases at the C_{H2S} = 1500 mg/dm^3. Grain size increases (Fig. 5f), deep cracks up to 10 μm wide with numerous branches extend perpendicular to the surface. The concentration of sulfur and nickel in this layer reaches 30 and 40 wt.% respectively. The content of chromium and iron is reduced (Fig. 5e). The structure of the inner zone, as well as at lower concentrations of hydrogen sulfide, is fine, but the sulfur content is higher (~ 6 wt.%).

In all cases, oxygen is present in the corrosion products (up to 25 wt.%) This is due to the oxidation of unstable sulfides in the air after completion of exposure to chloride-acetate environment. It is known [8] that unstable sulfides (makinavite) in the air can react with oxygen and turn into sulfates.

Conclusions.

1. Steel 07Cr16Ni6 in chloride-acetate solutions corrodes in the electrochemically active state regardless of the hydrogen sulfide concentrations. The presence of hydrogen sulfide in the solution does not change the nature of the cathode processes, but it accelerates them by 7… 9 times. Increase of hydrogen sulfide concentrations accelerates the anodic processes by 20… 35 times and changes its mechanism - the Tafel coefficient doubles. Unstable passivation was detected in solution with $C_{H2S} \leq 100$ mg/dm^3, which turns into pitting at higher potentials.
2. The corrosion rate of steel 07X16H6 in chloride-acetate solution at a C_{H2S}=100…1500 mg/dm^3 decreases by ~ 5 times for 720 h and is equal to 0.4… 0.5 g/(m^2·h). Corrosion products on the surface of steel include nickel sulfides. Corrosion products consist of two layers at $C_{H2S} \geq 500$ mg/dm^3, the upper of which loses continuity due to cracking.
3. Steel 07Cr16Ni6 absorbs ~4.2, ~8.0 and ~17.5 ppm of hydrogen during corrosion in chloride-acetate solution at concentrations C_{H2S} = 100, 500, and 1500 mg/dm^3 for 720 h. It is mostly diffusion-active hydrogen (C_{200} = 62… 70%), contained in traps with low activation energy. Defects in the corrosion layer can be a "reservoir" for hydrogen trapping.

References

1. M.S.Khoma, V.A.Vynar, M.R.Chuchman, Ch.B.Vasyliv Lecture Notes in Civil Engineering . **102** (2020) 231-239.
2. M. S. Khoma., V. R. Ivashkiv, S. A.Halaichak, M. R. Chuchman, Kh. B. Vasyliv, Materials Science, **55** (2019) 272–276.
3. Ma H., Cheng X., Li G., Chen S., Quan Z., Zhao S., Niu L. , Corros. Sci. 42 (2000) 1669–1683.
4. Genchev G.,Erbe A. Reference module in chemistry, molecular sci. and chem.eng (2017) P.221-231.
5. Khoma M., Holovei S., Ivashkiv V., Chuchman M., Vasyliv Ch. Materials Science, **53** (2018) 761-768
6. M. Askaria, M. Aliofkhazraeia, S. Afroukhteh Journal of Natural Gas Science and Engineering 71(2019). https://doi.org/10.1016/j.jngse.2019.102971
7. Huang F, et al. International Journal of Hydrogen Energy (2016), http://dx.doi.org/10.1016/j.ijhydene.2016.10.130.
8. Monnot M., Nogueira R. P., Roche V., Berthomé G., Chauveau E., Estevez R., Mantel M. Applied Surface Science. **394** (2017) 132–141.
9. Sun W., Pugh D. V., Smith S. N., Ling S., Pacheco J. L., Franco R. J., *CORROSION/2010*, paper no. 10278, Houston TX: NACE, 2010.
10. Castaneda H, Sosa E, Espinosa-Medina MA. Corros. Sci. – 2009;51:799e806.
11. International Journal of Hydrogen Energy (2016), http://dx.doi.org/10.1016/j.ijhydene.2016.10.130.
12. FangYu Ge, Feng Huang, Wei Yuan, Zhixian Peng, Jing Liu, Y. Frank Cheng International Journal of Hydrogen Energy, (2020) https://doi.org/10.1016/j.ij hydene.2020.02.149.

Influence of $CeCl_3$ on the inhibitory activity of imidazoline-based corrosion inhibitor

Tihomir Borko, INA, d.d., Zagreb, Croatia

Gordana Bilić, Faculty of Mining, Geology and Petroleum Engineering, University of Zagreb, Zagreb, Croatia

Abstract

In this paper, the effect of $CeCl_3$ on the efficacy of imidazoline based inhibitor on corrosion of J55 carbon steel in CO_2 saturated chloride-carbonate solution at 80 °C was investigated by weight-loss testing, electrochemical measurements and surface characterization. It has been noticed a synergistic effect of two inhibitors, as higher efficacy of the inhibitor mixture was observed compared to the efficacies of the individual inhibitors. The synergistic mechanism is attributed to the co-adsorption of Ce^{3+} cation from $CeCl_3$ and nitrogen from imidazoline on the surface iron atoms. The resulting surface film has better corrosion protection properties than the films formed in the presence of a single inhibitor due to the repulsive forces between the adsorbed identical inhibitor molecules.

Keywords: CO_2 corrosion, imidazoline based inhibitor, synergistic inhibition

Influence of Micro-Alloying Elements Upon the CO_2 Preferential Weld Corrosion Rate of Carbon Steel

Juliana L. Cardoso, Zehbour Panossian, Bruno B. Andrade, Marcos L. Henrique, Rodrigo S. Marques, Institute for Technological Research of the State of São Paulo, Petronio Zumpano Jr, Ilson P. Baptista, Petrobras, Brazil

This work evaluated the susceptibility to Preferential Weld Corrosion (PWC) of C-Mn and low alloy steel weldments of gas pipelines, containing low conductivity condensed water with CO_2. 79 different girth weld combinations were produced with different nickel, copper, chromium, and silicon content between parent metal (PM) and welding metal (WM).

Immersion and other tests were conducted aiming to promote PWC occurrence and to catch the influence of the chemical composition. The medium, simulating fresh condensed water, was CO_2 saturated deionized water (pH 3.9 and conductivity 45 µS/cm), kept at 25 °C ± 2 °C during the test. Each girth weld combination was tested twice. According to literature (1), condensed water is a low conductivity medium, not favorable to the formation of carbonates, because it is free from Fe^{2+} ions, it presents low pH (< 4.5) and the adopted test temperature was low (25 ºC).

Experimental results showed most of the specimens' grooves formed in the fusion line (FL) vicinity, mostly on the HAZ side, and some on WM side. Statistical analysis provided equation (**Eq.1**) predicting the general corrosion rate (*CR*) in the FL vicinity by the difference of Ni, Cu, and Si content between PM and WM and equation (**Eq.2**) predicting the local corrosion attack (LCA) by the difference of Ni, Cu and Cr content between PM and WM.

$$CR = 2{,}54 - 0{,}54*\Delta\mathrm{Ni} - 0{,}73*\Delta\mathrm{Cu} - 0{,}64*\Delta\mathrm{Si} \quad \textbf{Eq. 1}$$

$$LCA = 1{,}71 - 0{,}58*\Delta\mathrm{Ni} - 1{,}49*\Delta\mathrm{Cu} - 1{,}36*\Delta\mathrm{Cr} \quad \textbf{Eq. 2}$$

A work outcoming aiming for PWC mitigation is a method for welding consumable composition selection to weld a specific PM, based on the difference in chemical elements content between WM and PM. It is worth noting, that the proposed selection criterium is valid only within the studied elements ranges and in a low conductivity medium.

Reference: 1. DUGSTAD, A.; LUNDE, L.; VIDEM, K. Influence of alloying elements upon the CO_2 corrosion rate of low alloyed carbon steels. Corrosion 1991.

Q-BI^{TM} – Purple Yams Waste (*Ipomoea Batatas)* as Organic Corrosion Inhibitors for Carbon Steel in Oil and Gas Industry: Substitute of Chemical Compound

Gede Putra[1] , Hasbi Fahada, Arif Amrullah

[1]526 West 112th street #1, New York – New York 10025 - gw2440@columbia.edu

Abstract: The majority of research on the effectiveness of organic molecules and (nano)materials at inhibiting corrosion focuses on the discovery of novel compounds rather than the long-term viability of the material. As a result, the product was discovered but hasn't been widely used to replace chemical products that harm the environment, notably in the oil and gas industry, where sustainability and environmental issues are two major considerations in every decision. Chemical products that could inevitably end up becoming a complete waste in the construction of oil and gas facilities (fuel tanks, pipelines, and other equipment) require special consideration. To prevent corrosion of the carbon steel material during construction, the hydrotest process with fresh water or sea water requires particular chemical compound treatment. However, the subsequent effects of the disposal treatment on chemical corrosion inhibitor before it releases to the sea or ground caused a significant environmental problem. The efficiency of organic materials in preventing corrosion was evaluated using a thermodynamic corrosion test on high-quality ASTM A 283 Grade C plates by projecting the observed pH with a potential difference (volts) into the Pourbaix Fe diagram. The comparison below demonstrates the effectiveness of using Q-BI as an organic corrosion inhibitor for carbon steel in place of chemical inhibitors. We discovered that the corrosion rate of the plate with Q-BI was better than the other plate with chemical inhibitor, accounting for 3,35 mm/y compared to 6,21 mm/y, from the immersion test of the identical sample of plate. Anthocyanin concentrations of up to 700–800 mg/L were found in the extract of Ipomoea batatas waste in 600 g/L of tap water. The amount of chemical waste produced by hydrotest utilizing Q-Bi was less than the EPA's criterion, accounting for only 0.005 mg/L of the MCL of 0.1 mg/l. Finally, statistical research demonstrates that applying Q-BI to the oil and gas industry will enable us to save at least $10,000 on each hydrotest, translating into cost savings of over $1 billion annually. This Q-BI product, specifically when used in the oil and gas industry, is the safest Hydrotest solution, which leads to various implications that may have an impact on the environment. We believe the industry performs numerous hydrotests, treats water, and finds how to stop corrosion in carbon steel. This alternative is our suggestion for the best course of action.

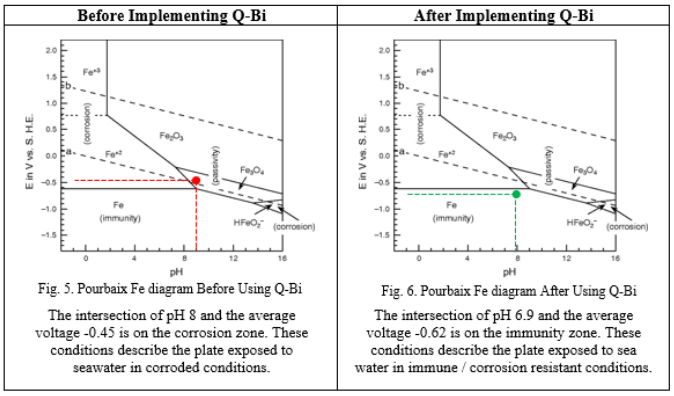

Fig. 5. Pourbaix Fe diagram Before Using Q-Bi

The intersection of pH 8 and the average voltage -0.45 is on the corrosion zone. These conditions describe the plate exposed to seawater in corroded conditions.

Fig. 6. Pourbaix Fe diagram After Using Q-Bi

The intersection of pH 6.9 and the average voltage -0.62 is on the immunity zone. These conditions describe the plate exposed to sea water in immune / corrosion resistant conditions.

Keywords: nondestructive test, hydrostatic test, organic inhibitor corrosion, ipomoea batatas

DIGICOAT: EIS and FTIR data analysis for protective coatings

Alejandro Gutierrez, Antonio Ruesca, Survey and Foresee Technologies SLL, Las Palmas de Gran Canaria/Spain

Digitalisation (Automation, Data Acquisition, Process Control)

Electrochemical Impedance Spectroscopy (EIS) and Fourier-Transform Infrared Spectroscopy (FTIR) are powerful techniques for characterization of protective coatings. Fitting EIS data to an equivalent circuit can provide information like barrier performance (based on coating resistance) and water uptake (based on coating capacitance). FTIR, on the other side, presents a unique chemical fingerprint of the coating that allows to monitor coating integrity. The complexity of EIS and FTIR data interpretation restricts its use to experienced users with advanced knowledge on both techniques fields (electrochemistry and spectroscopy) and coating technology, not always easy to find or train. It is also a waste of skilled personnel time to interpret high number of data produced by current multiplexer devices and online monitoring systems. Even though the prices of portable potentiostats and FTIR analyzers had become affordable since the past decade, this knowledge-related restriction presents a real roadblock to upgrade formulation labs and inspection procedures with this technologies.

We will present the last advances on DIGICOAT, a highly intuitive online platform that provide relevant data management tools to characterize protective coatings with these techniques. A case study with a real protective coating from industry will be used for the explanation.

Control of the degradation rate and corrosion resistance of ZK60 magnesium alloy by coating via HiPIMS and SolGel

Adrián Claver, Institute for Advanced Materials and Mathematics (INAMAT2), Universidad Pública de Navarra (UPNA), Pamplona/Spain

Iñaki Zalakain, Institute for Advanced Materials and Mathematics (INAMAT2), Universidad Pública de Navarra (UPNA), Pamplona/Spain

Iván Fernández, Nano4Energy SL, Madrid/Spain

José Antonio Santiago, Nano4Energy SL, Madrid/Spain

Ibán Quintana, Fundación Tekniker, Eibar/Spain

Lucia Mendizabal, Fundación Tekniker, Eibar/Spain

José Antonio García, Institute for Advanced Materials and Mathematics (INAMAT2), Universidad Pública de Navarra (UPNA), Pamplona/Spain

Magnesium is considered as one of the most promising candidates for biodegradable implants due to its mechanical properties thar are similar to those of the human bones. However, its fast degradation because of a poor corrosion resistance in human body environment has limited the use of magnesium alloys in biomedical applications. In this work TiN coatings doped with Cu were deposited via HiPIMS into ZK60 magnesium alloys for improving the corrosion resistance and antibacterial properties of the substrate, combined with an outer layer of TEOS-GPTMS based solgel coating. The structure and composition of the coatings were characterized using Scanning electron microscopy (SEM), Energy-dispersive X-ray spectroscopy (EDS), Fourier transform infrared (FTIR) spectroscopy, and X-ray diffraction (XRD). The roughness and contact angle of the surface were also measured. The corrosion resistance, mass change and hydrogen and PH evolution were studied, in addition to the electrochemical tests that were performed to evaluate the corrosion behavior of the samples. The results have shown that the corrosion resistance has been improved in the coated samples and they showed better hydrophilicity; that improves the ability to cell attachment of the surface.

Sub topic: Magnesium, HiPIMS, Corrosion resistance, SolGel, PVD, biomedic

Evolution in microstructure, wear, corrosion, and tribocorrosion behavior of Mo- containing high-entropy alloy coatings fabricated by laser

Yu Fu, University of Science and Technology Beijing, Beijing/China

Cuiwei Du, University of Science and Technology Beijing, Beijing/China

Xiaogang Li, University of Science and Technology Beijing, Beijing/China

Abstract

High-entropy alloy (HEA) is a novel alloy that contains multi-principal elements. Due to the four core effects, HEAs can simultaneously possess a variety of excellent properties, such as high strength, high ductility, good corrosion resistance and radiation resistance. Many scholars have utilized the design concept of this novel alloy to develop new materials with higher performance suitable for harsh environments.

In this work, we explored the non-equimolar HEA coating which was a broader space for the development of high-performance coatings. The microstructure, hardness, wear, corrosion, and tribocorrosion of $CoCr_2FeNiMo_x$ (x=0, 0.1, 0.2, 0.3, 0.4) coatings fabricated by laser cladding were investigated. The results showed that $CoCr_2FeNi$ HEA coating was a single FCC phase and Mo addition in the coating promoted the precipitation of σ-CrMo phase. The corrosion of the coatings preferentially occurred in the interdendrite region. Additionally, Mo addition significantly increased the hardness and wear resistance. $CoCr_2FeNiMo_{0.3}$ coating exhibited excellent performance during the synergistic effect of corrosion and wear in acidic 3.5 wt.% NaCl solution. The tribocorrosion mechanism of the Mo-containing coating was a combination of abrasion, adhesion wear, and corrosion. In summary, a suitable Mo addition in the HEA coating can simultaneously improves the corrosion and wear resistance due to the balanced stable passive film and hard precipitation.

Flash Plasma Electrolytic Oxidation of an Additively Manufactured Al-Si alloy

Marta Mohedano, University Complutense of Madrid, Spain

Esther Lopez, University Complutense of Madrid, Spain

Rubén del Olmo, Military University of Technology, Warsaw, Poland

Endzhe Matykina, University Complutense of Madrid, Spain

Raúl Arrabal, University Complutense of Madrid, Spain

An Additively Manufactured (AM) Al10Si1Mg alloy obtained via Direct Metal Laser Sintering (DMLS) was investigated in terms of characterization, surface modification and corrosion performance; the results were compared to those obtained for a conventional A361 cast alloy. The characterization (SEM) of AM alloy revealed α-Al cells enclosed in a fine 3D Si network and coarser microstructure at the melt pool borders. Thin (~5 μm) and energy-efficient PEO coatings (Flash-PEO) were successfully developed on the Al substrate in 100 s treatment. The influence of different parameters on the coating formation (voltage, current) was evaluated and the most promising results were obtained for the conditions: 350V and 100mA/cm^2. Flash-PEO of the AM alloy produces more uniform coating in comparison to the cast alloy due to enhanced Si oxidation. Electrochemical Impedance Spectroscopy (EIS) for short immersion times in 3.5 wt% NaCl aqueous solution, reveals that Flash-PEO coatings improved the corrosion behaviour of the materials

Development of an innovative quasi-ceramic layer for the hot forming of galvanized medium manganese steels with variable strengths

A. Anthes, W. Fürbeth , DECHEMA-Forschungsinstitut, Frankfurt am Main, Germany.

Safety-relevant components in the automotive industry are currently made of press-hardened manganese-boron steels like 22MnB5 or 20MnB8. This treatment offers the advantage of components with high strength and an inexpensive alloy concept. However, there are still problems in manufacturing that have not yet been resolved. During the hot stamping process an oxide scale is formed on the steel surface, which increases the wear on the pressing tool. In addition, this oxide scale must be removed for further processing. Therefore nowadays Al-Si-layers are mostly used to prevent steel oxidation at the moment. Unfortunately, these layers are not ideal either, as they adhere to the oven rollers and do not offer any active protection against corrosion. Alternatively zinc coatings can be used to protect the substrate against corrosion, but the press-hardening process must be adapted to prevent liquid metal embrittlement or the formation of brittle Zn-Fe phases. Today there is only one company which uses galvanized strip material in a patented indirect press-hardening process. So far these galvanized press-hardened components have reached only a market share of approx. 5%.

This poster will show the schematic approach of the development of a quasi-ceramic layer on medium manganese steels. Sol-gel chemistry is used for the formation of these SiO_2-based layers with low sintering temperatures. The dispersions are characterized by determination of the solid content by means of re-drying, measurement of the particle size distribution with dynamic light scattering and determination of the viscosity. The coatings applied by dip-coating are characterized by light microscopy and SEM on the substrate surface and at cross-sections.

Increasing the corrosion resistance of AZ91 magnesium alloy by plasma electrolytic oxidation

Milan Štrbák, University of Žilina, Department of Materials Engineering, Žilina/Slovak Republic

Branislav Hadzima, University of Žilina, Research Centre, Žilina/Slovak Republic

Ján Sovík, University of Žilina, Department of Materials Engineering, Žilina/Slovak Republic

Plasma electrolytic oxidation (PEO) is an effective surface treatment of valve metals to produce well-adherent oxide coatings that enhance wear and corrosion resistance in many aggressive environments. PEO process is accompanied by the electrochemical and plasma chemical reactions on the surface of the substrate materials immersed in the electrolyte. The impact of optimal process parameters on the overall electrochemical corrosion resistance of AZ91 magnesium alloy was studied. Voltage-time response for PEO process was graphically recorded in order to describe formation mechanism of PEO coating. The corrosion resistance of PEO coating was assessed using two different electrochemical methods: electrochemical impedance spectroscopy (EIS) and potentiodynamic polarization (PDP) in 0.1M NaCl at laboratory temperature. In addition to electrochemical methods, morphology of the oxidic coating was observed in the cross sectional and top surface view. The electrochemical characteristics obtained from the measurements show that the formation of PEO coating on AZ91 alloy has a beneficial influence on the coating's corrosion resistance in the given environment.

Enhancing corrosion resistance on magnesium alloy EV31 by PEO process

Vidžaja Knap, University of Žilina, Department of Materials Engineering, Žilina/Slovak Republic;
Branislav Hadzima, University of Žilina, Research Centre, Žilina/Slovak Republic;
Milan Štrbák, University of Žilina, Department of Materials Engineering, Žilina/Slovak Republic;
Veronika Obertová, University of Žilina, Department of Materials Engineering, Žilina/Slovak Republic

The plasma electrolytic oxidation is an efficient surface modification treatment that can increase the capability of wear protection and corrosion resistance in Mg and its alloys by the formation of oxide coating. The resultant coatings are surely not free from defects – indeed, they tend to contain porosity, inclusions, microcracks, etc. As there is a lack of research for PEO coating prepared on EV31 alloy this work aims to investigate properties of PEO coating and its overall impact on corrosion resistance of this alloy. Plasma electrolytic oxidation was performed in DC mode with constant current density of 0.05 A/cm^2 for 14 minutes. Evolution of voltage was measured and depicted graphically in order to describe PEO creation mechanism. Morphology and thickness of the PEO coating were examined together with corrosion resistance of the coating by measurements of electrochemical characteristics using electrochemical impedance spectroscopy (EIS) and potentiodynamic polarization (PD) after 1 hour in 0.1M NaCl. Results from these measurements showed significant increase in corrosion resistance of the sample treated by PEO.

Zr-Mo-Mn Conversion Coating as a Sealing Option to AA2024-T3 Anodized Layers

Jéssica Salles Pinheiro, Universidade Federal do Rio Grande do Sul, Porto Alegre/Brasil; Jane Zoppas Ferreira, Universidade Federal do Rio Grande do Sul, Porto Alegre/Brasil

AA2024-T3 alloy has been used for decades by the aerospace industry, since it has important properties for this application such as low weight and high mechanical strength. Despite its mechanical properties, suitable for structural use, this alloy is more vulnerable to corrosion compared to pure aluminum. Thus, surface treatments environmentally correct capable of effectively protect these surfaces against corrosive processes are necessary. Anodized aluminum alloys have a robust protective structure, formed by a barrier and a porous layer. To achieve greater corrosion resistance, the porous layer must anchor another coating or else be sealed. New sealing methods performed at low temperatures and for a short time, besides presenting the lowest possible toxicity have been sought. The present work brings contributions about a new sealing method for anodic layers of AA2024 produced in tartaric sulfuric acid (TSA). The method consists of immersion for 2 to 10 min in solutions containing H_2ZrF_6, Na_2MoO_4 and $KMnO_4$, at room temperature. The obtained layers were analyzed by scanning electron microscopy (SEM), X-ray spectroscopy with energy dispersion (EDS), contact angle, electrochemical impedance spectroscopy (EIS) and visual test after immersion in NaCl solution. They were compared to H_2ZrF_6 conversion coating and hydrothermal sealing. The results indicate that the Zr-Mo-Mn conversion coating formed on the anodic oxide film was able to seal its porous structure more efficiently than hydrothermal sealing as well as than the Zr-only coating. Nevertheless, the layers did not exhibit hydrophobicity and cracks were observed on the top of them when the immersion time was 5 and 10 min. Furthermore, there was a different precipitation, forming spherical deposits that could penetrate larger defects in some regions, probably attenuating eventual corrosion process. It can be postulated that the system formed by anodizing in TSA followed by sealing with Zr-Mo-Mn conversion coating is efficient to protect the AA2024 alloy against corrosion.

Plasma Electrolytic Oxidation (PEO) for Production of High-Performance Coatings on Ti-Al Intermetallic Compounds

Khaldon Munassar[a] *, Beatriz Mingo*[a]*, Aleksey Yerokhin*[a]

[a]*University of Manchester, Oxford Road, Manchester, M13 9PL, UK*

khaldon.munassar@postgrad.manchester.ac.uk

Abstract

The aerospace and automotive industries are evolving rapidly and with that, the need for environmentally friendly technologies is rising. Plasma Electrolytic Oxidation (PEO) is an environmentally friendly technology in the surface modification field with a promising potential to provide a wide range of ceramic coatings for several key light alloys that are used in the aerospace and automotive industries and the biomedical field. The ceramic coatings produced by Plasma Electrolytic Oxidation (PEO) provide high corrosion and wear resistance on light alloys, which is key in improving fuel consumption efficiency, tribological behaviour and commercial applicability of the alloys. This study aims to investigate the fundamentals of PEO by studying coating formation on pure titanium and aluminium as well as Ti-Al intermetallic materials. Understanding the fundamental science behind the formation of PEO ceramic coatings would enrich the overall understanding of PEO technology and shed light on new areas of research. In addition, this study aims to explore the potential use of Plasma Electrolytic Oxidation (PEO) to produce different ceramic coatings on Ti-Al intermetallic compounds using three different electrolytes (silicate-based, aluminate-based and phosphate-based electrolyte). This research will compare the different coatings and aim to select one of these electrolytes for future work on more tailored coating production. The physical and chemical properties of Ti-Al intermetallic compounds such as low density and thermal stability at high temperatures, make these compounds ideal for the aerospace and automotive industries. These coatings could have the potential to provide higher wear and corrosion resistance properties, which would add to the overall attractive properties of these intermetallic compounds.

Keywords: Plasma Electrolytic Oxidation (PEO); Ti-Al intermetallic compounds.

ZnO-based nanostructured electrodes for biosensors: Corrosion behavior in Ringer's physiological solution

Katarina Aleksić[1], Ana Stanković[1], Ivana Stojković Simatović[2], Smilja Marković[1]

[1] Institute of Technical Sciences of SASA, Belgrade, Serbia, [2] University of Belgrade, Faculty of Physical Chemistry, Belgrade, Serbia

Over the last decade, due to its numerous unique features that can achieve single biomolecule detection, zinc oxide have been examined as potential electrochemical biosensor for medical diagnosis. Previous studies proved success of ZnO-based materials in determining various biomolecules such as glucose, cholesterol, uric acid, etc. The materials being used as biosensors require special characteristics including high corrosion resistance.

The main goal of this study was to examine biocorrosion characteristics of ZnO materials in Ringer's physiological solution as a function of immersion time. Six different ZnO nanostructured powders were synthesized by microwave processing with an aid of citric acid and CTAB in different weight amount (5, 10, and 20 wt.%). To comprehend the influence of physicochemical characteristics of ZnO samples on biocorrosion, decisive features such as the crystal structure, morphology, textural properties, and surface chemistry were systematically investigated and correlated with biocorrosion activity. The biocorrosion activity of the samples was measured by potentiodynamic polarization technique. The measurements were performed on a potentiostat using a conventional three-electrode cell and a Ringer's solution as the electrolyte. Platinum foil and a standard calomel electrode (SCE) were used as the counter and the reference electrode, respectively, while FTO glass was used as the working electrode. The working electrode was coated with a thin film of ZnO ink prepared by mixing of a ZnO powder as an active material and Nafion solution as a binder. Prepared specimens were immersed in 100 ml of Ringer's solution for different immersion times ranging from 30 min to 7 days. The immersed specimens were then characterized by potentiodynamic polarization techniques in the potential range from −0.2 to +0.3 V vs SCE, at the scan rate of 0.1 mVs^{-1}. We found that all examined ZnO samples has low biocorrosion activity. Slight differences in biocorrosion activity between the samples are determined by particles morphology, textural properties and surface chemistry influenced by used surfactants.

Fabrication of Novel Hybrid Sol-Gel/Urethane Coatings for the Protection of Mild Steel Substrate against Corrosion in the Saline Medium

Rami K. Suleiman, Interdisciplinary Research Center for Advanced Materials, King Fahd University of Petroleum & Minerals (KFUPM), Dhahran 31261, Saudi Arabia

Banji M. Alkhuraim, Chemical Engineering Department, King Fahd University of Petroleum and Minerals (KFUPM), Dhahran 31261, Saudi Arabia

This work describes the successful fabrication of a novel hybrid sol-gel coating mixed with various additives that can be considered as waste material from human daily-life activities. The project succeeded in developing highly protective hybrid coatings that demonstrated excellent anti-barrier properties on the surface of mild steel substrate for the passage of the corrosive ions and ultimately protecting the steel substrate from corrosion in the saline medium.

The results obtained from this work are expected to open the door for further development in this field by exploring more waste additives or studying the synergistic effect of the additives of the current study with other sol-gel coating matrices. Furthermore, the application of the hybrid coatings developed in this study can be considered on other metallic substrates such as aluminum and magnesium which have significant impact in the aerospace and automotive industries. In addition, our developed coatings can be excellent candidates and promising alternatives to the commercially available, highly toxic chromate-phosphate conversion coatings.

Sealing of Anodized Aluminum Alloy by Acrylic Acid Polymerization

Adrian Dąbrowski, Zofia Buczko, Łukasiewicz - Institute of Precision Mechanics, Poland

Aluminum alloys are used on a large scale in industry, e.g. in the aviation industry. Aluminum alloys are anodized to protect against corrosion. A porous layer of aluminum oxide (AAO) have to be sealed. Sealing is necessary so that the coating has anti-corrosion properties and it is usually done in boiling water. This operation generates a large energy cost and it is expensive. Therefore, scientists are looking for new, more economical methods of sealing, which will provide the obtaining of coatings with similar anti-corrosion properties compared to coatings sealed in boiling water. In this study, AAO coatings were formed on the aluminum alloy (Al 99,5%) surface in the anodic oxidation process in sulfuric acid and then the porous coating was sealed in the acrylic acid polymerization process. This sealing process consists of 3 operations. The first operation is to cover the anodized aluminum alloy sample by the $K_2S_2O_8$ aqueous solution. In the second operation sample is covered by an acrylic acid aqueous solution. The final step is drying to polymerize acrylic acid. This is the classic „grafting" method, sealing takes place inside the porous oxide structure. The quality of the sealing was tested in dye-spot standard method according to ISO 2143. It was observed the same results for coatings sealed in acrylic acid polymer and coatings sealed in boiling water. Potentiodynamic polarization tests in 0,1 M NaCl aqueous solution were conducted to assess the corrosion resistance of the coatings. The value of passivation current density for the polymerization-sealed coatings is similar to the boiling water-sealed coatings, but the value of corrosion potential is shifted towards more negative potentials (-1,14 V vs. SCE) versus (-0,80 V vs. SCE) for the coatings sealed in boiling water. This proves a different mechanism of the corrosion course.

Physical and tribological properties of infrared dried coatings

Ivan Cindrić[1], Ivan Stojanović[1], Lovro Turkalj[1], Ivan Juraga[1], Daniela Rakela Ristevski[2]

[1]Faculty of Mechanical Engineering and Naval Architecture, University of Zagreb, Croatia

[2]Končar Steel Structures Inc., Zagreb, Croatia

Abstract

In the coating's selection process tribological resistance often takes a second place to corrosion resistance. Protective coating system is abraded and eroded over time which can lead to premature corrosion and material deterioration; thus, abrasion and erosion resistance must be considered when choosing coatings for specific conditions. Coatings are carefully chosen based on durability of the coating system, ease of maintenance, service environment and budget. Even though coatings resistant to abrasion and erosion wear last longer and better withstand heavy-duty environments, they tend to be significantly more expensive, both in material and labor costs. With polymer-based coatings superior adhesion and surface protection from mechanical and /or chemical damage can be achieved. These coatings are used in a variety of industries, from car manufacturing to metal construction.

In this paper, solvent-borne and water-borne 3-layer coating systems with zinc and without zinc in the epoxy primer, dried either with infrared (IR) radiation or at room temperature were evaluated. To assess the performance of the coating, the type of solvent, different drying methods, tribological and physical tests were performed. Also, to determine the resistance of a dry film to cracking or peeling from a substrate impact resistance test was done. Zinc-rich coatings have shown better resistance to abrasion and erosion wear, whereas IR-dried systems being more resistant to abrasion wear for all cases. The coating systems achieved satisfactory results regardless of the type of coating and the drying method.

Keywords: *abrasion, erosion, impact, coating resistance, coating hardness, infrared drying*

Influence of Hydrogel Coatings on Corrosion and Fatigue of Iron in Simulated Body Fluid

Jingyuan Huang[1], Markus Voigt[1], Steffen Wackenrohr[2], Christoph Ebbert[1], Adrian Keller[1], Hans Jürgen Maier[2], Guido Grundmeier[1]*

[1] Paderborn University, Technical and Macromolecular Chemistry, Warburger Str. 100, 33098 Paderborn, Germany.

[2] Leibniz Universität Hannover, Institut für Werkstoffkunde (Materials Science), Garbsen, 30823 Germany

Bioresorbable metallic implants provide desired functional properties for a certain time range and degrade safely within the body after their use phase. Iron based alloys have been increasingly considered for the development of biodegradable implants because of their mechanical properties [1]. However, their low degradation rate is a major concern. The production of corrosion products on the surface is considered to be an important cause of corrosion inhibition because it limits the diffusion of oxygen and ions to the metal surface.

Agar is a natural polymer with a suitable ionic conductivity, it has been discussed as an alternative for liquid electrolytes in the past [2]. In this work, surface corrosion and fatigue studies of pure iron were performed in modified simulated body fluid (m-SBF) with and without applied agar films. The electrochemical corrosion rates were measured by means of electrochemical impedance spectroscopy. The morphology and surface chemical composition of the samples after exposure were analysed by means of FE-SEM, XPS and Raman microscopy. The effect of applying agar films on the corrosion process was estimated. In addition, the study revealed a correlation between the surface corrosion process and the fatigue life of iron samples in physiological environments.

Acknowledgements

This research was funded by the German Research Foundation (Deutsche Forschungsgemeinschaft (DFG)) under project number 413259151.

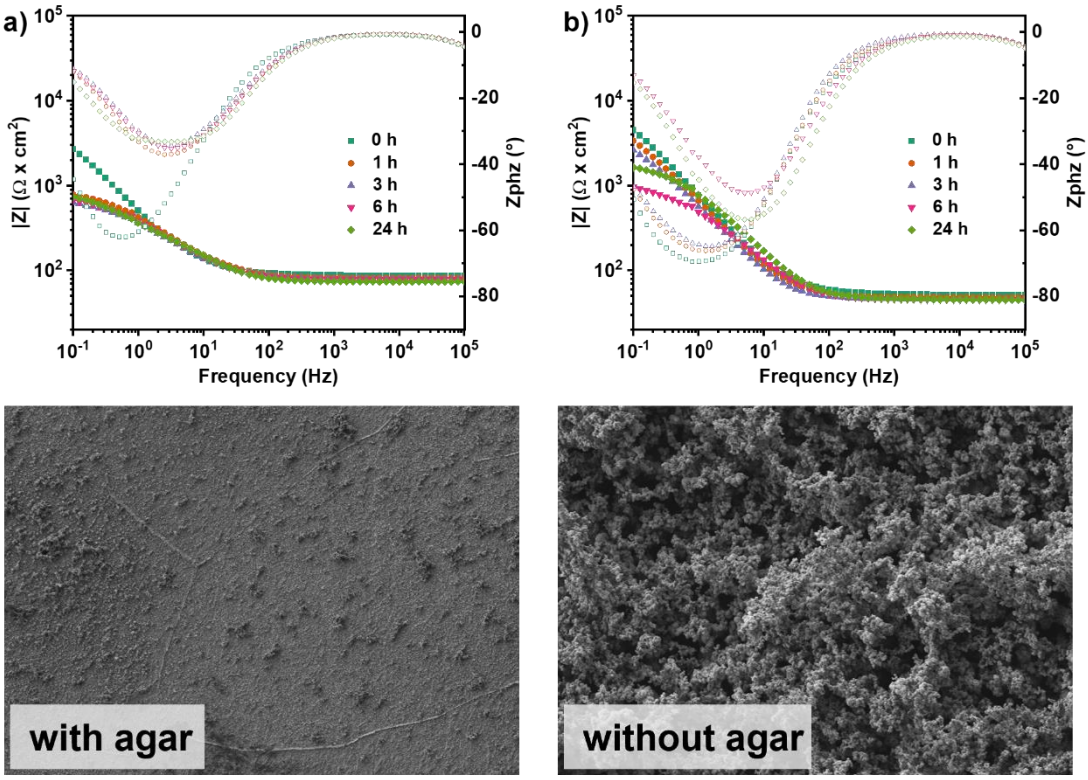

References

[1] Y. F. Zheng, X. N. Gu, F. Witte, *Materials Science and Engineering: R: Reports* **2014**, 77, 1–34

[2] A. Heyn, *IOP Conf. Ser.: Mater. Sci. Eng*. **2020**, 882, 12010.

Efficient coating process using robots and water-based coating material

Šimun Jurišić[1], Ivan Stojanović[1], Vinko Šimunović[1], Marin Kurtela[1], Vesna Alar[1], Marko Bilmez[2]

[1]Faculty of Mechanical Engineering and Naval Architecture, Zagreb, Croatia

[2]Ember kamin d.o.o., Velika, Croatia

Abstract: Nowadays, the need to reduce CO_2 consumption and increase energy efficiency is growing. The use of wood-burning stoves for space heating is energy acceptable because wood is considered a renewable energy source and, as a fuel, has an almost neutral impact on CO_2 emissions into the atmosphere. During the stove production process, manual electrostatic application of liquid coatings based on organic solvents is most often used, which significantly increases the negative impact on the environment that occurs in the production process. Organic solvents are based on carbon and its compounds and reducing carbon emissions into the environment is one of the most current topics in the field of environmental protection and sustainability. In this paper, the existing technology of manual electrostatic application of solvent-based coatings will be analyzed, as well as the introduction of new coatings and coating process improvement using robots. In order to minimize the impact on the environment, it is necessary to select a new protective coating material based on water, which leads to the elimination of carbon emissions. New protective coating material should be resistant to high temperatures (up to 600 °C), withstand high loads in heating and cooling processes, keep the color shade under load and be in line with the service life of the heating system. Introducing robots to the painting process leads to reduced paint consumption, improved product quality, increased efficiency, and a healthier and cleaner environment. The results of this analysis show the improvement of the painting process and the performance of the water-based protective coating which further increases the quality of the product.

Keywords: Organic solvents, water-based coating, process efficiency, robot application

Self-assembled monolayers of phosphonic acids for improved bronze protection by polyurethane coating

Nina Carek, Dajana Mikić, Angela Kapitanović and Helena Otmačić Ćurković, Faculty of Chemical Engineering and Technology, University of Zagreb, Zagreb/Croatia

Bronze objects, such as historical and cultural artefacts, are often exposed to outdoor environment where deterioration of their surface occurs due to the atmospheric corrosion. Organic coatings are often used for protection of bronze surfaces, but in the case of objects of cultural heritage only limited number of coatings, that satisfy criteria of conservation ethics, can be applied. For that reason, the obtained protection level and protection duration are limited. This work examines the possibility to improve the corrosion protection, offered by polyurethane coating, by pretreatment of bronze surface with long-chain phosphonic acids. They can form self-assembled monolayers on bronze surface which can act as adhesion promoters between the coating and the bronze substrate. The influence of two phosphonic acids on adhesion of polyurethane coating is examined. The level of bronze protection in simulated acid rain solution is studied by the means of electrochemical impedance spectroscopy. Additionally, bronze samples covered by polyurethane coating are exposed to high humidity conditions and afterwards characterized by optical microscopy and SEM, as well as by electrochemical impedance spectroscopy.

This work has been fully supported by Croatian Science Foundation under the project IP-2019-04-5030.

Poly-aminoindoles as alternative coatings against corrosion: Electrochemical study in simulated seawater

Erik Castañeda[1,2], Francisco Armijo[1,2], Ignacio Vargas[1,2], (1) Pontificia Universidad Católica de Chile, Santiago. (2) Marine Energy Research and Innovation Center (MERIC), Chile.

Indoles with different substituent groups have been used to modify surfaces for different applications. This is because of its good thermal stability and high redox activity compared to other polymers [1]. In addition, indoles can be easily electro-polymerized over conductive substrates, such as stainless steel (SS). This has motivated the study of the anticorrosion properties [2]. The poly-aminoindoles belong to the family of poly-indoles. Their Physico-chemical properties, synthesis methods, and anticorrosive behavior have not been completely understood.

This work obtained poly-n-aminoindoles (n = 5 and 6) electrodeposition onto AISI 304 SS surfaces through cyclic voltammetry and pulse potential techniques to generate a protective coating towards corrosion. To study polymer's different structures and thickness, the obtained materials were characterized by FESEM technique. In addition, electrochemical studies including open circuit potential (OCP), linear polarization resistance (LPR), Tafel diagrams, and electrochemical impedance spectroscopy (EIS) were performed in coupons exposed for different times to simulated.

The OCP values of the coatings show a shift towards more positive potentials than bare SS, indicating an ennoblement process. Finally, LPR and EIS data show the effect of the tested coatings on corrosion mitigation. Indeed, results suggest that the protection over time depends on each polymer's morphology and conductive properties. Finally, our findings indicate that these materials emerge as a promising alternative to avoid SS corrosion in saline environments. A multi-technique approach including electrochemical and spectroscopic studies will lead us to develop novel anticorrosion coating for metals.

References

[1] Zhou, W., & Xu, J. (2017). Progress in conjugated polyindoles: synthesis, polymerization mechanisms, properties, and applications. *Polymer Reviews*, *57*(2), 248-275.

[2] Deshpande, P. P., & Sazou, D. (2016). *Corrosion protection of metals by intrinsically conducting polymers*.

The impact of bioactive coatings on bone implants corrosion

Dragana Bjelić & Matjaž Finšgar, Faculty of Chemistry and Chemical Engineering, University of Maribor, Smetanova ulica 17, 2000 Maribor, Slovenia

Background: Corrosion is one of the main factors limiting the biocompatibility of bone implants and increasing the need for revision surgery due to the shorter lifespan of implants. Particles released into the tissue environment as a result of corrosion trigger an inflammatory response and lead to aseptic loosening [1]. The lifespan of the implant can be extended and thus the revision operation can be postponed by choosing the method of fabrication and processing of the implant [2]. The susceptibility of the implant material to corrosion must be checked after each coating and the corrosion rate should not increase compared to uncoated material [3, 4]. We have observed in the past that several bioactive coatings promote corrosion, which is an undesirable effect.

Methods: Coatings of chitosan, chitosan-alginate, and alginate were applied by drop-casting method on Ti6Al4V disks and Ti6Al4V 3D printed samples. The corrosion susceptibility was tested using the electrochemical impedance spectroscopy (EIS) and cyclic polarization (CP) techniques. EIS measurements were carried out after 1, 3, 5, 7, and 10 h of immersion in 0.9 wt% NaCl at 37 °C to simulate time-dependent corrosion behavior in the human body. An analysis of the rate of degradation of the coating was also performed by analysis of swelling and degradation. The results were statistically evaluated, and correlations were determined.

Results: The applicability of the bioactive coatings on the implant materials was demonstrated for all developed coatings and both tested materials. Based on the EIS and CP measurements, a corrosion mechanism was proposed and rate determining corrosion reaction was determined. Since the coated material did not corrode faster than the uncoated one, the applicability of such a composite design can be used for further testing, i.e. biocompatibility, cell viability and gene expression analysis of cells exposed to tested materials.

V. M. S. Muthaiah, S. Indrakumar, S. Suwas and K. Chatterjee, *Bioprinting* **2022**, *25*, e00180.
S. Pal, M. Finšgar, T. Bončina, G. Lojen, T. Brajlih and I. Drstvenšek, *Materials & Design* **2021**, *211*, 110184.
U. Maver, K. Xhanari, M. Žižek, L. Gradišnik, K. Repnik, U. Potočnik and M. Finšgar, *Carbohydrate Polymers* **2020**, *230*, 115612.
M. Finšgar, A. P. Uzunalić, J. Stergar, L. Gradišnik and U. Maver, *Scientific Reports* **2016**, *6*, 26653.

Modified epoxy coatings on cast iron

Marin Kurtela[1], Vinko Šimunović[1], Vesna Alar[1], Marina Samardžija[2]

[1]Faculty of Mechanical Engineering and Naval Architecture, University of Zagreb, Croatia

[2]Faculty of Mining-Geology-Petroleum Engineering, University of Zagreb, Croatia

Abstract

The application of organic coating on cast iron is one promising strategy for extending its service life by providing a passive physical barrier between the corrosive environment and metal surface. Among these protective properties of organic coating, epoxy coating is the most broadly applied material for industrial and engineering applications due to their advantages of good protection effect, simple method, good adhesion to metals, high corrosion resistance and low cost. However, water, oxygen and corrosive ions can diffuse into the epoxy resin through coating defects derived from improper curing, low cross-link density and local shrinkage resulting in coating delamination and substrate corrosion. Such wear can be seen in lower protective efficiency resulted from blistering, cracking, increase of pore volumes and number as well as from loss of adhesion to the substrate. Therefore, under the influence of aggressive media, epoxy coatings undergo both chemical and mechanical degradation which results in decrease of their operational durability.

In this paper, commercial epoxy was modified by adding micro metal powders (Cu, Ni, Al, Zn and Ag) and coated on cast iron. Also, laboratory tests of modified epoxy coated on the cast iron samples were performed, in which the physical and chemical properties of the coating were tested after exposing the samples to corrosive conditions of the salt and humid chamber. Furthermore, the resistance of the coating was examined by electrochemical impedance spectroscopy (EIS), during which the samples were immersed in 3.5 % NaCl aqueous solution at a temperature of 20 °C and 50 °C. The electrochemical results revealed that protective performance of epoxy coatings provide good protection in NaCl solution at both temperatures.

Keywords: *corrosion, modified organic coatings, micro metal powders, electrochemical impedance spectroscopy (EIS), chloride medium*

Assessment of the Antibiofilm Performance of Chitosan-Based Surfaces in Marine Environments

Marta Lima[1,2], Luciana C. Gomes[1,2], Maria J. Romeu[1,2], Jesus Valcarcel[3], José Antonio Vázquez[3], Miguel A. Cerqueira[4], Lorenzo Pastrana[4], Ana I. Bourbon[4], Ed.D. de Jong[5], Jelmer Sjollema[5] and Filipe J. Mergulhão[1,2]

[1]LEPABE-Laboratory for Process Engineering, Environment, Biotechnology and Energy, Faculty of Engineering, University of Porto, Rua Dr. Roberto Frias, 4200-465 Porto, Portugal.
[2]ALiCE - Associate Laboratory in Chemical Engineering, Faculty of Engineering, University of Porto, Rua Dr. Roberto Frias, 4200-465 Porto, Portugal
[3]Grupo de Reciclado y Valorización de Materiales Residuales (REVAL), Instituto de Investigaciones Marinas (IIM-CSIC), C/Eduardo Cabello, 6, CP36208 Vigo, Galicia, Spain.
[4]International Iberian Nanotechnology Laboratory, Department of Life Sciences, Av. Mestre José Veiga s/n, 4715-330 Braga, Portugal.
[5]Department of Biomedical Engineering, University of Groningen, University Medical Center Groningen, Groningen, The Netherlands.

Marine biofouling is a natural process often associated with biofilm formation on submerged surfaces. It is responsible for surface corrosion and for the increasing drag resistance, which leads to higher maintenance costs and fuel consumption, creating a massive economic and ecological burden. Although several biocides, cleaners and antifouling agents have been used to prevent biofouling, most of them can affect marine ecosystems and human health, emphasizing the need to develop new and environmentally friendly antifouling approaches such as bio-based coatings. Chitosan (CS) is a polysaccharide that can be extracted from chitin (found in by-products from the fishery industry) and with outstanding biological properties such as non-toxicity and antimicrobial activity.

This work aimed to produce and characterize CS-based surfaces with antimicrobial and antifouling properties. For this purpose, polylactic acid films were coated with CS of different molecular weight (Mw) and concentrations by dip coating. The antimicrobial activity of the produced surfaces was assessed against Cobetia marina, a ubiquitous bacteria isolated from aquatic ecosystems, for 7 weeks under controlled hydrodynamic conditions. Results demonstrated surfaces treated with 0.5% and 1% (w/v) of CS exerted a significant antimicrobial performance by reducing the number of culturable cells up to 58% and 69%, respectively, compared to control. Additionally, results suggest that CS coatings using lower Mw CS had higher antimicrobial activity. The antifouling effect was corroborated by Optical Coherence Tomography, as 0.5% and 1% (w/v) CS treated surfaces reduced the biofilm thickness by up to 16% and 31%, respectively, being their activity dependent on CS Mw. Overall, CS coatings showed to be a promising approach to reducing biofouling under the marine environmental conditions mimicked in this work, contributing to the valorization of marine waste and encouraging further research on this topic.

An effective poly (ethylene) oxide sol-gel coating reinforced with SiO_2 nanoparticles to enhance the corrosion resistance of PEO-coated AZ31B Mg alloys

E. Merino[1], A. Durán[1], Y. Castro[1], Instituto de Cerámica y Vidrio, CSIC, Campus de Cantoblanco, 28049 Madrid, Spain

Magnesium and its alloys have become a hot research topic for a variety of industries due to its excellent mechanical and physical properties; particularly, its low density and high strength-to-weight ratio. Unfortunately, their high susceptibility to corrosion strongly limits its wide applications. To improvement of the corrosion resistance performance of Mg alloys without adversely affecting the mechanical properties, multilayer deposition systems obtained through the combination of plasma electrolytic oxidation (PEO) and sol-gel techniques can be considered as promising solution. However, in terms of corrosion protection, the deposition of a highly cross-linked and crack-free silica sol-gel coating allows for a rapid deterioration of the system to be avoided. Under this perspective, it is important to control the synthesis parameters of the sol-gel coating. In our case, the incorporation of SiO_2 nanoparticles together with an organo-functional group, such as GPTMS (3-(glycidyloxypropyl) trimethoxysilane), and boron trifluoride diethyl etherate (BF_3OEt_3) as ring epoxy opening agent, could increase the stiffness and density of the network, and therefore the corrosion resistance.

Thus, the aim of this work focuses on the development of a *highly cross-linked hybrid poly (ethylene) oxide sol-gel coating* reinforced with SiO_2 nanoparticles to increase the corrosion protection of the Mg Alloy. The results showed that an increment of the BF_3OEt_3 amount promotes the inorganic and the organic polymerization at the same time through the formation of a poly (ethylene oxide) chain. The structural and electrochemical characterizations of the different hybrid coatings were performed using ^{13}C and ^{29}Si Solid State NMR Spectroscopy and Electrochemical Impedance Spectroscopy (EIS), respectively. Since the organic and the inorganic polymerization reactions are in competition, a good control of both processes allows for the best corrosion resistance performances to be obtained.

The optimized silane coating was further deposited on a PEO coated AZ31B Mg alloy. The results reveal that the combination of PEO with the appropriate sol-gel formulation is a promising solution to controlling the corrosion performance of Mg alloys.

Ultrasonically enhanced cerium based conversion chemistry for the corrosion protection of aluminum alloys

Lukas Ruhm, Paderborn University, Paderborn/Germany

Pascal Vieth, Paderborn University, Paderborn/Germany

Guido Grundmeier, Paderborn University, Paderborn/Germany

Ultrasound (US) can be used to modify the microstructure and chemistry of metal surfaces[1] and therefore could be of advantage for the development of sustainable surface treatments of aluminum alloys. The effectiveness of the method has already been demonstrated by the formation of cerium oxide conversion coatings on aluminum and magnesium alloys.[2] However, the influence of the alloy composition on the effect of the ultrasound remained unclear so far. In this work, the morphology, surface chemical composition, and corrosion properties of AA 2024 and AA 7075 as treated in cerium nitrate and zirconium oxynitrate solutions under US enhancement were comparatively studied. Additionally, the influence of the pH on the effect of the ultrasound was investigated. The morphology was analyzed by means of scanning electron microscopy (SEM), revealing a significantly different effect of the sonication process for the two alloys. The corrosion resistance was studied electrochemically by means of linear sweep voltammetry (LSV) and electrochemical impedance spectroscopy (EIS). The chemical composition of the surface was analyzed by infrared reflection absorption spectroscopy (IRRAS) and X-Ray photoelectron spectroscopy (XPS), showing that an effective corrosion inhibition was achieved by very low surface concentrations of cerium and zirconium. The delamination resistance of the surfaces was measured after application of a model epoxy-amine adhesive. The US-supported treatment clearly led to an improved wet adhesion and reduced delamination kinetics.

[1] E. V. Skorb, D. G. Shchukin, H. Möhwald, D. V. Andreeva, *Nanoscale* **2010**, *2*, 722.

[2] a) E. Skorb, D. Shchukin, H. Möhwald, D. Andreeva, *Langmuir* **2010**, *26*, 16973; b) C.-N. Liu, M. Wiesener, I. Giner, G. Grundmeier, *Front. Mater.* **2015**, *2*, 68.

Cost effective sealing of porous PEO coating on AZ31 magnesium alloy by removable water and oil based preservatives

Filip Pastorek, University of Žilina, Research Centre, Žilina/Slovak Republic;
Milan Štrbák, University of Žilina, Department of Materials Engineering, Žilina/Slovak Republic;
Branislav Hadzima, University of Žilina, Research Centre, Žilina/Slovak Republic,
Jana Pastorková, University of Žilina, Research Centre, Žilina/Slovak Republic

Plasma electrolytic oxidation (PEO) provides a thick and adherent ceramic-like coating on magnesium alloys performing high wear resistance and improving the corrosion resistance. However, this corrosion resistance is limited under long-term exposure in aggressive chloride-containing environments due to the presence of defects as pores and cracks in the PEO layer. A major strategy to overcome this problem is to seal these defects by second layer that would fill the pores and even improve the overall surface qualities. However, generally used techniques of post-treatment create a permanent surface layer that is not suitable for applications where just temporary corrosion protection of PEO is required (for example a marine transport of semi-final Mg products treated by PEO) and many of these techniques are not cost effective. Presented research deals with an alternative solution of anti-corrosive temporary protection enhancement of PEO coating prepared at AZ31 magnesium alloy in aggressive corrosive environments by impregnation of the layer with commercially available transparent preservative products containing corrosion inhibitors allowing direct dipping application and removability by standard alkaline cleaners. The evaluation of the effect of the performed surface treatment was performed using electrochemical methods, namely electrochemical impedance spectroscopy (EIS) and potentiodynamic polarization (PD) in 0.1M NaCl, as well as using exposure methods such as immersion test in 3.5% NaCl and salt spray test according to STN EN ISO 9227. The obtained results confirmed sufficient improvement of corrosion resistance reached by PEO sealing in all tested aggressive environments compared to pure PEO coating on AZ31 surface.

Effect of Laser Surface Melting on the Corrosion Resistance of Adhesive/Al 7075 Alloy Interfaces

P. Vieth[a], M.-A. Garthe[a], M. Voigt[a], C. Ebbert[a], C. Weinberger[b], M. Tiemann[b], G. Grundmeier[a]

[a]Paderborn University, Technical and Macromolecular Chemistry, Warburgerstr. 100, 33098 Paderborn, Germany

[b]Paderborn University, Inorganic Chemistry, Warburgerstr. 100 33098 Paderborn, Germany

High strength aluminum alloys are used in a wide range of applications such as aircraft or automotive industries although they are affected of local corrosion due to the presence of intermetallic particles in the aluminum oxide matrix. Therefore, laser surface melting treatments have gained increasing attention as an alternative to improve corrosion resistance of high strength aluminum alloys such as Al 7075.

Surface laser melting of 7075-T6 alloy prior to the application of epoxy adhesives films was performed under different oxygen containing and pure nitrogen gas atmospheres by means of a continuous laser operating at a wavelength of 1064 nm. The surface near changes in microstructure and chemical composition were analysed by means of FE-SEM, XRD and XPS analysis.

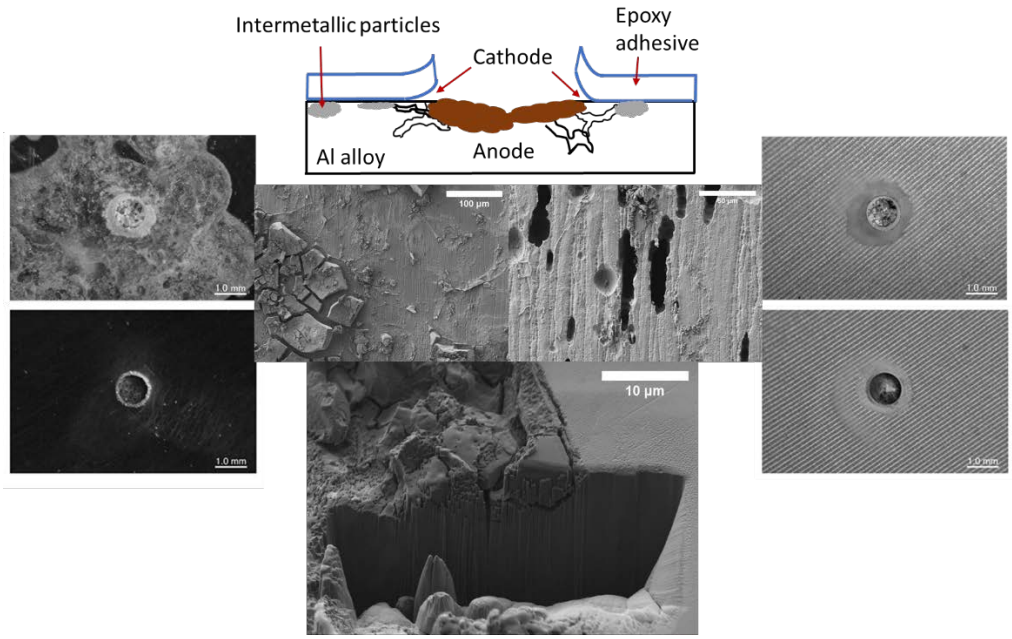

Figure 1: Microscopic images of corrosion at epoxy/Al 7075 interfaces as a function of the interface chemistry

The aim of this research study was to fundamentally understand how the surface near region of the alloy is modified and how this affects the adhesion and corrosive delamination of adhesives. The additional adsorption of phosphonic acid monolayers led to an overall increase of interface stability, which could be assigned to the inhibition of interfacial corrosion reactions and to the formation of acid-based interactions between the phosphonic acid group and the Al-oxide surface.

Acknowledgement

The authors acknowledge the partial funding of the project by the German Science Foundation (SPP 2122, GR 1709/26-1).

Fabrication and characterisation of additive manufactured Ti-6Al-4V parts by laser powder bed fusion (L-PBF) technique

N. Godja [1], A. Schindel [1], L. Payrits [1] Z. Pasztor [2], B. Hegedüs [2]

[1] CEST Kompetenzzentrum für electrochemische Oberflächentechnlogie GmbH, Wiener Neustadt/Austria ; [2] Premet Kft, Budapest/Hungary

To improve aircraft resource-efficiency and to decrease fuel consumption and CO_2 emissions innovative solutions with superior mechanical properties for advanced structures are in development. Ti6Al4V alloys, due to a high strength-to-weight ratio compared to steel or aluminium can keep the structural weight and size ratio low. However, lightweight construction with this alloy is currently only possible with conventional techniques as CNC machining, casting that lead to a high proportion of raw material removal. This is not cost-efficient and works with a high ecological footprint. A primary alternative for fabrication of advanced functional lightweight metallic parts is additive manufacturing (AM), offering benefits in terms of weight, design and functionality, lead time and cost/manufacturability and allowing for alternative geometric shapes, thereby decreasing the weight of the component without sacrificing component strength and safety. However, AM has not yet been approved for structural components with high safety requirements to date, as there are still technology gaps: material property control, correlation between process and structural properties, effect of defects, quality control. Material and mechanical properties of AM parts differ substantially from the properties of the same parts produced by conventional casting. Therefore, a damage tolerance assessment needs to be performed for AM parts in commercial aircraft applications to meet functional and safety requirements. Currently, pores and other defects cannot be completely avoided, but they should be kept as low as possible at the stage of manufacturing. Mechanical properties of the as-built parts can be further improved by the application of different treatments. The influence of different treatment methods (heat treatment, CNC milling, electropolishing, chemical polishing) and operation parameters has been investigated by SEM / EDX, XRD, EBSD and FIB measurements in view of surface roughness, potential anomalies in chemical composition at the surface, and potential cracking. Characterization results of as built and treated samples will be discussed and presented in this work.

Hybrid PEO/sol-gel coatings loaded with Ce for corrosion protection of AA2024

Esther López, Complutense University of Madrid, Spain

Rubén Del Olmo, Military University of Technology, Poland

Endzhe Matykina, Complutense University of Madrid, Spain

Marta Mohedano, Complutense University of Madrid, Spain

Raúl Arrabal, Complutense University of Madrid, Spain

Abstract:

Plasma Electrolytic Oxidation (PEO) has emerged as an eco-friendly alternative to conventional protection methods in the transport industry as it produces multifunctional ceramic coatings with excellent wear and corrosion performances. Coating thickness is usually in the range between 50 and 100 μm and sealing is often required due to the inherent porosity of the coating allowing aggressive species to reach the substrate. These aspects limit the industrial mass production of conventional PEO and, in particular, restrict their use for fatigue sensitive applications.

In order to overcome these drawbacks, the present work combines two cutting-edge routes for the corrosion protection of alloy AA2024-T3: (i) the development of thin or Flash-PEO coatings (<10 μm, 100 s) and (ii) their combination with hybrid sol-gel (HSG) coatings that incorporate Ce (III) as corrosion inhibitor.

Coatings characterization was carried out using different techniques such as X-ray diffraction (XRD), scanning electron microscopy (SEM) and Fourier transform infrared spectroscopy (FTIR). Corrosion performance of the coatings was assessed by using electrochemical impedance spectroscopy (EIS) and an immersion test in 3.5 wt.% NaCl aqueous solution.

Flash-PEO coatings were successfully developed and sealed with a uniform top HSG layer. The incorporation of Ce in the latter provided self-healing properties to the hybrid system, thus showing the potential of these coatings as a Cr-free alternative for protection of aluminium alloys.

Aluminium alloy corrosion inhibition by two-stage modified zeolite

S.Korniy,I. Zin*, L. Kwiatkowski**,M.-O. Danyliak*,O. Khlopyk**

**Karpenko Physico-Mechanical Institute, NAS of Ukraine,*
Naukova Str., 5, 79060, Lviv, Ukraine
*** Łukasiewicz Research Network - Institute of Precision Mechanics,*
Duchnicka Str., 3, 01-796 Warsaw, Poland

A two-stage synthesis of anti-corrosion pigments for organic primer coatings based on synthetic zeolite was performed. New inhibiting pigments retain the zeolite framework structure, in the nanopores of which the amorphized phosphate phase is formed. The synthesized complex pigments effectively reduce the corrosion of an aluminium alloy in chloride solution due to mixed cathodic-anodic control. The most effective pigment is obtained by mechanochemical modification of zeolite with calcium cations, followed by liquid-phase treatment with a solution of zinc nitrate and sodium phosphate. The phosphate component of the complex pigments is easier to hydrolyze compared to aconventional zinc phosphate due to its nanostructured and amorphous nature. It is likely, the phosphate phase, intercalated in nanopores and deposited on the surface of the zeolites, slowly dissolves, releasing Zn^{2+}, Ca^{2+} and phosphate ions into the chloride solution. Then they interact with each other, cations of the substrate metal and hydroxyl ions, forming a protective film on the cathode and anode sections of the aluminum alloy, which includes sparingly soluble hydroxides and phosphates. The pigments can become promising inhibitory components of primer paints used for the protection of structures made of aluminium alloys in an industrial atmosphere environment.

Acknowledgment. The work was performed within the project No. 2020.02/0063 “Synthesis and properties of new complex anti-corrosion pigments for paint coatings based on aluminosilicate nanocontainers” of the National Research Foundation of Ukraine.

Effect of boron dispersion phase content on the microstructure and corrosion resistance of the Ni-B/B composite coatings

Katarzyna Skroban, Anna Gajewska-Midziałek, Grzegorz Cieślak, Marta Gostomska, Tinatin Ciciszwili, Edyta Pęśko, Anna Kapuścińska, Maria Trzaska, Zofia Buczko
Łukasiewicz Research Network – Institute of Precision Mechanics, Warsaw/Poland;

The paper presents the results of studies of composite coatings with nickel-boron matrix and boron particles as a dispersion phase produced by the chemical reduction method on a steel substrate. Three variants of composite coatings differ in the content of the dispersion phase in bath were produced as well as a nickel-boron coating without dispersion phase.
The topography and surface morphology using the scanning electron microscopy (SEM) were presented. Characterization of the structure of the produced materials was performed using X-ray diffraction analysis and light microscopy. The corrosion tests of the Ni-B and Ni-B/B coatings were carried out with electrochemical potentiodynamic method.
The conducted research allowed to determine the effect of the dispersion phase content in the bath on the corrosion resistance of the produced coatings.

Acknowledgements:
The project „New electroless Ni-B/B and Ni-B/MoS_2 composite coatings with improved mechanical properties” benefits from a €200 000 grant from Norway. The aim of the Small Grant Scheme (SGS) call is to support applied research projects led by female scientists in technical sciences.

Keywords: Ni-B, electroless deposition, composite coatings

New waterborne zinc primers

I. Gajecka[*], *S. Piłat*[*], *L. Komorowski*[**], *A. Królikowska*[**], *I. Kunce*[**],
M. Urbański[**], *D. Wojda*[**], *K. Zacharuk*[**], *E. Langer*[***], *M. Zubielewicz*[***]

[*]*Polish Corrosion Society, Gdańsk (Poland), e-mail: sekretarz@psk.org.pl*
[**]*Road and Bridge Research Institute, Warsaw (Poland), e-mail: akrolikowska@ibdim.edu.pl*
[***]*The Łukasiewicz Research Network - Institute for Engineering of Polymer Materials and Dyes, Gliwice (Poland), e-mail: malgorzata.zubielewicz@impib.lukasiewicz.gov.pl*

Keywords:

waterbased zinc-pigmented primers, ecological paint, primers with reduced zinc content

Abstract

The main problem in the preparation of zinc-containing waterborne primers is to avoid the evolution of hydrogen in the contact of the zinc particles with water, which results in the risk of explosion or coating failures.

The aim of the project under the acronym EcoWaterZinc, implemented under the CORNET Initiative, is to develop new primers with the lower content of the zinc with special modified zinc particles and good anticorrosion properties.

Corrosion-induced hydrogen absorption and embrittlement of Ultra-high-strength steel with Zn-based coatings in neutral aqueous conditions

Hye Rin Bang[a], *Jin Sung Park*[a], *Yong Bum Park*[a], *Seung-Pill Jung*[b], *Sung Jin Kim*[a]

[a]*Sunchon National University, Suncheon, Jeonnam, Republic of Korea*

[b]*Hyundai-Steel, Dangjin, Chungnam, Republic of Korea*

Ultra-high-strength steel sheets with a tensile strength of more than 1000 MPa have been developed and attracted the attention of the scientific and industrial communities. Despite their superior mechanical properties, their susceptibility to hydrogen embrittlement are regarded as a critical drawback that has restricted their commercial applications to auto-parts. In addition, their susceptibility can be dependent upon the types of coating on their surfaces. In particular, the hydrogen absorption and penetration, induced by corrosion can be considered as a controlling factor for the embrittlement.

In this work, the susceptibility to corrosion-induced embrittlement of two types of Zn-based coated steels (galvanized (GI) and galvannealed (GA) coatings) was compared in terms of hydrogen evolution, absorption, and cracking behaviors in neutral aqueous conditions. The results showed that the hydrogen evolution and absorption behaviors were controlled primarily by the electrochemical potential differences between the Zn-based coating and exposed steel, and the localized damage pattern of the coating in an advanced state of corrosion.

Improvement of the tribocorrosion properties of tungsten carbide (WC-Co) samples coated via PVD

José Antonio García Lorente, Institute for Advanced Materials and Mathematics (INAMAT2), Universidad Pública de Navarra (UPNA), Pamplona/Spain

Adrián Claver, Institute for Advanced Materials and Mathematics (INAMAT2), Universidad Pública de Navarra (UPNA), Pamplona/Spain

Mikel Marqués, Institute for Advanced Materials and Mathematics (INAMAT2), Universidad Pública de Navarra (UPNA), Pamplona/Spain

Eluxka Almandoz, Centre of Advanced Surface Engineering (AIN), Cordovilla/Spain

Jonathan Fernandez de Ara, Centre of Advanced Surface Engineering (AIN), Cordovilla/Spain

José Fernandez Palacio, Centre of Advanced Surface Engineering (AIN), Cordovilla/Spain

This study aims to investigate the improvement of the tribocorrosion properties of WC-Co substrates by coating them with hard coatings such as AlCrSiN using cathodic arc deposition. WC-Co is commonly used in the fabrication of machining and cutting tools; however, there are some materials like titanium or stainless steel that are difficult to work with; furthermore, in aggressive environments or under high temperatures the performance of the machining tools can be affected, and a failure may occur. This coating is intended to ensure the correct performance of the tools in any conditions. The coatings were characterized by Glow Discharge Optical Emission Spectroscopy (GDOES), Scanning Electron Microscopy (SEM) and X-ray diffraction (XRD). Tribocorrosion, tribology and corrosion tests were performed to evaluate the tribocorrosion properties of the samples. Furthermore, mechanical and adhesive properties of the coating were studied using scratch and nanoindentation tests. The results showed improved tribocorrosion properties of the samples combined with good adhesive and mechanical properties. These results show the possibility of using these coated materials in the most demanding cutting and machining applications.

Sub topic: Tribocorrosion, PVD, Tungsten carbide, cathodic arc, machining

Galvanic corrosion between Ti and CoCrMo alloy in human synovial fluids

Abstract: Ti/CoCrMo coupling is widely used in joint prostheses due to its outstanding corrosion resistance and mechanical properties. In this study, the galvanic corrosion behavior between Ti and CoCrMo alloy in human synovial fluids is investigated with electrochemical techniques, including open circuit potential (OCP), potentiodynamic methods and electrochemical impedance. The results show the corrosion behavior of Ti is patient-dependent, with the corrosion can be one magnitude different. However, the corrosion behavior of CoCrMo alloy varies little with patients. The OCP values of both materials are very close, with the highest difference being lower than 0.2 V, indicating this is no galvanic corrosion between Ti and CoCrMo alloy in human synovial fluids.

Sol-Rec2 Case Study: Assessment of Corrosion Behaviour of Aluminium and Degradation of Polymers During Delamination of Multi-Material Packaging Systems

Berenika Syrek-Gerstenkorn, Shiladitya Paul, Andrew P Abbott,

University of Leicester, UK

Currently, multi-material packaging waste continues to pose a major challenge for recycling due to the difficulty in separating the individual components from other plastic waste streams. Blister packs, crisp packets or yoghurt lids are typically composed of multiple materials including two or more types of polymers and an aluminium layer, requiring appropriate separation methods.

A possible candidate for separation of layers in multi-material packaging is the use of deep eutectic solvents. These solvents are considered "green" - due to their low toxicity. They also offer a number of beneficial properties such as ease of preparation and handling and low cost.

In this project (Sol-Rec2, funded by the European Union's Horizon 2020 research and innovation programme under grant agreement N° 101003532) several deep eutectic solvents were developed and tested for efficacy in separating of multi-layer packaging waste. The solvents were then assessed based on their corrosivity towards the aluminium film as well as reactivity with polymeric layers (PP, PE and PVC). Electrochemical methods were employed to assess the corrosion rate of aluminium. A potential dissolution of the polymers was studied based on the mass change and microscopic evaluation of samples immersed in selected liquids at elevated temperature.

Long-term corrosion monitoring: A prediction tool using the "SOCORRO" system

Burak Karabulut, KU Leuven, Sint-Katelijne-Waver/Belgium

Brent Verhoeven, KU Leuven, Sint-Katelijne-Waver/Belgium

Geert Potters, Antwerp Maritime Academy, Antwerpen/Belgium

Shahin Gelareh, University of Artois, Béthune/France

Raf Dewil, KU Leuven, Sint-Katelijne-Waver/Belgium

Barbara Rossi, University of Oxford, Oxford/United Kingdom

Abstract

Tackling the corrosion problem in a more efficient way is possible with a systematic approach where corrosion prediction models/algorithms are deemed prominent. The Interreg project "SOCORRO" is launched to develop a general approach to combat the corrosion problem in a more effective, structured, and smart way. The ultimate goal of this project is to develop a prediction algorithm that estimates the corrosion risk under a given set of environmental markers. Thanks to the prediction tool, it is possible to take actions against corrosion such as: hinder it from happening or optimize the choice of preventive actions with respect to life cycle performance of the designs. For this algorithm to function properly, it should be trained by real set of data (both laboratory and field data). One of the case studies that is chosen is wastewater treatment plants which is what this paper covers. Corrosion rates of grade A carbon steel were monitored in a water purification system which works on the principal of a moving bed bioreactor (MBBR). Correlations between environmental parameters and corrosion were evaluated via principal component analysis (PCA) and correlation matrices. For minimizing the noise involved in corrosion datasets, commonly applied digital filters were used. The conclusions on the efficiency of these filters were drawn based on variation in samples of the statistical population. The measured laboratory dataset was used for training the prediction algorithm which was furthermore optimized by real dataset obtained in the field demonstration. The overall conclusion was that the prediction tool works effectively for the recorded databases and could be used extensively for corrosion modelling of such water purification units.

New process for interior pipe rehabilitation with environmentally friendly coating materials

Ralf Feser, Heike Jost, Eva Tarfeld, Haiko Blache, Dennis Kovoussoglou, Tobias Tillmann,
Fachhochschule Südwestfalen University of Applied Science Iserlohn
Dirk Mollenhauer, Sebastian Grahammer, Nadira Grässle, Fa. Warnecke&Böhm

Galvanized steel and copper pipelines destroyed by corrosion cause damage worth billions every year. A sustainable renovation of these lines saves costs and protects the environment. A new process for safe and long-lasting pipe interior renovation with a new type of coating system should be developed.

A new method of rehabilitation is being researched that should avoid the complete replacement of the pipes in the future. There are already attempts to renovate the inside of pipes of this type, but the previous methods are often unsuccessful because they do not completely remove the corrosion products that caused the pipe damage and corrosion later spreads again to the newly coated pipes. In addition, the previously used epoxy coatings are not longer allowed in drinking water applications.

Instead, the new process is based on a combination of cleaning the inner surface of the pipes so that they are suitable for coating, preparatory surface treatment that conforms to drinking water regulations, and then a new type of coating. This should compensate for the disadvantages of the previous methods. Corrosion protection begins at the interface between the metal and the coating. A clean metal surface is a basic requirement.

The application of a subsequent corrosion-inhibiting coating then forms a dense, durable protective film that significantly extends the life of the inner pipe coating. The adsorption of the inhibitors is verified with contact angle measurements, the structure of the surface is assessed with scanning electron microscopic investigations. The coating is tested and further developed with the help of various electrochemical processes and corrosion tests.

The process is funded by the German Federal Environmental Foundation (DBU).

Restoration of iron supporting structure of historic suspension bridge

Hana Geiplova[1], Marketa Vlachova[1], Pavlina Fialova[1], Lubomir Mindos[1]

[1]SVUOM Ltd., Prague/Czech Republic,
geiplova@svuom.cz, vlachova@svuom.cz, fialova@svuom.cz*, mindos64svuom.cz*

Abstract
In 2021 the pre-restauration research and restoration of surface treatment of wrought iron part of historic suspension bridge listed as Czech national cultural monuments was performed. The iron parts had been protected against atmospheric corrosion by various coatings during the decades of exposure. The last coating consists from multilayer system which had been totally failed. The research of material and coating system was performed. The technology of complete renovation of surface treatments was proposed.

Keywords: wrought iron, bridge structure, material composition, painting system, corrosion attack, corrosion protection

Introduction

The principle of building chain bridges was patented in 1801 by James Finley of Pennsylvania in the USA. The first chain bridge in Europe is the Union Bridge over the Tweed River in Great Britain, designed by Samuel Brown, built in the years 1819-1820 and still serves today. Chain bridges were built with popularity in the USA, England, Italy and Russia. The most famous in Czech country was the František Josef Bridge in Prague (construction in the years 1839 - 1841), as well as bridges in Postoloprty, Jaromer, Strakonice, Podebrady, Loket, Podolsko, etc.. The fame of chain bridges was relatively short, most of them were gradually replaced by more modern and stronger ones - only the Podolsko bridge has been preserved.

In 2021 the pre-restauration research and restoration of surface treatment of wrought iron part of historic suspension bridge listed as Czech national cultural monuments was performed. It is the last surviving suspension bridge built in empire style in the Czech Republic. Originally, between 1848–1960, it spanned the Vltava river near Podolsko – Figure 1, South Bohemian region. The bridge served for many years until 1960 when it was decided to take it down. The bridge was dismantled, documented and stored for ten years. After the relocation on the Luznice river near Stadlec, the bridge has been in operation since 1975 – Figure 2 [2].

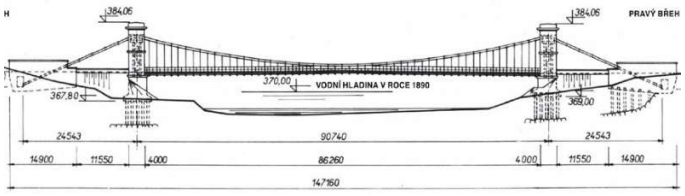

Figure 1 – Original bridge locality and its layout

Figure 2 – Bridge construction cross Luznice near Stadlec

The bridge was dismantled into 2,000 stone blocks and 1,100 steel parts and then reassembled. The total weight of the iron parts was 102 tons.

Wroght iron supporting structure

The basic supporting structure consists of four chains arranged in two pairs. Each link of the chain consists of six lamellae, at the ends provided with eyelets for connecting pins between the centres of the eyelets – Figure 3. These are connected to the wooden deck by vertical rods. The chains are pulled through the holes in the two stone pylons bounding the bridge and anchored in the bricked stone blocks.

Figure 3 – Wrought iron parts (left - chain pin, right – chain link)

During the replacement the chemical composition analysis and basic mechanical properties of selected parts of structure had been done – Table 1.

Wrought iron is an iron alloy with a very low carbon content (less than 0.08%) in contrast to that of cast iron (2.1% to 4%). It is a semi-fused mass of iron with fibrous slag inclusions (up to 2% by weight), which gives it a "grain" resembling wood that is visible when it is etched,

rusted, or bent to the point of failure. Wrought iron is tough, malleable, ductile, and corrosion resistant [3].

Table 1 - Chemical composition analysis and basic mechanical properties of bridge parts

material sample	tensile strength (MPa)	yield strength (MPa)	hardness (HB)	chemical composition (wt. %)				
				C	Mn	Si	P	S
wrought iron	< 340	min 230	-	0.03-0.09	0.02-0.08	0.20	0.10-0.50	max. 0.050
chain pin	375	259	136	trace	0.06	0.18	0.31	0.011
chain link	379	268	129	trace	0.07	0.21	0.30	0.009
bridge hinge	385	299	120	0.02	trace	0.25	0.20	0.003
anchor pin	331	196	117	0.02	0.11	0.09	0.17	0.005

Paint system on wrought iron structure

A direct written mention of the primary original bridge coating was not found, but in the Allgemeine Bauzeitung 1844, an article concerning the opening of the similar bridge in Podebrady in 1842 states that all iron material and wood on the bridge were painted with graphite mixed with coal tar.

After the replacement of bridge, the all paints had been mechanically removed. The new paint system had been applied consisting from the primer oil paint with minium pigment Pb_3O_4 in one coat and two coats of seed oil paint i.e., the classic paint used in 70ties years. All coatings were done before assembly of chains. The wrought iron parts had been protected against atmospheric corrosion by various coatings during the next decades of exposure. According to the data obtained, the paint system of bridge structure was restored in 1981.

The thickness of paint system was measured on representative surfaces including the thickness of mill scale layer. The results are given in Table 2.

Table 2 – Thickness of layers on bridge surfaces

surface	thinkness of layer (μm)		
	average	minimum	maximum
chain pin	494	133	760
chain link	177	58	302
mill scale	58	27	110

The sample of painting system was withdrawn for cross-section evaluation and FTIR analysis. The painting system was created by 6 layers (Figure 4) – 3 layers of painting system applied on 1981 and probably next 3 layers applied as new system without removal of previous layers. There are cracks passing trough whole layers open for diffusion of moisture and pollution species to iron surface and penetration of corrosion products above the painting system surface.

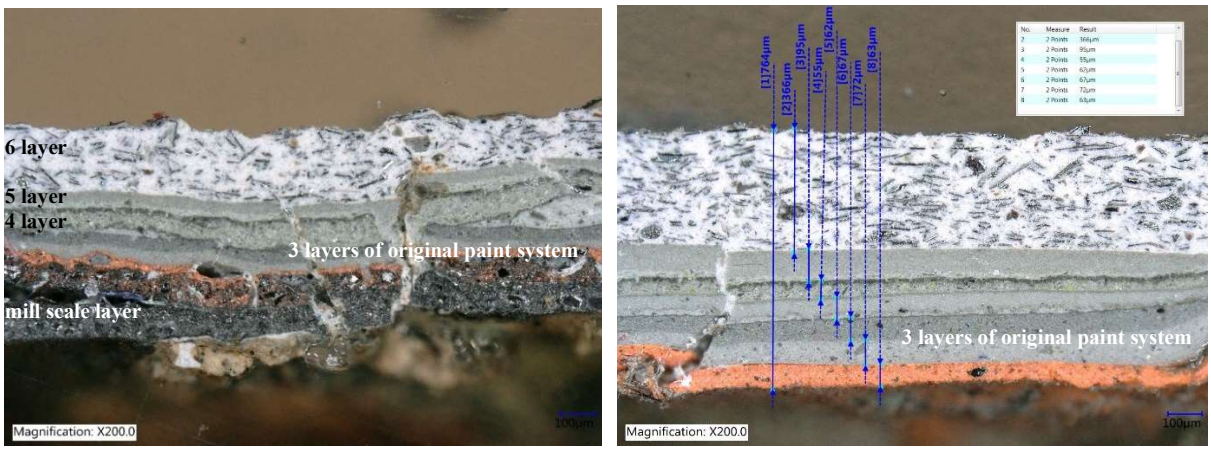

Figure 4 – Cross section of painting systems applied on wrought iron structure

IR spectres were measured on FT-IR spectrometer Nicolet iS5 with ATR module with single-anechoic diamante crystal at spectrum range 4000 – 500 cm^{-1} at resolution 4 cm^{-1}, DTGS detector. The IF spectrum of the first paint layer shows the composition of seed oil with $PbSO_4$ which is result of chemical reaction of minium pigment with air SO_2 pollution – Figure 5. Other layers were based on alkyd resins filled by $BaSO_4$ or kaolin and top layer was based on epoxyester resin filled by talc.

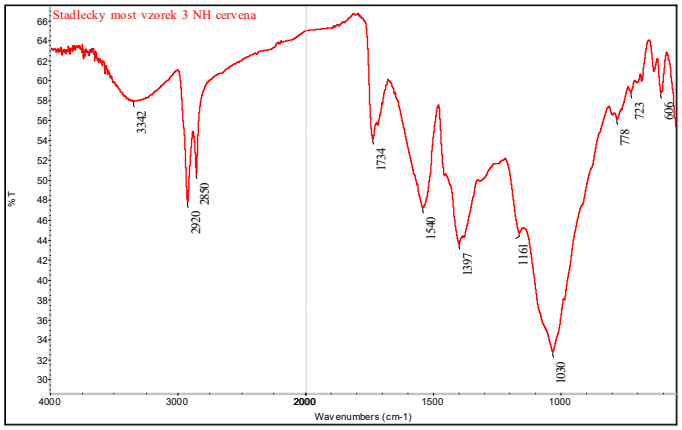

Figure 5 – The IF spectrum of the first paint layer – seed oil with minium pigment

The last coating consists from multilayer system which had been totally failed (cracking, delamination of individual layers) and the primer with minium pigment was evident, on some surface also the mill scale – Figure 6. The most degraded were places on the edges, near joints and crevices. Locally the corrosion of wrought iron occurred.

Based on this preliminary evaluation it was decided for complex renovation of paint system after removal of all non-adhesive layers.

Figure 6 – Defect of painting system – typical examples

Renovation of paint system

Surface pretreatment

The renovation of paint system was done without disassembly of any parts by mechanical tool. After the mechanical cleaning with power tool the residual surface ~~shows~~ were found traces of adhering mill scale, structure of wrought iron, local corrosion attack and the first paint layer with minium pigment – Figure 7. The cleanliness of surface may be estimated as degree St3, locally St2 according to ISO 8501-1.

Paint application

The estimated corrosion category for the bridge site environment is C2 for carbon steel according to EN ISO 9223.

The coating system had to obtain corrosion protection for a long service life - 15 - 20 years, due to limited possibilities of application of coatings in field conditions without disassembly of chains, design of chains, climatic influences and especially the possibilities of surface preparation. As the whole structure of the chain bridge is very subtle, with a large number of slots and joints, this was the reason why it was necessary to choose a coating system that does not produce a hard coating, but soft and flexible ones.

Figure 7 – Appearance of cleaned chain surface

The new painting system was applied as three layers – two layers of primer (red and grey layers) and 1 layer of top coating with total thickness of paining system 180 μm. The paint basis was epoxyester resin.

Figure 8 – Appearance of newly painted surface

Conclusion

At the time the first iron and steel bridges were being built there was little knowledge about the special advantages and disadvantages of these new materials. With appropriate corrosion protection the corrosion loss of structural materials is negligible even after more than 100 years and the bridge structure may serve for transport (limited ones) as and excellent example of technical development of previous centuries.

The crucial for long-term service life of newly applied painting system was the maximally thoroughness preparation of surface and removal of all non-adherent layers on the all surface of the chain.

Acknowledgements

This paper was prepared with financial support of DKRVO project from MPO ČR.

References

1. M. Bussell, The Building Conservation Directory, (2011).
2. F. Stejskal, Stavebnictvi, **9** (2007) 18 (in Czech).
3. C.N. McCowan, T.A. Siewert, J.D. McColskey, K. Hildebrand, D.L. Olson, Materials characterization, **62** (2011) 807

Indoor environment and its aggressivity toward cultural heritage objects made of Lead and its alloys

Dušan Majtás, Institute of Theoretical and Applied Mechanics of the Czech Academy of Sciences, Czech Republic, Pavlína Fialová, SVÚOM ltd., Czech Republic,

Although lead is supposed to be resistant to inorganic acids it is prone to corrosion in organic acids and their fumes. For proper storage of cultural heritage objects both in repositories and in exhibits not only indoor temperature and humidity have to be monitored. It is also necessary to monitor concentration of formic and acetic acid fumes that may evaporate from both objects in the area and containers these objects are kept in; be it exhibit cabinet or storage shelf. Additionally one should be aware of synergic effect that may occur, causing more corrosive environment than expected. Aim of the research was at first to monitor and specify indoor environments of both exhibits and repositories and further modelling indoor conditions using standard corrosion chamber to examine whether there indoor environment conditions may lead to synergic effect. The Indoor conditions in monitored locations were taken into account when designing corrosion tests. Instead of favouring more aggressive conditions to shorten the simulation time desired aim was to produce more realistic corrosion environment. In such setup: what is occurring during the simulation should be corresponding to the real corrosion situation.

As a byproduct of the research question has arisen whether or not spectro-colourimetry can be of any use to monitor corrosion of cultural heritage objects. As the method is relatively cheap and easy to use, it may be suitable for preliminary monitoring in the exhibit or repository. It could not provide information on phase composition of examined corrosion product, but can determine change in surface colour properties and thus warn curators there is aggressive environment causing corrosion to occur and proceed.

Modification of tartaric-sulphuric acid anodizing bath by addition of a short-chain monocarboxylic acid

Eva Šrámková[1], Vít Záliš[2]

[1] Czech Aerospace Research Centre, Beranových 130, 199 05 Praha – Letňany, Czech Republic, sramkova@ vzlu.cz
[2] Czech Aerospace Research Centre, Beranových 130, 199 05 Praha – Letňany, Czech Republic, zalis@ vzlu.cz

Abstract

Nowadays, tartaric-sulphuric acid anodizing (TSA) is widely accepted as an environmentally friendly alternative to chromic acid anodizing (CAA) in aerospace industry. It provides the aluminium substrate with an oxide layer, meeting the requirements such as high corrosion resistance, paint adhesion or low effect on fatigue strength. However, new modifications of TSA process are still searched for with the aim to further improve the properties of TSA anodic layers. In this work, two TSA-based anodizing baths containing additives were studied. The first additive was a molybdenum salt, already discussed in the literature. The second additive was a short-chain monocarboxylic acid. The objective was to compare the modified baths with the traditional TSA and CAA. Also, the effect of two-step sealing procedure based on trivalent chromium on corrosion resistance was evaluated. Following properties of the anodic layers were studied to compare the tested anodizing baths: corrosion resistance, paint adhesion, thickness, or hardness across the substrate-layer. Although the phenomenon was not yet explained, the monocarboxylic acid addition into the TSA bath seemed to intensify the positive effect of two-step sealing on corrosion resistance in the neutral salt spray test. The data presented in this comparative study might also contribute to a better understanding of both modified and traditional TSA anodizing processes.

Keywords

Anodizing, chromic acid anodizing, tartaric acid anodizing, hexavalent chromium replacement, anodic layer sealing

Introduction

Despite the intensive development of composite materials, aluminium, specifically its alloys, is still an unreplaceable material in the aircraft construction [1]. Aluminium is relatively stable in neutral pH environment. However, particularly copper-rich alloys are susceptible to corrosion in acidic or alkaline environment and a proper surface treatment is required. Anodic oxidation in chromic acid (CAA) is a traditional time-tested surface treatment technology of aluminium and its alloys in the aerospace industry. Its history dates to the 1920's [2]. Due to the high toxicity of hexavalent chromium, chromium oxide has been classified as SVHC (Substances of Very High Concern) by the European Community Regulation on Chemicals (REACH) and its specific use is subject of authorization [3]. Although the replacement of this technology is challenging, the health and environmental risks associated with operating the chromate baths are too high despite all the advantages of this technology, such as high corrosion resistance with self-healing properties, good adhesion properties and minimal impact on fatigue properties of the base material.

One of the most promising processes to replace CAA is the anodization in a mixture of tartaric and sulphuric acid (TSA process) [4]. In fact, it is a modification of sulphuric acid anodization. This process has several advantages compared with CAA, such as lower time required to formation of a layer of the same thickness, lower applied voltage, and finally lower environmental impact [5]. Parameters of CAA and TSA processes reported in the literature are given in the following table.

Table 1: Parameters of CAA and TSA processes [5]

Process	CAA	TSA
Time of anodization	45 min	25 min
Temperature	38–42 °C	36–39 °C
Layer thickness	3–5 μm	3–5 μm
Voltage	21±1 V or 40±1 V	14±1 V
Current density	0,3–0,4 A/dm^2	0,6–1 A/dm^2
Electrolyte	65 g/l chromic acid	40 g/l sulphuric acid, 80 g/l tartaric acid

Mechanism of the effect of tartaric acid on the growth and properties of anodic layer is discussed in the literature. Determination of the elemental composition of anodic layer in the cross section shows that tartaric acid is incorporated in the porous structure of the anodic layer only in a small amount, compared with the number of detected sulphur atoms [6]. It seems that tartaric acid as a weak acid does not directly contribute to the formation of the anodic layer, the main source of mobile protons involved in the layer growth is sulphuric acid. Based on these findings, it can be assumed that the main function of tartaric acid is to slow down the dissolution of the anodic layer. This assumption is also confirmed by the observed decrease in the value of steady current during anodization at constant voltage about 20 % in a bath with the addition of tartaric acid. These phenomena can be explained by adsorption of organic groups at the anodic layer and electrolyte interface, followed by reduced dissolution of the oxide layer. The same mechanism is applied during the open circuit state, for example at the end of anodization when parts are being removed from the bath [6], [7], [8]. Another discussed mechanism of tartaric acid role in aluminium anodizing is the chelation of copper ions (in the case of aluminium alloys) dissolved in the anodic layer pores and their removal from the inner pore walls during sealing (i. e. at pH when tartaric acid is in deprotonated form of tartrates) [8].

To obtain required corrosion resistance, porous anodic layers need to be sealed. Chromates (sodium or potassium dichromate solutions) have been traditionally used in this step. A simple ecologic replacement of this process is a hydrothermal sealing in boiling demineralized (DEMI)

water. However, this process does not impart high corrosion resistance to the layers. Verdauger [5] claims, that in case of Al 2024, Al 6061 and Al 7075 alloys anodized in TSA and sealed in boiling DEMI, the corrosion resistance in neutral salt spray (NSS) is only up to 96 hours. Such corrosion resistance is not satisfying and adequate to standard EN 4704 [9] and only closely meets the requirements of the standard EN 4827 [10]. Therefore, new modifications of the TSA process (including sealing step) are proposed and studied. One of the options to increase the corrosion resistance of anodic layers is the addition of various additives to the anodic bath, or into the sealing bath. For example, additives based on inorganic salts, e. g. molybdenum, cerium, vanadium, or manganese are discussed [11], [12]. Trivalent chromium sealing baths have been reported as promising. Where acceptable, longer anodizing times leading to thicker anodic layers are an option to increase corrosion resistance – "TSA long cycle" reported in [7]. One of the TSA bath modifications discussed in the literature is the addition of molybdenum salt into the anodic bath. The positive effect of molybdenum on corrosion resistance is probably due to the ability of molybdenum to change the oxidation state easily. As a result, it can oxidize or reduce by-products of anodizing reactions, having a positive effect on bath stability. TSA bath with molybdenum (Mo-TSA) was patented by Airbus [13]. Another modification discussed in this paper is based on the addition of a short chain monocarboxylic acid into TSA solution (SCHA-TSA).

Experimental

Sample preparation

Aluminium panels (Al 2024-T3, Al 6061-T6, Al 7075-T6) with dimension 75*50*0.8 mm and 125*75*0.8 mm were utilized for this study. Pretreatment of the samples was following: Alkaline degreasing, alkaline etching, and acid desmutting with included rinsing steps in DEMI water between each process. Basic anodizing solution was prepared from H_2SO_4 (p. a., PENTA s. r. o.), L-tartaric acid (p. a., Lach-Ner, s r. o.) and DEMI water. Molybdenum salt, i. e. sodium molybdate (p. a., PENTA s. r. o.), was used to prepare Mo-TSA bath. The second tested anodizing bath was prepared by the addition of a short-chain carboxylic acid. The concentrations of each component except of SCHA-TSA are based on data from literature and are given in Table 2.

Table 2: Chemical composition of baths for anodic oxidation

Bath	Concentration [g/l]			
	H_2SO_4	$C_4H_6O_6$	Na_2MoO_4	SCHA
TSA	40	80	X	X
Mo-TSA	40	80	50	X
SCHA-TSA	40	80	X	<10

Anodizing process was carried out in an experimental galvanic line, equipped with thermostatic regulation of heating, air agitator and external power supply EA-PS 5040-40A driven by computer sequencing. Inox steel plates (AISI 304) were used as cathodes. Titanium racks were used to fasten the samples. There were proper rinsing steps after anodization (three level rinsing). Sealing step was carried out in boiling DEMI water (T > 96 °C). Time of exposure in sealing bath was adjusted according to layer thickness (approximately 3 min/μm). During the two-step sealing process, samples were first sealed in a Cr (3+) bath for a few minutes at laboratory temperature and subsequently hydrothermally sealed in boiling DEMI. After this step, samples were dried at 50–55 °C for 20 minutes. For purpose of organic paint adhesion testing, anodized samples were only dried immediately after anodization and rinsing, and the

sealing step was omitted. Organic paint application was performed within 4 hours after anodization. An epoxy-based primer was used with the thickness of dried layer 30–70 μm.

Anodic layer thickness measurement

A non-destructive (ND) eddy current method was used for rapid layer thickness control (Defelsko PosiTector 6000). Because of low layer thickness, values obtained by ND method were checked by a cross section microscopy measurement.

Corrosion testing

Corrosion resistance of anodized samples was tested in neutral salt spray (NSS). The tests were performed in a calibrated climatic chamber Liebisch SKB 1000 A-TR according to ASTM B 117. Several series of NSS tests were performed to find the optimal process parameters and to verify the results. Based on the information from standard EN 4827 [10], 504 hours in NSS with no visible signs of corrosion was identified as a satisfactory corrosion resistance.

Paint adhesion testing

The adhesion of the epoxy primer coating was tested by a cross-cut test according to EN ISO 2409 [14]. Cross-cut tests were performed with 1mm distance between cuts. Unbound/peeled coating was removed by adhesive tape (Gamin s. r. o.) in both directions.

Nanoindentation

Nanoindentation measurements were performed with Hysitron Tribolab TI-700 (Berkovich indentor) at CEMHUB Laboratories of Nanoindentation and Experimental Micromechanics of Materials, Czech Technical University, Faculty of Civil Engineering, Dpt. of Mechanics, Prague. Al 2024 samples anodized in TSA, Mo-TSA and SCHA-TSA baths (40 minutes anodizing time), as well as CAA reference sample all sealed in boiling DEMI were used for nanoindentation measurements. Two different methods were used – force control test and displacement control test. Hardness (GPa) across the anodic layer/base material interface was evaluated.

Results and discussion

Film growth

In Table 3, anodic layer thickness after 40 minutes of anodizing (45 min for CAA) is presented, depending on the alloy type and tested anodizing bath. The layer thickness was significantly lower on Al 2024 alloy compared with 6061 and 7075 alloys, regardless of the anodizing bath composition. The influence of bath composition on anodic layer thickness was observed as well, the layer thickness increasing in the order of CAA–Mo-TSA–SCHA-TSA≈TSA.

Table 3: Influence of alloy type and bath composition on anodic layer thickness after 40 minutes anodizing, comparison of destructive (D) and non-destructive (ND) method

Bath	TSA		SCHA-TSA		Mo-TSA		CAA	
Thickness by method [μm]/ Alloy	ND	D	ND	D	ND	D	ND	D
Al 2024	8±1	6.7	8±1	6,2	5±1	5.9	2	1.6
Al 6061	12±1	11.7	11±1	11.1	6±1	7.1	2	2.4
Al 7075	12±1	11.5	11±1	10.8	8±1	8.3	2	2.5

The growth rate of anodic film in SCHA-TSA bath is presented in Graph 1. To meet the normative requirement of layer thickness for CAA replacement – up to 8 μm [9], [10], the process time needs to be 30 min, respective 20 minutes in the case of Al 7075-T6 alloy in SCHA-TSA, as well as TSA bath.

Graph 1: Growth rate of SCHA-TSA anodic layer vs. aluminium alloy type

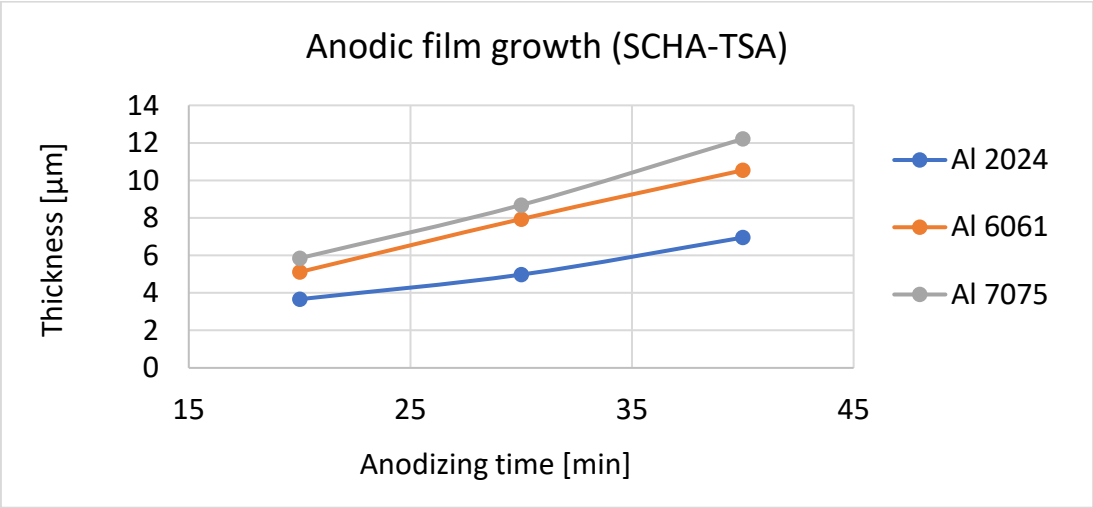

Corrosion resistance

In the first step, verification of optimal anodizing parameters and effect of two-step sealing process was carried out on a set of samples (dimension 75*50*0.8 mm). Several process parameters (i. e. temperature and voltage) settings were tested. Based on "long TSA process", a fixed anodizing time of 40 minutes was applied for all samples. Results of the corrosion test are summarized in Graph 2.

Graph 2: Corrosion resistance (ASTM B 117), effect of bath composition, aluminium alloy and sealing procedure (40 minutes anodizing, 9 samples were tested for every bath-alloy-sealing procedure combination)

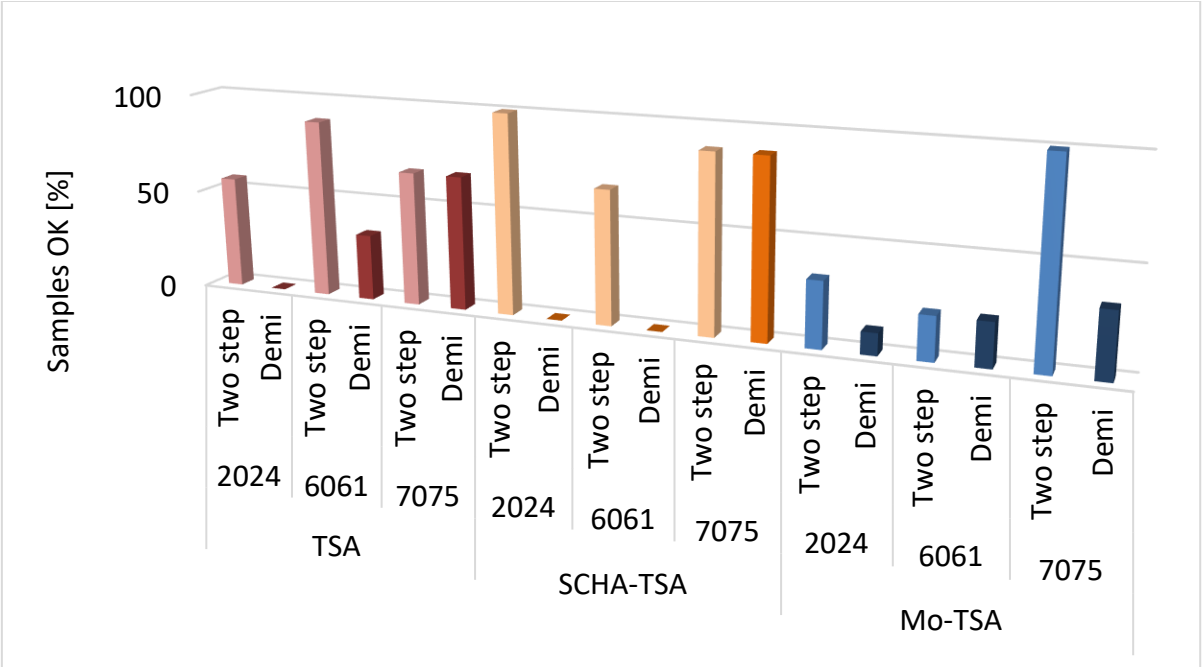

It is obvious that the two-step sealing process provided better corrosion resistance in all three tested TSA bath modifications. The effect of two-step sealing was most significant for Al 2024 and Al 6061 alloys. In the case of Al 7075 alloy, the effect showed only in Mo-TSA bath. Corrosion resistance of Al 2024 samples sealed in boiling DEMI water was comparable for both TSA and SCHA-TSA bath. However, when two-step sealing in Cr (3+) was applied, SCHA-TSA showed generally higher corrosion resistance than TSA on Al 2024.

Repeatability of this phenomenon was showed in the next step, when a new set of samples (125*76*0.8 mm) was prepared with fixed optimal anodizing parameters (temperature, voltage), anodizing time of 40 minutes and two-step sealing. Results after 504 hours exposition in NSS (presented in Table 4) confirm the SCHA-TSA/two-step sealing as the most promising procedure of the three tested TSA modifications, providing good corrosion protection across all tested alloys, including Al 2024.

Table 4: Percentage of samples passing 504 hours in NSS without any signs of corrosion – effect of alloy and bath composition (40 minutes anodizing, two-step sealing, 3 samples were tested for every bath-alloy combination)

Bath composition	Alloy	OK 504 h [%]
TSA	2024	33
	6061	100
	7075	100
SCHA-TSA	2024	100
	6061	100
	7075	100
Mo-TSA	2024	67
	6061	33
	7075	100

In the next step, SCHA-TSA/two-step sealed samples were prepared with shorter anodizing times (20–30 minutes), to meet the requirements of the standard regarding maximum layer thickness 8 μm [9, 10] (see Graph 1). As expected, the corrosion resistance was lower for lower anodizing times. For every alloy, minimum 75 % samples with acceptable layer thickness passed 504 hours NSS test.

Table 5: Percentage of samples passing 336 and 504 hours in NSS without any signs of corrosion – effect of alloy and anodizing time (SCHA-TSA, two-step sealing, 4 samples tested for every anodizing time-alloy combination)

Alloy	Anodizing time [min]	Layer thickness Ø [μm]	OK 336 h [%]	OK 504 h [%]
2024	20	4.0	100	0
	30	5.5	100	75
6061	20	5.5	0	0
	30	8.0	100	75
7075	20	5.5	100	100
	30	8.5	100	100

Paint adhesion

In Graph 3, percentage of successful samples in cross-cut test (i. e. result S0 or S1) is presented as a function of bath composition and alloy type. There was only minor difference between the tested bath-alloy combinations.

Graph 3: Percentage of samples exhibiting cross-cut test results S0 or S1 – effect of alloy type and bath composition (40 minutes anodizing, unsealed, for every alloy-bath combination at least 14 samples tested)

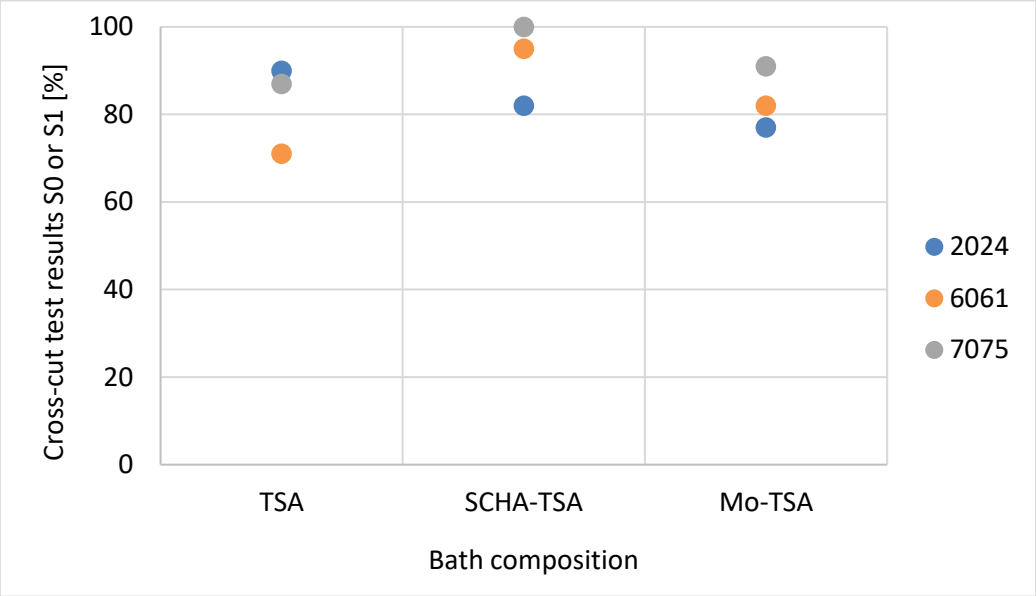

Nanoindentation

Hardness as a function of the distance from the base material/anodic layer interface is presented in Graphs 4–7. In all samples, there is a discontinuous increase of hardness value on the side of anodic layer. Then, the hardness decreases towards the outer edge of the anodic layer. Similar behaviour was observed in all samples, including the reference CAA sample. The difference between the anodic layer hardness slope values is caused mainly by different layer thickness at the measured points.

Graph 4: Hardness vs. distance from the base material/anodic layer interface, Al 2024, CAA, sealed in boiling DEMI

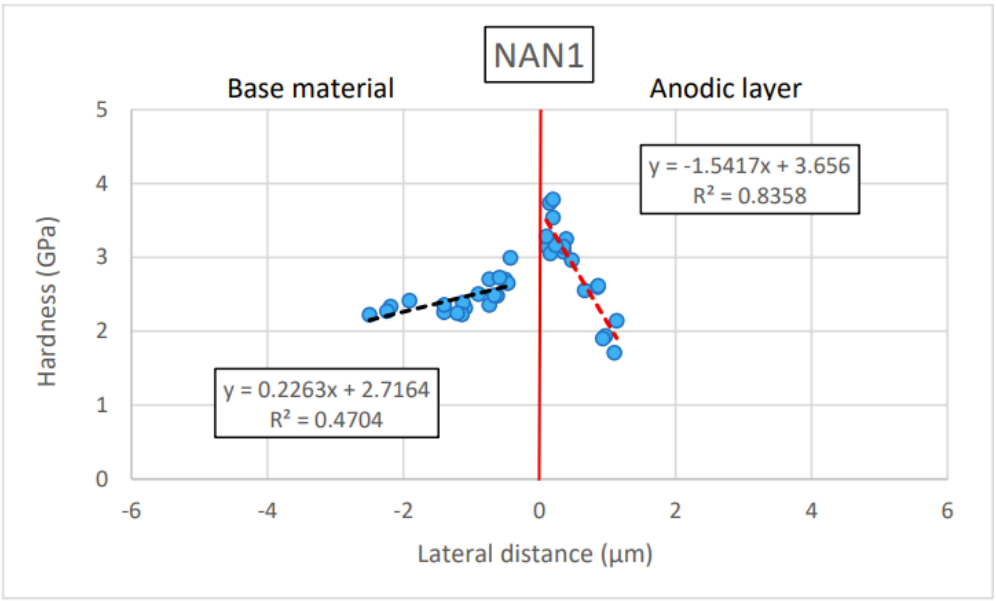

Graph 5: Hardness vs. distance from the base material/anodic layer interface, Al 2024, TSA, sealed in boiling DEMI

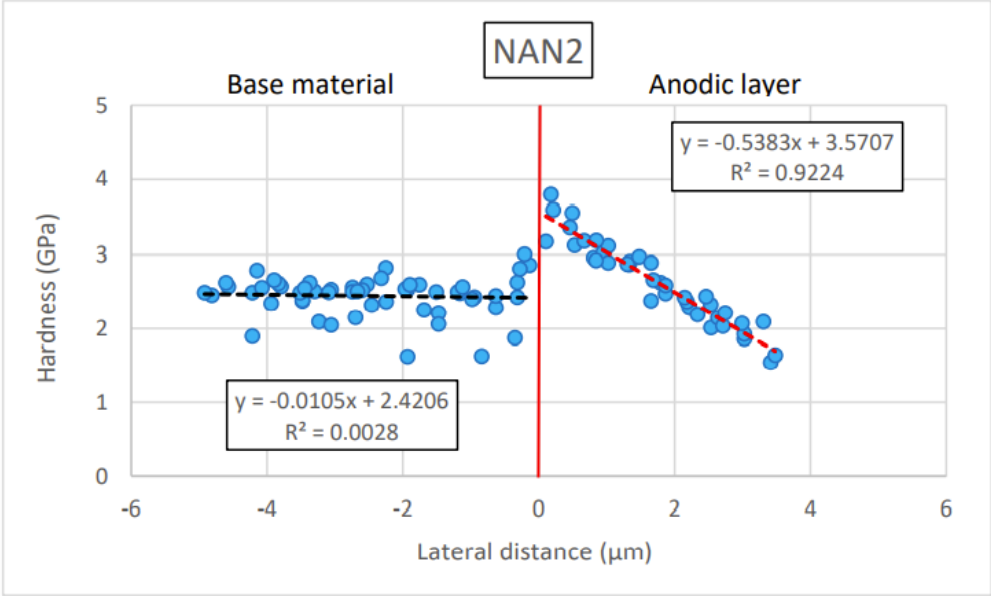

Graph 6: Hardness vs. distance from the base material/anodic layer interface, Al 2024, SCHA-TSA, sealed in boiling DEMI

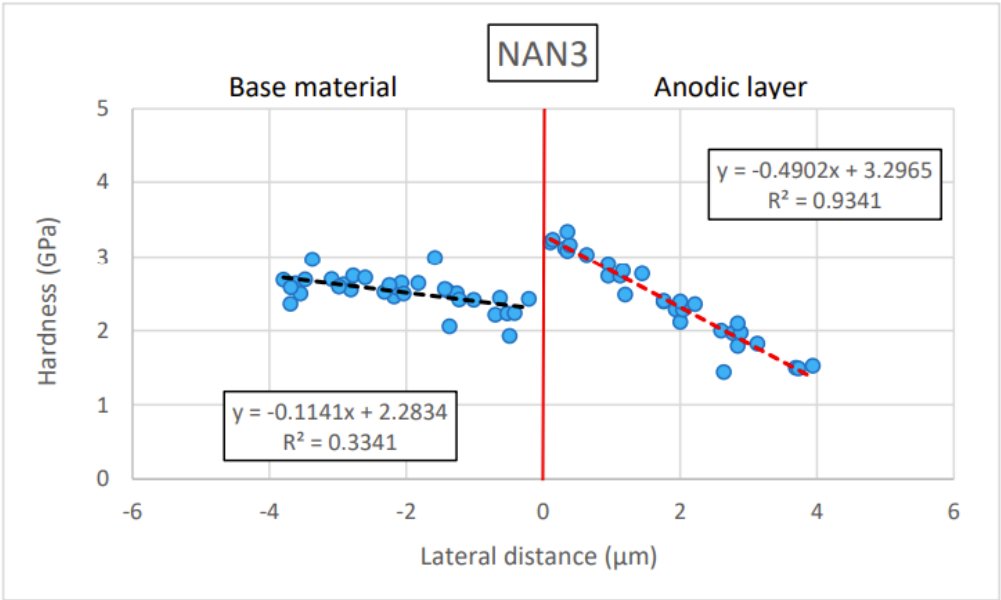

Graph 7: Hardness vs. distance from the base material/anodic layer interface, Al 2024, Mo-TSA, sealed in boiling DEMI

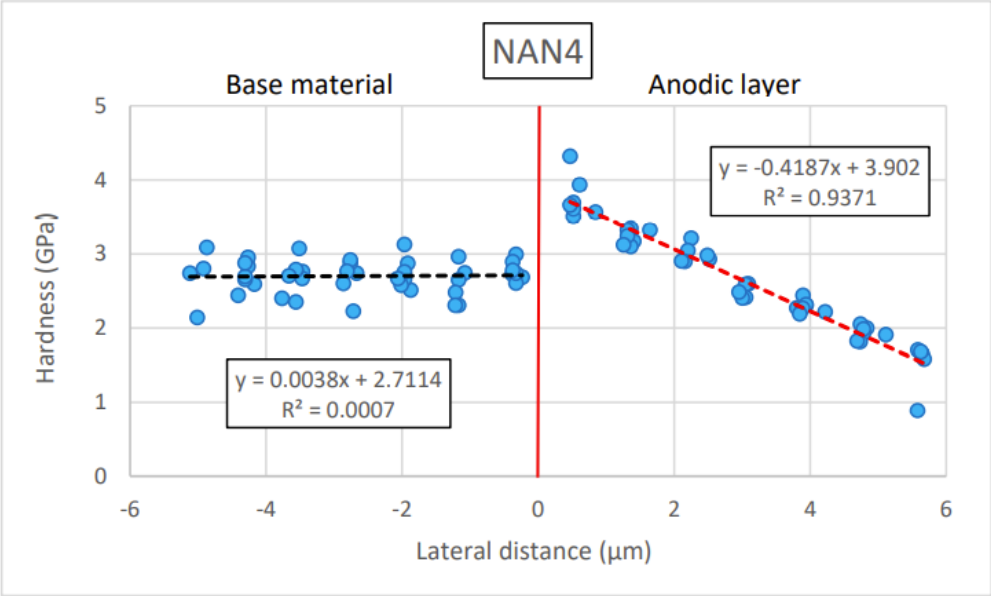

Conclusion

Comparison of three TSA-based anodizing baths and two sealing procedures in terms of corrosion resistance, anodic layer growth parameters, paint adhesion and hardness, is presented. The positive effect of two-step sealing in Cr (3+) bath on corrosion resistance of anodic layers was verified on three aluminium alloys relevant for aerospace industry. Also, an interesting phenomenon was observed, that the addition of a short-chain monocarboxylic acid into TSA bath seems to enhance the two-step sealing effect on corrosion resistance, particularly on copper-rich alloy Al 2024. As a result, among the three tested TSA-based baths, SCHA-TSA combined with two-step sealing provided the best corrosion resistance on all the three tested aluminium alloys. To explain the mechanism of this effect, further research is needed. At the same time, there was no significant difference between TSA and SCHA-TSA processes in terms of anodic layer growth rate or paint adhesion. Hardness across the substrate/anodic layer interface measured via nanoindentation is presented for the tested TSA-based baths as well as CAA reference sample.

Acknowledgement

T A
Č R

The text has originated in the framework of the solution of project number FW01010017 “Replacement of surface anticorrosive and sliding layers of aerospace materials with more environmentally friendly technologies “. This project is financed from the state budget by the Technology Agency of the Czech Republic and the Ministry of Industry and Trade within the TREND Programme.

Literature

1. M. García Rubio, "Optimisation of a non-chromium-containing tartaric acid/sulphuric acid anodising bath for aluminium alloys for aerospace industry application," Madrid. Dissertation. Universidad Autonóma de Madrid. Advisor Pilar Ocón Esteban, Ignacio Manuel García Diego.

2. S. Ebnessajad, assisted by C. Ebnessajad. Surface treatment of materials for adhesive bonding. 2nd edition. Elsevier Inc., 2014, 306 s. ISBN 978-0-323-26435-8.

3. REACH, Annex XIV to Regulation (EC) No 1907/2006, 2013.

4. Alenia Aeronautica S.p.A., "Anodizing process with low environmental impact for a woodpiece of aluminum or aluminum alloys". USA Patent US 2002/0157961 A1, 8 October 2002.

5. D. S. Verdaguer, "Alternative surface treatments without chromium content in aeronautical aluminium alloys: Tartaric sulphuric acid anodising," Master's thesis, July 2015

6. V. R. Capelossi; et al., "Corrosion protection of clad AA2024 anodized in sulphuric and tartaric acid sealed with sol-gel hybrid coatings," Electrochimica Acta, vol. 124, p. 69–79, 2014.

7. M. Beneke and S. Nixon, "Chromate free surface pre-treatments for aluminium alloys, AIRBUS," ASETS Defense, 2016.

8. M. A. Arenas, "Effect of acid traces on hydrothermal sealing of anodised layers on 2024 aluminium alloy," Electrochimica Acta, vol. 55, p. 8704–8708, 2010.

9. ČSN EN 4704. Letectví a kosmonautika – Eloxování hliníku a tvářených slitin hliníku v kyselině vínové a sírové (TSA) na ochranu proti korozi a úprava před nátěrem. Úřad pro technickou normalizaci, metrologii a zkušebnictví, 2012. 13 p.

10. ČSN EN 4827. Letectví a kosmonautika – Eloxování hliníku a slitin hliníku bez přítomnosti šestimocného chromu. Úřad pro technickou normalizaci, metrologii a zkušebnictví, 2020. 22 p.

11. R. del Olmo; et al., "Effect of cerium (IV) on thin sulfuric acid anodizing of 2024-T3 alloy," Journal of Materials Research and Technology, vol. 15, p. 3240–3254, 2021.

12. S. U. Ofoegbu; et al., "The sealing step in aluminum anodizing: A focus on sustainable strategies for enhancing both energy efficiency and corrosion resistance," Coatings, vol. 10, 2020.

13. Airbus España, S.L. 28906 Getafe (Madrid) (ES), "Procedure for anodizing aluminium or aluminium alloys". Patent EP 2 055 810 A2, 6 May 2009.

14. EN ISO 2409:2020 - Paints and varnishes - Cross-cut test

Practical methods for Moisture Level Indication inside Printed Circuit Boards

Jan Bjerre Christensen, FORCE Technology, Denmark

For electronic equipment high level of humidity can in addition to corrosion cause damage to the Printed Circuit Board (PCB) . High moisture content combined with temperature variation are problematic for a PCB and can results in failures due to creeping currents, delamination and disconnection of electrical connections. At FORCE Technology, we have developed a sensor that can indicate the accumulated moisture level inside PCB's. We call it a Moisture Level Indicator, MLI. This presentation will give a short introduction to MLI with examples of test results, implementation and verifications.

Electronic equipment used in humid environments have a risk that humidity will penetrate the encapsulation and functional product failures will occur over time. Many manufactures do not have the knowledge of the humidity condition for every individual product. To make it a good business case for the producer of electronic equipment the cost and space needed is optimized. With the knowledge from a Moister Level Indicator inside a Printed Circuit Board, moister conditional monitoring can be made and predicted actions will limit damages and ensure maximum life time of each individual product. This can be beneficial for both users and producers of electronic equipment. The goal is that Moister Level Indicator will limit the global amount of electronics scrap for the benefit of our descendants. This presentation will give an overview of the:

- Project background
- The diversity of use
- Verification results
- Examples of MLI in real products

Effect of solder mask surface properties and water film build-up on PCBA failure

A.R. Lakkaraju[1], H. Conseil-Gudla[1], D. Schucht[2], J. Tekath[2] and R. Ambat[1]

[1] Materials and Surface Engineering, Department of Mechanical Engineering, Technical University of Denmark, 2800 Kongens Lyngby, Denmark.
[2] Lackwerke Peters GmbH & Co. KG, Hooghe Weg 13, 47906 Kempen, Germany.

The electronics industry adopts an increased device miniaturization, and devices are expected to perform optimally in a multitude of climatic conditions worldwide, which adds to the list of possible failure modes. Changing temperature and humidity are a major driving force for condensation regime on the electronics surface, which can eventually lead to failure. The surface chemistry and morphology of printed circuit boards will influence the formation of water droplets size on the surface, and therefore the bridging pathway between two connector pads. Surface properties of the printed circuit board comprise the surface roughness of the laminate and the chemical coatings like solder masks etc., which are often overlooked.

Simulated condensation experiments on test PCB laminates have been performed. A test setup using a heat-exchanger allows the cooling of the laminates while being exposed to high-humidity conditions at room temperature, , resulting in water layer build up on the test PCBs coated with different solder masks.

The water layer formation on the test PCBs has been monitored using both qualitative (in-situ Digital Microscope) and quantitative (Impedance and leak current measurements) methods, in order to create a correlation to measured surface roughness parameters, surface morphology and hydrophobic/hydrophilic nature of the solder masks.

The results give an insight into the bridging of condensed water droplets on the solder mask surfaces, which can be correlated to changes in measured impedance. Leakage current values of the test PCBs have also been measured on test PCBs with different connectors geometry and pitch distance. Ultimately, a unified picture of the effect of surface parameters such as roughness values and water droplet angle on potential PCBA failure has been hypothesized. Selection of the appropriate surface roughness and wetness angle parameter can be used to rank and potentially predict solder mask characteristics contribution to PCBA failures.

Keywords: Humidity, Impedance, Printed circuit board laminate, Solder Mask, Surface roughness, Temperature, Water droplet angle, Water layer formation

Electrochemical testing for characterization of sinterability of DCB substrates with Cu, Ag and NiAu metallization

***Sandy Klengel*[1], *Janine Dumke*[2], *Dorit Wilke*[2], *Michael Hahn*[2]**

Fraunhofer Institute for Microstructure of Materials and Systems IMWS
Elektrochemie Halle GmbH

Silver sintering is a common technology in packaging technology for the electrical and mechanical contacting of semiconductor components. Reliable sinterable surfaces are therefore a basic requirement for the cost-effective and efficient production of power electronic modules for the energy transition and electromobility. The quality and sintering ability depends mainly on the chemical properties of the surfaces to be joined. Currently, there is no method available that allows the assessment of surfaces for sinter technology upfront the sintering process.

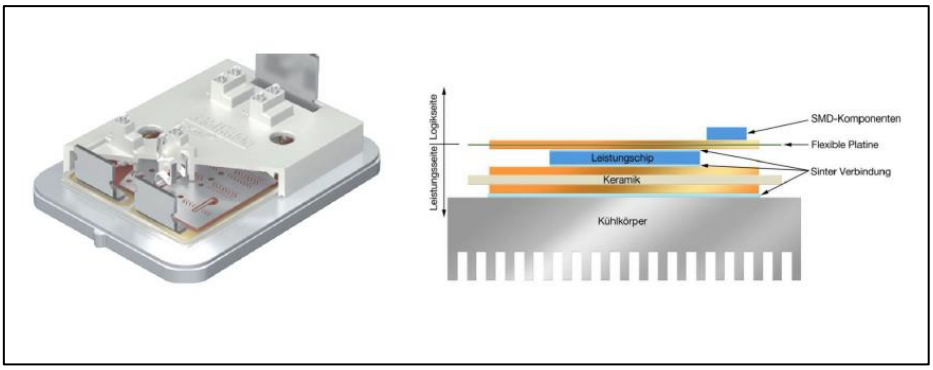

Figure 1: left: SKiN- module of Semikron Elektronik GmbH &Co. KG with sinter contacts [1], right: Scheme of a power electronic module with sinter contacts [2]

For the development of a new characterization method for surface quality assessment, we analyzed the surface characteristic of different metallization systems of DCB (direct copper bonded) substrates by high resolution methods (SEM, TEM, XPS) in comparison of boards in initial condition and after temperature treatment (typical industry processing parameters). Afterwards the samples were tested by miniaturized electrochemical analyses (cyclovoltammetry) [3]. The results were correlated to each other and to the sinter ability of the surface. Following results could be observed:

NiAu-Finish: temperature treatment worsens the sinter ability of the surface – root cause is Ni diffusion to the surface and chemical transformation to NiOH/NiOOH

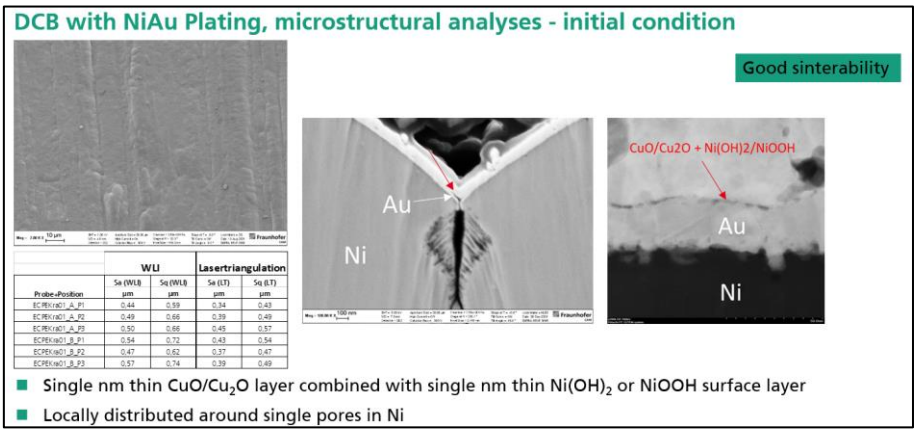

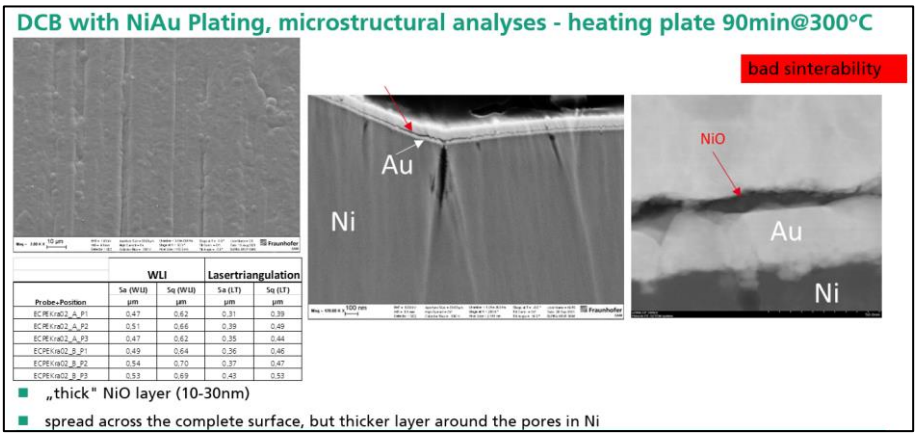

The chemical changes of the surface conditions could be detected by the electrochemical method. Additionally, for sinterable NiAu surface the electrolyte was able to attack the surface (no passivation effects).

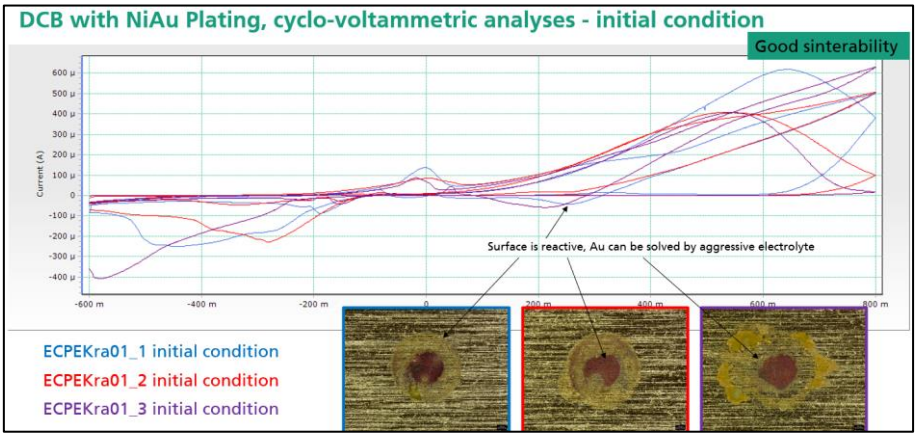

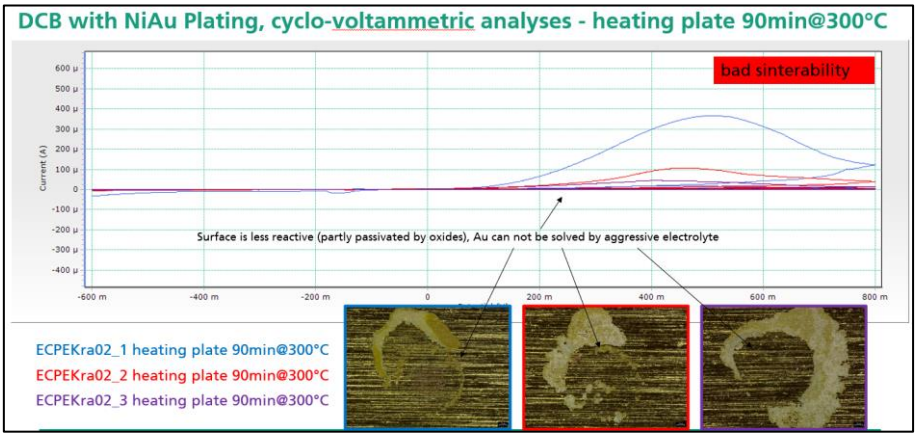

Cu-Finish (without corrosion inhibitors): temperature treatment worsens the sinter ability of the surface – root cause is a CuO/Cu2O formation with layer thickness of 100nm

DCB with Cu Plating, microstructural analyses- initial condition

Good sinterability

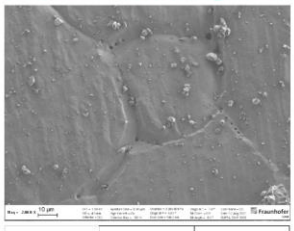

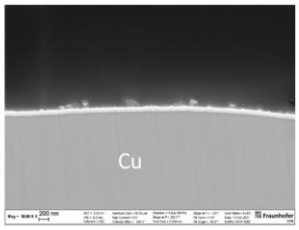

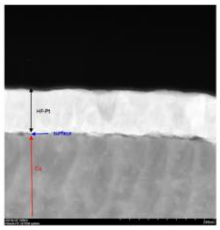

	WLI		Lasertriangulation	
Probe+Position	Sa (WLI) µm	Sq (WLI) µm	Sa (LT) µm	Sq (LT) µm
ECPEKra07_A_P1	1,15	1,57	1,27	1,63
ECPEKra07_A_P2	1,11	1,51	1,28	1,65
ECPEKra07_A_P3	1,17	1,60	1,26	1,64
ECPEKra07_B_P1	1,44	2,00	1,56	2,07
ECPEKra07_B_P2	1,17	1,67	1,24	1,63
ECPEKra07_B_P3	1,14	1,67	1,17	1,54

- Surface contains mostly metallic Cu and single nm thin CuO/Cu_2O layer

DCB with Cu Plating, microstructural analyses, heating plate 90min@300°C

bad sinterability

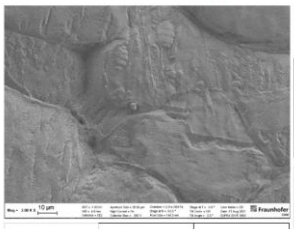

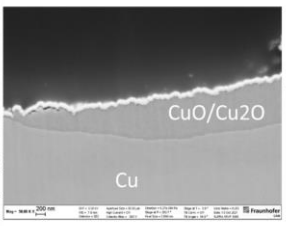

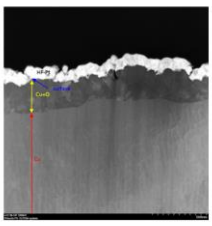

	WLI		Lasertriangulation	
Probe+Position	Sa (WLI) µm	Sq (WLI) µm	Sa (LT) µm	Sq (LT) µm
ECPEKra08_A_P1	1,45	1,83	1,08	1,45
ECPEKra08_A_P2	1,48	1,87	1,27	1,69
ECPEKra08_A_P3	1,21	1,59	1,16	1,57
ECPEKra08_B_P1	2,14	2,54	0,94	1,24
ECPEKra08_B_P2	1,70	2,13	1,04	1,35
ECPEKra08_B_P3	1,76	2,18	1,09	1,41

- Surface shows a thin CuO layer followed by a µm thick Cu_2O layer

DCB with Cu Plating, cyclo-voltammetric analyses - initial condition

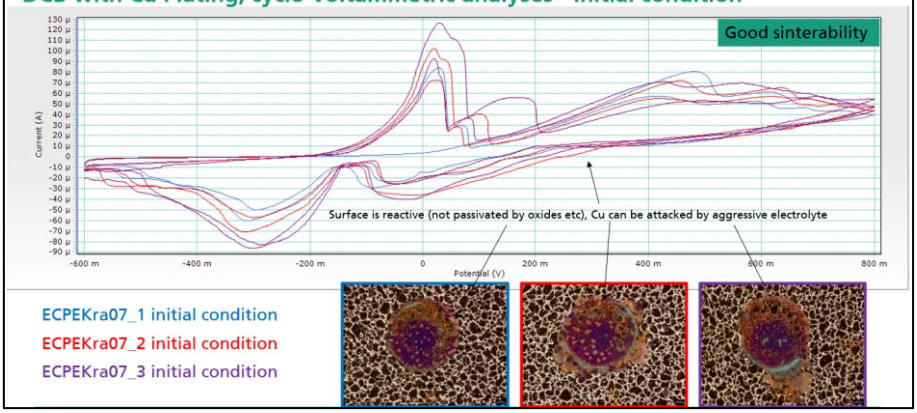

DCB with Cu Plating, cyclo-voltammetric analyses, heating plate 90min@300°C

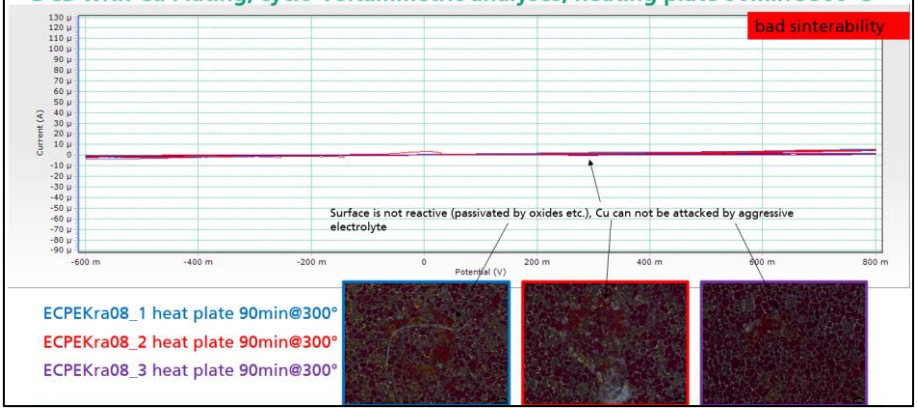

Ag-Finish: temperature treatment doesn't lead to changed surface characteristic resulting in a good sinter ability in all conditions

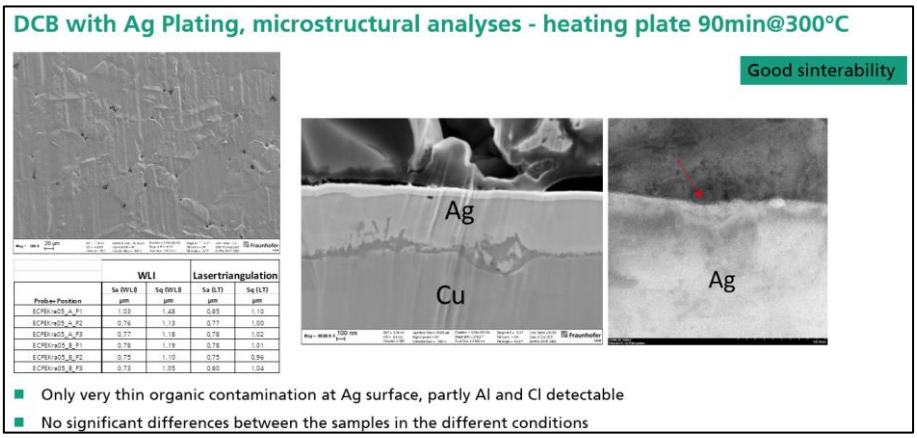

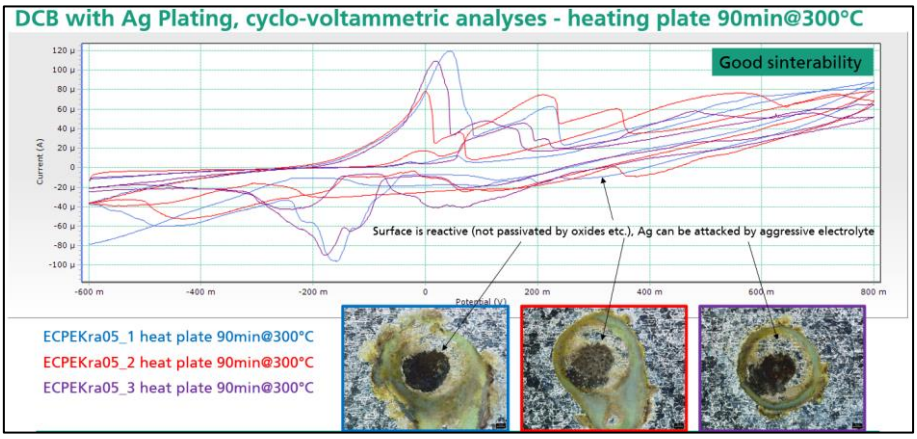

Acknowledgement:
The work presented received financial support from the European Regional Development Fund in Saxony-Anhalt, Germany by project number FuE 023/21 (ZS/2021/05/156729). Furthermore, the authors would like to thank the European ECPE network for funding the basic work of this paper via the "ECPE Joint Research Programme".

Literature:

[1] SEMIKRON_Flyer-Compilation_Power-Electronic-Stacks_2016-09-26_EN.pdf
[2] https://www.all-electronics.de/elektronik-entwicklung/einen-schritt-voraus.html, Bild Semikron International
[3] Klengel, S., Klengel, R., Stephan, T., Mühs-Portius, B., Wilke, D., & Hahn, M. (2021, September). A new method for local electrochemical measurements at PCBs. In 2021 23rd European Microelectronics and Packaging Conference & Exhibition (EMPC) (pp. 1-6). IEEE.

Developing strategies for protecting Li-ion powered hearing aids from the user environments.

Markus Asikainen[*1], *Abhijeet Yadav*[*2], *Rajan Ambat*[*1]

[*1]*Department of Mechanical Engineering, Technical University of Denmark, DK 2800 Lyngby, Denmark*

[*2] *WS Audiology A/S, DK 3540 Lynge, Denmark*

In recent years, Li-ion-based rechargeable hearing aids (HA) have entered the market replacing the conventional zinc-air technology. Li-ion-powered HAs offer better welfare for users due to the possibility of recharging and ease of use and therefore, a further shift of the market towards Li-ion products is expected. The user environments for hearing aids are harsh due to the synergetic effect of body fluid contact and the external environment such as high humidity and temperature. These factors have proven to cause serious corrosion reliability issues for HA devices in the field. Moreover, the combined effect of higher voltage and the predominant trend towards design miniaturization possess challenges for Li-ion devices to have corrosion-related issues caused by user environments. This makes it crucial to develop protection strategies for the Li-ion powered hearing aid to be competitive in the market for performance, safety, and robustness. In this study, the performance of several liquids - and gas-phase conformal coatings are investigated by conducting experiments such as sweat drop test and immersion test, which mimics the user environment exposure and conditions. Coatings were applied and tested on the power supply module (PSM), which is one of the key components in the existing rechargeable Li-ion-powered HAs. Its role is to provide power from the Li-ion battery, control the charging/discharging cycles and ensure safe usage of the Li-ion battery. Afterward, a thorough analysis was performed by using a light optical microscope (LOM), scanning electron microscope (SEM), and energy dispersive spectroscopy (EDS). In the analysis, the focus was to identify and analyze the effect of the design and material choices of the device and the quality of the applied coating on the performance evaluation of the conformal coating. Hence, to evaluate whether the coatings would perform with the acceptable level in the field. Some of the key findings from this investigation were: poor adhesion of the liquid conformal coatings, non-coverage of conformal coatings under the capillary areas, and

localized corrosion attacks through pinholes and defects were observed. Considering the full picture of results obtained, it provides an in-depth discussion of the quality and performance of tested conformal coatings against humidity and sweat and their future potential to be used in microelectronic devices such as hearing aids.

Author list:

1. Markus Asikainen (mkaas@mek.dtu.dk)
Department of Mechanical Engineering, Technical University of Denmark, DK 2800 Lyngby, Denmark (Presenting author)

2. Abhijeet Yadav (abhijeet.yadav@wsa.com)
WS Audiology A/S, DK 3540 Lynge, Denmark

3. Rajan Ambat (ram@mek.dtu.dk)
Department of Mechanical Engineering, Technical University of Denmark, DK 2800 Lyngby, Denmark

Water absorption in dense phase CO_2

Bjørn Helge Morland, Arne Dugstad, Gaute Svenningsen,
Institute for Energy Technology, Kjeller/Norway

CO_2 from Carbon Capture plants must be sufficiently dry before it can be transported to the storage site. However, liquid water could accidentally be present due to upset conditions. One main question is how long it takes for liquid water pools in the bottom of line to dissolve in the bulk CO_2 stream (i.e. how long corrosion can take place).

Dissolution of water in dense phase CO_2 (60 – 80°C, 20°C) was tested experimentally in the present work. Dense phase CO_2 was fed slowly through a small pipe section that was filled with 4 ml of liquid water. The pipe was submerged in a water bath with temperature control. The water content in the exhaust CO_2 was continuously measured with a dew-meter. The CO_2 flow rate was 0.5 – 3 Nl/min, which gives a residence time of 30 - 5 minutes, respectively.

The test conditions simulate a fluid flow of 0.2 – 2 cm/min in the pipeline. The water content was in the range of 500 – 800 ppm-mol, varied with temperature and CO_2 flow rate. The observed water content is far below the equilibrium which is 2000 – 3000 ppm-mol. This illustrates that the dissolution of water in CO_2 is a slow process, and accidental water ingress could cause corrosion problems for a long period. The dissolution rate of the water pool that was about 4 mm deep was in the order of 1 mm/day.

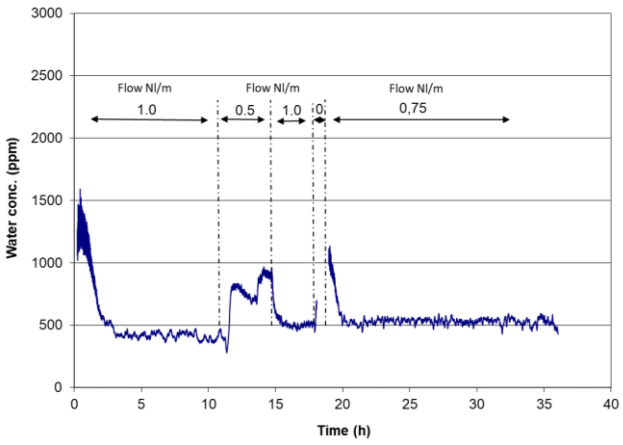

Figure 1: Water content in the exhaust CO2 for different flow rates at 20°C (60 – 80 bar).

Deposition of Chloride Ions in the Vicinity of Road I/11 in the Czech Republic

Miroslav Vacek[1], Vit Krivy[2], Katerina Kreislova[3], Monika Kubzova[4]

[1] Department of Structures, Faculty of Civil Engineering, VSB – Technical University of Ostrava, Ludvika Podeste 1875/17, Ostrava – Poruba, Czech Republic, miroslav.vacek@vsb.cz
[2] Department of Structures, Faculty of Civil Engineering, VSB – Technical University of Ostrava, Ludvika Podeste 1875/17, Ostrava – Poruba, Czech Republic, vit.krivy@vsb.cz
[3] SVUOM Ltd, U Mestanskeho pivovaru 934-4, Prague, Czech Republic, kreislova@svuom.cz
[4] Department of Structures, Faculty of Civil Engineering, VSB – Technical University of Ostrava, Ludvika Podeste 1875/17, Ostrava – Poruba, Czech Republic, monika.kubzova@vsb.cz

Abstract
Chloride ions occur near the roads primary in form of sodium chloride like a deicing salt or a brine. Usage of salt has many benefits for population, for example safer travel, reduction the number of traffic accident or saves fuel. On the other hand, it brings negatives, mainly high airborne salinity and high corrosivity categories of atmosphere. In this context, it was found that corrosion map is good for wide surroundings, but for construction directly adjacent to the road the values of salinity are higher. This directly affect the speed of corrosion and degradation of the construction. The aim of this article is to measure the deposition of chloride ions near the roads. Measurement in the first locality is about deposition at graduated distances from the road with maximum distance from the road I/11 about 200 m. Second one is more focused on surroundings of the road, in this case to the road cut and bridge. The maximum distance from the road is circa 15 m. These two measurements provide more information about the local microclimate in vicinity of road I/11. Main season of deicing is in the winter month when the difference in the position of the test equipment is most noticeable. The authors are also researching additional measurements on other roads for better understand deposition of chloride ions. The measurement is carried out using the method of wet candle and the method of dry desk in vertical and horizontal position.

Keywords
Chloride; bridge; steel; road

Introduction

The service life of structures located in the vicinity of the roads can be significantly adversely affected by chloride deposition [1]. Chloride deposition on the surfaces of structures occurs either by direct rain leaking, e.g. from leaking bridge drainage systems, or by airborne deposition, where dust debris and/or aerosol is emitted from the road surface by road vehicles. Chlorides deposited on the surface of load-bearing structures can significantly accelerate degradation processes, especially corrosion damage to structural steel or concrete reinforcement [2, 3]. The deposition rate of chlorides in the vicinity of the roads depends on many factors and their combination. Among the most important influences are:

- the intensity of road traffic;
- the amount of gritting salts used in winter maintenance (depending mainly on the amount of precipitation and the temperature in winter);
- the season (deposition is significantly higher in winter compared to the rest of the year [1]);
- the location of the structure in relation to the road (as an example, different deposition rates for bridges that are part of the road and bridges that run over the assessed road [4]);
- the geometric layout of the structure (significant differences in deposition rates for different typical surfaces of the structure [1, 5]);
- the topography of the terrain around the road (effects of road cuts, retaining or noise walls, surrounding vegetation).

Experimental verification of the effects related to the topography of the surrounding terrain and the location or design of construction objects in the vicinity of roads should be carried out under the assumption that other influences (traffic intensity, amount of spreading salts used, climatic conditions at the time of measurement) are not significantly different. It is therefore advisable to carry out individual comparison measurements on a suitably selected section of road, optimally between two crossroads.

In this case, the measured data is the distribution of chloride ions in the vicinity of roadways near the bridge structures of the I/11 road in the Czech Republic. Data collection is carried out periodically every month from installed test stands. The measured values for the year 2021 are presented in the text together with climate data at two locations. A non-linear regression analysis is performed on the data from the locality that covers the wider area above the crown of the road cut.

Locality

The test stands are located in the vicinity of two road bridges near the I/11 road. The first location is near the village of Josefovice and bridge 11-134G, the location of the test stands is shown in Fig. 1. This part of the research focuses on the wider vicinity of the road above the crown of the road cut between approximately 5 m and 180 m from the guide strip.

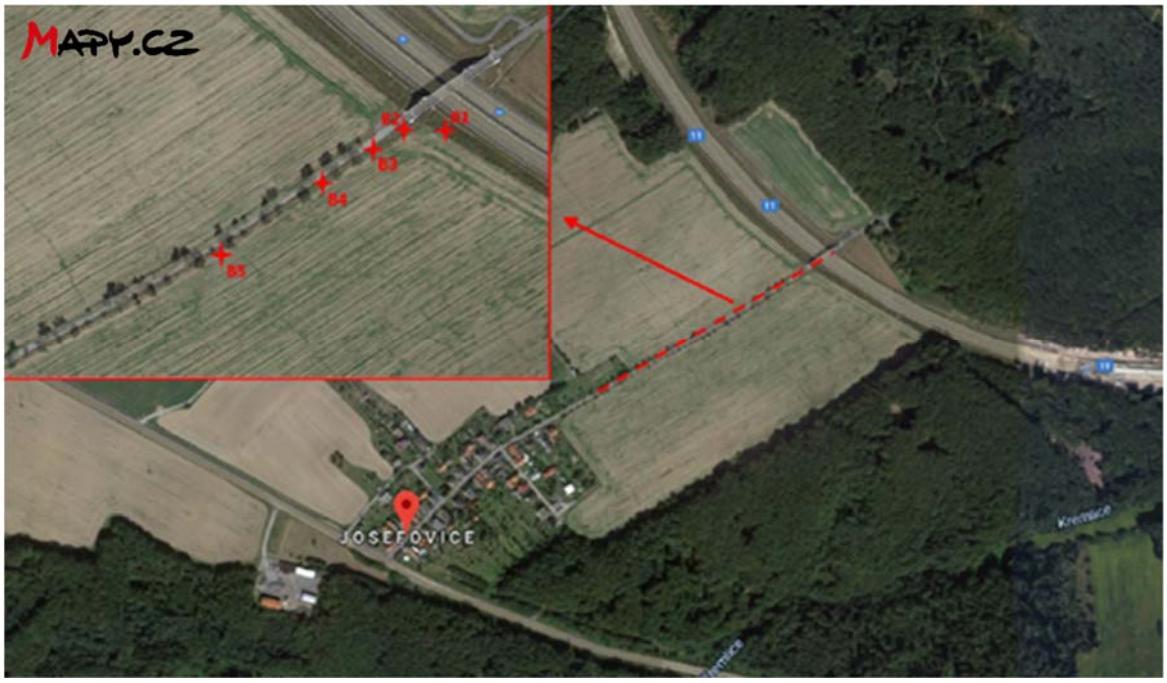

Fig. 1: Locality near Josefovice and bridge 11-134G (source: mapy.cz)

The second analyzed location is near the village of Vřesina at bridge 4692-2, the location of the test stands can be seen in Fig. 2. The research at this location focuses on chloride ion transport in the I/11 road cut. The distances of the test stands from the guide strip range from approximately 3 m to 18 m. This location was established in September 2021. Periodical sample exchange takes place at both locations of interest.

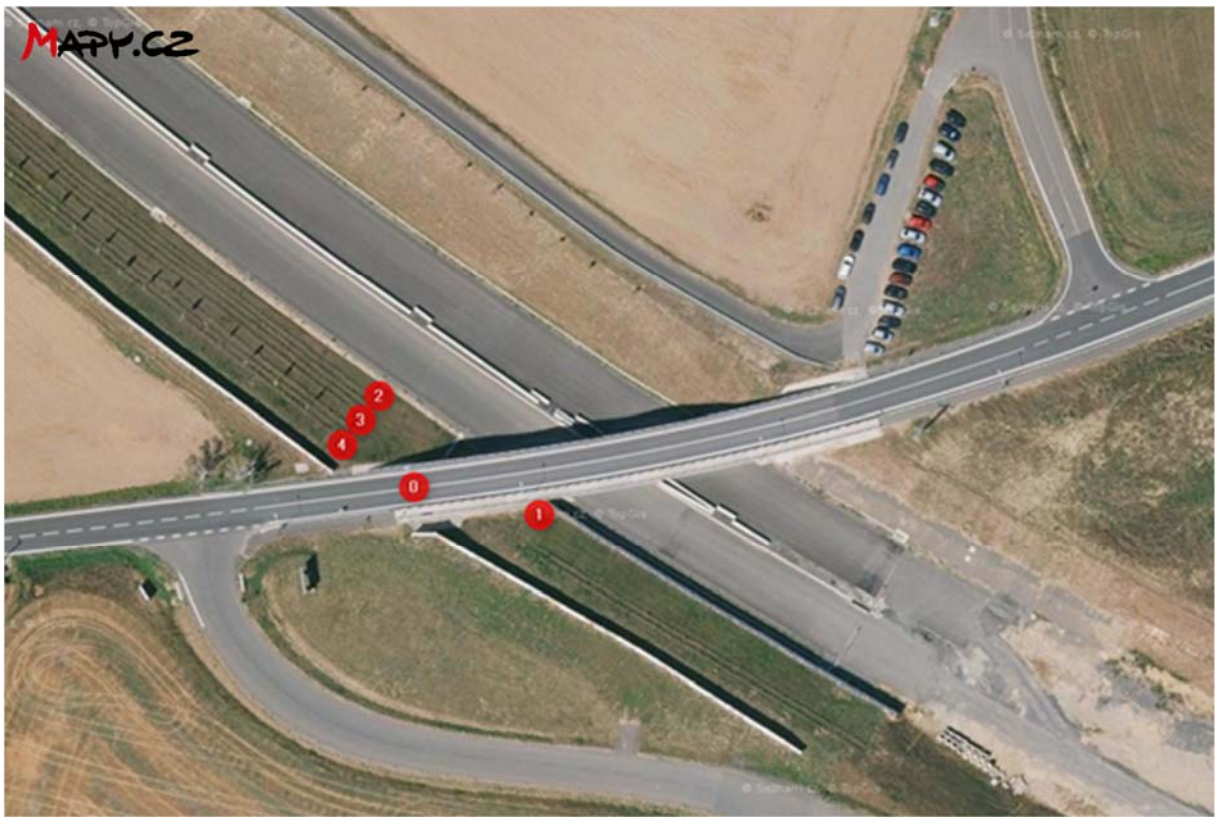

Fig. 2: Locality near Vřesina and bridge 4692-2 (source: mapy.cz)

Test methods

Test methods and sample analysis are performed according to EN ISO 9225 [6]. The standard wet candle test method is applied unchanged. In view of the experience based on the research work of Ing. Monika Kubzová, Ph.D. [1], the dry desk test method is modified against the norm by using 100% polyester fabric from EWAC [7] instead of gauze. The dry desk method is specified in EN ISO 9225 [6] only as a vertical desk. In the experimental measurement by the authors a horizontal dry desk method is also used. All the methods mentioned are located on test stands, see figure Fig. 3 for a typical stand. The analyses of the collected samples are carried out using HACH Pocket Colorimeter™ II and cuvette tests HACH LCK311, available from [8], in accordance with the standard EN ISO 9225 [6] and the equipment manufacturer's regulations and test regulations.

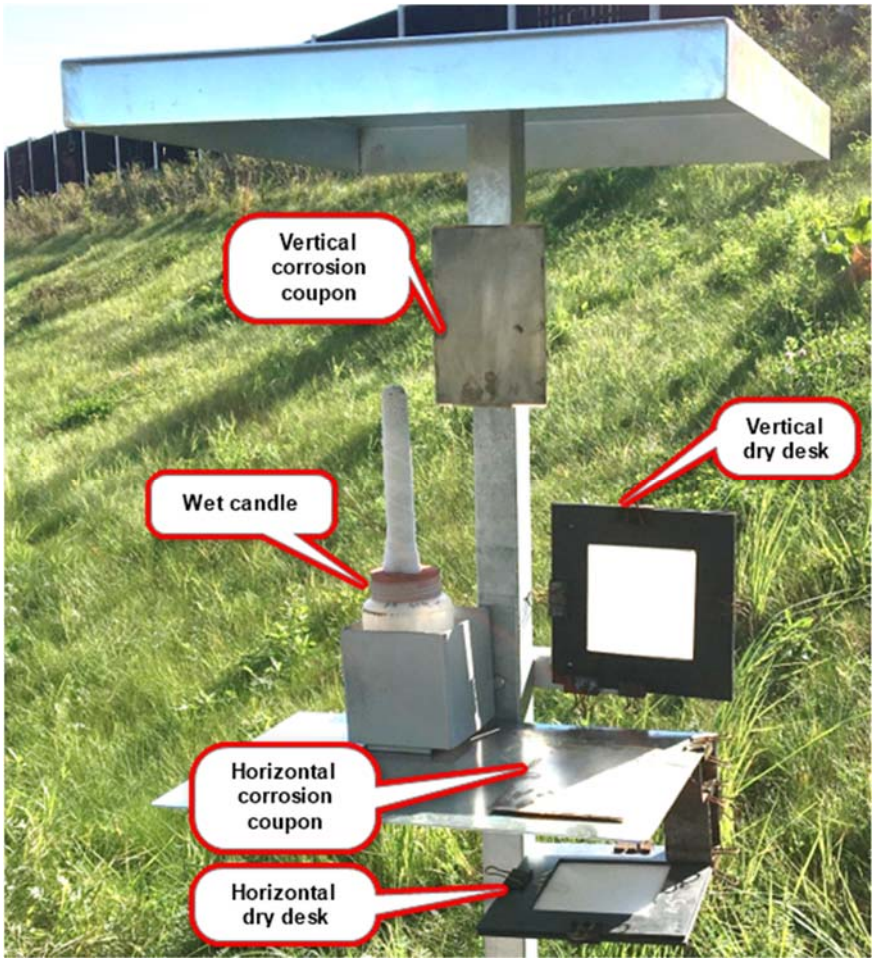

Fig. 3: Typical stand

Measured data

The data are from measurements carried out in 2021. The samples were collected at the beginning of each month, after approximately 30 days of exposure. This time also corresponds to the distribution of monthly mean temperature and other climatic data obtained from the Czech Hydrometeorological Institute [9], which respect the beginning and end of calendar months.

Locality Hrabyně

Seven measuring stations are installed in the area near the Josefovice and the bridge 11-134G near the I/11 road. Two stations are located at the bridge abutment near the bridge bearings closer to the lane towards Opava. Both of them are equipped with a horizontal dry desk only. Five stations are equipped with a stand and are located with increasing distance from the I/11 road in close proximity to the dirt road towards the village of Josefovice. The nearest of the measuring stands is at a distance of 20 metres from the road and the furthest one is at a distance of 180 metres. All stands are equipped with a horizontal dry desk (designation PH), a vertical dry desk (designation PV) and a wet candle (designation C).

The slope of the cut of the road is approximately 35° and the depth of the cut is approximately 6 metres. The slope of the cut of the road is without shrubs or trees, only grass.

The site is focused on the wider surrounding microclimate to a distance of approximately 180 metres from the roadway guide strip in the cut of the road. The stands on this site are exposed above the crown of the road cut.

The measured values from the standard analysis using ferric thiocyanate containing tests (hereafter referred to as LCK311 tests) are illustrated in Table 1. The distance of the measuring stands is also specified in Table 1.

Locality 4692-2

Six measuring points are installed in the area around the bridge 4692-2 (designation Rudná 1). The stands with measuring equipment are located on the side adjacent to the traffic lanes leading towards Ostrava. Two measuring points are fitted with only one horizontal dry desk (designation PH) and are located near the bridge bearings at the bridge abutment towards of Vřesina. The four measuring stations are equipped with a horizontal dry desk (designation PH), a vertical dry desk (designation PV) and a wet candle (designation C). All stands are located outside the plan projection of Bridge 4692-2. One of the racks is in close proximity to the gabion heavy duty retaining wall and three stands are in equidistant distances are located on the slope cut of the road of the I/11 roadway.

The slope of the cut of the road is approximately 40°, the depth of the cut is approximately 6 metres. For the direction of the road to Ostrava the slope of the cut of the road is in the place of the gabion heavy support wall (from the bridge closer to Ostrava) without shrubs or trees, only grass, then small shrubs and trees in the outermost circle. On the side from the bridge 4692-2 closer to Opava, where three stands are located at equidistant distances, the slope is planted with small shrubs and trees at several height levels. The remaining area is naturally overgrown with grassland. At a distance of approximately 5 metres from the crown of the cut, there is a noise barrier of approximately 3 metres in height. On the side of the I/11 road towards Opava, closer to Ostrava, on both sides of the bridge there is a small growth of bushes and trees.

This locality, due to its very short distances to the guide strip of the road, is mainly focused on the local microclimate in the immediate vicinity of the road and the effect of the cut of the road. The area of interest is the area between the base and the crown of the cut of the road.
The measured values from the norm analysis using LCK311 tests, are illustrated in Table 2. The spacing of the measuring stands is also specified in Table 2.

Table 1 (part 1): Measured data and distance from guide strip from locality Hrabyně (bridge 11-134G)

average monthly value	Temperature (°C)		-0,1	-0,7	3,7	6,4	12,2	19,4
	Rel. humidity (%)		83	80	72	70	69	66
	New snow (cm)		20	20	2	3	0	0
	Rainfall (mm)		40.1	41.0	26.4	64.8	110.3	72.9
Locality	Position	Distance (m)	1/21	2/21	3/21	4/21	5/21	6/21
Hrabyně	A-PH	5	29.7	26.0	4.1	1.3	2.0	Stolen
Hrabyně	B-PH	5	30.2	13.0	5.2	1.5	1.6	Stolen
Hrabyně	B1-C	7	33.1	82.4	16.3	11.6	7.7	3.3
Hrabyně	B1-PH	7	13.8	24.1	10.0	1.7	1.1	2.5
Hrabyně	B1-PV	7	48.0	21.6	Stolen	0.4	1.5	0.5
Hrabyně	B2-C	20	15.8	66.2	13.1	13.0	9.1	3.7
Hrabyně	B2-PH	20	7.7	10.8	7.2	0.8	1.2	1.0
Hrabyně	B2-PV	20	11.3	10.2	3.3	0.4	0.4	0.4
Hrabyně	B3-C	45	9.3	49.3	8.4	13.4	8.1	5.0
Hrabyně	B3-PH	45	4.2	9.6	3.8	0.5	0.5	1.1
Hrabyně	B3-PV	45	6.6	6.7	2.0	0.5	0.4	0.7
Hrabyně	B4-C	80	13.6	30.0	6.7	8.1	9.3	4.1
Hrabyně	B4-PH	80	2.5	4.5	2.7	0.9	0.4	2.6
Hrabyně	B4-PV	80	4.8	6.7	2.9	1.6	0.4	1.3
Hrabyně	B5-C	180	3.8	5.7	6.1	14.3	8.8	4.6
Hrabyně	B5-PH	180	5.8	4.4	1.0	0.4	0.9	2.3
Hrabyně	B5-PV	180	6.2	5.4	1.3	1.4	0.4	1.0

Table 1 (part 2): Measured data and distance from guide strip from locality Hrabyně (bridge 11-134G)

average monthly value	Temperature (°C)		20,4	17,3	14,6	9,1	4,8	0,4
	Rel. humidity (%)		70	75	75	72	82	83
	New snow (cm)		0	0	0	0	25	8
	Rainfall (mm)		67.8	172.9	31.3	20.1	50.2	35.7
Locality	Position	Distance (m)	7/21	8/21	9/21	10/21	11/21	12/21
Hrabyně	A-PH	5	0.8	0.8	2.7	4.7	4.5	14.3
Hrabyně	B-PH	5	0.4	1.3	2.4	2.8	3.8	8.5
Hrabyně	B1-C	7	5.6	9.4	12.4	1.9	16.0	30.0
Hrabyně	B1-PH	7	0.4	0.7	2.3	3.9	4.2	20.9
Hrabyně	B1-PV	7	0.4	1.3	0.7	2.6	4.6	10.9
Hrabyně	B2-C	20	5.5	9.9	7.4	4.9	9.8	13.3
Hrabyně	B2-PH	20	0.4	0.4	1.0	2.4	4.0	14.7
Hrabyně	B2-PV	20	0.4	1.3	1.1	2.5	1.3	7.0
Hrabyně	B3-C	45	5.1	8.4	9.8	Stolen	Stolen	11.2
Hrabyně	B3-PH	45	1.3	0.7	1.2	3.3	2.0	6.5
Hrabyně	B3-PV	45	0.4	1.2	0.9	2.3	1.7	2.1
Hrabyně	B4-C	80	5.3	4.8	7.3	5.0	3.9	15.7
Hrabyně	B4-PH	80	1.0	1.1	0.9	2.6	1.5	2.3
Hrabyně	B4-PV	80	0.4	0.8	1.2	1.4	1.2	1.8
Hrabyně	B5-C	180	7.5	8.5	7.6	0.9	6.2	8.7
Hrabyně	B5-PH	180	1.0	0.9	1.2	1.7	2.0	1.0
Hrabyně	B5-PV	180	0.9	1.1	1.2	1.6	0.8	0.6

Table 2: Measured data and distance from guide strip from locality near the bridge 4692-2

average monthly value	Temperature (°C)		14,5	9,7	5,3	0,5
	Rel. humidity (%)		76	70	81	83
	New snow (cm)		0	0	11	12
	Rainfall (mm)		35.3	14.0	42.3	22.5
Locality	Position	Distance (m)	9/21	10/21	11/21	12/21
Rudná1	A-PH	18	0.8	1.8	3.9	14.0
Rudná1	B-PH	13	0.6	1.5	6.8	10.9
Rudná1	R1-C	3	8.8	3.1	47.4	130.4
Rudná1	R1-PH	3	2.6	5.3	22.9	64.1
Rudná1	R1-PV	3	1.1	2.9	21.2	74.5
Rudná1	R2-C	5	10.5	4.0	51.9	173.2
Rudná1	R2-PH	5	0.8	2.8	8.7	39.6
Rudná1	R2-PV	5	0.5	1.6	10.3	50.1
Rudná1	R3-C	9	8.6	4.1	23.3	68.1
Rudná1	R3-PH	9	0.7	2.2	6.6	24.0
Rudná1	R3-PV	9	0.6	1.3	8.2	26.9
Rudná1	R4-C	13	7.0	3.9	19.3	42.6
Rudná1	R4-PH	13	1.2	1.9	6.0	17.4
Rudná1	R4-PV	13	0.4	1.7	3.8	9.9

Non-linear regression analysis

Non-linear analysis is performed for the horizontal dry desk values at the Hrabyně locality and stands above the road crown in the cut of the road. Because the authors are trying to find a predictive model for the measured chloride deposition, a statistical analysis is needed. Nonlinear regression analysis with multiple variables proved to be a suitable method for this case. For this case, the variables are temperature and distance from the guide strip.

In the statistical non-linear regression analysis, the minimum and maximum value of the residual is observed in Table 3. The residual is obtained by subtracting the model prediction value from the measured value. The residual value is important for the subsequent sum of the squared residuals (hereafter SSR), which determines the quality of the prediction model. The minimum and maximum prediction value is also observed and compared with the measured values, see Table 4. The value of the prediction model is constrained from below by the value of 0.4, which is the minimum measurable value in the dry desk analysis used and is therefore considered to be insignificant (background value).

Table 3: Minimum and maximum value of residuum

Residuum	
min	0.0
max	5.5

Table 4: Minimum and maximum value of measured and predicted value

	Measured	Prediction
min	0.4	0.4
max	24.1	18.5

In the case of non-linear analysis, the R^2 is not the telling factor, so the SSR is observed in this analysis [10]. From the measured values, it can be seen that the measured value from the horizontal dry desk analysis increases with decreasing temperature and decreasing distance.

The equation with the smallest observed SSR is of the form (1), the coefficients and SSR are listed in Table 5, and the resulting equation is then (2). The results can be graphically displayed in a graph (Fig. 4) or three-axis geometry (Fig. 5), where the x-axis denotes the average monthly temperature, the y-axis denotes the distance from the road guide strip, and the z-axis denotes the measured (red crosses) and predicted (blue crosses) chloride deposition value on the horizontal dry desk. This prediction equation can only be used for structures located above the road crown in the cut of the road.

$$PH = x * e^{a+temp} + y * dist^{b} + const \geq 0{,}4 \quad (1)$$

where
PH – predicted value of horizontal dry desk analyses (mg/m^{2}day)
x, y, a, b, const – constant (see Table 7)
temp – temperature (°C)
dist – distance from guide strip (m)

Table 5: Variables for predicted equation

Variables	
a	-5.80
b	-0.34
x	-44.38
y	47.48
const.	-5.89
SSR	228.6165

$$PH = -44{,}38 * e^{-5{,}80+temp} + 47{,}48 * dist^{-0{,}34} - 5{,}89 \geq 0{,}4 \quad (2)$$

Table 6: Predicted value

Predicted value (mg/m^{2}day)		Average monthly temperature (°C)											
		-0,1	-0,7	3,7	6,4	12,2	19,4	20,4	17,3	14,6	9,1	4,8	0,4
Distance (m)	7	18.5	18.5	13.2	0.4	0.4	0.4	0.4	0.4	0.4	0.4	2.3	18.4
	20	11.1	11.2	5.8	0.4	0.4	0.4	0.4	0.4	0.4	0.4	0.4	11.1
	45	7.0	7.1	1.7	0.4	0.4	0.4	0.4	0.4	0.4	0.4	0.4	6.9
	80	4.7	4.7	0.4	0.4	0.4	0.4	0.4	0.4	0.4	0.4	0.4	4.6
	180	2.1	2.2	0.4	0.4	0.4	0.4	0.4	0.4	0.4	0.4	0.4	2.0

Fig. 4: Measured and predicted value of chloride deposition

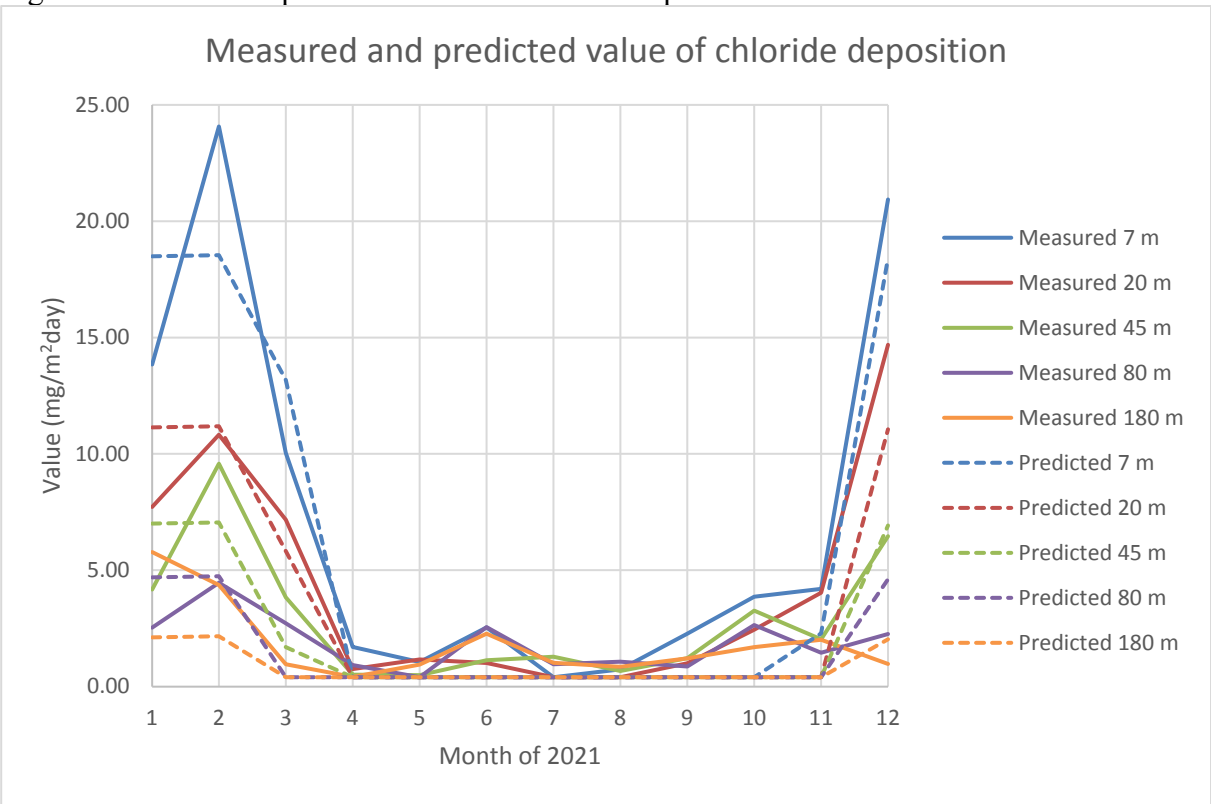

Fig. 5: Three-dimensional graphical representation of measured (red crosses) and predicted (blue crosses) chloride deposition value

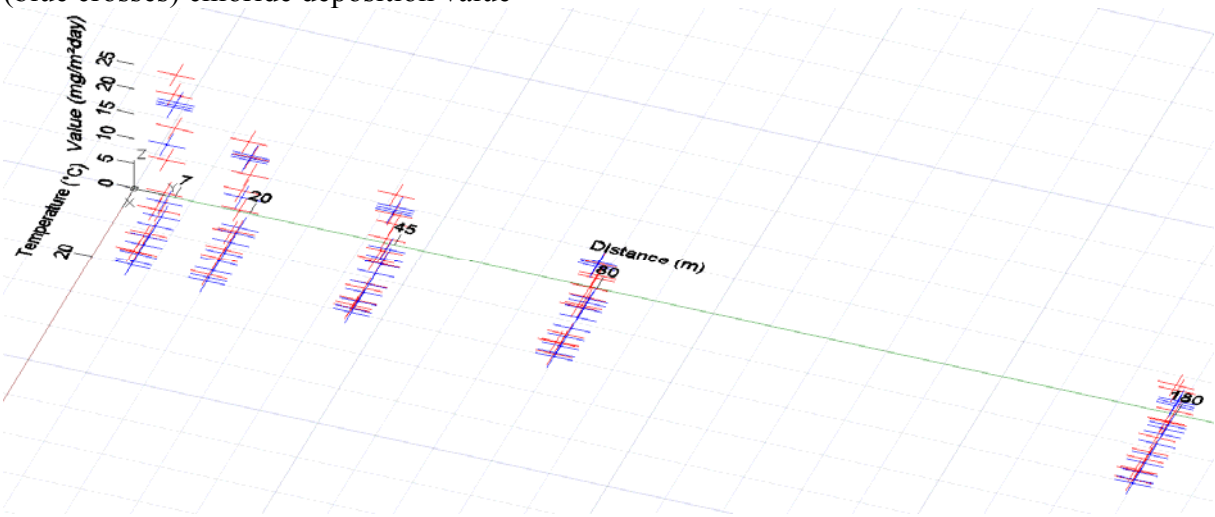

Conclusion

The paper presents measurements from two sites in the vicinity of the I/11 road. The data from the analysis of the horizontal dry desk over the road crown in the cut of the road from the locality Hrabyně are analyzed by means of nonlinear regression. The output of this analysis is a prediction equation of the value on the horizontal dry desk.

From the measured values at bridge location 4692-2, it is evident that the values continue to increase on the slope of the roadway cut of the road. Due to the limited amount of data, these results are mentioned but no further statistical analysis is performed on them. However, the

authors are carrying out further measurements at the two mentioned and other selected localities to deepen their understanding of the mechanism of chloride deposition in the vicinity of roads.

Acknowledgement

The work was supported by the Student Grant Competition of VŠB-TUO. The project registration number is SP2020/37.

References

1. M. Kubzová. Studium korozních procesů na ocelových konstrukcích ovlivněných usazováním chloridů. Ostrava, 2020. VSB-TU Ostrava.
2. V. Křivý; M. Kubzová; P. Konečný; K. Kreislová. Materials. 2019, vol. 12, No. 7. issn 1996-1944.
3. P. Konecny; P. Lehner; D. Vorechovska; M. Somodikova; M. Hornakova; P. Rovnanikova. IOP Conference Series: Materials Science and Engineering. 2019, vol. 659, No. 1.
4. D. Ungermann; P. Hatke. ECCS - European Convention for Constructional Steelwork, 2021.
5. V. Křivý; V. Urban; M. Kubzová. Procedia Engineering. 2016, vol. 142, p. 56–62.
6. EN 9225:2012 Corrosion of metals and alloys — Corrosivity of atmospheres — Measurement of environmental parameters affecting corrosivity of atmospheres.
7. EWAC spol. s r.o. Planá, 2022. Available from: https://ewac.cz/catalog/226.
8. HACH Company. USA, 2022. Available from: https://www.hach.com.
9. Český hydrometeorologický ústav. Praha, 2022. Available from: https://www.chmi.cz.
10. Spiess, Andrej-Nikolai, Natalie Neumeyer. BMC Pharmacology. 2010; 10: 6.

Resistometric sensors for atmospheric corrosion monitoring of surface treated or naturally corroded metals

Matěj Reiser, František Bayer, Adéla Marešová, Šimon Sebastian Havíř, Milan Kouřil,
University of chemistry and technology, Prague, Czech Republic

This work focuses on the preparation and testing of surface modified resistometric sensors. The aim of the chosen surface treatments is to obtain more accurate data on the corrosion rate of the resistometric sensors. The surface treatment was performed on several types of resistometric sensors in order to obtain a surface that can be considered as a real surface. It does not make sense to measure the corrosion rate of a metal that has been exposed outside for years and is corroded, using a new sensor.

The following surface treatments were chosen for a surface with a low or no corrosion attack: pickling in HCl, grinding and blasting. However, corroded surfaces often occur. For such a case the following surface treatments were chosen: precorrosion, corrosion products removal in H_3PO_4 or HCl and passivation of the surface. The process of precorrosion was carried out by exposure to an aggressive environment or prolonged exposure to the outdoor atmosphere.

The sensors we worked with were carbon steel and zinc with different metal track designs and thickness. Sensors with the same surface finish and with different designs were compared. The sensors were exposed to a corrosive environment in order to compare the effect of the surface treatment to corrosion response.

The sensors with protective surface treatments confirmed protective action of conversion coatings, sealers and passivating agents. On the other hand, the precorroded sensors confirmed elevated corrosion rate of active surface under mild atmospheric conditions. Artificially formed corrosion products on steel and zinc correctly represents corrosion behaviour of naturally corroded materials.

Waterborne coating for bronze corrosion protection

Angela Kapitanović, Helena Otmačić Ćurković, Faculty of Chemical Engineering and Technology, Zagreb/Croatia

Cultural heritage objects are often made of bronze. When placed outdoors, they are prone to corrosion due to the presence of aggressive atmospheric compounds. As a result, they get covered with patina. The most common method for their protection is the use of Paraloid B-72, an acrylic varnish. Paraloid B-72 shows good protective properties but only for a relative short period of time. It contains an organic solvent, which can have a negative impact on the environment and human health. Legal regulations restrict the use of organic solvents, which led to the development of waterborne coatings. Their disadvantages are poor surface wetting, corrosion of the metal substrate and a lower level of protection. The aim of this research is to examine the possibility of bronze protection by an acrylic waterborne coating. In order to improve the corrosion protection of studied waterborne coating, self-assembled monolayers of long-chain phosphonic acids are formed on bronze surface prior to coating application. They can act as both adhesion promoters and corrosion inhibitors, as was previously observed in case of their combination with Paraloid B-72. Studies are conducted on bare and patinated bronze surfaces.

The long-term corrosion behaviour of protected samples in simulated acid rain is studied by electrochemical impedance spectroscopy. The film structure and the surface composition are examined by Fourier transform infrared spectroscopy and scanning electron microscopy. Pull-off adhesion tests are conducted before and after exposure to corrosive medium in order to validate the influence of phosphonic acids on coating adhesion.

This work has been fully supported by Croatian Science Foundation under the project IP-2019-04-5030.

Applicability of the paste electrolyte cell for the evaluation of atmospheric corrosion of cultural heritage metals

Ines Šoljić, Sanja Martinez

Faculty of Chemical Engineering and Technology, Zagreb/Croatia

Various electrochemical techniques can be used to obtain information about the condition of metallic cultural artefacts during the exposure to outdoor atmosphere in situ. Electrochemical impedance spectroscopy (EIS) as a widely spread corrosion evaluation tool is one of them. The challenges of its application in the field are well known. One approach to solving these challenges is the application of the paste electrolyte cell. This approach is used in this study for EIS testing of leading (copper, bronze, zinc, Cor-Ten) and modern (aluminium, stainless steel) cultural heritage metals exposed to urban atmospheric environment.

Two surface treatments of copper and zinc, five surface treatments of bronze, and one surface treatment of Cor-Ten are used to compare the natural and artificially applied patinas and the effectiveness of the applied coatings. The corrosion behaviour of aluminium and anodized aluminium and two types of stainless steel are also compared. This results in a total of 18 cases, which are initially characterized by EIS measurements in 3.5% NaCl solution, tap water, simulated rainwater and the aforementioned electrolyte paste cell (QCQ method). According to ASTM G50, untreated and treated metal specimens are exposed to the external corrosive environment. Exposure conditions (humidity and temperature) are monitored and specimens are periodically characterised using spectroscopic techniques. Corrosion behaviour is monitored over a six-month period using the non-destructive QCQ method, which shows promise for on-site measurements of cultural heritage objects without compromising their integrity.

Acknowledgment: This work has been fully supported by Croatian Science Foundation under the project IP-2019-04-5030.

Determination of the corrosion product layer resistance on zinc samples by using gel electrolytes

Crash barriers, railings, lamp posts, waste glass containers - these are just a few of the many examples of galvanized surfaces. They withstand wind and weather for decades, which is possible thanks to a protective layer made of corrosion products. When designing the atmospheric durability of galvanized components, a linear corrosion loss is assumed. In the past 30 years, however, the surrounding atmosphere has changed a lot. Due to the restriction of sulfur exhaust air, acid rain completely disappeared in Europe and Germany, which has a direct influence on the type and protective effect of the corrosion products. Under the influence of current atmospheric conditions, zinc layers are significantly more resistant and no longer show any linear corrosion loss. The established test methods cannot correctly map this change in neither short-term nor long-term tests and thus provide incorrect results. In order to solve this problem, a new measurement method was developed at BAM that can assess the protective effect of the formed surface layers in a minimally invasive manner without damaging the sample and in short test times. For this new method, gel electrolytes are used and the so-called corrosion product layer resistance R_L, which is made up of various surface resistances, is measured electrochemically. As a single measurement, the surface layer resistance can provide information about the existing corrosion protection, while time-dependent measurements assess the stability of the layer. Thus, it is possible again to evaluate the corrosion protection layer. Furthermore, this method can also be used for field measurements on real components.

Study of the anodized Al sealing process, using new sealing solutions that are more respectful of the environment

Hichem Salhi[1], Abderrazak Chilali[2]

[1a]*Département de Matériaux, Centre de Recherche & Developpement des Forces Aeriennes, BP 142Dar El Baida 16033, Alger, Algeria,salhihichem61@gmail.com*
[2]*Département de Technologie, Ecole Nationale Préparatoire aux Etudes d'Ingéniorat, BP05Rouiba, Alger, Algeria,chilalilism@gmail.com*

Abstract

The most commonly used surface treatment of aluminum alloys is sulfuric anodization. It is an electrochemical conversion of the substrate surface inducing a deposit that is more important, resistant and thicker than the naturally formed layer. This treatment is generally followed by a sealing process which consists in reinforcing the aluminium oxide layer by filling its porosities. This work aims mainly at finding a solution to substitute hexavalent chromium used during the sealing process, a carcinogenic element for humans. The aluminum alloy considered in this work concerns particularly the alloy 2024. For this purpose, a new sealing process based on cerium sulphate was developed. This new process is more environmentally friendly but also belongs to the cerium salts, very promising inhibitors.

Keywords: "Aluminum alloys; Surface treatment; Sulfuric anodization; Sealing; Hexavalent chromium; Cerium sulfate".

Introduction

Aluminum and its alloys have the ability to spontaneously cover themselves with an alumina layer of a few nanometers thick when they are in contact with the oxygen in the air. This layer is generally too thin to provide effective protection against corrosion. Thus, in order to promote the growth of this oxide layer, an "anodic oxidation" step commonly called "anodization" is necessary. This treatment is generally followed by the so-called "sealing" process, which consists of reinforcing this aluminum oxide layer by sealing its porosities.

Anodized aluminum sealing treatments, practiced industrially or under development, aims at improving the resistance to corrosion, the mechanical qualities of the surface, or even the adhesion of paints. They are particularly numerous such as sealing with boiling water, dichromate, cerium sulphates, etc. Anodizing is an electrochemical treatment leading to increase the thickness of the natural oxide layer present on the substrate surface, and thus giving it interesting functional properties. The range of anodization currently used in the treatment of aluminum alloy 2024 parts is anodization in a porous sulphuric medium having a negative effect on their mechanical properties. Sealing is a complementary process of anodization, which aims to seal the porous anodic layer and strengthen its resistance to corrosion.

The main objective of this study is to develop and characterize a new sealing process based on cerium sulphates of anodized 2024 aluminum alloy, which is also compatible with the new environmental standards. European directives state that the use of hexavalent chromium-based compounds must be reduced or even eliminated in the very near future, as these have been recognized as carcinogenic for humans and toxic for the environment. Recently, many works have been done in this field, but today most alternatives do not have the same performance level as the hexavalent chromium-based processes. Among the most promising inhibitors are cerium salts: cerium nitrates, cerium acetates and cerium sulphate on which our study will be based.

Experimental work

Materials and anodizing process

The approach consists of carrying out a certain number of anodization operations, sealing and characterization of the corrosion phenomenon affecting the AL 2024 alloy using the electrochemical method.

The electrochemical approach is essential but it should not be considered separately. The chemical composition of the material, the applied surface treatment, the anodizing and sealing processes, the electrochemical and metallographic characterization were considered in this work. The chemical composition of the studied 2024 aluminum alloy is summarized in Table1.

Table 1. Chemical composition of the studied 2024 aluminum alloy.

Element	Al	Cu	Si	Mg	Mn	Fe	Zn	Pb	Cr	Ti	Ni	Sn
%	bal	4.48	0.06	1.47	0.71	0.17	0.054	0.00	0.008	0.03	0.00	0.00

The anodization treatment of the 2024 aluminum alloy samples required the use of an experimental assembly carried out in the corrosion laboratory (figure 1). The experimental assembly consists of the following elements:

- A direct current generator, which can output a current of up to 3 A and deliver a voltage of up to 30 V of the GP-1305 type. We used a current density of 1.5 A/dm²;
- A bain-marie to maintain the temperature;
- A lead cathode, of a rectangular shape, which gives good current distribution;
- A stopwatch to indicate the anodizing time;
- A magnetic stirrer, which ensures the homogeneity of the medium;
- The electrolyte used is sulfuric acid (H_2SO_4) at 180 g/l;
- A stand that serves as a support to hold the sample.

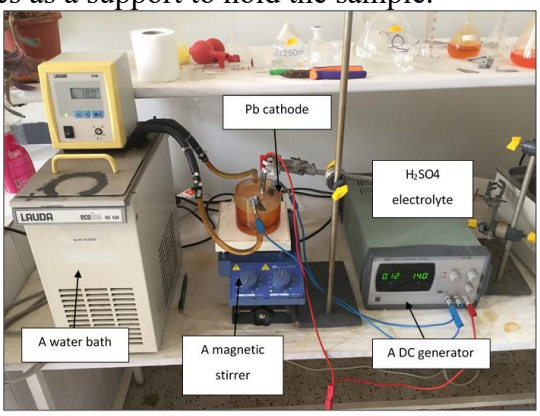

Figure 1: Experimental anodizing device

The sulfuric anodizing parameters are shown in table 2:

Table 2: Sulfuric anodization parameters

Anodizing parameters	concentration	temperature	anodizing time	Current density
Value used	180 g/l	18 °C	60 min	1.5 A/dm²

Sealing of the anodic layers

The sealing treatment of the 2024 aluminum alloy samples was performed on an experimental assembly consisting of the following elements: a thermostatic bath, a 150 ml beaker and a stand that serves as a support to hold the beaker and the sample (figure 2).

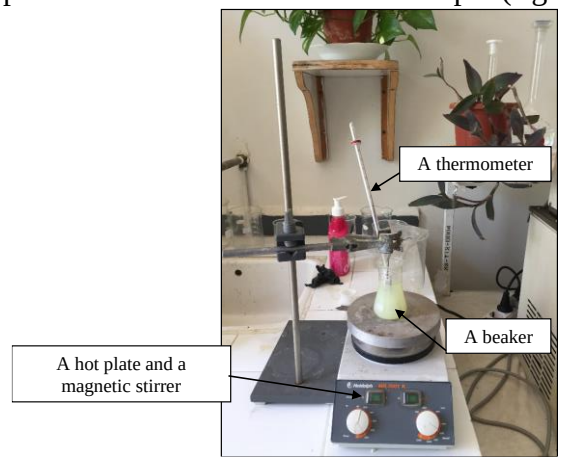

Figure 2: Sealing device

In order to optimize the sealing process, we have used the cerium sulfate inhibitor Ce $(SO_4)_2.4H_2O$ by varying the sealing parameters (table 3).

Table 3: Sealing parameters

Sealing parameters / Type of Sealing	Concentration	Temperature	anodizing time	pH
Distilled water	/	98°C	30 min	7
Potassium bichromate $K_2Cr_2O_7$	40 g/l	98°C	30 min	6
Cerium Sulphates $Ce(SO_4)_2.4H_2O$	10^{-2}M $3x10^{-2}$M $5x10^{-2}$M $7x10^{-2}$M	37°C 55°C 75°C 85°C 98°C	20 min 30 min 40 min 50 min 60 min	5

Results and discussions

Optimization of cerium sulphate concentration

The influence of the cerium sulphate concentration of the sealing solution on the anodized layer corrosion behaviour was analysed. To this end, the evolution of the OCP of cerium as a function of time (1 hour of immersion) of 2024 aluminum samples immersed in an electrolyte containing 35 g/l of NaCl at ambient temperature was studied (figure 3).

The concentrations used in this work are 10^{-2}M, $3x10^{-2}$M, $5x10^{-2}$M and $7x10^{-2}$. These concentrations were chosen based on the reference [1] which revealed that for low levels of inhibitor, corrosion resistance is better.

The evolution of the OCP indicates the corrosion of the studied samples with the occurrence of corrosion products (oxides of Al, Mn and/or Si). Besides, in the absence of cerium sulphate, stabilization is reached after 1 hour of immersion at -640 mV. On the other hand, for the same period of immersion in the cerium sulphate medium, a potential ennoblement can be observed indicating that a protective layer (probably Al_2O_3) is formed on the metal surface.

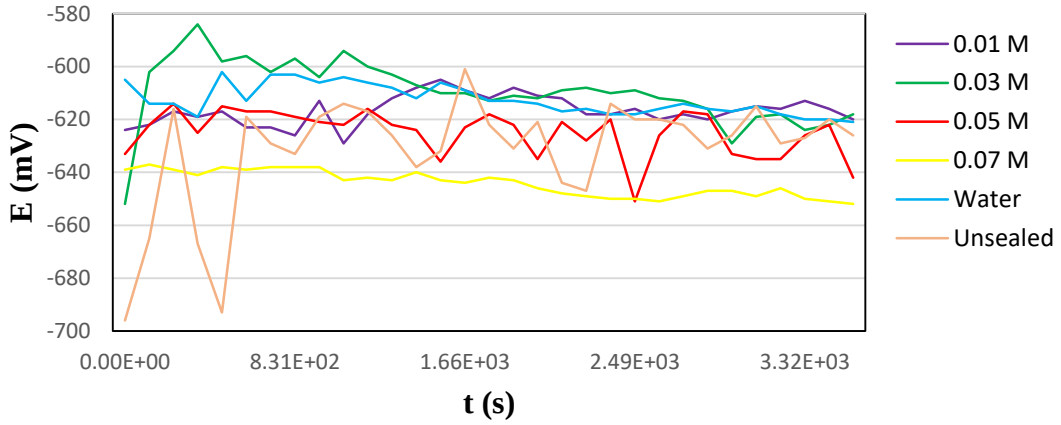

Figure 3: Evolution of the OCP during 1 h of immersion in 35 g/l NaCl for different concentrations of $Ce(SO_4)_2.4H_2O$.

In addition, the effect of the inhibitor on the anodic and cathodic partial reactions can be estimated from the linear polarization curves in a three-electrode electrochemical cell for different concentrations of cerium sulphate (figure 4). The polarization measurements were carried out in the potential range of -800mV to -500mV with respect to the free potential with a scanning speed of 1 mV/min. We depict in figure 4 the polarization curves for sealed with cerium sulphate and unsealed Al 2024 alloy.

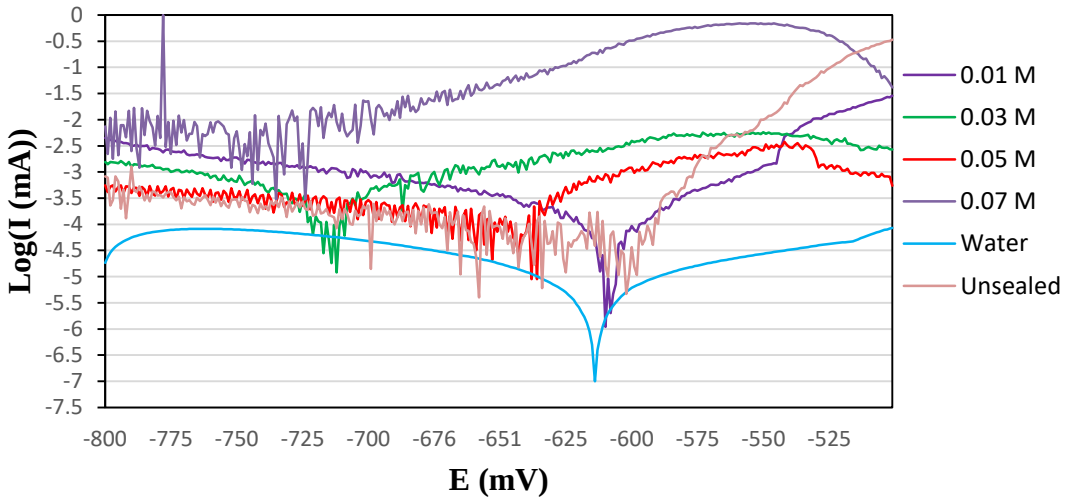

Figure 4: Polarization curves of anodized and sealed samples for different concentrations of $Ce(SO_4)_2.4H_2O$ in 35 g/l NaCl.

It can be noticed that the addition of the different concentrations of cerium sulphate shifts the corrosion potential towards more cathodic values and leads to a decrease in the anodic corrosion current densities. A change in the curves shape can also be observed with a large area of cathodic passivation.

In order to compare the effectiveness of the different cerium sulphate concentrations, we calculate the corrosion current density Icorr which represents the porous layer modifications induced by the sealing process (table 4). Icorr was determined by the intersection of the anodic and cathodic Tafel slopes.

Table 4: Corrosion current densities as a function of cerium sulphate inhibitor concentration

Concentration (M)	10^{-2}	$3x10^{-2}$	$5x10^{-2}$	$7x10^{-2}$	Water	Unsealed
Icorr (mA)	$3.5x10^{-9}$	$2.9x10^{-8}$	$6.16x10^{-9}$	$4.90x10^{-6}$	$3.16x10^{-12}$	$5.42x10^{-9}$

Table 4 shows that for low concentrations, the corrosion resistance is higher due to the optimal protective effect of cerium sulphate inducing then the formation of a protective layer on the sample surfaces. The current density decreases for low concentrations of cerium sulphate. Moreover, the inhibitor seems to act as an "impurity" by attaching itself to the pores surfaces by an adsorption process. This limits the transformation of alumina into aluminum hydroxide. Since adsorption depends on concentration, it seems obvious that when the inhibitor is more concentrated, itss adsorption will be higher (high-incorporated cerium content) and the sealing level will be lower in agreement with the reference [1].

Optimization of sealing time

In this part, the alloy samples were sealed at 10^{-2}M and at 98°C. The objective is to find the sealing time corresponding to the highest corrosion resistance. First, we followed the evolution of the OCP for different sealing times as a function of time, i.e. 1 hour of immersion of the 2024 aluminum samples in an electrolyte at 35 g/l of NaCl at room temperature. The sealing times were chosen based on the references [2, 3], concluding that the pores resistance increases very quickly in contact with the sealing solution during the first 20 -30 minutes of treatment while it increases very slightly beyond 30 minutes of treatment. The optimum sealing time was found to be equal to the anodization time or 80% of the anodization time [3]. These sealing times are 20, 30, 40, 50 and 60 min. The evolution of the OCP during 1 h of immersion in 35 g/l NaCl for different sealing times based on $Ce(SO_4)_2.4H_2O$ is shown in Figure 5.

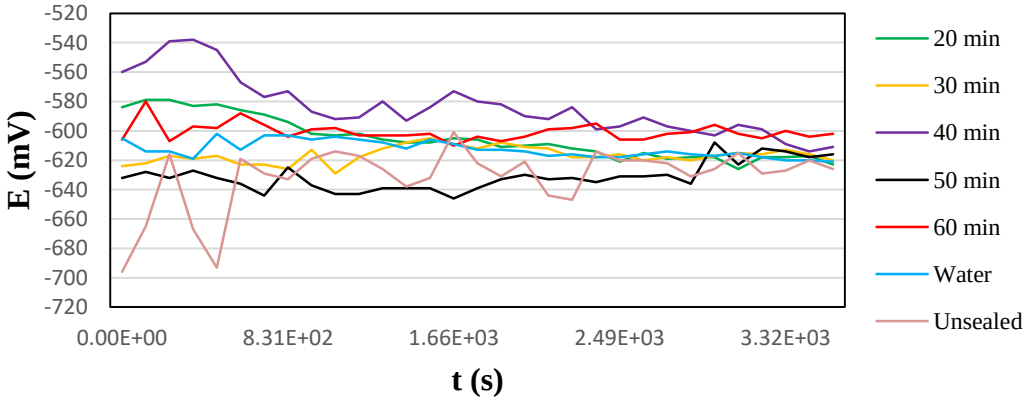

Figure 5: Evolution of the OCP during 1 h of immersion in 35 g/l NaCl for different sealing times based on $Ce(SO_4)_2.4H_2O$.

The potential evolution of the test performed without inhibitor characterizes, as before, the sample corrosion with the formation of corrosion products. It can be noticed that the stabilization at a value of -610mV of the OCP was reached after 1 hour of immersion. Besides, the stabilization of the clogged samples was observed after 1 hour of immersion at -615mV. It is worth noting that the OCP is less noble for high sealing times.

In order to optimize the cerium sulphate-based 2024 aluminum sealing time, the linear polarization curves are plotted in an electrochemical cell of 03 electrodes for different cerium sulphate sealing times (figure 6). The polarization measurements were carried out in the potential range of -800mV to -500mV with respect to the OCP with a scanning speed of 1 mV/min.

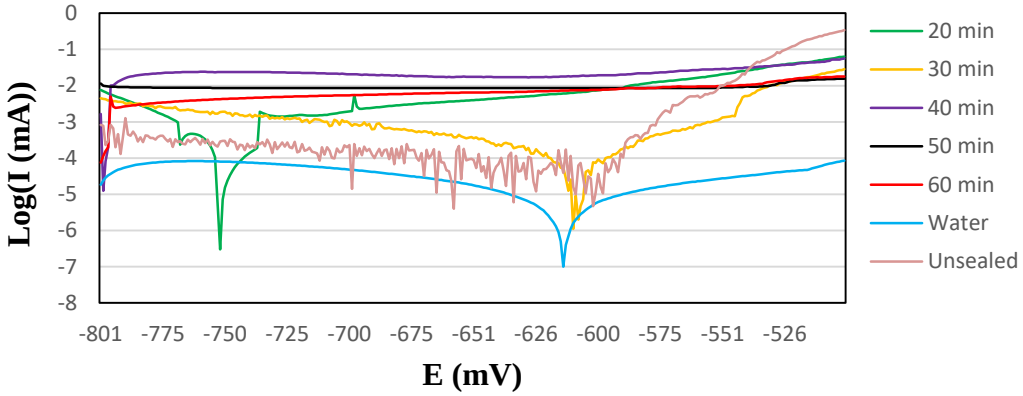

Figure 6: Polarization curves of cerium sulphate-based 2024 aluminum for different sealing times based on $Ce(SO_4)_2.4H_2O$.

The polarization curves show that for the sealing times of 20 and 30 min there is clearly a chemical attack, and therefore an anodic and cathodic polarization which results in corrosion sensitivity. The corrosion current densities are summarized in table 5.

Table 5:Corrosion current densities as a function of sealing time.

Time (min)	20 min	30 min	40 min	50 min	60 min	Distilled water	Unsealed
Icorr (mA)	$5.20x10^{-10}$	$3.5x10^{-9}$	AP	AP	AP	$3.16x10^{-12}$	$5.42x10^{-9}$

Optimization of sealing temperature

In this part, the aluminum samples are sealed at 10^{-2} M for 50 min, and the aim is to find a sealing temperature when the corrosion resistance will be the highest.

The OCP evolution at different sealing temperatures with cerium sulphate as a function of time was followed as depicted in figure 7. The choice of sealing temperatures was based on the work of B.E. Yoldas [4], which showed that the hydrolysis temperature plays a major role in the form of the obtained aluminum hydroxide. Indeed, the hydrolysis of aluminum alkoxide in “hot” water (T ≥80°C) leads to the formation of boehmite under shape of fibres of approximately 0.1 µm long and which do not undergo no change over time. On the other hand, when the hydrolysis is conducted at a temperature below 80°C, a very amorphous aluminum hydroxide (50 to 60%) is obtained, mixed with boehmite (20 to 30%) and small crystals of bayerite.

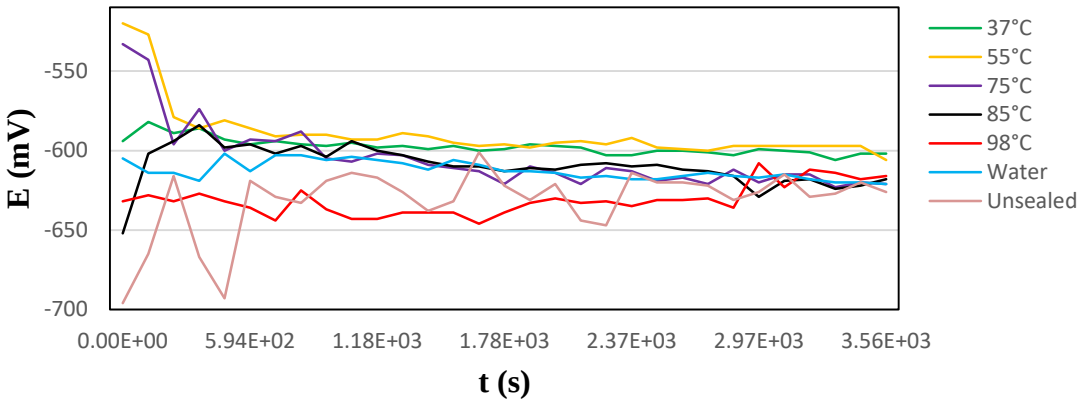

Figure 7: Evolution of the OCP during 1 h of immersion in 35 g/l NaCl for different sealing temperatures based on $Ce(SO_4)_2.4H_2O$

The potential evolution without inhibitor characterizes the sample corrosion of with the development of corrosion products. It was found that the stabilization was reached at a value of -610mV of the OCP after 1 hour of immersion. The stabilization of the clogged samples was observed after 1 hour of immersion at –615 mV. In addition, the potential was found to be less noble for high sealing temperatures.

In order to optimize the sealing temperature of cerium sulphate-based 2024 aluminum aluminum 2024 based on cerium sulphate, we plotted the linear polarization curves in a three electrodes electrochemical cell for different cerium sulphate sealing temperatures (figure 8). The polarization measurements have were carried out in the potential range of -800mV to -500mV with respect to the OCP with a scanning speed of 1 mV/min.

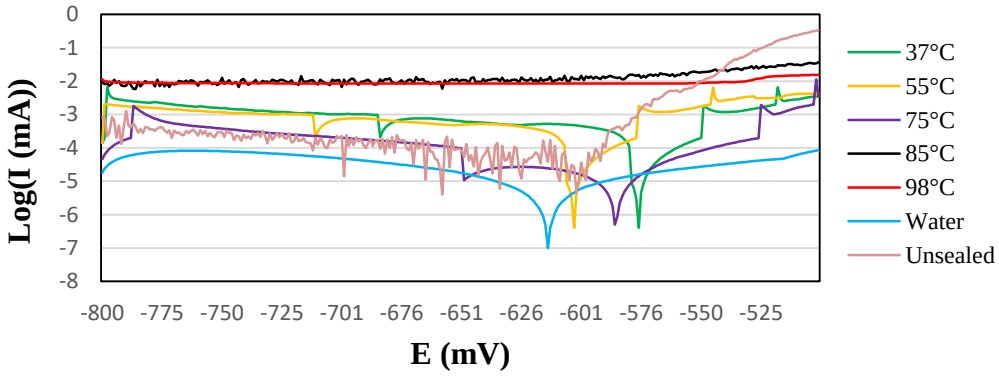

Figure 8: Polarization curves of anodized and sealed samples for different sealing temperatures based on $Ce(SO_4)_2.4H_2O$

It can be seen from figure 8 that, for the temperatures of 75°C, 55°C and 37°C, there is clearly a chemical attack, and therefore an anodic and cathodic polarization which results in sensitivity to corrosion. The corrosion current densities as a function of sealing temperature are summarized in table 6.

Table 6: Corrosion current densities as a function of sealing temperature

Temperature (°C)	37°C	55°C	75°C	85°C	98°C	Distilled water	Unsealed
Icorr (mA)	$9.12x10^{-10}$	$4.7x10^{-10}$	$4.98x10^{-12}$	AP	AP	$3,16x10^{-12}$	$5.42x10^{-9}$

Figure 9 depicts the polarization curves as function of OCP in 35 g/l of NaCl with the optimized parameters of each inhibitor. The optimized parameters are 10^{-2} M, 50 min and 98°C.

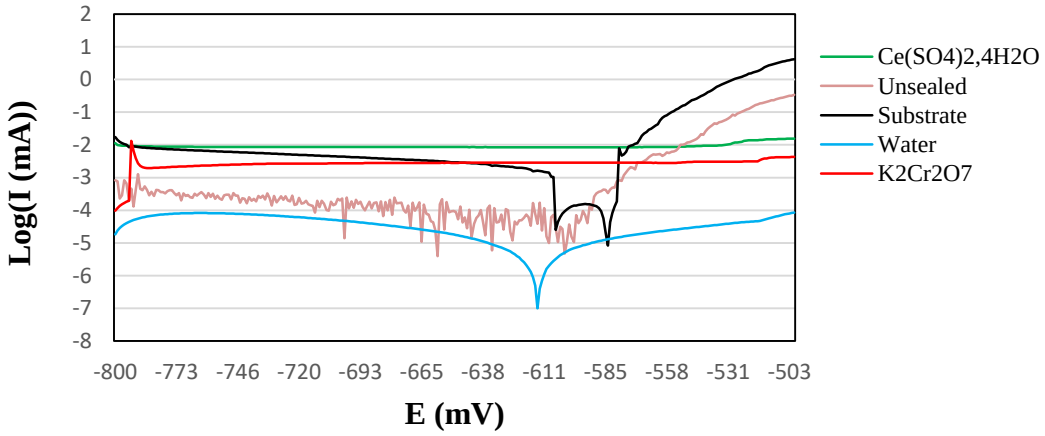

Figure 9: Polarization curves as function of corrosion potential in 35 g/l of NaCl with the optimized parameters of each inhibitor

Study of ageing

In order to study the properties evolution of aluminum over time under the effect of different inhibitors, we immersed our anodized and sealed samples with: cerium sulphate, potassium dichromate and water in aggressive medium of NaCl (35g/l) for different immersion times from 1 hour to 7 days. The effectiveness of inhibitors will be compared using polarization curves and corrosion potential evolution.

Study of ageing for cerium sulphate

Figure 10 presents the polarization curves as function of the corrosion potential in 35 g/l of NaCl for different ageing times, and table 7 summarizes the corrosion current densities obtained as function of ageing time.

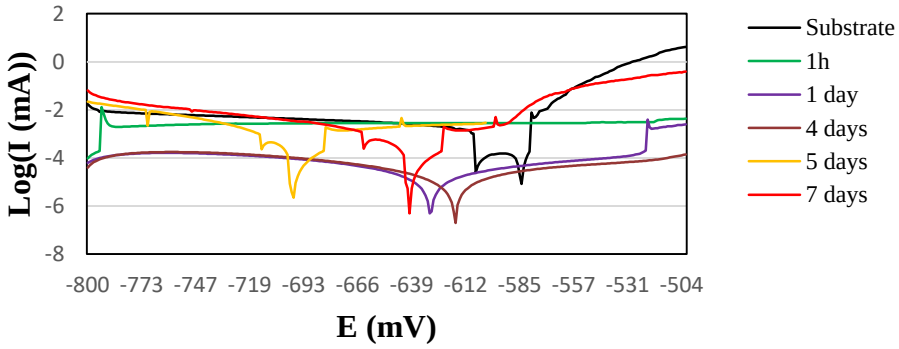

Figure 10: Polarization curves as function of the corrosion potential in 35 g/l of NaCl for different ageing times.

Table 7: Corrosion current densities as a function of aging time.

Time	substrate	1h	1 day	4 days	5 days	7 days
Icorr (mA)	$8.26\text{x}10^{-8}$	AP	$1.25\text{x}10^{-11}$	$6.3\text{x}10^{-10}$	$1.9\text{x}10^{-12}$	$7.9\text{x}10^{-12}$

It can be seen from figure 10 and table 7 that, after one hour of immersion in a solution of NaCl, a total passivation of the layer is observed, which means that the anodic layer sealed with cerium sulphate is homogeneous and compact.

After 1 day of immersion in a NaCl solution, the protective layer is attacked by chloride ions, showing some resistance because the attack is not strong with a very low current density of $1{,}25x10^{-11}$ mA. After 04 days of immersion in a NaCl solution, a slight weakening of the protective layer and an increase in the current density are noted. This means that the chloride ions have succeeded in penetrating deeper into the layer and that the oxides of cerium have not yet exerted their protective effect. After 05 days of immersion in a NaCl solution, we observe a strong reinforcement of the protective layer and a decrease in the current density ($1{,}9x10^{-12}$ mA). This results in the effect of repassivation or self-sealing of cerium sulphate oxides in pitting areas. After 07 days of immersion in a solution of NaCl, a stabilization of the layer resistance can be observed and even an improvement in its resistance with a current density of $7{,}9x10^{-12}$ mA. This means that the chloride ions may penetrate the protective layer because there is no total passivation.

In order to better study the reaction mechanism of the sealed and aged anodic layer, we will focus on the appearance of the obtained curves. We notice a shift in the corrosion potential of sealed and aged anodic layers towards more noble values for longer ageing times. This can be explained by the fact that, at the beginning, the cerium sulphate oxides have not attain their protective effect, and that after a strong attack and a repassivation (self-sealing) a layer has been formed with a more noble potential of corrosion. By comparison with the substrate polarization curve, it appears that for the cerium sulphate sealed samples, the chlorides could not reach the aluminum and therefore cross the barrier of the protective layer.

Study of ageing for potassium dichromate

Figure 11 depicts the polarization curves as function of the corrosion potential in 35 g/l of NaCl for different ageing times, and table 8 summarizes the corrosion current densities obtained as function of ageing time.

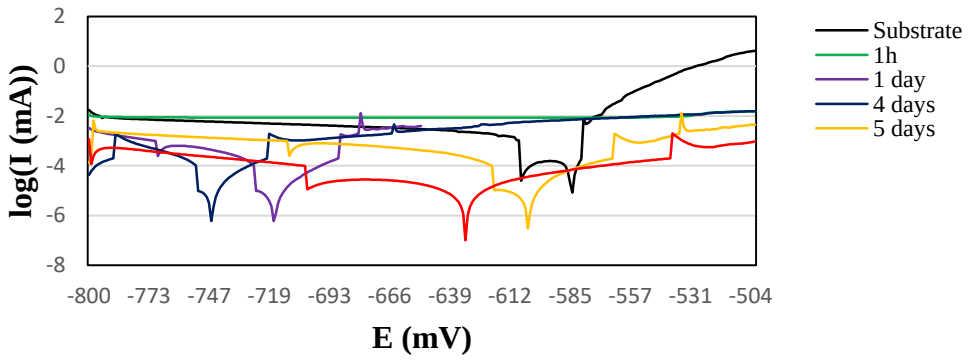

Figure 11: Polarization curves as function of the corrosion potential in 35 g/l of NaCl for different ageing times

Table 8: Corrosion current densities as a function of ageing time.

Time	substrate	1h	1 day	4 days	5 days	7 days
Icorr (mA)	$8.26x10^{-8}$	AP	$1.25x10^{-11}$	$5x10^{-13}$	$5.3x10^{-8}$	$1.3x10^{-8}$

A total passivation of the layer was observed after 1 hour of immersion in a NaCl solution. This means that the potassium dichromate-sealed anodic layer is homogeneous and compact.

After 1 day of immersion in a NaCl solution, the protective layer was attacked by chloride ions. However, the protective layer showed some resistance with a very low current density of $1{,}25x10^{-11}$ mA. After 04 days of immersion in a NaCl solution, it was found that the

corrosion resistance of the protective layer has remained the same as after 1 day of immersion, which proved the very high corrosion resistance of a potassium dichromate-sealed layer. After 05 days of immersion in a NaCl solution, a marked weakening of the protective layer resistance was recorded with an increase in the current density, reaching $5{,}3x10^{-8}$ mA. This implies that the chloride ions penetrated successfully the layer deep, and that the chromium oxides have not yet exerted their protective effect. After 07 days of immersion in a solution of NaCl, a stabilization of the layer resistance and even degradation of its resistance were observed with a current density of $1{,}3x10^{-8}$ Ma, indicating that the chloride ions penetrated the protective layer.

In order to better study the reaction mechanism of the potassium dichromate-sealed and aged anodic layer, the appearance of the obtained curves was analysed. We remarked a shift of the corrosion potential of the sealed and aged anodic layers towards more noble values for higher ageing times reaching up to 05 days. Nevertheless, a considerable reduction in the corrosion potential and a shift towards more negative values. After 05 days of ageing, this can be justified by the fact that at the beginning the aluminum hydroxybichromate ensure its protective effect, and after a strong attack, the layer resistance decreased and the self-sealing time was considerably long. By comparison with the substrate polarization curve, we can conclude that for the potassium dichromate-sealed samples the chlorides could not reach the aluminum and therefore cross the barrier of the protective layer.

Conclusion

Through this work, the following conclusions can be drawn:

• The optimal parameters for the sealing process based on cerium sulphate are 10^{-2}M, 98°C and 50 min;

• Cerium sulphate is an inhibitor which is effective even after a certain period of ageing. It has a very rapid self-sealing or repassivation capacity;

• Potassium dichromate is an inhibitor, which gives a very good corrosion resistance to the anodized layer. However, its self-sealing capacity is slower than that of cerium sulphate;

• The anodic layers sealed with water are thicker than the anodic layers sealed with potassium bichromate and cerium sulphate;

• Cerium sulphate and potassium dichromate act on the anodic layer by coating the walls of the pores unlike water, which acts by filling.

References

1.S. Mohsen, J. Mehdi and V. Sareh, Anodising of 2024-T3 aluminium alloy in electrolyte of sulphuric- boric-phosphoric mixed acid containing cerium salt as corrosion inhibitor, journal of Transactions of Nonferrous Metals Society of China Volume 27, Issue 3, March 2017, Pages 711-721.

2.B.J.Usmana, F.Sceniniab and M.Curioni, The effect of exposure conditions on performance evaluation of post-treated anodic oxides on an aerospace aluminium alloy, journal of Surface and Coatings Technology, Comparison between salt spray and immersion testing, Volume 399, 15 October 2020.

3. A.Charles, Anodizing of aluminum, journal of Metal Finishing Volume 97, Issue 1, Supplement 1, January 1999, Pages 476-493.

4. E. Bulent and Yoldas, Hydrolysis of aluminium alkoxides and bayerite conversion, Journal of Applied Chemistry and Biotechnology 23(11), 803-812, 1973.

Corrosion of Pt in fuel cell electrodes of different structure

A. O. Krasnova[a], A. A. Nechitailov[a], N. V. Glebova[a], A. G. Kastsova[a], N. K. Zelenina[a], A. Seyeux[b], P. Marcus[b], N. Cam[c], P. Volovitch[b]

[a]Ioffe Institute, Saint-Petersburg, Russia;

[b]Institut de Recherche de Chimie Paris (IRCP), Paris, France

[c]Placamat, UMS 3626, 87 av. du docteur Schweitzer, Pessac, France

email : annkrasnova.ak@gmail.com

Among different green energy solutions, electrochemical energy devices such as proton-exchange membrane (PEM) fuel cells offer high efficiency of energy conversion, high specific energy intensity of energy carriers, low noise and high autonomy. However, sustainability of newly developed materials for these devices needs to be verified and the degradation mechanisms which can lead to the efficiency loss need to be understood in order to control them. Recent works demonstrated that addition of carbon nanotubes (CNT) and graphene-like materials in the electrodes is beneficial for both the electrode activity [1] and the mass transport processes. Moreover, ageing tests demonstrated that addition of CNT reduces the degradation rate of Nafion-carbon based PEM electrodes with Pt catalyst. The degradation mechanisms of these electrodes with and without addition of CNT are studied in the present work. X-ray powder diffraction showed the increase of Pt nanoparticles size during ageing. In highly porous electrodes (with CNTs) the size of Pt nanoparticles increased to a lesser extent. Pt migration in aged electrodes was confirmed by Auger electron spectroscopy and time-of-flight secondary ion mass spectrometry depth profiling.

A speculative mechanism of improved sustainability of the electrodes in the presence of CNT is proposed. In this mechanisms Pt recrystallization under electrochemical action is suggested to occur with the participation of the proton-conducting polymer Nafion. In the samples without CNTs, Pt recrystallization leads to the reduced electrochemically active surface area and decrease in localized strain. The presence of CNTs introduces a spatial mismatch resulting in decrease of the direct contacts between Pt and Nafion and hence reduces its mobility.

1. Glebova, N.V., et al // ETACP-2019. Journal of Physics Conference Series journal, V. 1236, Article Number 012004, 2019. DOI: 10.1088/1742-6596/1236/1/012004

Evaluation of the susceptibility to hydrogen-induced corrosion of various metallic materials for offshore power-to-X plants

Sven Schewe, DECHEMA-Forschungsinstitut, Frankfurt am Main/Germany;
Wolfram Fürbeth, DECHEMA-Forschungsinstitut, Frankfurt am Main/Germany

Hydrogen will play a substantial role in global efforts to reduce emissions of harmful greenhouse gases and decarbonization in various fields. The energy required to produce carbon-free green hydrogen must come only from renewable sources, e.g. offshore wind farms. Within the framework of the German hydrogen strategy, various projects are concerned with the offshore production of hydrogen as well as downstream products. These products, also known as Power-to-X (PtX), include methane, methanol, ammonia and Fischer-Tropsch synthesis products.

What we aim to do

An evaluation of application-related corrosion resistant materials for plant components and piping regarding their suitability for the usage in contact with hydrogen and hydrogen containing (or evolving) PtX plant media is conducted. An electrochemical characterization of the diffusion tendency will be performed using Devanathan cells. In addition, slow tensile tests will evaluate influences on the mechanical properties. Furthermore, analyses of diffusible hydrogen by thermodesorption mass spectrometry as well as various metallographic and electron microscopic methods will be used to characterize the interactions between hydrogen and the different materials.

Carbon steel corrosion and fusion bonded coating deterioration in the liquid phase of anaerobic digestion

Xiaoqi Wen, University of Southampton, Southampton, U.K.

Anaerobic digestion (AD) is an established method to recover energy from biogas by-products and simultaneously convert nutrients into digestate, making it an efficient alternative to treat waste within a circular resource economy. The AD conditions are generally mild, with a neutral pH and low redox potentials; however, adverse surface degradation, such as abrasion and corrosion can occur. Key factors affecting coating lifetime in AD are still unclear for alternative epoxy-based coatings. Consequently, further studies are necessary to explore the interaction between the chemical and biochemical conditions, and the coating properties when exposed to AD conditions. Combining electrochemical methods and immersion tests, this work aims to initially investigate the corrosion performance of bare and fusion-bonded epoxy (FBE) coated carbon steel in the AD liquid phase from digested sewage sludge (supernatant chemical composition: 0.79 g L^{-1} Cl^-, 0.07 g L^{-1} PO_4^{3-}, 1.85 g L^{-1} NH_4^+, 0.11 g/L total volatile fatty acids).

To benchmark the corrosion performance of bare carbon steel in the supernatant, as well as 3.5% NaCl and 0.165% NaCl test solution, was initially investigated at room temperature, 35°C, and 55°C with a low dissolved oxygen level (<0.2 mg/L). Both electrochemical impedance spectroscopy (EIS) and potentiodynamic polarisations suggest the corrosion kinetics of carbon steel in the supernatant were predominately mixed-controlled (charge transfer and diffusion processes). This study provides insights into the feasibility to define a simplified simulant sludge supernatant as a test electrolyte for industrial practice. In addition, bare carbon steel and partially damaged FBE coated carbon steel (scribed) were immersed in digested sludge at room temperature, 35°C, and 55°C for 12 weeks (in 20 L reactors). Ex situ EIS data were consistent with the development of corrosion products/deposits with immersion time. For the bare carbon steel, the results indicate that the corrosion process was affected by temperature, with corrosion products and surface deposits most evident on the surfaces retrieved from the 55°C reactors. For the scribed FBE coatings, corrosion products/deposits covered the exposed steel, while the coating surfaces remained unaffected, indicating as expected the FBE coating have a good chemical resistance to the digested sludge.